A NOVEL 3D TRANSITION ZONE SEISMIC SURVEY, SHOAL POINT, PORT AU PORT PENINSULA, NEWFOUNDLAND: SEISMIC DATA PROCESSING AND INTERPRETATION

CRAIG A. ROWE

A Novel 3D Transition Zone Seismic Survey, Shoal Point, Port au Port Peninsula, Newfoundland: Seismic Data Processing and Interpretation

by

© Craig A. Rowe

A thesis submitted to the

School of Graduate Studies

in partial fulfillment of the

requirements for the degree of

Master of Science

Department of Earth Sciences (Geophysics)
Memorial University of Newfoundland

August, 2003.

St. John's Newfoundland

ABSTRACT

The west coast of Newfoundland is a region of considerable interest for petroleum exploration. Interest is focused in several specific areas, but especially in the vicinity of the Hunt et al. discovery at Port-au-Port. The primary target is the carbonate bank sequence deposited on the margin of the ancient North American continent (Laurentia) in Cambro-Ordovician time. The geological setting of this area is extremely complicated and dominated by extensive thrusting dictating that only a 3D technique could yield acceptable results. The integration of 2D land acquisition combined with a novel style of "3D" wide-angle transition zone seismic surveying allows for a different and efficient technique of seismic acquisition in shallow water. The survey was conducted in the vicinity of the PanCanadian et al. Shoal Point K-39 well. The processing challenges associated with this style of seismic acquisition fall predominantly in the realm of extremely long offset data combined with low fold coverage. The testing and application of less conventional processing techniques was essential for optimal results, and a better understanding of the geology of the area.

The primary goal was to develop a better understanding of the complex geology of the area. The objective is to create a 3D surficial map of the Ordovician carbonate platform using the 3D seismic data. Detailed processing followed by careful consideration of surrounding pre-existing seismic surveys aided in the final interpretation of the stacked 3D dataset and creation of 3D surface maps.

Overall the final sections and 3D surfaces compare favorably with the drilling results and surrounding seismic therefore meeting the project objectives and desired goals.

Acknowledgements

I would like to express sincere gratitude and appreciation to the following organizations: Landmark Graphics Corporation for the donation of the necessary software to the Department of Earth Sciences, the Government of Newfoundland and Labrador for funding the Industrial Development Fund for the field data acquisition, PanCanadian Petroleum (now EnCana) for the early permission to use K-39 well logs and Shearwater Geophysical Corporation for study leave to complete the project.

The thesis would not have been possible without the assistance of several individuals who generously contributed their time and knowledge. I would like to thank Mr. Ian Atkinson, Mr. Paul Barnes, Dr. Chris Pike and my supervisor Dr. Jim Wright who initiated the project; providing direction and instruction throughout all stages of planning, processing and report compilation.

Table of Contents

List of Figures

List of Tables

1.0 Introduction

The Port au Port Peninsula is located on the southwestern edge of the Province of Newfoundland. Geologically situated along the frontal edge of the Humber zone, this is the western-most of five regional tectono-stratigraphic Appalachian zones (Figure 1.1). The Humber zone represents a Cambro-Ordovician passive margin regionally deformed and displaced during various phases of deformation related to the formation of the Appalachian Mountains and the closing of the Proto-Atlantic Iapetus Ocean during Ordovician / Silurian time.

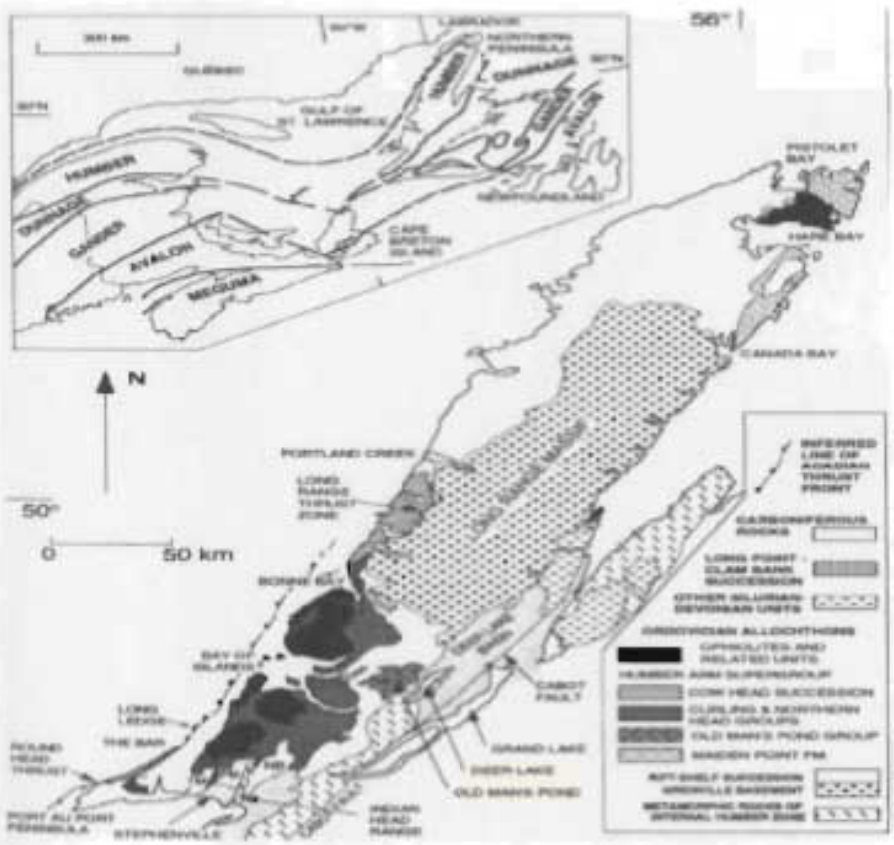

Figure 1.1. Geological map of the Western Newfoundland Humber zone.

Traditionally western Newfoundland has displayed excellent hydrocarbon potential with the discovery of oil seeps and exploration dating back to the late 1800's. Documented shallow wells throughout the 1900's have indicated varied amounts of hydrocarbons and possible reservoirs helping contribute to industry interest and modern seismic exploration and drilling operations during the 1990's. To date the Port au Port peninsula and surrounding bays have been the site of thousands of line kilometers of 2D seismic and a handful of exploration wells (Figure 1.2). Interest is focused in several specific areas but especially in the vicinity of the 1996 Hunt et al. discovery well, Port-au-Port # 1. The primary Western Newfoundland exploration targets tend to be either Carboniferous or Cambro-Ordovician plays. On the Port au Port peninsula it is generally the carbonate bank sequence deposited on the margin of the ancient North American continent (Laurentia) in Cambro-Ordovician time that is of primary interest. This equivalent setting also exits in the proven Anadarko Basin of the Southern United States.

Western Newfoundland (i.e: Humber zone) and the Eastern United States as far south as the Gulf of Mexico originally developed as a continental shelf in the Late Cambrian as the eastern coast of the Laurentian continent. An early Paleozoic passive margin the Humber zone is characterized by a Cambro-Ordovician carbonate platform that has undergone extensive folding and faulting controlled by multiple orogenies related to the opening and closing of the Iapetus ocean (To be discussed further in Chapter 2 Geology). The geology of the peninsula is

extremely complex being extensively faulted and dominated by a regional structural feature known as the Round Head fault.

Various exploration programs have resulted in the unsuccessful drilling of numerous exploration wells yielding "non-commercial" quantities of oil and gas reserves. In 1999 PanCanadian (now EnCana) and partners drilled the K-39 well (Figure 1.2) at the tip of Shoal Point to test a possible footwall anticline structural high. Following abandonment of K-39 as a dry hole, exploration and participation by oil and gas majors has decreased leaving the area with an unfortunate stigma.

This thesis extends the geophysical study and research of the area using modern marine and land seismic techniques. In the fall of 2000 the Center for Earth Resources Research (Memorial University of Newfoundland), along with local seismic companies Shearwater Geophysical Corp. and GeoScott Exploration received a contract from the Government of Newfoundland and Labrador to design and acquire a non-conventional 3D seismic transition zone survey. Figure 1.2 shows the location of the survey area within Port au Port bay centered directly over a central peninsula known as Shoal Point. This location is of particular interest to both the Government of Newfoundland and Labrador and the petroleum industry as it is situated directly over the 1999 Shoal Point K-39 well.

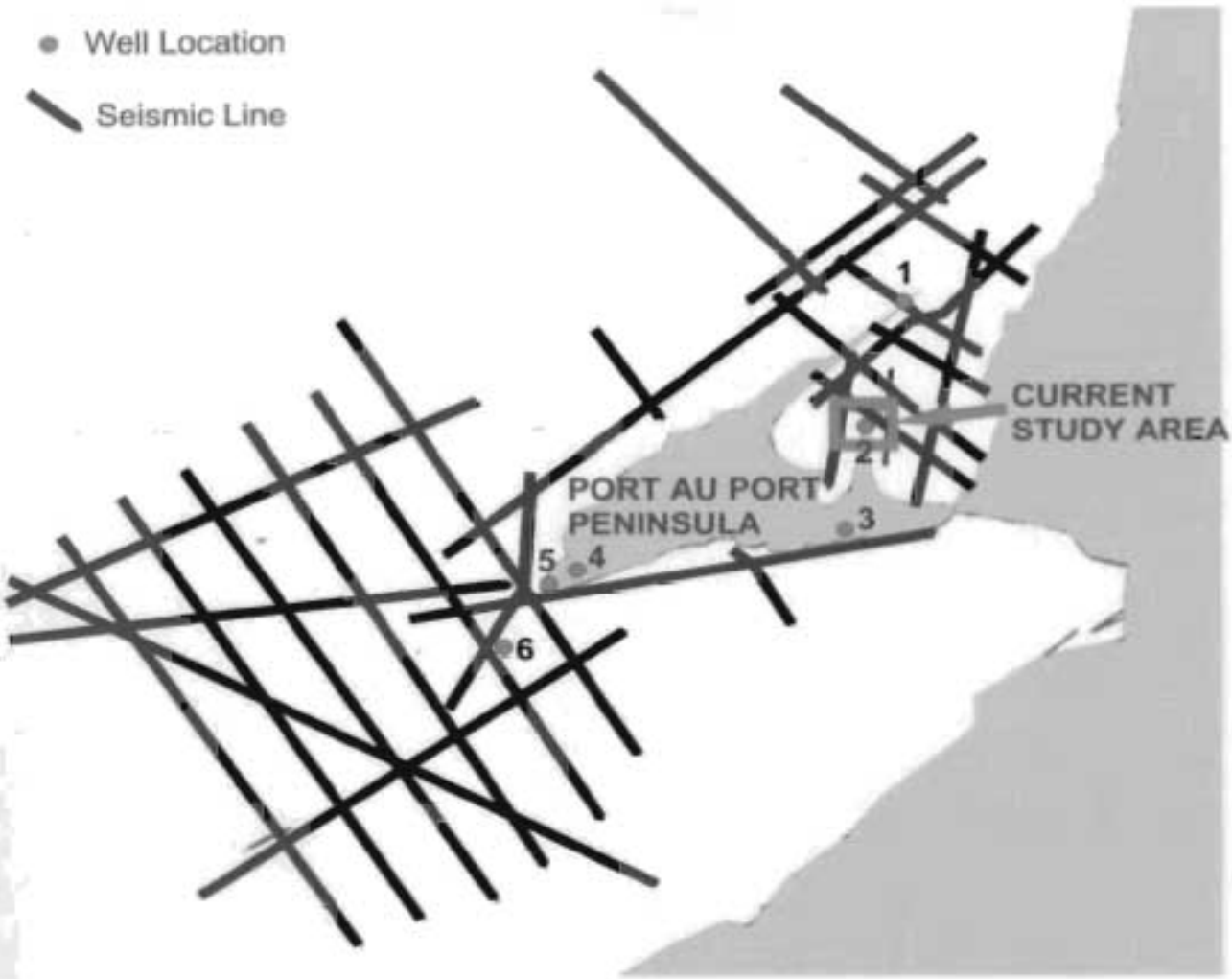

Figure 1.2. Map of the Port au Port peninsula overlain by well locations, marine seismic line locations and the current study area.

Table 1.1: Well location legend

WELL	OPERATOR
1	NHOC / PCP (Long Point M-16)
2	PanCanadian et. al (Shoal Point K-39)
3	Inglewood (Man of war)
4	NHOC / PCP (Port au Port # 1)
5	Talisman et al (Long Range A-09)
6	NHOC / PCP (St. George's)

The goals of the research project are the following:

- To demonstrate a novel and cost-effective technique to acquire, process and interpret 3D data in a shallow water transition zone.
- To provide a seismic image at the Shoal Point K-39 well location.
- Create a 3D mapped surface to the top of the Ordovician carbonate platform.
- To develop a better understanding of the complex geology and tectonic history of the area.

This thesis discusses and describes the techniques and processes undertaken to achieve the above goals. It considers all aspects from survey design and acquisition to complete 2D and 3D seismic data processing. The final result is an interpretation of structure and dominant geological characteristics of Port au Port Bay and specifically the Shoal Point area. Generation of 3D surficial maps to the top of the Ordovician carbonate platform will allow analysis of the PanCanadian well, analysis of the area for other possible hydrocarbon targets and an increased understanding of the local geology and structural expressions.

2.0 Geology

2.1 Introduction

The island of Newfoundland is located in the North Atlantic Ocean along the eastern coast of Canada. Geologically complex, Newfoundland is world renowned for its various expressions of rare geological settings and structures. Divided in to five tectono-stratigraphic zones by Williams (1979) the current study area is located on the Port au Port Peninsula and belongs to the western-most Humber zone (Figure 2.1).

The Humber zone originally developed in the Late Cambrian as a continental shelf off the eastern coast of the Laurentian continent. This early Paleozoic passive margin (Waldron and Stockmal, 1994) is generally characterized by a Cambro-Ordovician carbonate platform overlain regionally by an Early to Middle Ordovician emplaced allochthon and underlain by a Grenvillian crystalline basement (Stockmal et al., 1998). The regional geologic formations of the area have undergone extensive folding and faulting during numerous phases of orogenic deformation related to the opening and closing of the Iapetus ocean.

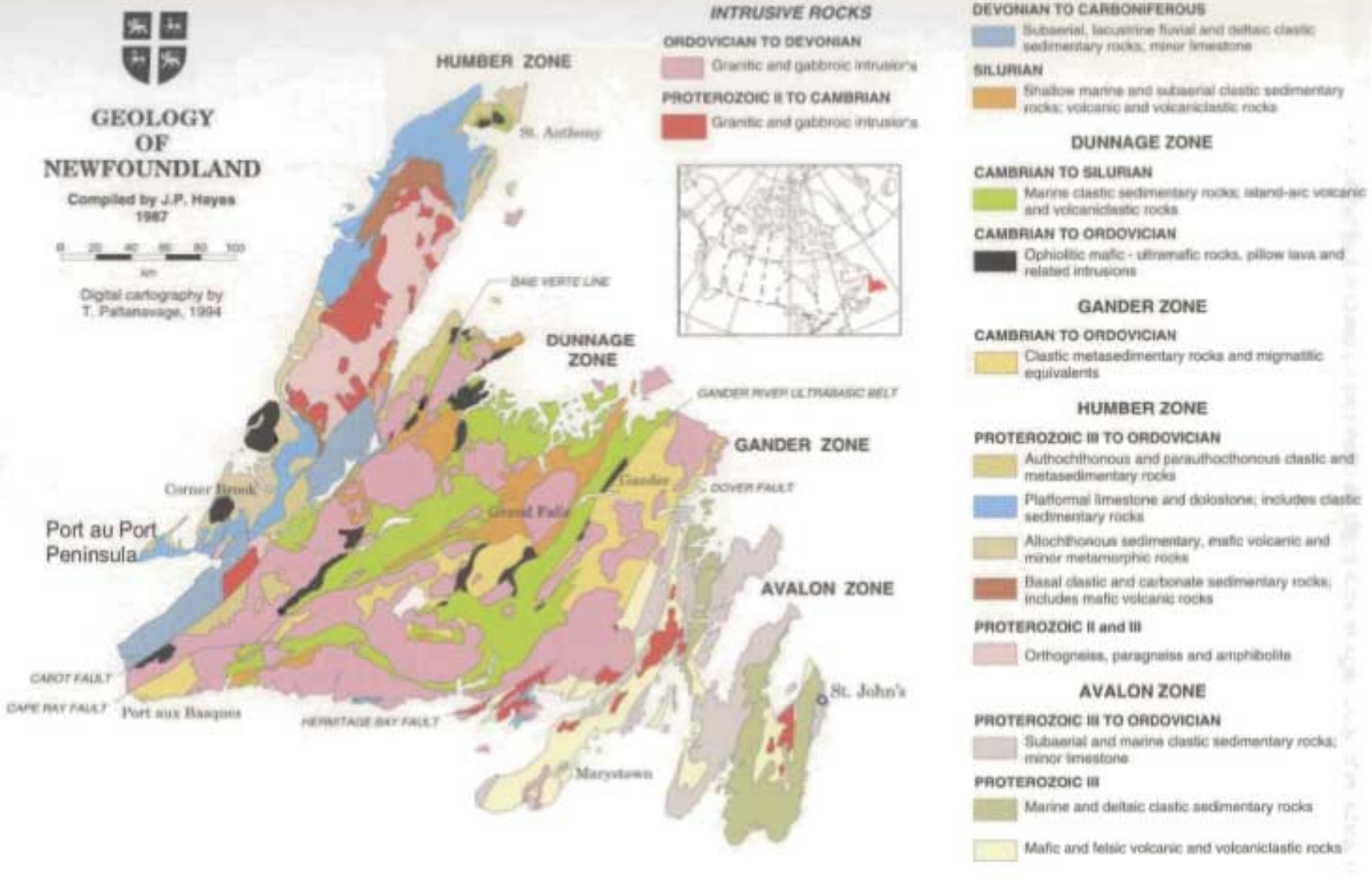

Figure 2.1. Geological map of Newfoundland (Government of NL, Department of Mines and Energy).

Due to the substantial increase in seismic data coverage over the area in the past 10 years there have been numerous revisions of the initial hypothesis and geologic models constructed during the 1970's, 1980's and even up to the early 1990's. The following geologic overview is drawn predominantly from the more recent literature (Cooper et al., 1998, Stockmal et al., 1998, Waldron et al., 1994).

2.2 Regional Stratigraphy and Geologic Evolution

The geologic formations of the Humber zone and particularly the Port au Port Peninsula are composed of complex folded and faulted Lower Paleozoic sediments. It is generally accepted that the deformation and structural relationships of the Port au Port stratigraphy result directly from three primary phases of deformation: The Mid to Late Ordovician Taconic Orogeny, the Silurian Salinic Orogeny and the Devonian Acadian Orogeny.

Cooper et al., (1998) divide the Paleozoic stratigraphy into the following six distinct tectono-stratigraphic megasequences that directly effect sedimentation and basin development of the Humber Zone.

1. Late Proterozoic-Early Cambrian siliclastic synrift sediments deposited during the formation of the Iapetus Ocean: This sequence is composed of the Bradore Formation of the Labrador Group and is

believed to have its upper boundary at the base of the Forteau Formation (Figure 2.2).

2. Early Cambrian-Early Ordovician passive margin strata containing shallow water carbonates that pass eastward into deeper marine shales: This gradation to deeper water sediments is directly related to thermal subsidence of the shelf post active rifting of the margin. This sequence begins with the Forteau Formation of the Labrador Group and continues upwards into the carbonates of the Port au Port Group and the Early Ordovician St. George's Group (Figure 2.2).

3. The Early Ordovician-Middle Ordovician sequence beginning at the St. Georges Unconformity: A depositional hiatus of 3-4 m.a., it is believed that the unconformity is a direct result of extensional faulting due to westward migration of the flexural forebulge of the Taconic foreland basin. This sequence is composed of the Table Head Group containing predominantly shallow to deep subtidal limestones, and the Goose Tickle Group that is dominantly a muddy Taconic flysch including the Mainland Sandstones (Stenzel et al., 1990) (Figure 2.2).

4. This Taconic Foreland Basin Megasequence spans approximately Middle Ordovician-Early Silurian and is defined at its lower boundary by the Taconic Unconformity. This sequence is characterized by the

emplacement of the Taconic allochthon via overthrusting of basinal sediments. The Taconic allochthon is then overlain and onlapped by shallow marine siliclastic sediments of the Long Point Group (Figure 2.2).

5. The Late Silurian Salinic Orogeny provided continued imbrication and additional westward displacement of the Taconic allochthon along with erosion of the hinterland Salinic foreland and deformation of the eastern Cambro-Ordovician platform. Bounded at its base by a substantial 20 m.a. unconformity, the sequence contains fluvial sands and shales of the Clam Bank and Red Island Road Formations (Figure 2.2).

6. The youngest preserved sediments in the area, this sequence is represented by the Carboniferous strata of the Codroy, Angille and Barachois Groups. The sediments display transtensional dextral reactivation of preexisting extensional faults (i.e.: Round Head Thrust) following the compressional deformation of the Late Devonian Acadian Orogeny. These groups vary between fluvial sandstones, silts, shales and local lacustrine source rocks with marine evaporites.

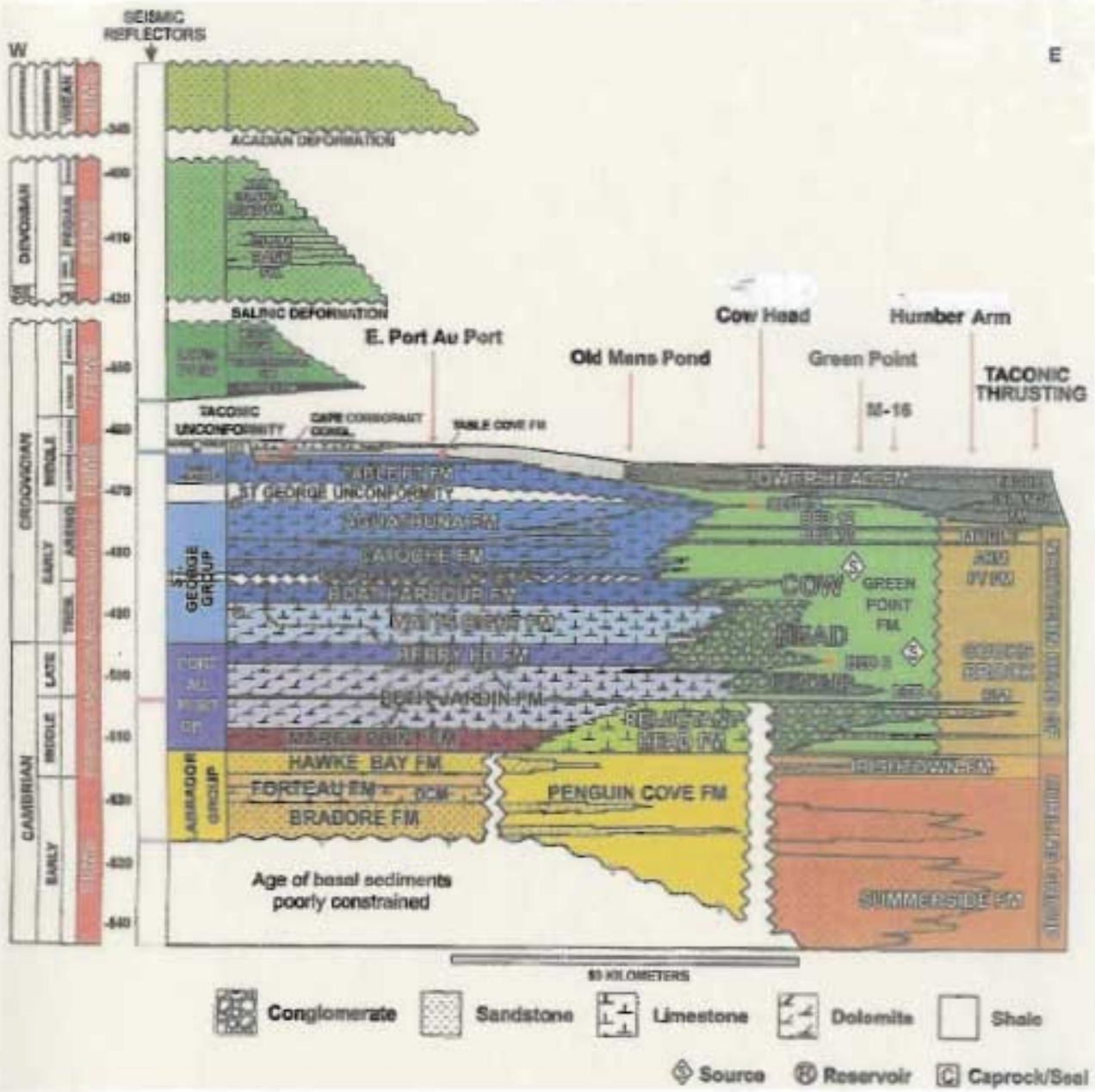

Figure 2.2. Chronostratigraphic summary of western Newfoundland Paleozoic strata. Lithostratigraphic units are colored and ornamentation indicates rock type (From Cooper et al., 1998).

2.3 Seismic Expression of Key Structural Features

2.3.1 Triangle Zone

A regional expression created late in the Acadian Orogeny, the triangle zone was originally recognized as a thrust front by Cawood and Williams (1988) and later further constrained by Stockmal and Waldron (1990) as a triangle zone. The triangle zone geometry is defined by an upper detachment thrust (Waldron and Stockmal, 1991) (Figures 2.3a, 2.3b), bounded at its base by a lower detachment surface located at the base of the allochthonous sediment package.

The triangle zone involves Taconic allochthon basinal sediment thrust slices being forced between the Goose Tickle shales and the Lourdes Limestone of the Long Point Group. The compressional force and westward motion of the allochthon has caused the peeling back and westward dip of the Carboniferous strata (Figures 2.3a, 2.3b). This compression has created the roof thrust upper detachment edge of the triangle zone at the base of the Lourdes Limestone. The subsequent basal detachment surface for the frontal tip of the Humber Arm allochthon in my opinion corresponds to the top of the carbonate platform sequence. Figure 2.3b clearly demonstrates an allochthonous wedge of thrust slices riding over a continuous package of seismic reflectors corresponding to the autochthonous carbonate platform. Waldron and Stockmal (1994) have interpreted considerable displacement of the Taconian allochthon westward from

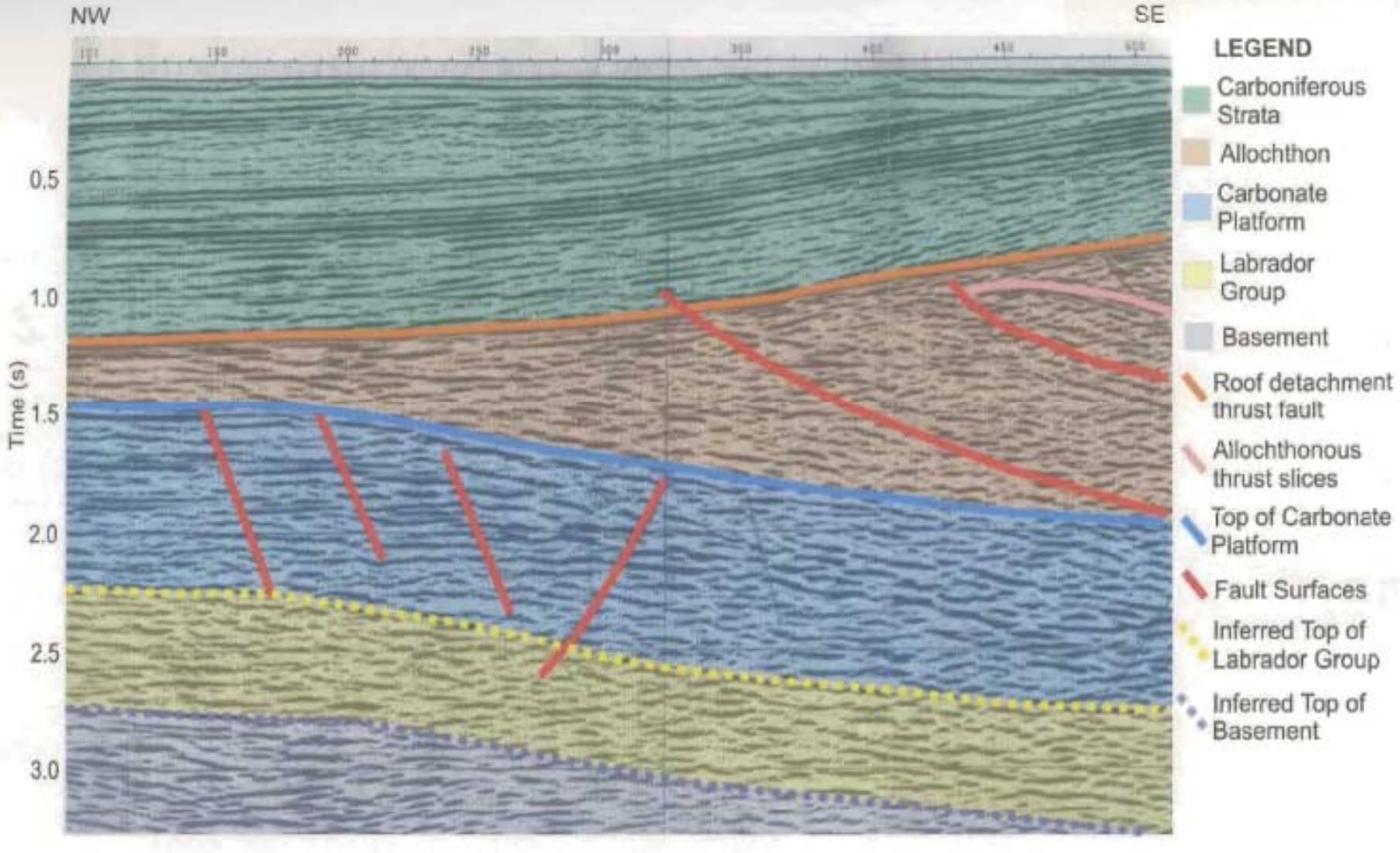

Figure 2.3a. Seismic line 91-1560, a typical expression of the frontal tip of the Triangle zone annotated for stratigraphy and characteristic structural expressions (see figure 2.6 for location).

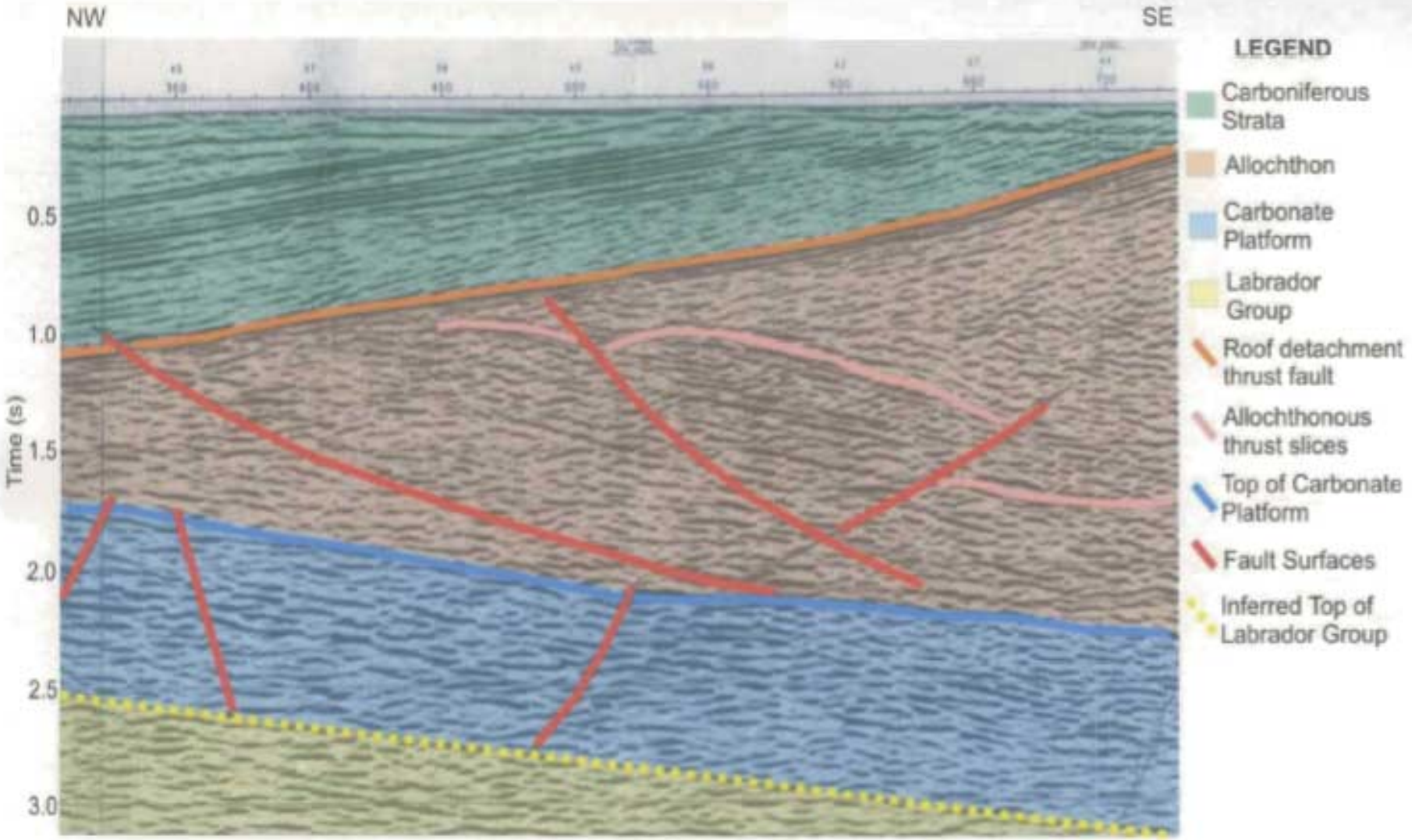

Figure 2.3b. Seismic line 91-1561, a typical seismic expression of the Triangle zone. In comparison to 5.3a the above figure gives a wider picture of the Taconic allochthon and its internal structure of thrust sheets (see figure 2.6 for location).

its original location during the Acadian Orogeny as an accommodation for the triangle zone wedging.

2.3.2 Round Head Fault

Originally interpreted by many as the Round Head thrust, this feature is the dominant structural expression of the Port au Port peninsula. It is present on land at the western edge of Port au Port as a large thrust fault that offsets the carbonate platform in some locations in excess of 3 kilometers of vertical offset (Figure 2.4). Orientation of the fault is less clear as it tracks off of the coast into Shoal Bay where prior to the late 1990's little seismic coverage existed.

Stockmal and Waldron (1991) surmised that the Round Head thrust was actually a reactivated and inverted extensional normal fault that was formed initially during the Taconian extension. It is generally accepted that compressional forces brought on during the Acadian Orogeny inverted motion on this pre-existing fault plane, thereby accommodating the present day expression previously discussed for the Port au Port Peninsula.

Analysis of recent seismic data has allowed for a modified version of previous interpretations of the Round Head thrust and its expression and orientation within Shoal Bay. Cooper et al. (1998) used proprietary Hunt / PanCanadian seismic data from within the Bay to achieve what I believe is the most accurate

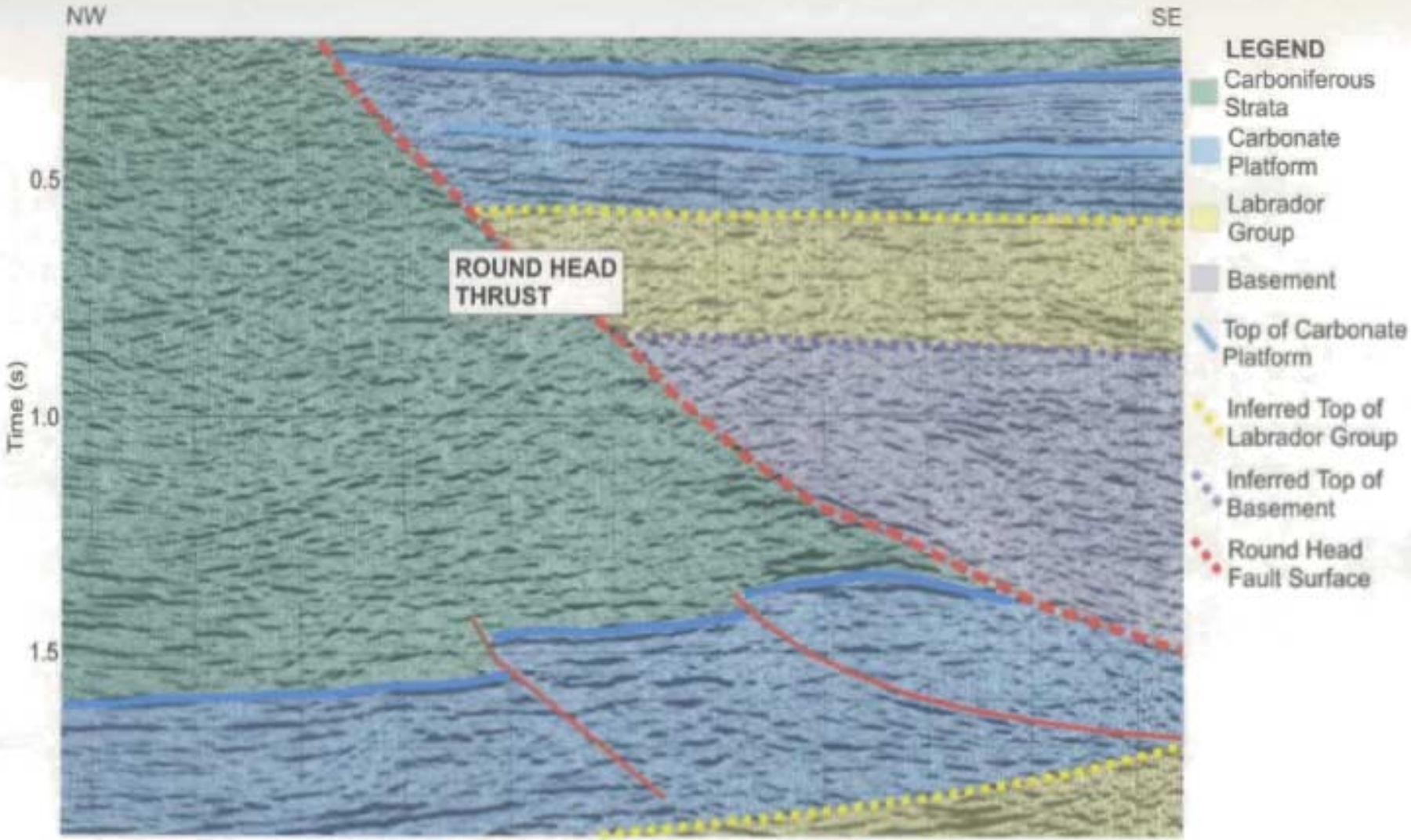

Figure 2.4. Seismic line CAH 93-5, a NW-SE onshore transect (see figure 2.6 for location) displaying the extensive offset as the entire geological sequence including basement has been thrust on top of the carbonate platform.

interpretation to date. They re-interpret the Round Head thrust as the Round Head fault, which remains in net extension within the Bay increasing in lateral offset as the fault tracks northward.

Cooper et al. (1998) states that the thrust visible on land (Figure 2.4) tapers to a zero offset null point somewhere within the Shoal Bay west of the tip of Shoal Point. The fault continues east and curves northward to the top of the Bay constantly in net extension.

Figure 2.5 is a sample of one of the now public Hunt / PanCanadian lines used by Cooper et al. (1998) for the re-interpretation. The southeastern portion of the seismic line images the carbonate platform reflectors offset in extension to the southeast in comparison to the northwest end of the line. In the area of the Round Head fault the platform is not as cleanly offset as the thrust motion exhibited on the peninsula in figure 2.4. Figure 2.5 (OBC line 300) is interpreted with hanging wall and footwall cutoffs whose faults sole out into the same detachment surface. This structure is consistent on all of the seismic lines within the bay and will be mapped in greater detail in Chapter 6 (Interpretation).

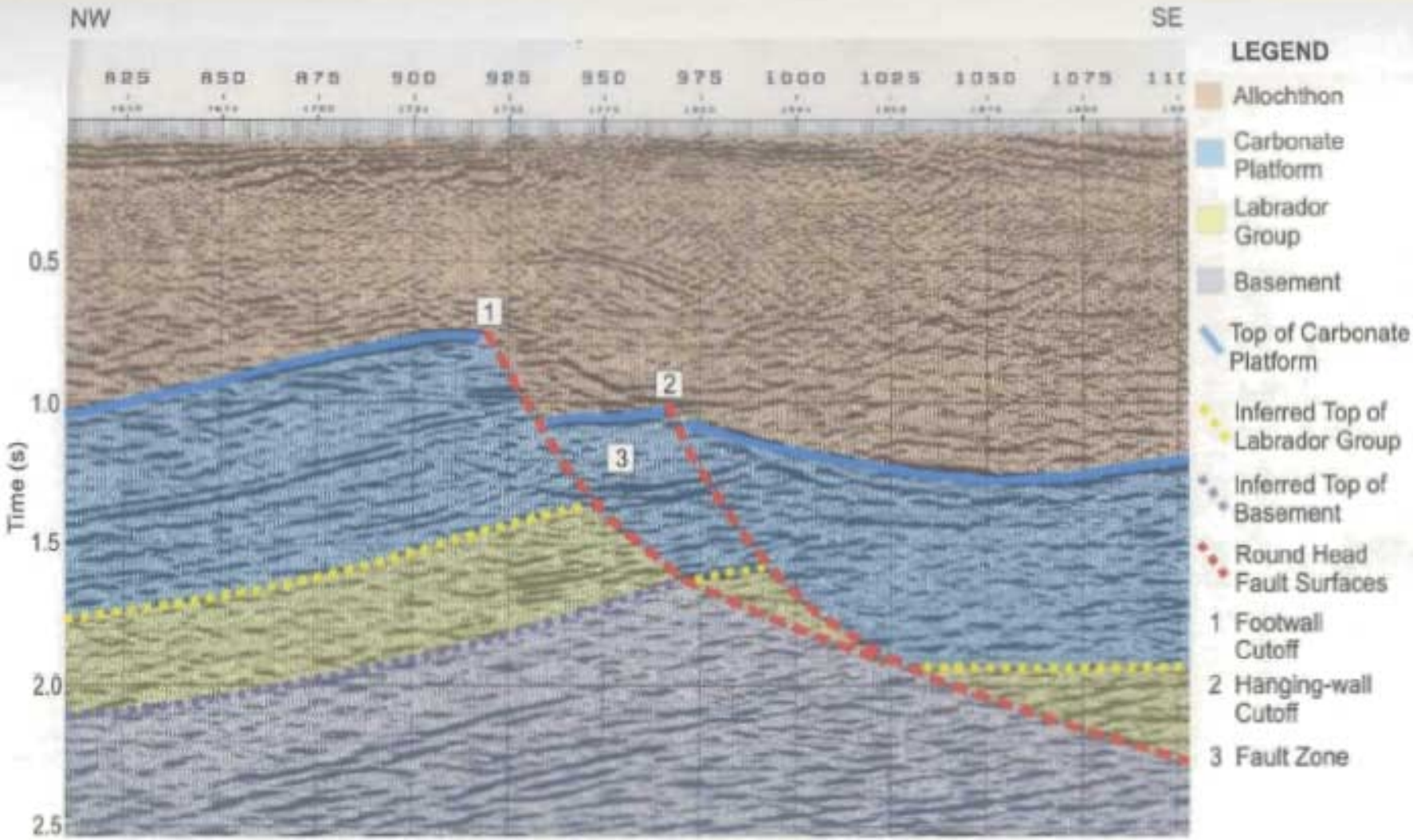

Figure 2.5. Hunt OBC line 300 (see figure 2.6 for location). Line 300 displays the extensional expression of the Round Head Fault within Shoal Bay discussed by Cooper et al. (1998).

2.4 Seismic Exploration Data

The seismic exploration data volume for the West Coast of Newfoundland and Port au Port area has increased significantly over the past 15 years. Interest by majors such as Hunt, PanCanadian and Mobil during the mid to late 1990's has generated a seismic data volume that has allowed a more detailed and better controlled interpretation of the region.

2.4.1 Seismic Program 8924-H028-004E (Shoal Bay)

During the summer of 1996 Hunt and partners acquired a 7-line exploration seismic program directly within Port au Port Bay (Figure 2.6). The seismic survey was acquired by Western Geophysical using ocean bottom cables (OBC) and was designed to further understand the expression of the Round Head thrust within the bay. It appears that Hunt was seeking similar footwall anticline traps within the top of the carbonate platform such as that drilled in 1994 as Port au Port #1 (Figure 2.7).

This Hunt survey generated new direct evidence of the Round Head thrust expression and orientation within Shoal Bay, such evidence allowed for the above interpretation by Cooper et al. (1998) as net extension of the Round Head thrust and therefore renaming of the structure as the Round Head fault (Figure 2.5).

Figure 2.6. Seismic line locataions acquired by Hunt and partners in 1996 for the Shoal Bay exploration program.

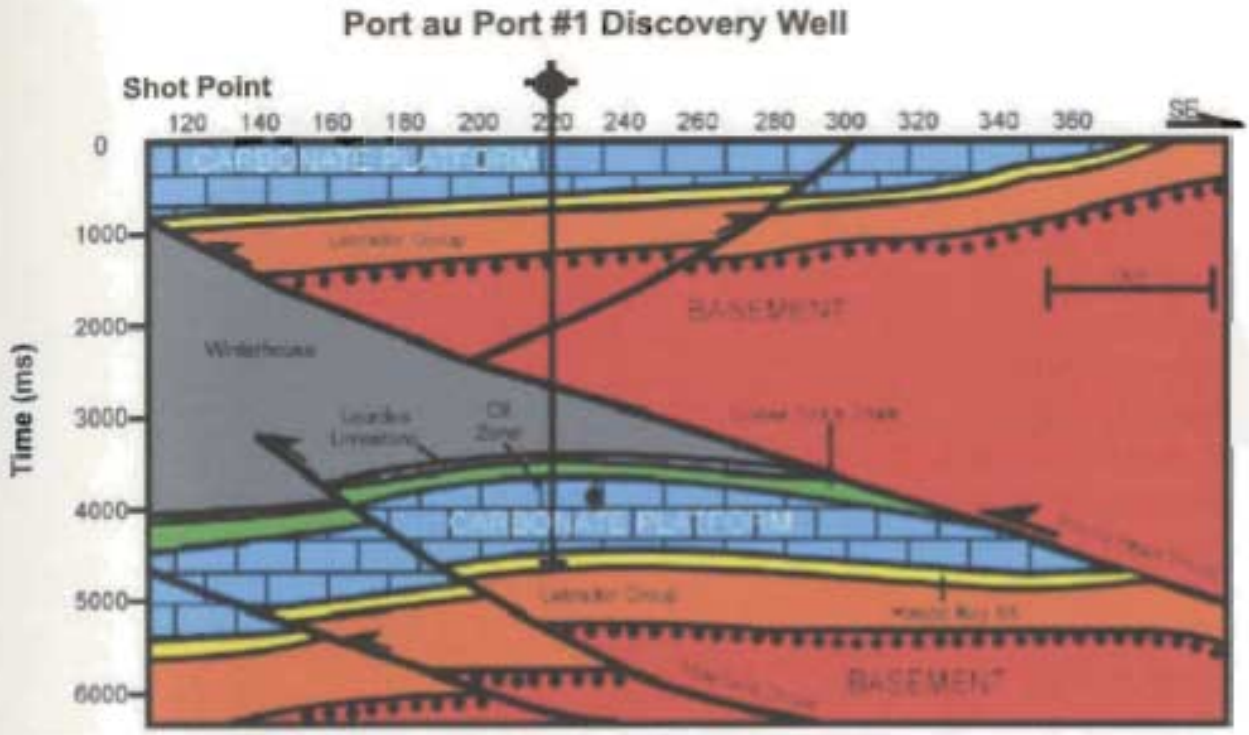

Figure 2.7. Cartoon of Hunt/PanCanadian Port au Port #1 discovery well. Interpretation is based on line CAH 93-5, figure 2.4 (Government of NL, Department on Mines and Energy, 2003).

Public release of the Hunt data in 2002 was instrumental during the interpretation phase of this current study. Three of the Hunt lines are located directly on the north, west and east sides of the current 3D volume (Figure 2.6). The high quality of the Hunt seismic lines adds excellent control to the interpretation as interpolations are necessary across poor data quality areas between the current 2D / 3D seismic data and the 1996 2D Hunt data. Chapter 6 (Interpretation) will include a more detailed look at all of the Hunt seismic lines and the current data;

how the datasets interrelate and how the Hunt data provides control on the interpretation in poor data quality areas.

2.5 Exploration Drilling Data

The number of exploration wells that have been drilled in and around the Port au Port area is limited in comparison to a similar geographic area of Western Canada (i.e. Alberta) but has continued to grow throughout the 1990's. Currently the Newfoundland and Labrador Department of Mines and Energy registers the total number of wells drilled in the Humber zone including sidetracks at 18 (Figure 2.8). Directly on the Port au Port Peninsula and adjacent in near shore waters the Government lists the total number of exploration wells at 8 (Figure 2.9).

2.5.1 Shoal Point K-39

The Shoal Point K-39 well drilled in 1999 is located at the center of the current study area (Figure 2.9). It appears that the K-39 well location was selected using the previously discussed seismic of the 1996 8924-H028-004E Hunt et al. seismic program. The desired target for drilling was expressed by the partners as a closed carbonate platform structural high on the footwall of the Round Head fault just NNW of the tip of Shoal Point.

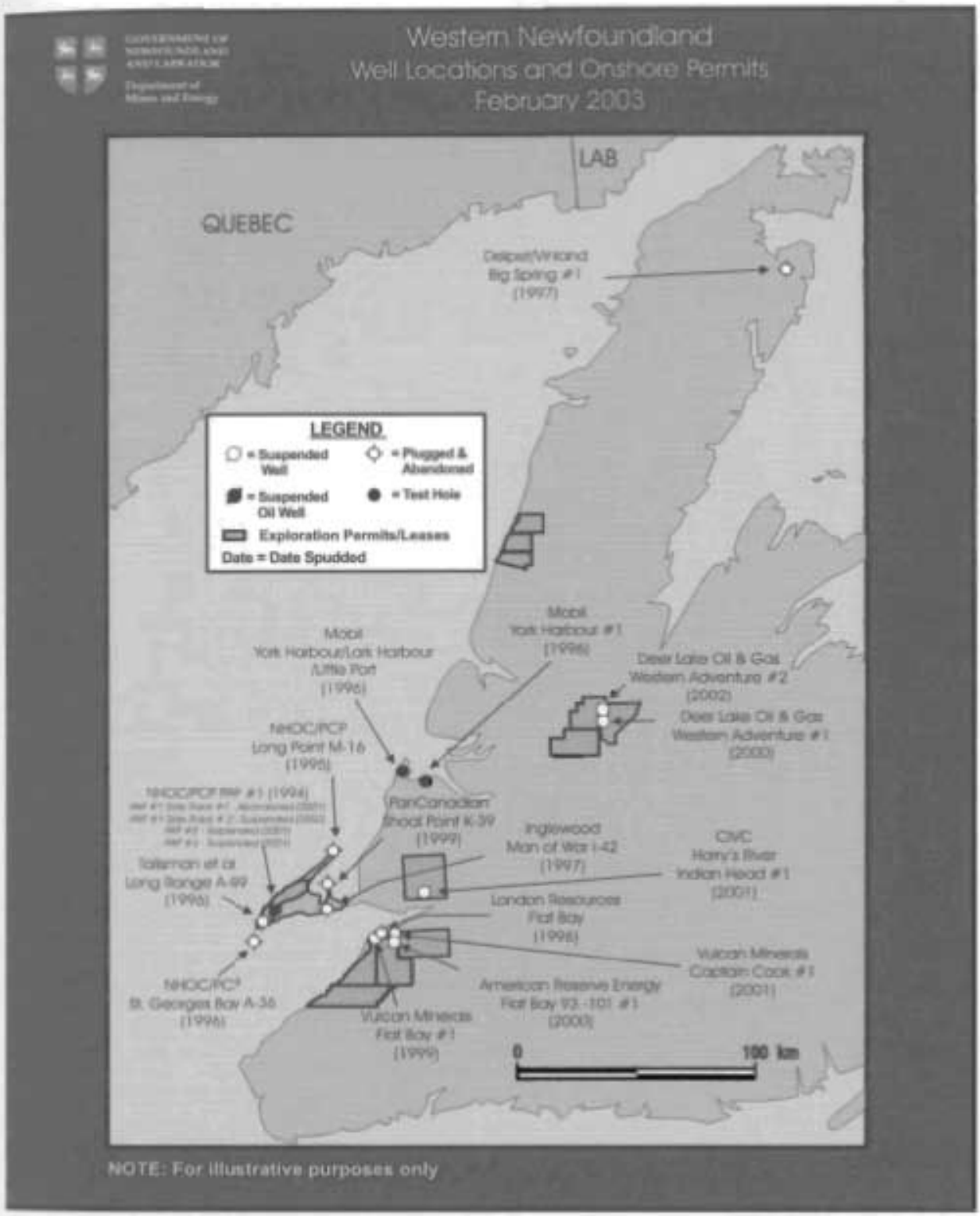

Figure 2.8. **Location of exploration oil and gas wells for Western Newfoundland as of February 2003 (Government of NL, Department of Mines and Energy).**

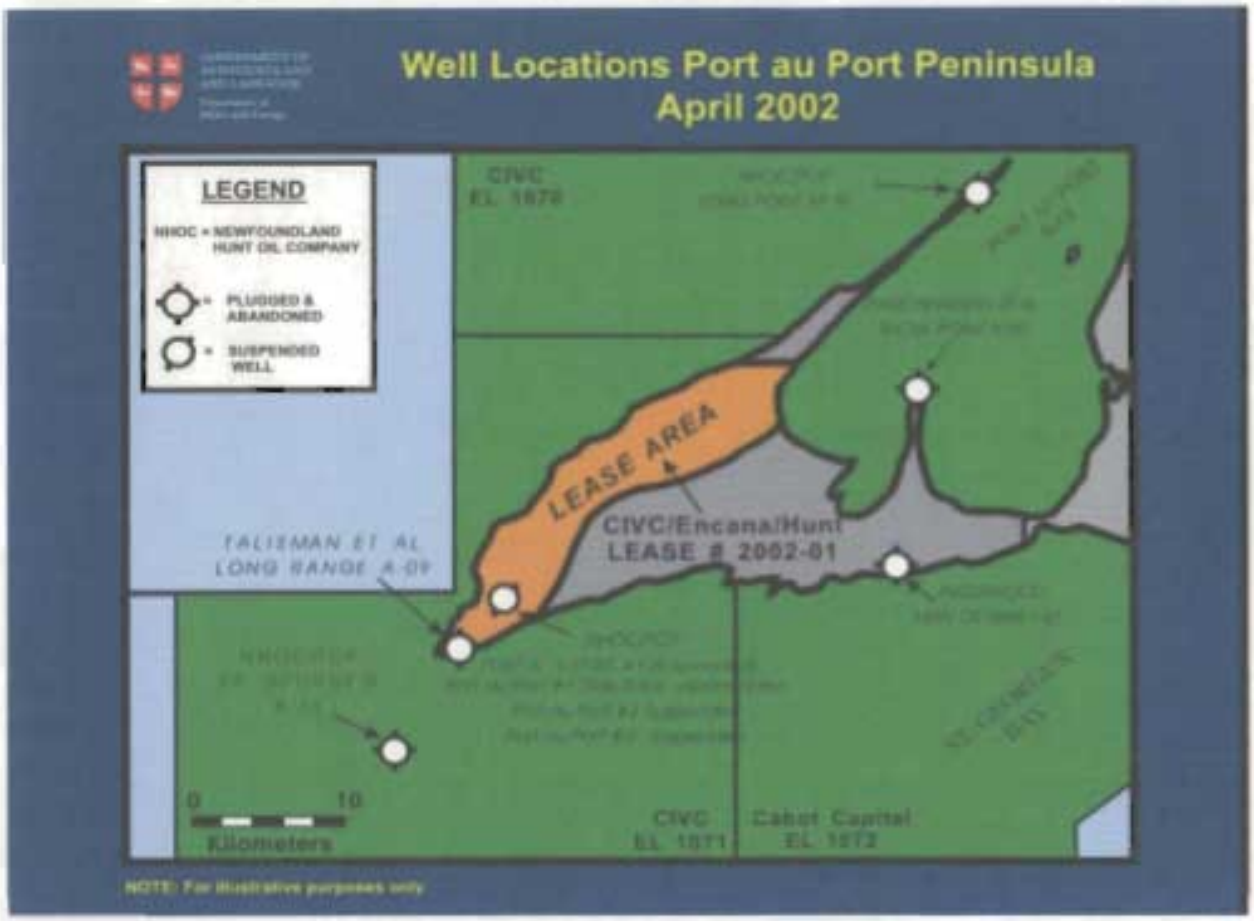

Figure 2.9. Location of exploration oil and gas wells on the Port au Port peninsula as of April 2002 (Government of NL, Department of Mines and Energy).

2.5.1.1 Drill Results

As previously stated the K-39 well was plugged and abandoned as a water wet dry hole. The following table is a Hunt / PanCanadian geological summary of the well representing a condensed synopsis of the geological strip log. The Round Head fault intersection is annotated in yellow and corresponds to a TVD of

1899m, this fault is extremely important because to correctly test the top of the footwall carbonate platform the well should have exited the fault into a geological formation above the Table Head Group (Figure 2.2).

Table 2.1. Complete list of geological tops for Shoal Point K-39 (From released drilling operations report).

FORMATION	LOG TOPS (m)	TVD (m)	THICKNESS (m)
KB		10.56	0
Humber Arm Allochthon Shales	Surface	Surface	1031.5
Humber Arm Allochthon Carbonates	1031.5	943	1175.5
Round Head Fault	2207	1899	
Catoche	2207	1899	134
Fault 1	2251	1940	
Fault 2	2296	1980	
Boat Harbour 1	2341	2021	292.5
Boat Harbour Discon. 1	2369	2047	
Fault 3	2452	2122	
Boat Harbour 2	2461	2131	
Boat Harbour Discon 2	2490	2158	
Fault 4	2535	2200	
Fault 5	2570	2234	
Petit Jardin			
- Felix Mem.	2636.5	2298	45.5
- Big Cove Member	2682	2343	39
- Campbells Member	2721	2381	190
March Point	2911	2571	22
Hawke Bay	2933	2933	102
FTD	3035		

The following figures are VSP and the sonic log displays from the K-39 well. Both figures are annotated for key faults and stratigraphy in TWT, TVD and measured depth. These results allow correlation between the actual cuttings of the strip log to a measured quantitative geophysical technique. Consideration of all three information volumes therefore enables the accurate selection of the Round Head fault location along with important geological tops.

The overall importance of this well information is that during the final interpretation of the current seismic data volume there can be a comparison of interpreted fault locations and horizon tops with known results from the K-39 well. This comparability will allow a better understanding of the overall validity of the current studies seismic data.

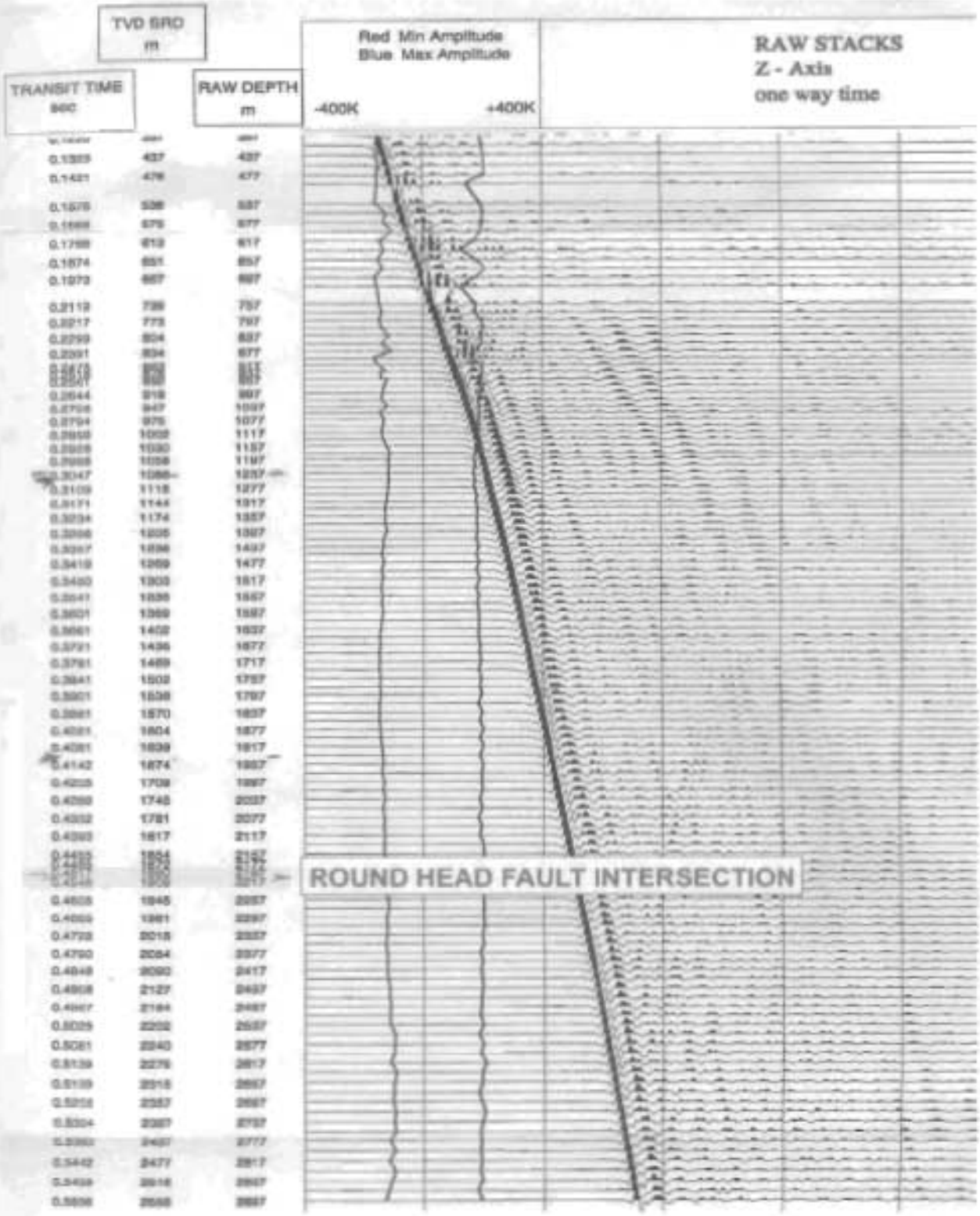

Figure 2.10. K-39 VSP results showing corresponding values for one-way transit time, true vertical depth (TVD) and raw depth (modified from PanCanadian VSP). Round Head fault location is inferred from geological strip log information.

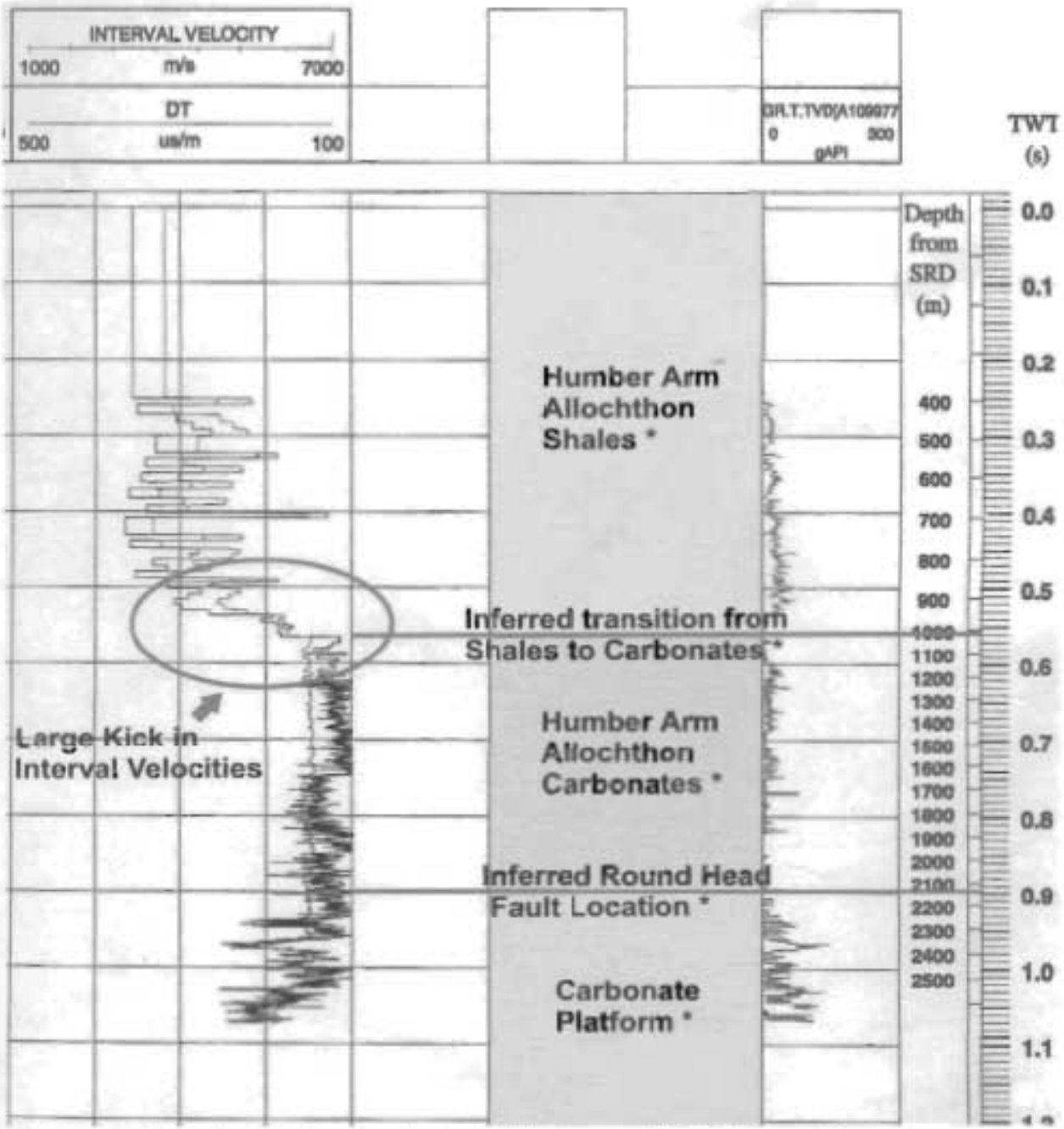

* Interpretation based on geological strip log and VSP information.

Figure 2.11. K-39 sonic log and measured interval velocities overlain with geological information extracted from the strip log and VSP.

2.6 Geological Summary

Dominated by complex structures and discontinuous heavily faulted stratigraphy, the Shoal Point area will require consideration of all available seismic and well data from the area. The interpretation section of the thesis will focus in from the six distinct tectono-stratigraphic megasequences of Paleozoic stratigraphy previously defined by Cooper et al. and discuss the basin stratigraphy by subdivision of the basin geology into four dominant geological and stratigraphic units, which are as follows:

1. Taconic Allochthon sequence (Carbonates and basinal shales from the Ordovician platform sequence).
2. Ordovician Carbonate platform sequence (Port au Port Group, St. George Group, Table Head Group, Goose Tickle Group).
3. Pre-Ordovician Labrador Group (Primarily clastics of the Hawke Bay, Forteau and Bradore Formations).
4. Grenvillian Basement.

3.0 Data Acquisition

3.1 Acquisition Overview

The completion of the Shoal Point survey with the achievement of the previously stated goals while adhering to a strict budget, timetable and environmental commitment proved demanding and included numerous logistical and technical obstacles.

Logistically the survey was complex due to the liaison between marine and land seismic crew and equipment. The acquisition included aspects of land geophones, marsh geophones, land dynamite sources, marine air gun sources, a large crew, land vehicles and several vessels, including Memorial's research vessel the M.V. Lauzier. Technical obstacles included the use of a conventional streamer as an ocean bottom cable (OBC), obtaining adequate fold coverage and offset distribution, and sensitivity to the area's active shellfish and groundfish industry.

3.2 Seismic Survey Design

Design of the Shoal Point seismic survey focused around obtaining the highest quality data given the logistical and technical challenges of the area. Three key initial issues constraining the design of the survey were:

- Shallow water depth of Port au Port bay.
- Maintaining high data fold coverage.
- Obtaining near offset seismic data.

Due to the extremely shallow water depths in the bay around Shoal Point it is impossible to obtain conventional marine seismic within 1000m of land and the primary area of interest just north of the tip of Shoal Point. Because of this it was decided that optimal fold coverage and offset distribution would be achieved using three different configurations of seismic data acquisition.

1. A conventional 2D seismic landline running N-S on Shoal Point.
2. A series of 11 marine source-only lines firing into the land receivers.
3. Three conventional 2D marine seismic lines running along the perimeter of the survey area where water depth was sufficient.

3.2.1 Land Seismic

The receiver spread for step 1 was designed to contain 111 land geophones and 37 transitional marsh hydrophones at 25m intervals (Figure 3.1). MUN's high-resolution solid marine streamer was also considered for use in the receiver spread as an OBC. The marsh hydrophones combined with the OBC were key to improving the distribution of near trace offsets and data coverage at the tip of the point in the primary zone of interest. The streamer would add an additional 120 channels at 12.5m to the receiver spread. The seismic source for land acquisition was a single 2kg dynamite charge set at a 5m depth at 50m intervals.

3.2.2 Marine shot lines

A series of marine shot lines with 25m shot intervals was designed to be fired into the same receiver spread used for the land acquisition (Figure 3.1). Line layout was positioned such that the survey would achieve maximum fold and source-receiver offset distribution. The seismic source for the marine shots involved an air gun array of 320 in^3 (5.24 *L*) as 8 X 40 in^3 (0.66 *L*) cubic inch air guns timed to fire simultaneously.

In figure 3.2, the 3D survey is designed for the marine shots into the land receiver spread. Note the gap in fold coverage at the south central section of the fold

display, this area corresponds to the location of Shoal Point and is a seismic dead zone.

3.2.3 Conventional marine lines

Three 2D marine seismic lines were strategically placed on the north, east and west sides of the point. Acquisition of the 2D marine lines was planned to help constrain data and velocity information from within the 3D area and to provide near-offset data for the 3D bins that otherwise would have few or no CDP traces.

Consideration of all three aspects for maximum data coverage and best possible geological information led to the final pre-acquisition survey design (Figure 3.3). This shows a rough location of the seismic sources and receivers with respect to the bay and surface bathymetry / topography.

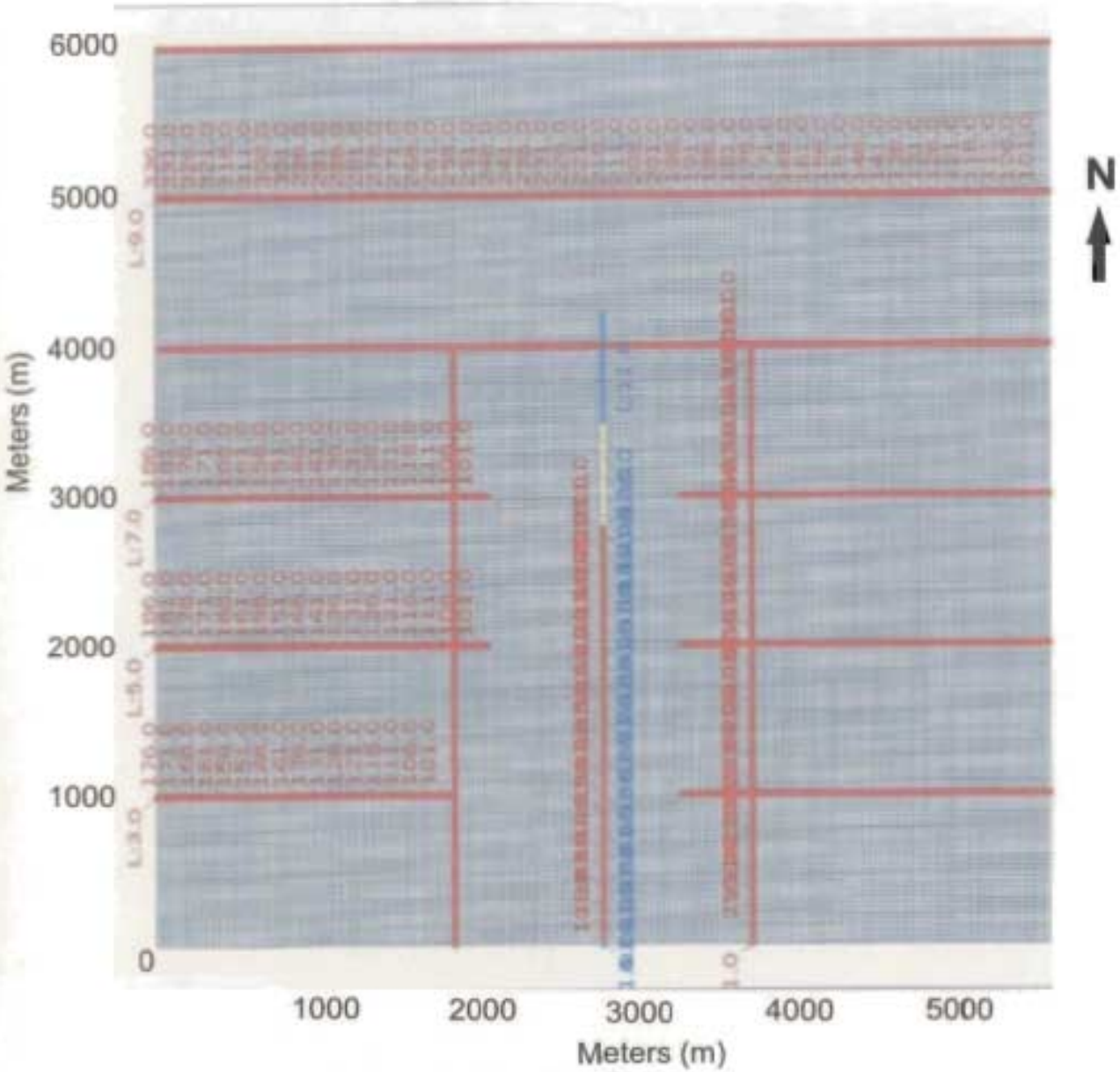

Figure 3.1. The initial acquisition model showing binning (25m X 25m), the marine shot lines (red), the land receivers (center-line red), the transitional marsh receivers (white) and the OBC cable (blue).

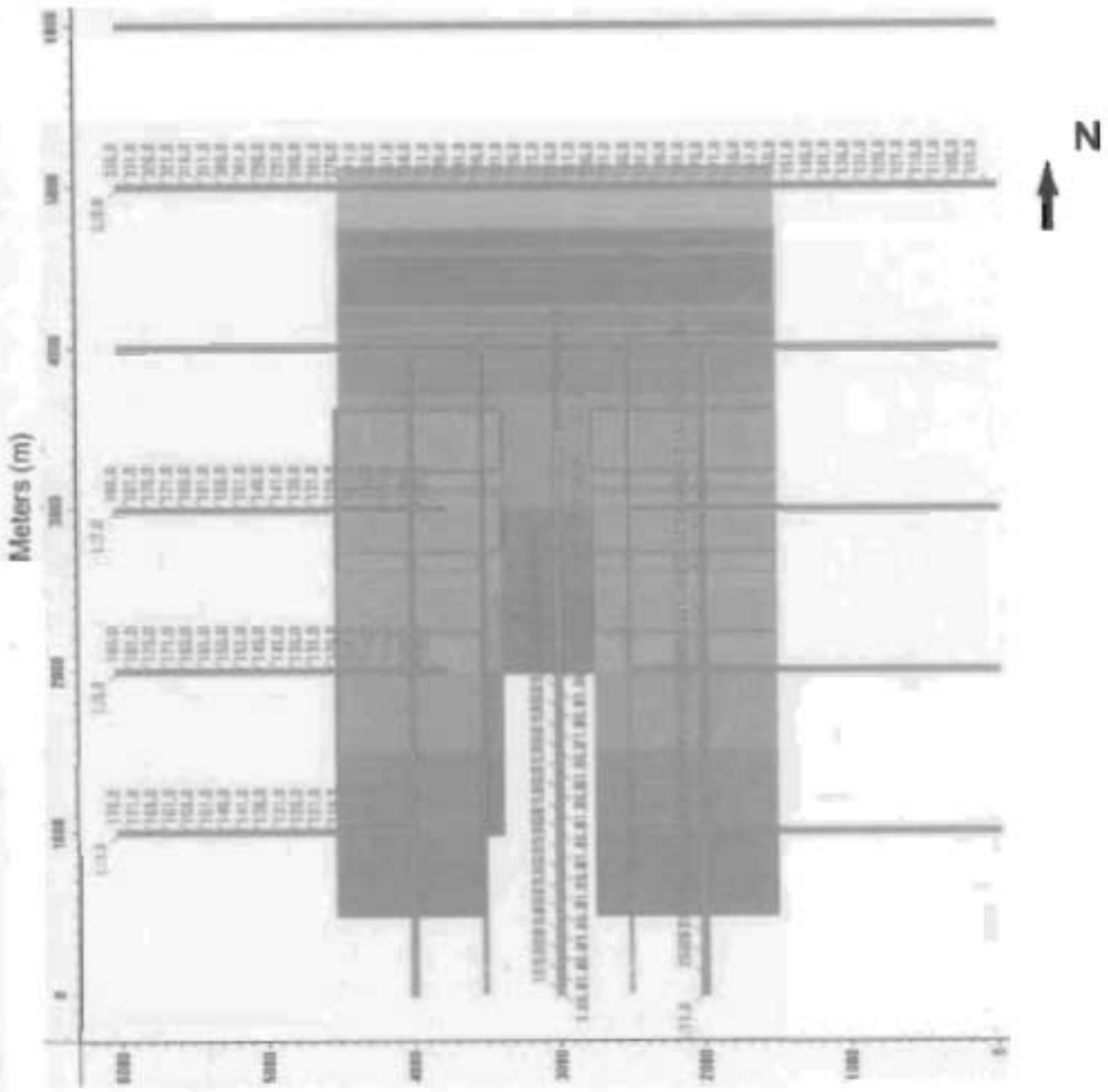

Figure 3.2. Design fold model for marine shot lines into the land receiver spread. (Maximum fold of 50 = orange, light blue = 25, deep blue = 5).

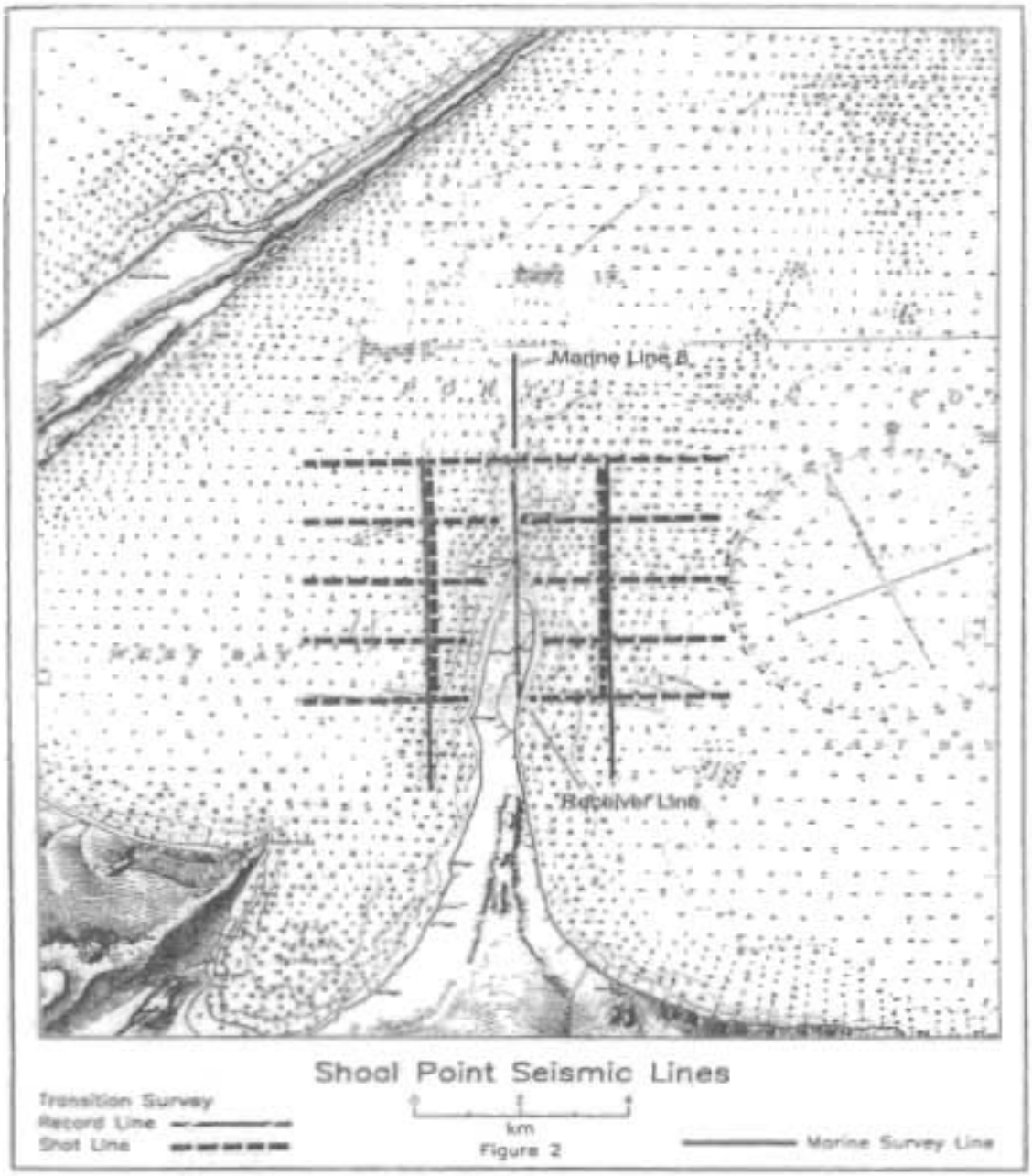

Figure 3.3. Initial survey model outlining positioning of the seismic survey around the existing topography.

3.3 Seismic Acquisition

Geographically the Shoal Point acquisition was within Universal Transverse Mercator map projection (U.T.M) zone 21, with all source / receiver coordinates referenced to the North American Datum 83 (NAD 83). The 3D binning grid that was designed to cover the acquisition footprint is as follows:

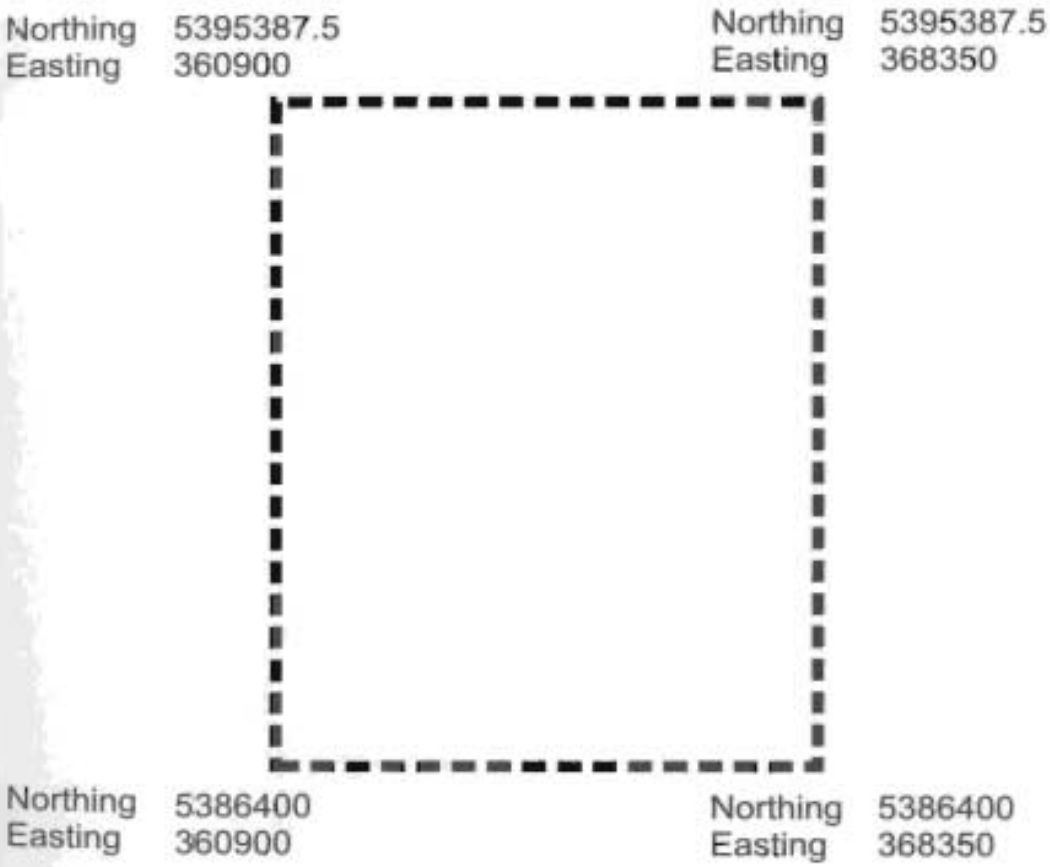

Figure 3.4. UTM locations corresponding to corner locations of the 3D bin grid.

Seismic acquisition was planned for early fall (weather and fisheries concerns) but began on November 30th 2000 with a budgetary timetable allowing for a

maximum of 2 weeks of acquisition. Upon arrival the acquisition plan was to adhere to the above design parameters and begin with collection of the 2D seismic landline. Due to extremely poor weather, it was not possible to deploy the marine streamer as an OBC. Therefore this part of the acquisition was deleted from the project plan. Emplacement of the marsh geophones also proved difficult as problems were encountered with anchoring them to the sea floor because of a strong rip tide at the tip of Shoal Point. High seas combined with strong currents led to all 37 of the marsh phones being extremely noisy when they were in place.

3.3.1 Land Acquisition

The Shoal Point 2D line PP-01 was acquired as a conventional crooked seismic landline (Figure 3.5). Data were recorded in SEG-Y format using an ARAM-24 system. Acquisition source and receiver parameters in Table 1 are consistent with the desired parameters modeled during the design stage. The line geometry seen in figure 3.5 is a result of the geophones being positioned along the shoulder of an existing roadway. This configuration was deemed adequate and a straight N-S line was not used primarily due to timing, environmental and cost constraints.

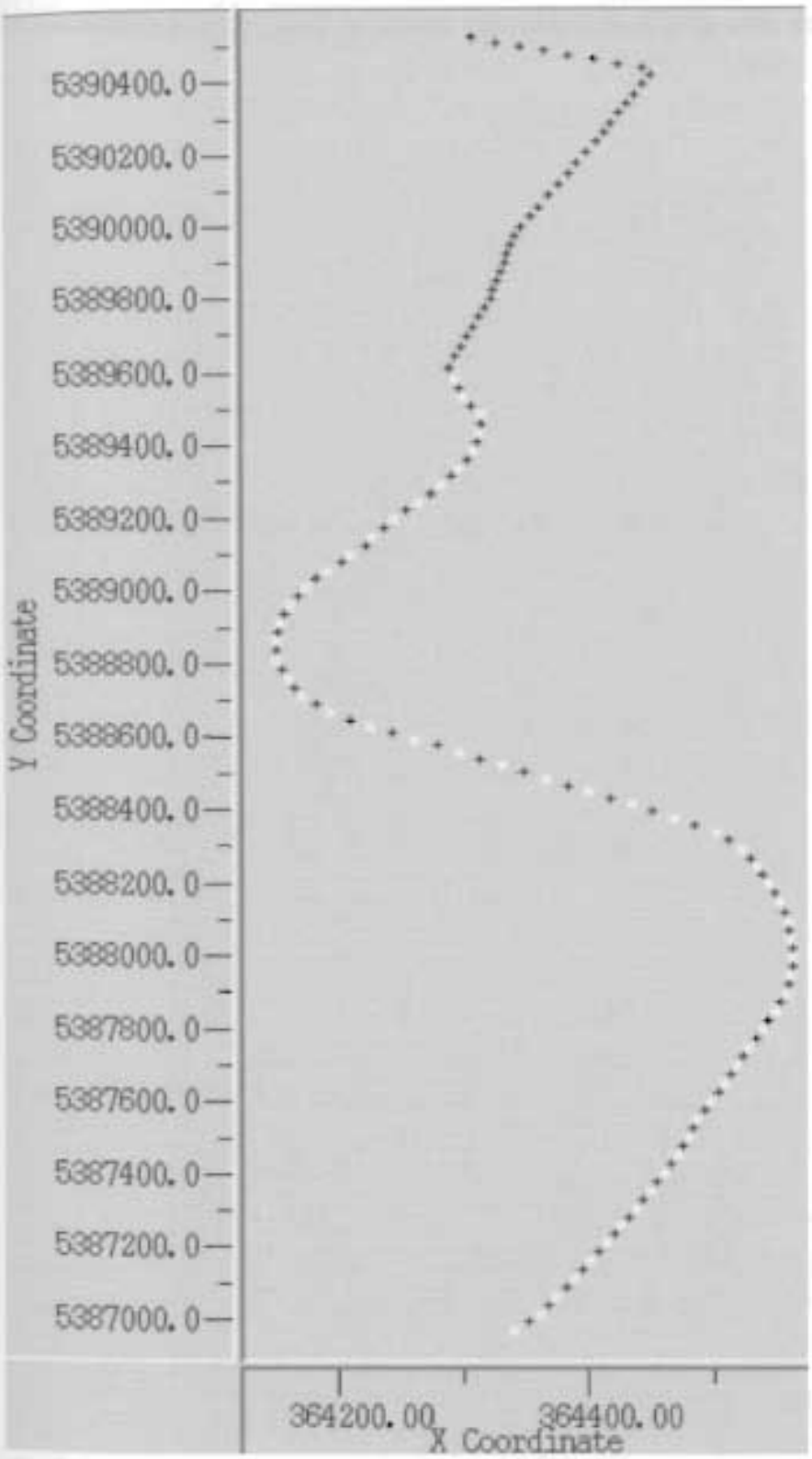

Figure 3.5. Shot point map for the 2D land seismic portion, note receiver positions are annotated in black and source positions in white.

Acquisition source and receiver parameters along with instrumentation specifications are listed in tables 1 and 2. The final land seismic line acquired was a 3km, 56 shotpoint, 148 channel record dataset recorded for 6sec TWT with a sample rate of 1ms. Seismic acquisition began at the southern end of the line and stepped northward. A recording truck, located on Shoal Point between stations 1103 and 1104 controlled acquisition of the dynamite source data.

Table 3.1: Survey Source / Receiver Parameters

Marine Source		Land Source	
Energy Source	Sleeve Gun Array	Energy Source	Dynamite
Displacement	5.24 *L*	Charge Size	2 kg
Pressure	14.0 MPa	Average Depth	5.0 meters
Average Depth	3.0 meters	Source Interval	50 meters
Source Interval	25 meters	Receiver interval	25 meters
Receiver Interval	25 meters		

Table 3.2: Instrumentation Specifications

Recording System	ARAM24	
Number Channels	148	
Auxiliary Channels	3	
Sampling Interval	1.0 millisecond	
Record Length	6.0 seconds	
Recording Filter	Low Cut: 3 Hz	
	High Cut: 410 Hz	
Tape Format	SEG-Y	
Geophone Type	Mark Products	
	Frequency	10 Hz (UM-2)
	Array	6 over 25 m
Spread Description	All live, no roll/gap	

3.3.2 Marine Acquisition

The 3D survey acquisition involving the marine shot lines was also affected by weather. Hurricane force winds caused excessive sea conditions and therefore numerous consecutive days of downtime. Even in the relative shelter of the bay, the sea-state was too rough for safe operating near land. The final 3D shot line distribution seen in figure 3.6 includes a total of 11 marine shot lines fired into the land receiver spread. The survey map is underlain by the resultant actual fold distribution of the marine shot portion. Due to the poor weather resulting in substantial downtime and the 2 week timetable, we were not able deploy the streamer to collect any of the designed conventional 2D marine seismic data.

3.3.3 Acquisition Summary

Labeled a transition zone seismic survey, it is important to understand that the project is not truly transition zone nor is it conventional. The combination of final techniques used was primarily focused around marine shots being fired at long offset into a spread of geophones that were all on land. In all, the field operations resulted in the acquisition of 60 gathers equaling 9060 traces of 2D land data and 1591 gathers equaling 192263 traces of 3D transition zone data. These two datasets form the basis for the processing and interpretation in this thesis.

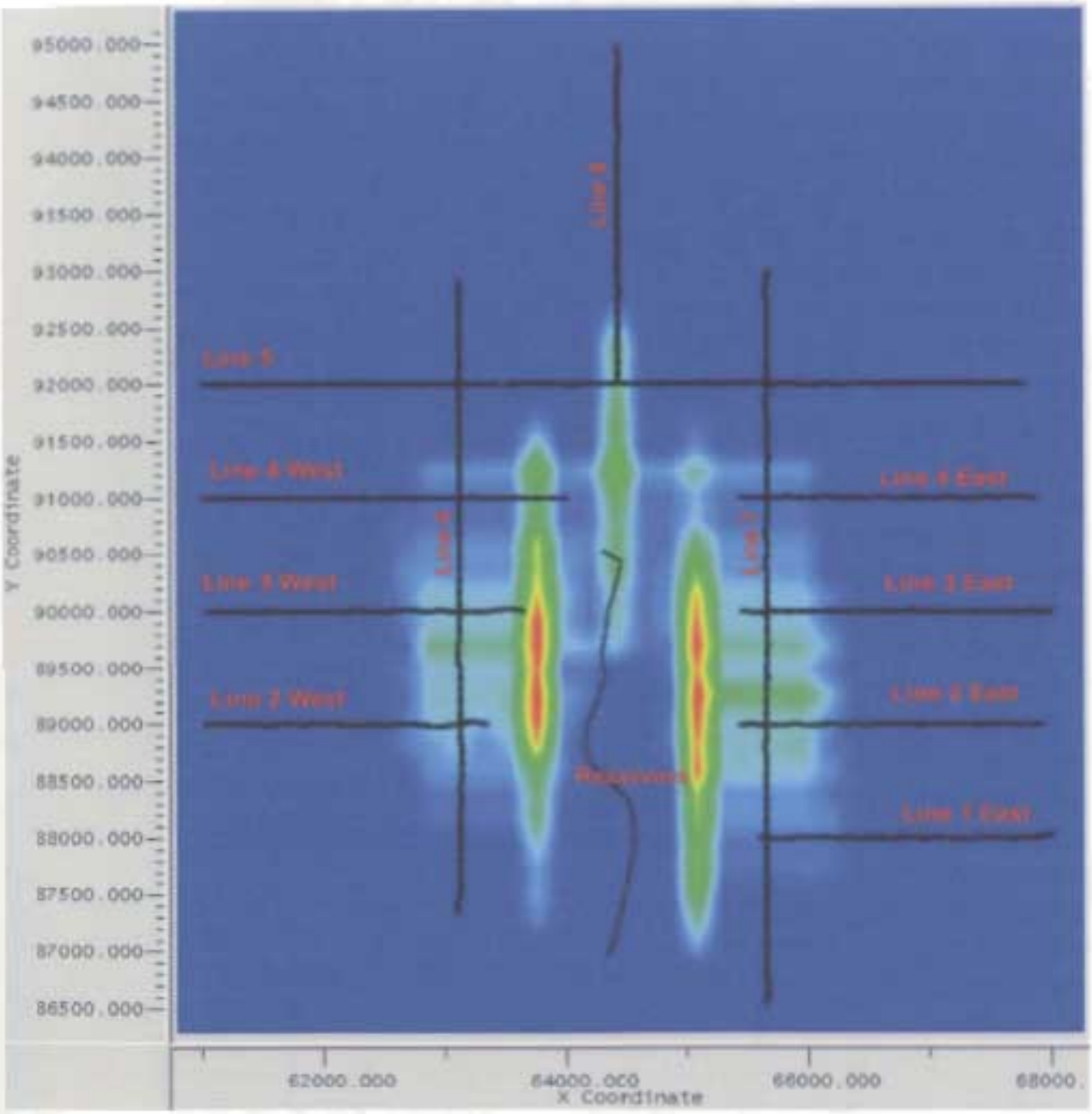

Figure 3.6. **Shot point and receiver** map showing positions of acquired marine lines and land receivers along with data fold distribution (red = 50+ fold, green = 25, light blue = 5, deep blue = 0).

3.4 Seismic Data Quality

The quality of collected seismic data varies significantly from shot line to shot line over the survey area. Overall the marine shot lines must be described as poor to extremely poor quality data. The records are extremely noisy with the marsh hydrophones being excessive to the point of not being usable. The following figures represent several typical raw shot records with no filters or scaling. Note that there is commonly abundant ringing of the first arrivals with few identifiable primary seismic events.

Due to the exclusion of the marsh phones and the inability to use the streamer as an OBC, the overall source-receiver offset distribution of the dataset has become even more heavily weighted to long offset traces. The majority of the data falls into offset ranges of 2000m to 4000m, with the nearest offset data available being on the order of 900m. As a result of this data quality and the offset issues many processing challenges arise. Conventional processing techniques and "rules of thumb" cannot be applied to the dataset. This is discussed more extensively in chapters 4, 5 (2D and 3D seismic data processing).

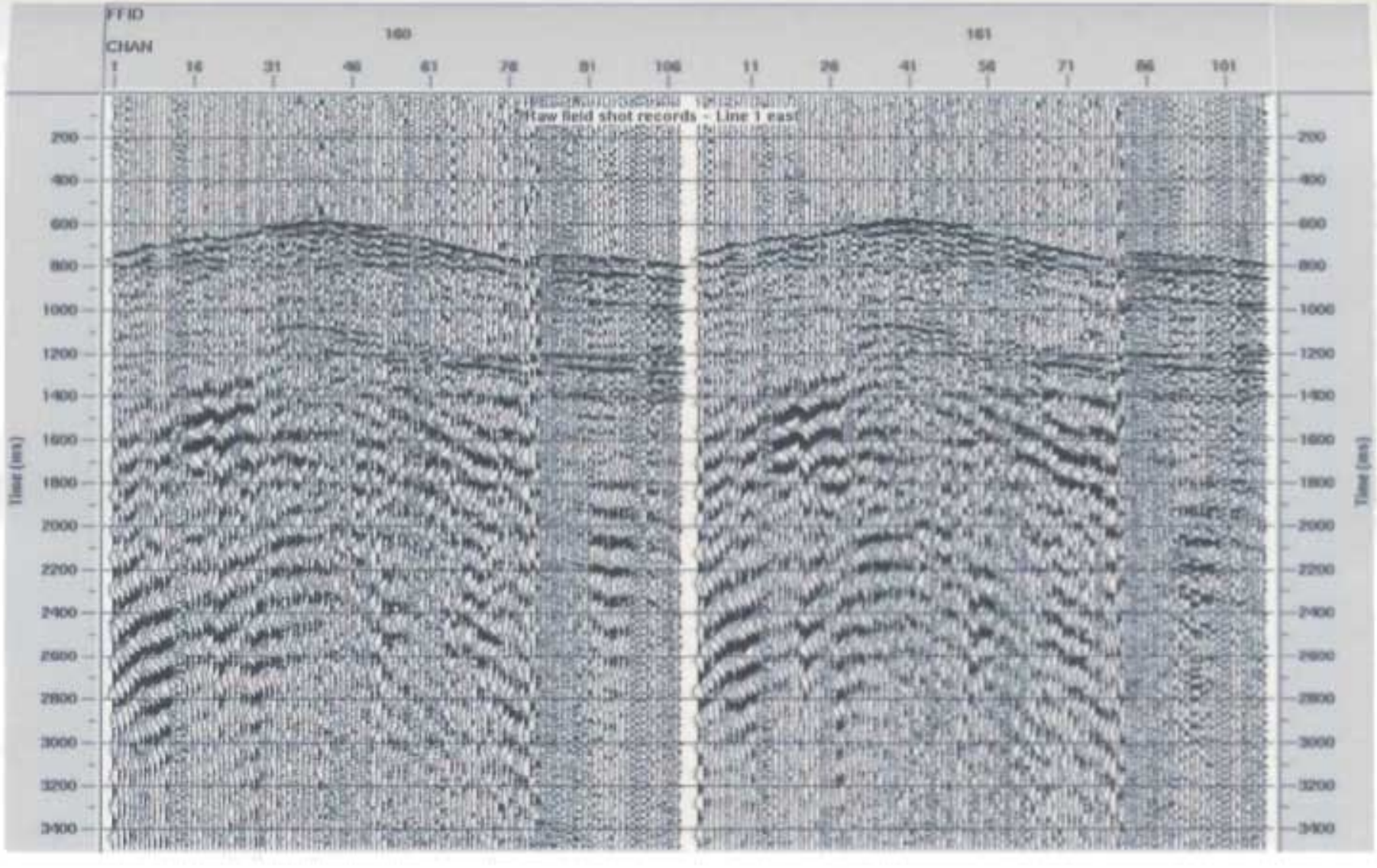

Figure 3.7a. Sample unfiltered/unscaled shot records for line 1 east of the marine 3D survey.

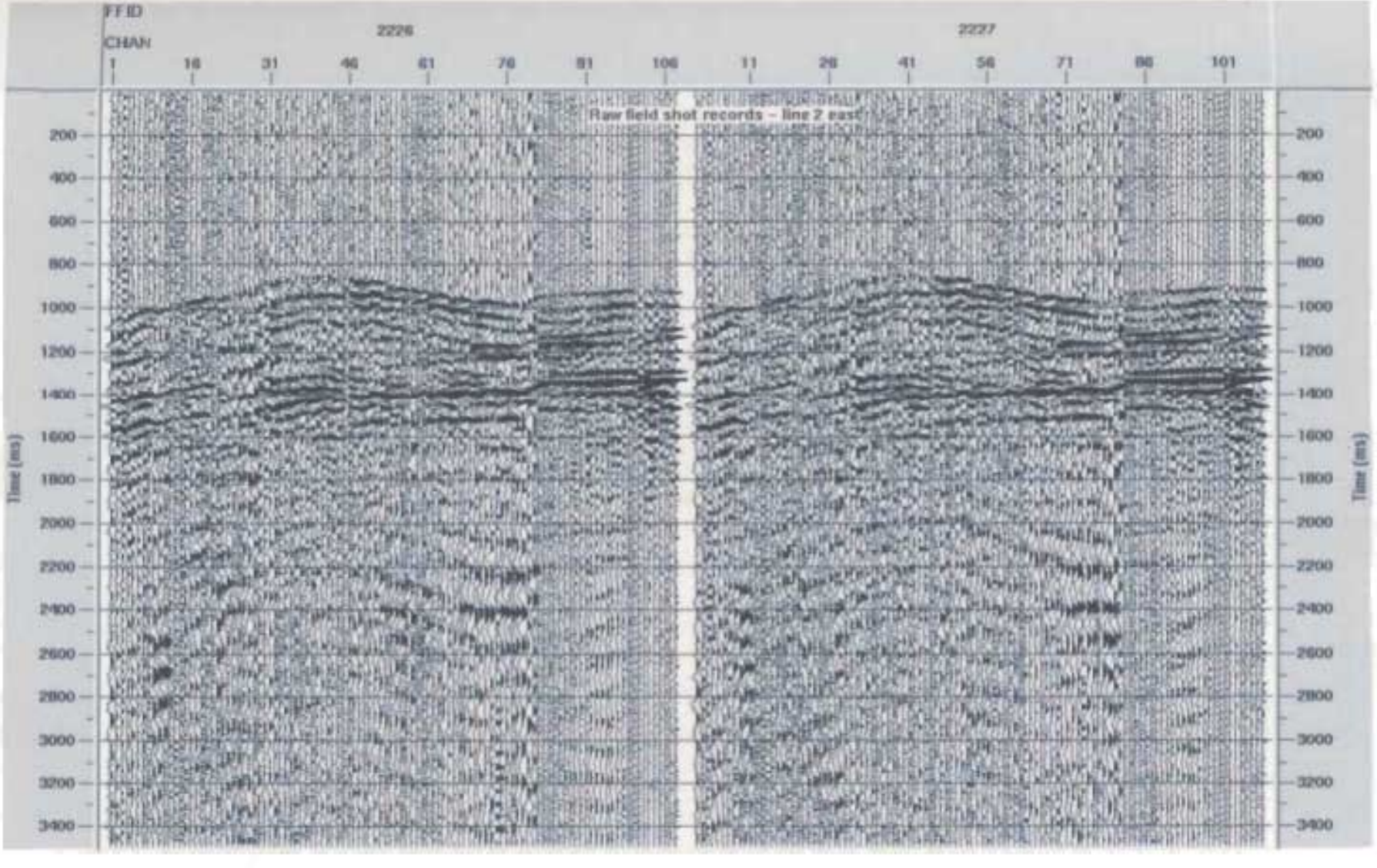

Figure 3.7b. Sample unfiltered/unscaled shot records for line 2 east of the marine 3D survey.

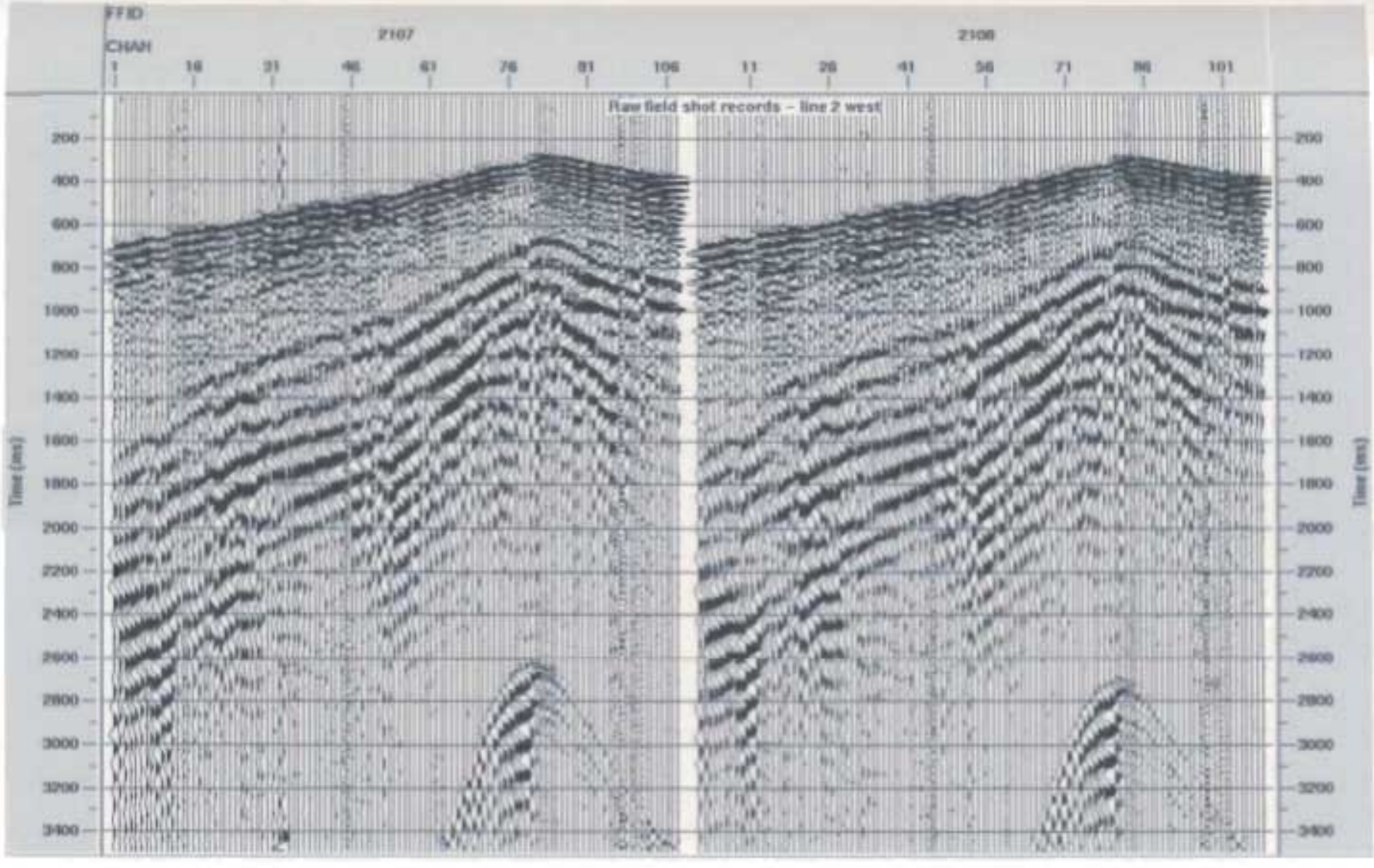

Figure 3.7c. Sample unfiltered/unscaled shot records for line 2 west of the marine 3D survey.

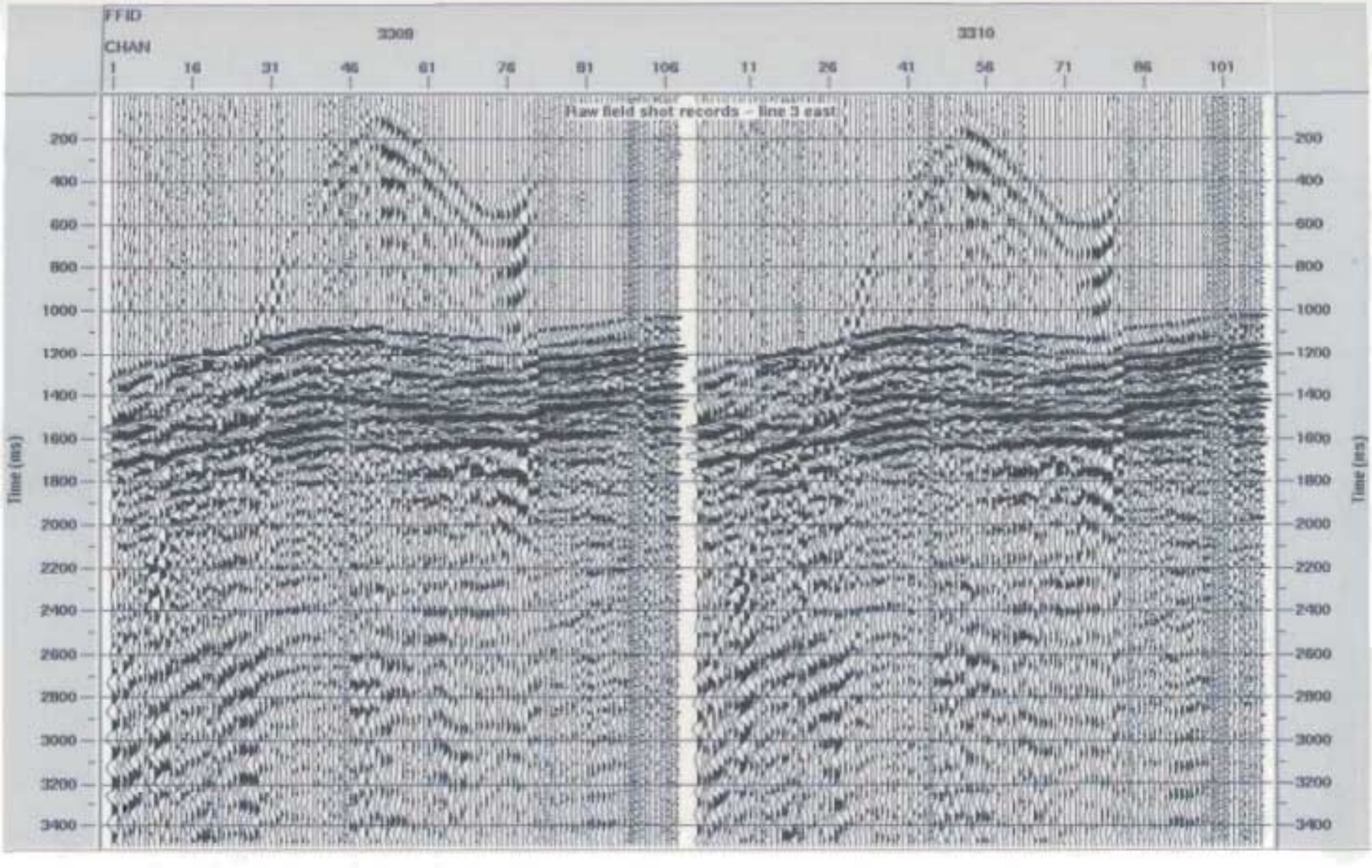

Figure 3.7d. Sample unfiltered/unscaled shot records for line 3 east of the marine 3D survey.

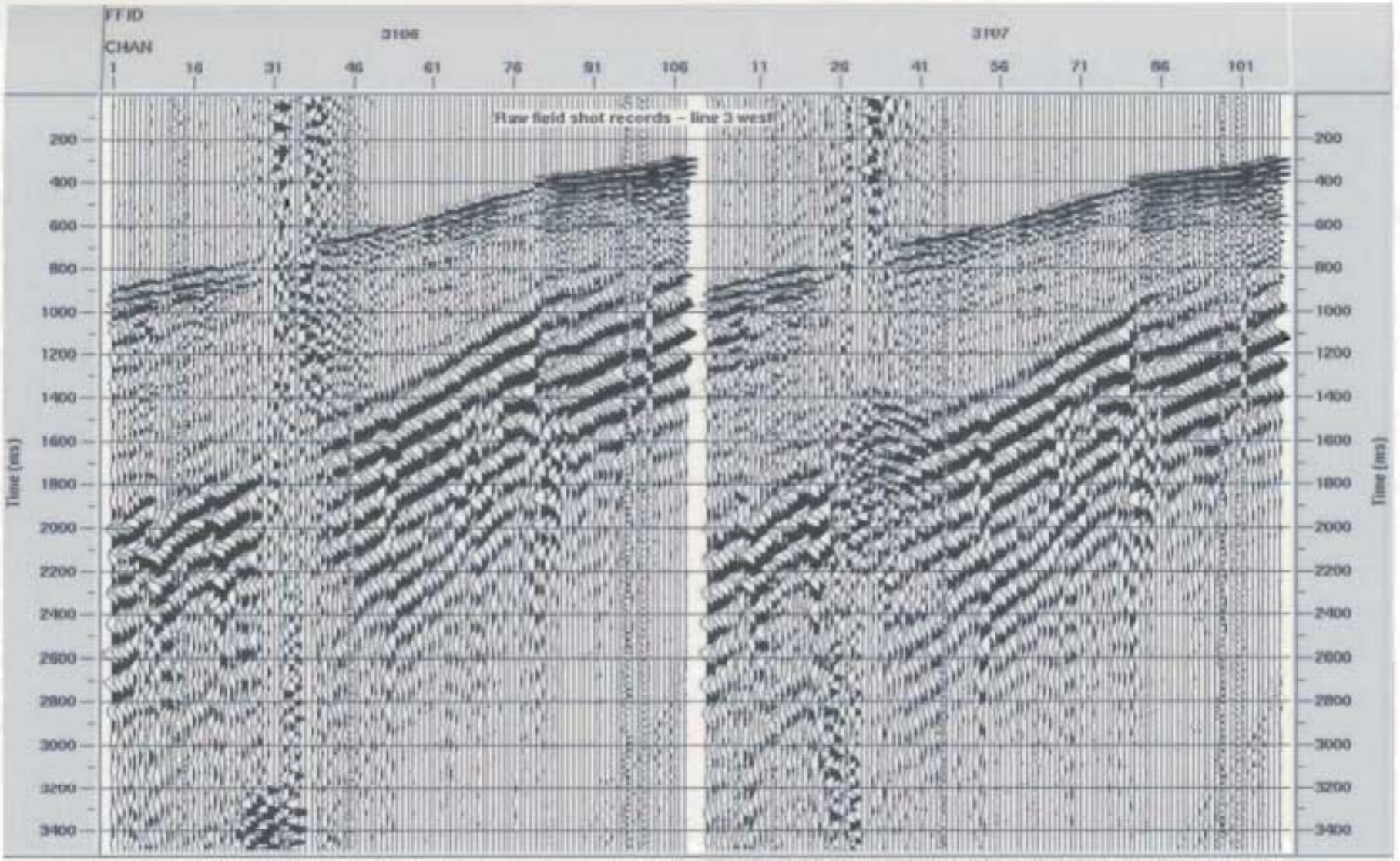

Figure 3.7e. Sample unfiltered/unscaled shot records for line 3 west of the marine 3D survey.

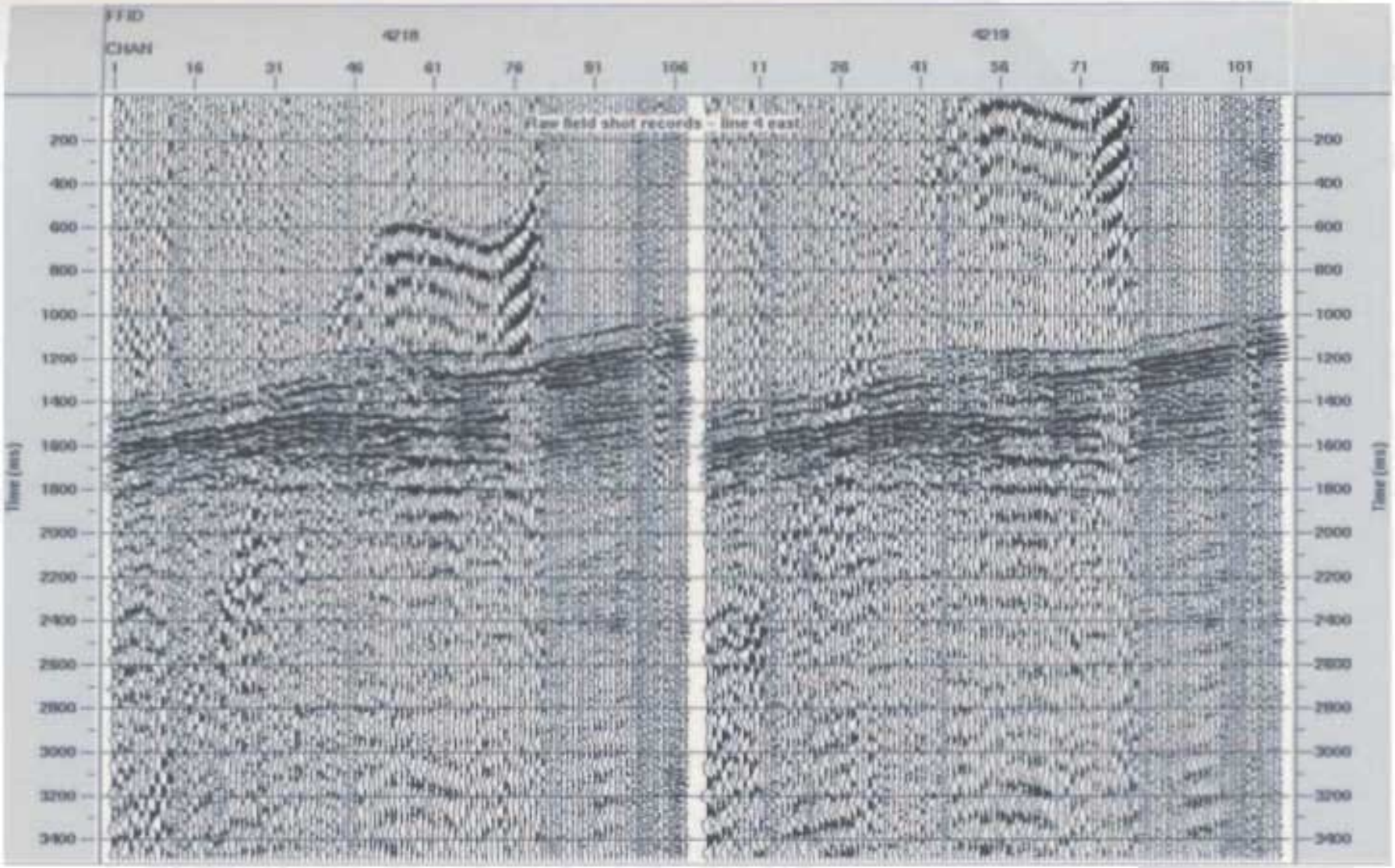

Figure 3.7f. Sample unfiltered/unscaled shot records for line 4 east of the marine 3D survey.

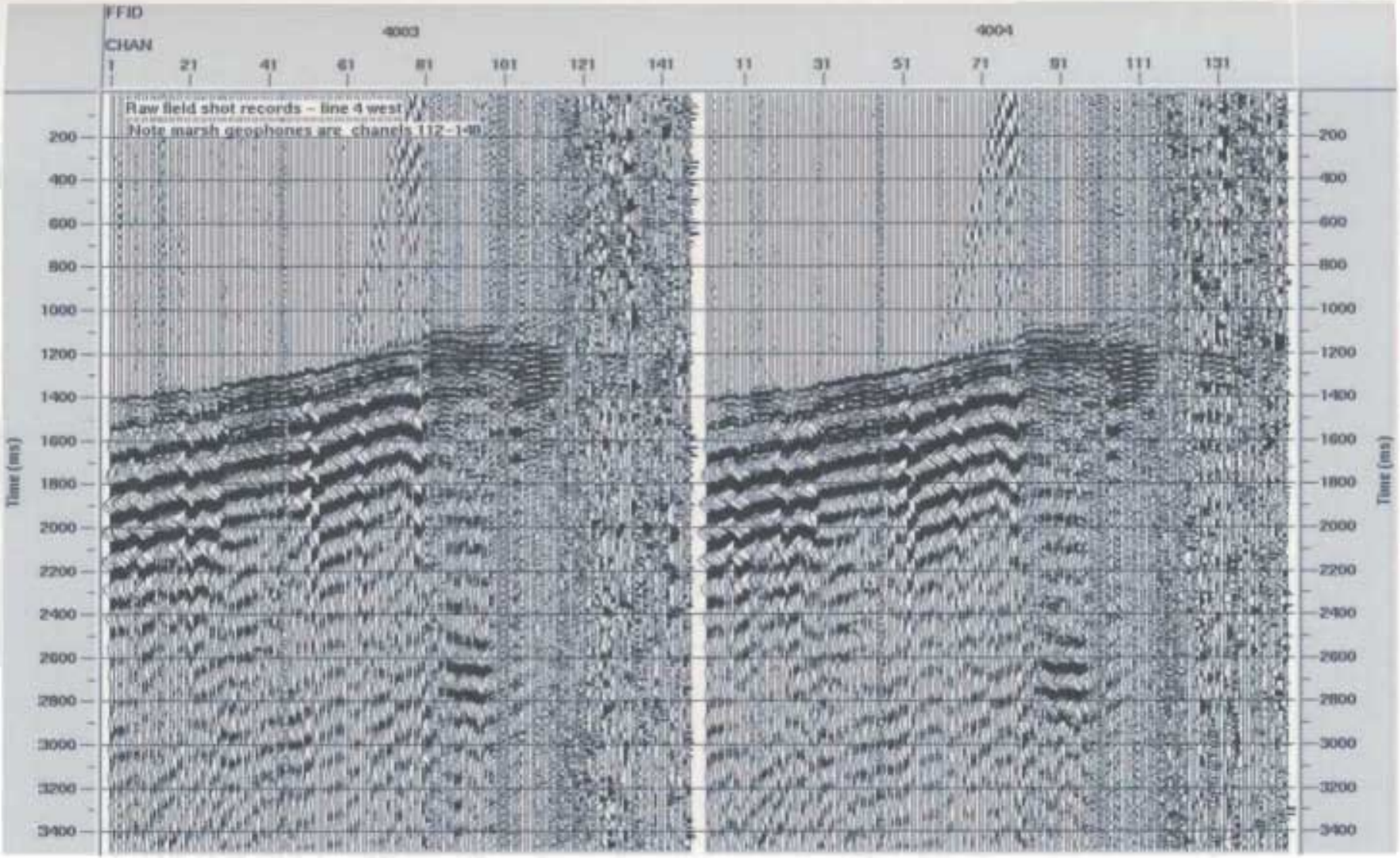

Figure 3.7g. Sample unfiltered/unscaled shot records for line 4 west of the marine 3D survey.

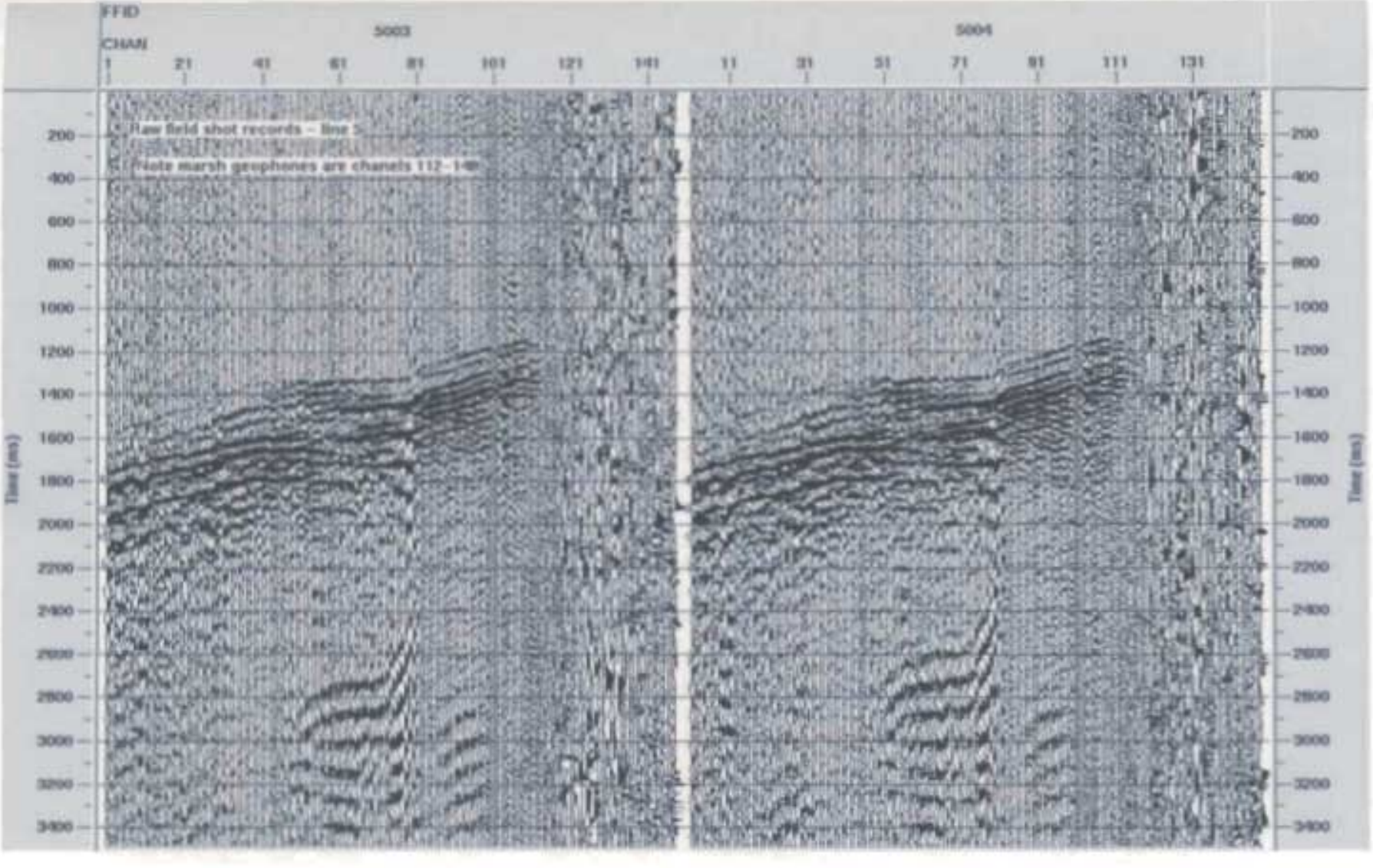

Figure 3.7h. Sample unfiltered/unscaled shot records for line 5 of the marine 3D survey.

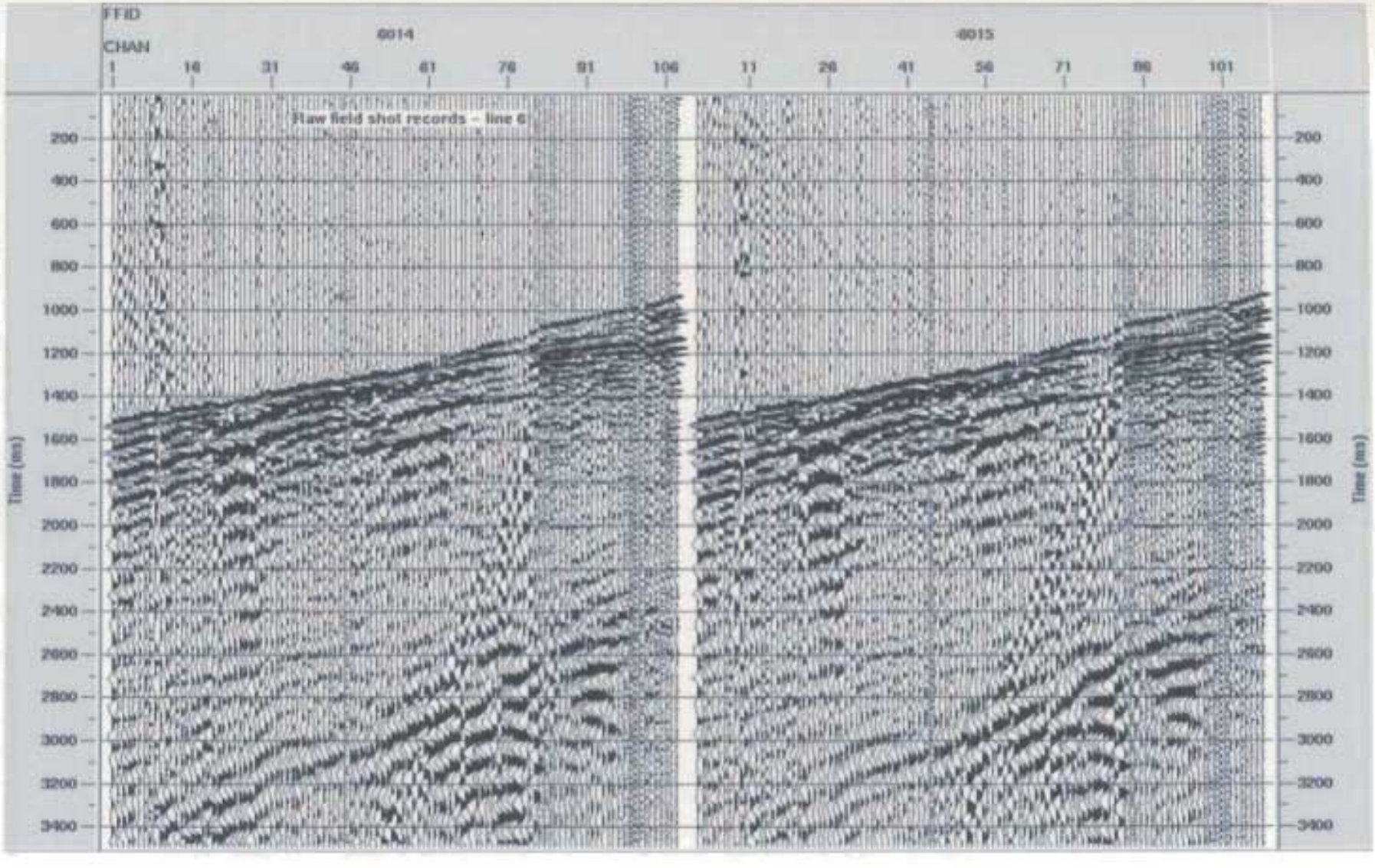

Figure 3.7i. Sample unfiltered/unscaled shot records for line 6 of the marine 3D survey.

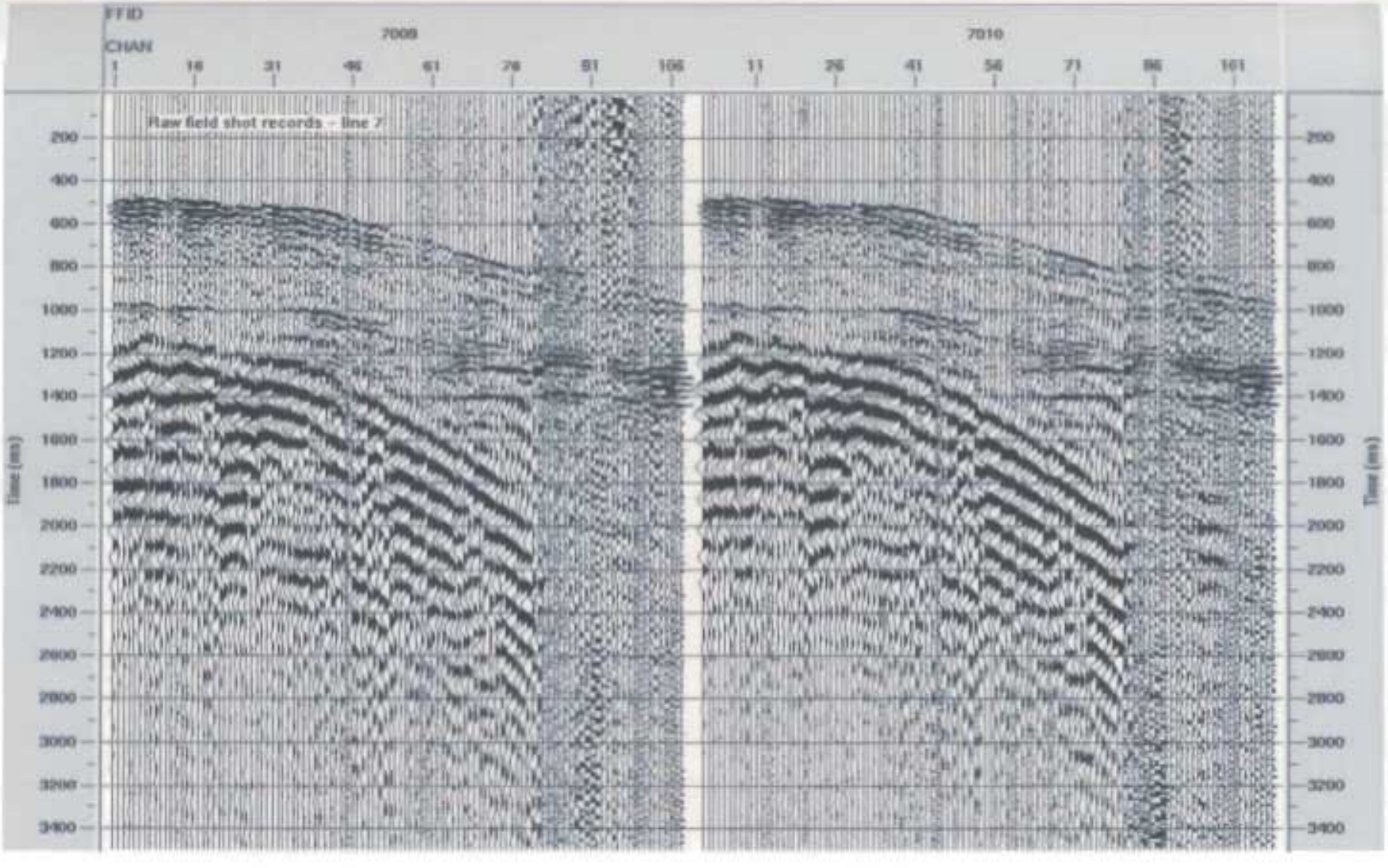

Figure 3.7j. Sample unfiltered/unscaled shot records for line 7 of the marine 3D survey.

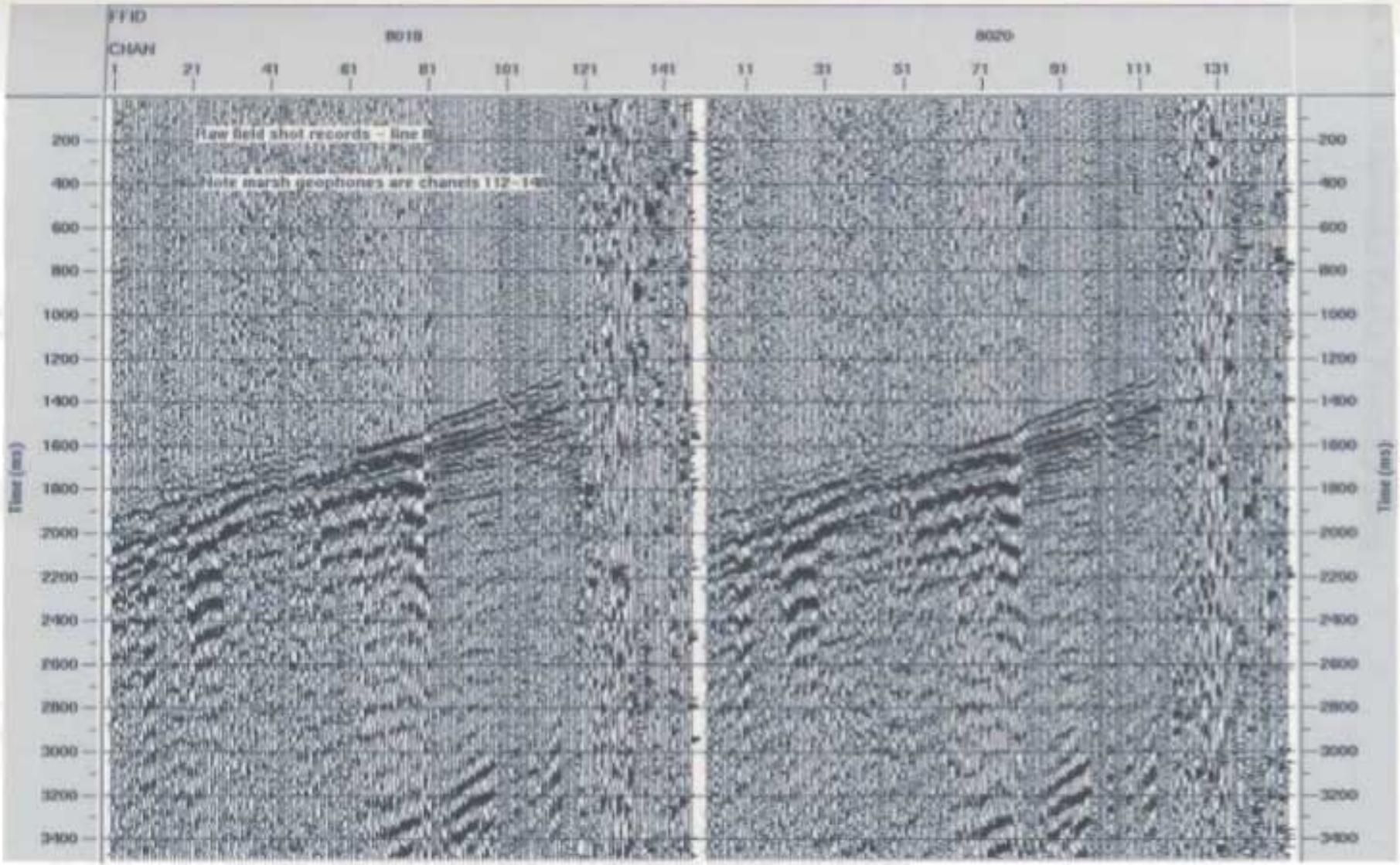

Figure 3.7k. Sample unfiltered/unscaled shot records for line 8 of the marine 3D survey.

4.0 2D Seismic Data Processing

As discussed in Chapter 3, 2D acquisition generated a conventional 60 record 2D landline. All of the following processing was completed with accomplishment of the initial project goals in mind. The Shoal Point 2D landline will be extremely important to the processing and interpretation 3D phases of the project.

4.1 Processing Overview

The immediate goal of almost any seismic processing operation is the production of the best possible stacked or migrated section. Completion of this goal involves an extensive sequence of testing and application of various filters and algorithms that manipulate the data to achieve the best possible result. This chapter includes a detailed description of the testing and techniques used to achieve the best stack for the Shoal Point 2D dynamite landline.

4.2 Hardware / Software

4.2.1 Hardware

All processing and interpretation of seismic data was completed on dual monitor UNIX based Silicon Graphics work stations at Memorial University of

Newfoundland, in the Earth Sciences Department's seismic processing laboratory.

4.2.2 Vista®

A Seismic Image Software (SIS) package, Vista® was used for the modeling portion of the survey design. This seismic processing package is capable of both 2D and 3D processing and runs on an NT platform.

4.2.3 ProMAX® / Seisworks®

ProMAX® and Seisworks® are both software packages from the Landmark Graphics Corporation suite of geological and geophysical processing and interpretation tools donated to Memorial by Landmark. ProMAX® is considered industry standard and was used to complete all of the 2D and 3D seismic data processing. Seisworks® an industry standard interpretation package was used for both the 2D and 3D seismic interpretation.

4.2.4 Gocad®

Gocad® is an extremely powerful earth science software package developed by Earth Decision Sciences. For the current data Gocad® was used for 3D visualization and mapping of the interpreted seismic surfaces from Seisworks®.

4.3 2D Data Testing and Processing Parameters

4.3.1 Data Loading

Field file data was recorded in SEG-Y format to 8mm Exabyte digital audio tapes (dat). Files were extracted at Memorial using UNIX workstations at which point the data was read in to ProMAX® and converted to a Landmark Graphics proprietary format for data processing.

4.3.2 Crooked Line Geometry Assignment

Due to the use of the existing roadbed for the line, the receiver layout was a "crooked" seismic line needing crooked line binning strategies for geometry application. Crooked line processing is different from conventional straight line processing in that the processor can select the CDP binning track to follow the bends of a crooked receiver line. This is contrasted to straight line geometry where the CDP binning track has to be a straight line. Use of a straight line geometry with an extremely crooked receiver line will destroy the fold and CDP offset distributions. Therefore to maintain a broad distribution of trace offsets and higher fold levels, crooked line binning strategies are necessary.

Navigation data collected during acquisition using a portable DGPS Trimble system for both shot and receiver positions was converted to ASCII format and

merged with seismic data in the ProMAX® geometry spreadsheets. Figure 4.1 contains a sample from the source and receiver spreadsheet displaying some of the key parameter fields such as field file identification (FFID), station #, X coordinate, Y coordinate and the Z coordinate. Figure 4.2 is a plot of surfical elevation along the point; note there is very little relief with elevations varying from 5m to just below sea level for the marsh transition hydrophones.

In figure 4.3 the CDP locations are illustrated and are colored to indicate varying source-receiver offset ranges (note the position of the receiver locations and the coverage of the overall data distribution). The s-shape of the receiver-shot line (black) has produced an east-west range of traces such that most CDP bin locations regularly have offsets longer then 3500m.

Mark	Block	Source	Station	X	Y	Z	FFID	Offset	Skid	Uphole	Hole Depth	Pattern	Num Chn
1		1000	1000	364340.5	5386970.5	3.7	1000		0.0	12.5	6.0	1	148
2		1002	1002	364360.6	5387016.0	3.5	1001		0.0	12.5	6.0	1	148
3		1004	1004	364374.3	5387064.5	3.7	1003		0.0	12.5	6.0	1	148
4		1006	1006	364388.1	5387113.5	3.8	1004		0.0	12.5	6.0	1	148
5		1008	1008	364401.2	5387161.5	3.6	1006		0.0	12.5	6.0	1	148
6		1010	1010	364413.6	5387210.5	3.5	1007		0.0	12.5	6.0	1	148
7		1012	1012	364425.5	5387259.0	3.2	1008		0.0	12.5	6.0	1	148
8		1014	1014	364437.2	5387307.5	3.3	1009		0.0	12.5	6.0	1	148
9		1016	1016	364448.6	5387355.5	4.0	1010		0.0	12.5	6.0	1	148
10		1018	1018	364459.7	5387405.5	3.5	1011		0.0	12.5	6.0	1	148

(a)

Mark	Block	Station	X	Y	Elev	Static
1		1000	364340.4	5386970.5	3.7	0.0
2		1001	364350.5	5386993.5	3.6	0.0
3		1002	364360.6	5387016.0	3.5	0.0
4		1003	364367.5	5387040.0	3.6	0.0
5		1004	364374.3	5387064.5	3.7	0.0
6		1005	364381.2	5387089.0	3.7	0.0
7		1006	364388.1	5387113.0	3.8	0.0
8		1007	364394.7	5387137.0	3.7	0.0

(b)

Figure 4.1. (a) Source spreadsheet (b) receiver spreadsheet from the ProMAX geometry assignment process showing the primary parameters required for geometry application.

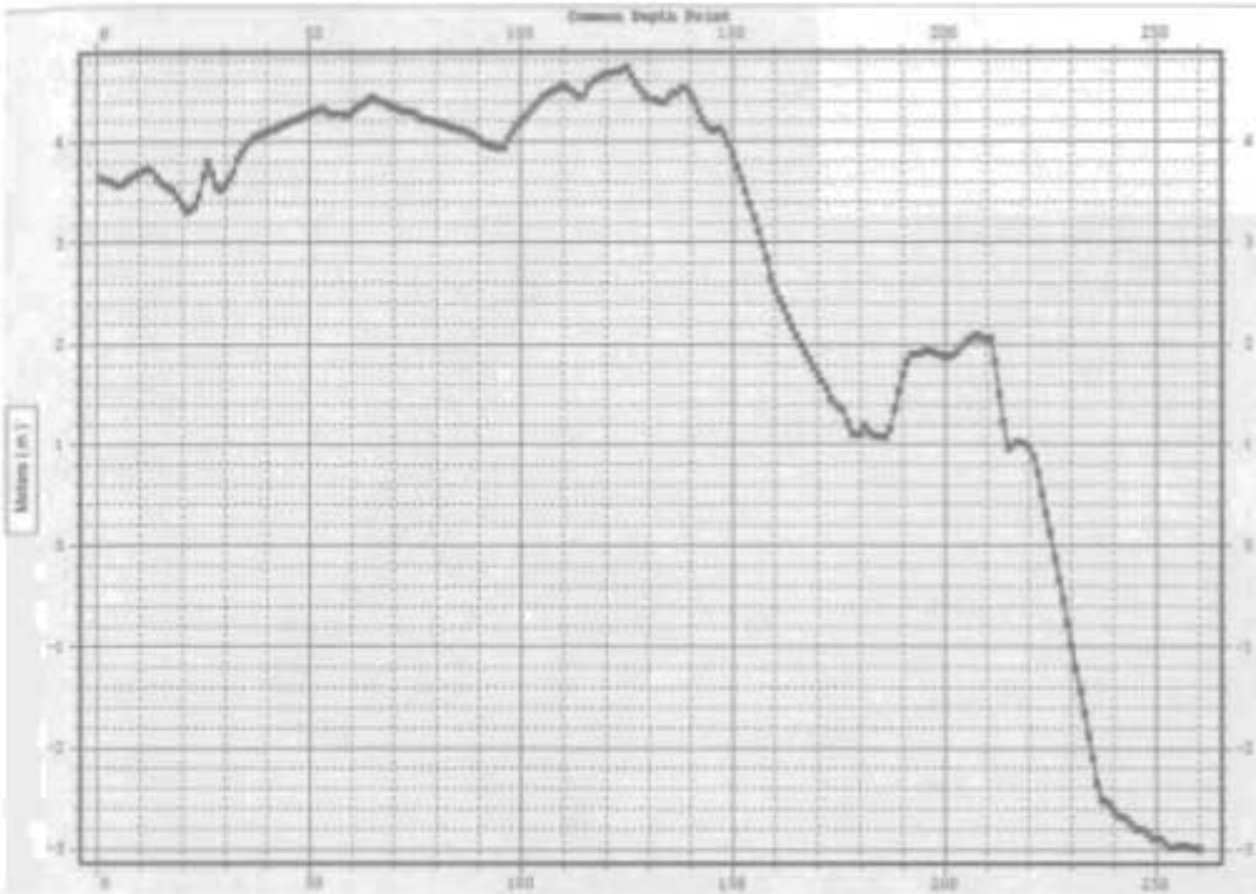

Figure 4.2. Cross-plot of CDP elevation in meters along the Shoal Point landline (including marsh geophones).

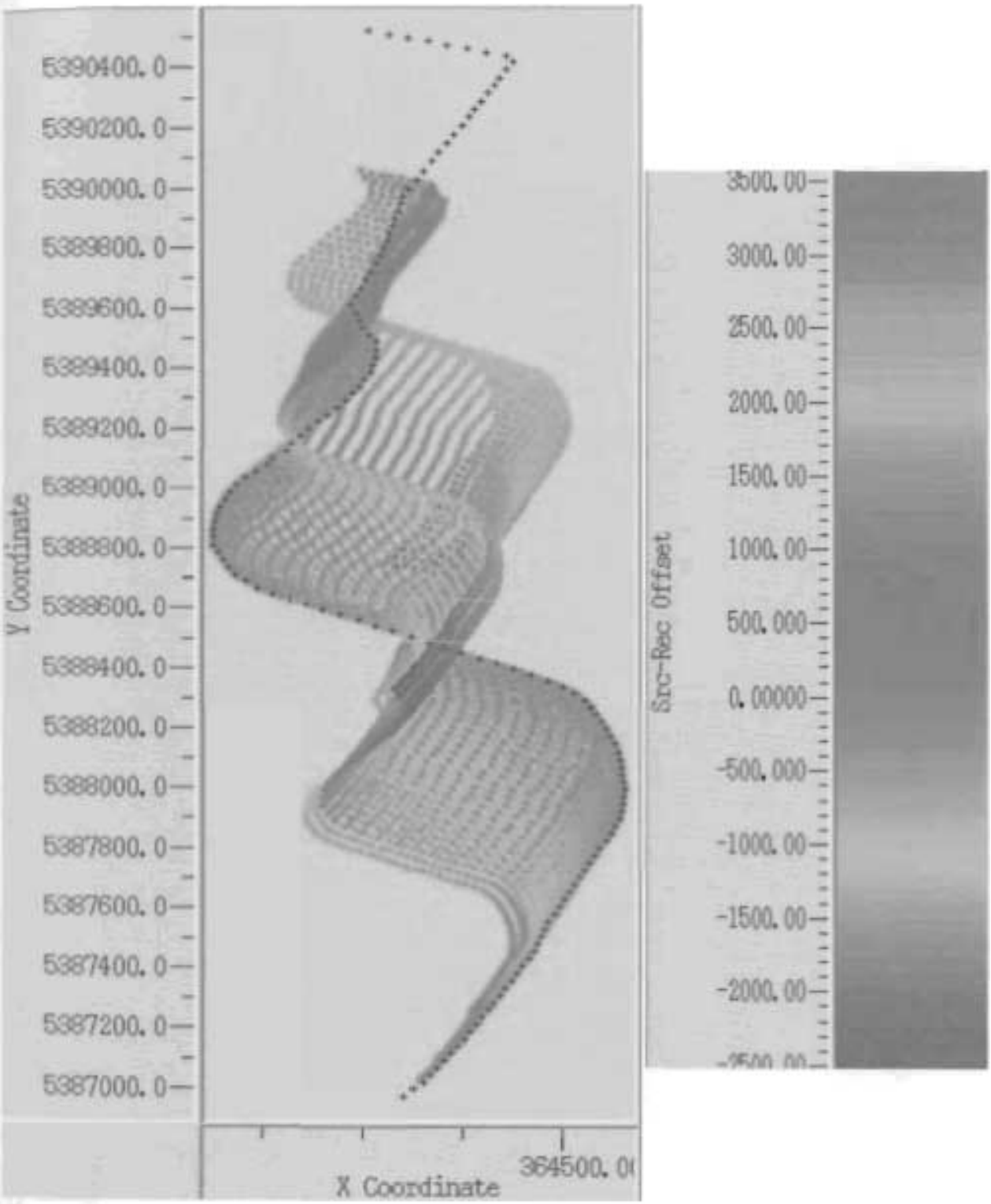

Figure 4.3. Diagram of source-receiver layout overlain by CMP distribution, which has been colored for source-receiver offset in meters.

4.3.2.1 Binning

The use of the crooked line geometry process allows definition of the exact size and location of the binning diagram. Using the above figure a binning track was designed to follow the general trend of the receiver line while allowing for the inclusion of maximum CDP's and offsets in each bin. Various bin dimensions were tested with particular care given to the value in the X direction. Due to the large surficial range of CDP locations it would be detrimental to the final output to design an oversized bin that would be large enough to contain each and every CDP. In doing so the data would be smeared excessively across the bin, when in theory it should represent a single point location on the reflecting surface. Final bin parameters of 12.5m (inline) x 100m (xline) were selected for optimal fold and source-receiver offset distribution. Figure 4.4 represents the final binning diagram showing bin size, and source-receiver locations. The designed binning diagram generates an average fold coverage of approximately 25 traces per bin.

4.3.3 Trace Kills / Editing

In general the land data was fair in quality with moderate signal to noise ratios. The 37 marsh transition hydrophones were extremely noisy with very poor signal level (Figure 4.6). For this reason I chose not to include any of these channels in the data processing.

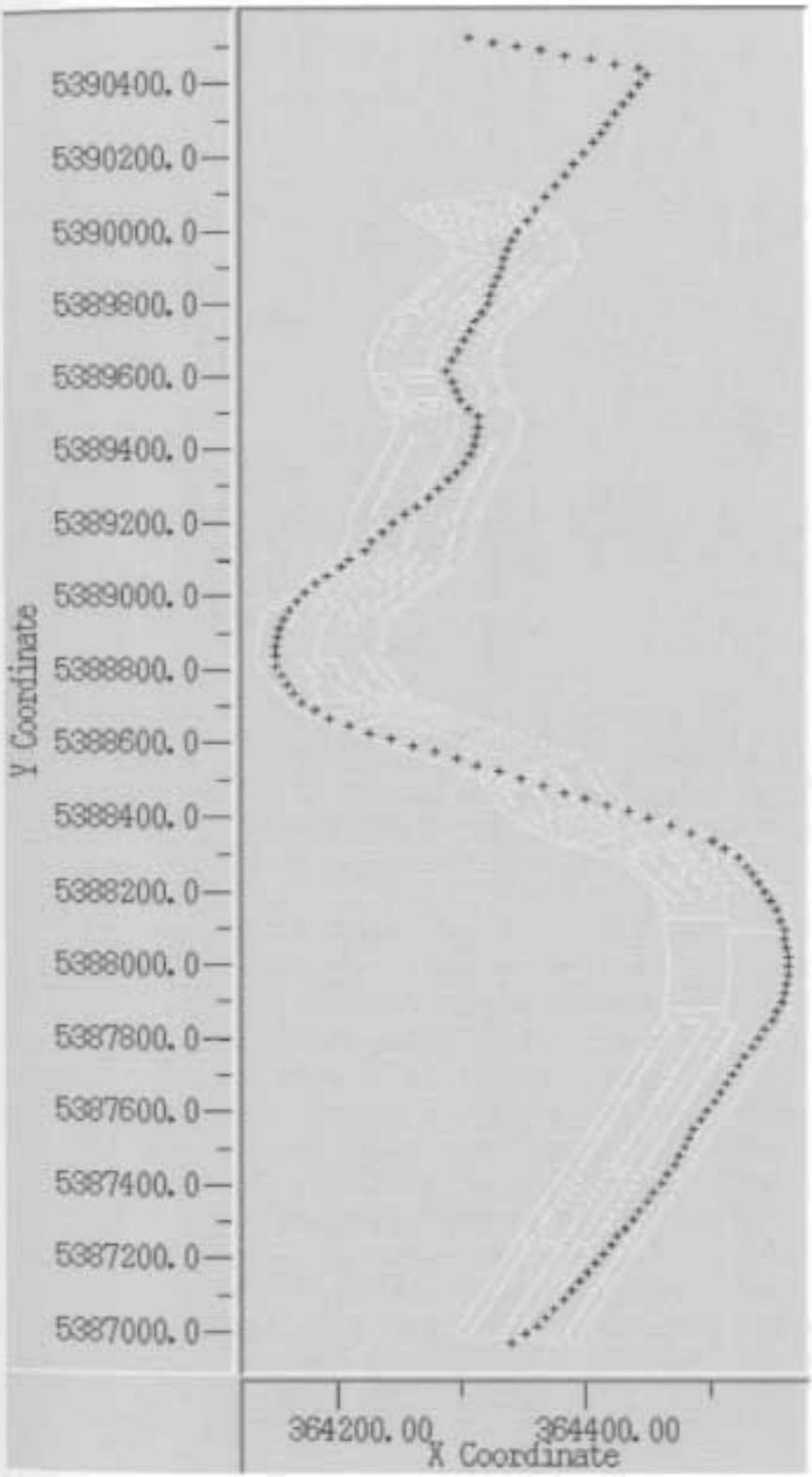

Figure 4.4. **Receiver spread locations overlain by finalized binning locations.**

Misfires / dead shot gathers that were killed included files 1002,1005 and 1035. All FFID's were digitally displayed and analyzed for frequency content, noise levels and dead traces.

In the following figure a typical field file / amplitude spectrum is displayed. It is clear the dominant frequency range is low in the 10Hz – 30Hz range and that little signal is present above 50Hz.

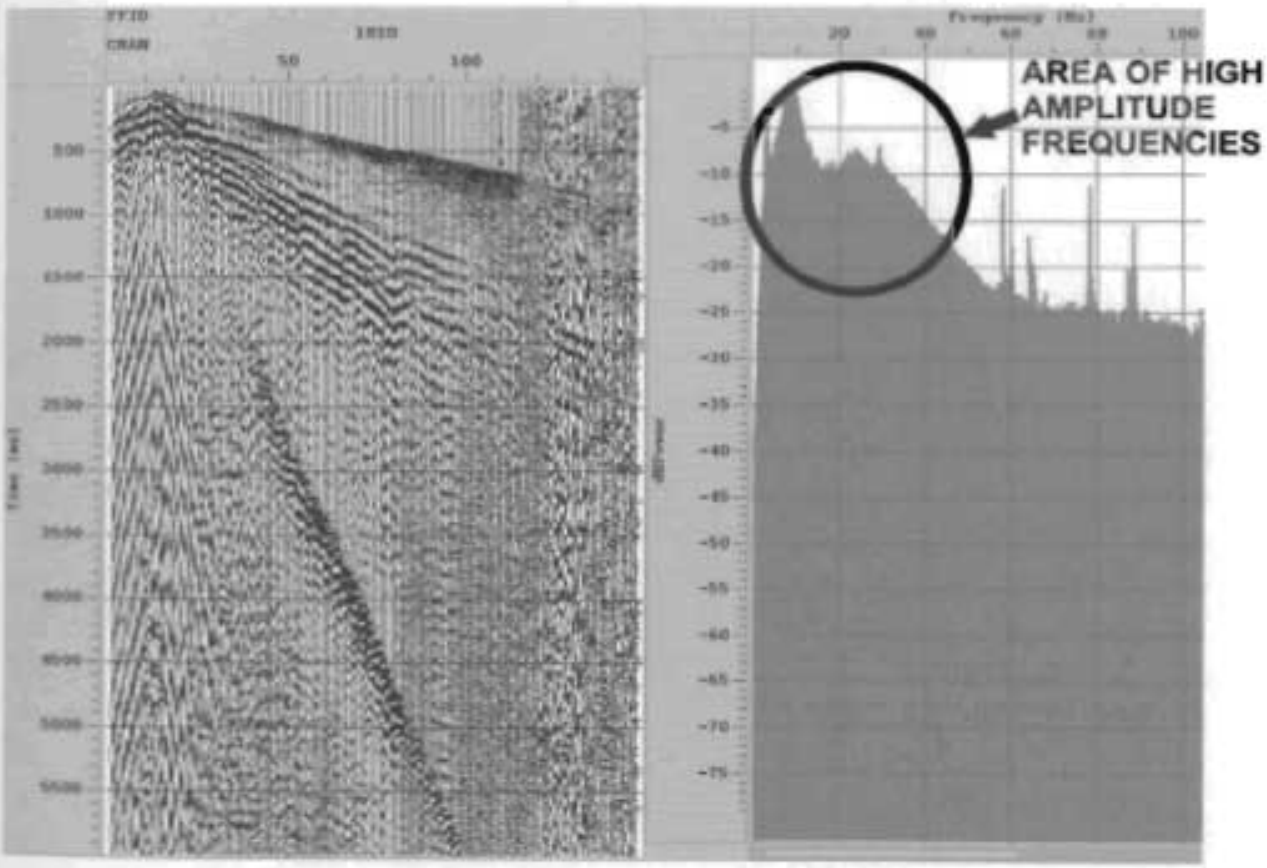

Figure 4.5. A typical shot record adjacent to its corresponding amplitude spectrum.

Each field file was edited to have all noisy traces, dead traces, misfires, signal bursts and noise trains such as ground roll and air blasts removed.

The following shot record is representative of the dataset and is annotated demonstrating typical features of land seismic data:

1. First arrival
2. Primary arrival
3. Air blast
4. Ground roll
5. Noisy channels

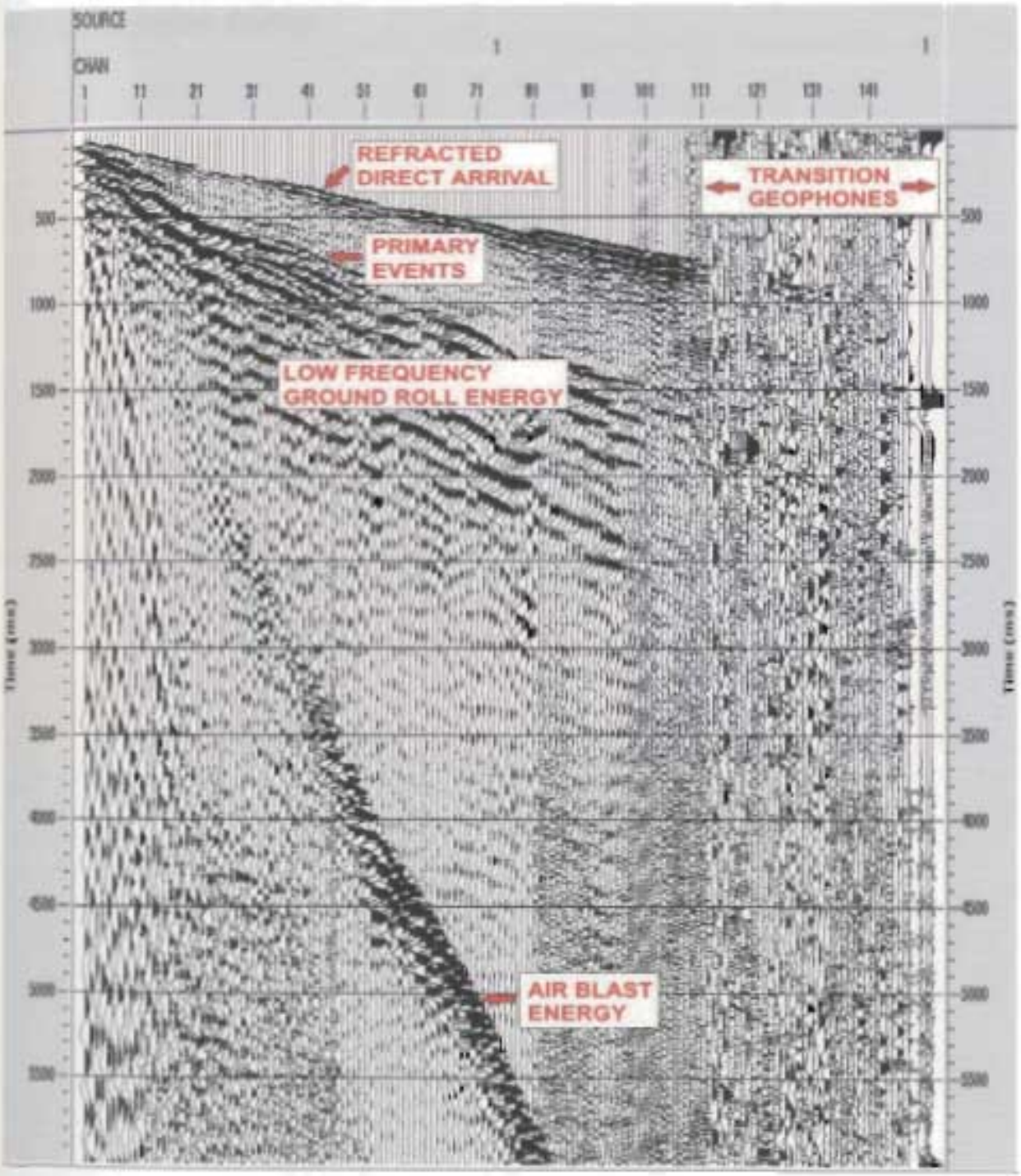

Figure 4.6. Representative land shot record annotated for its characteristic seismic attributes.

4.3.4 Refraction Statics

In land seismic acquisition reflection times are affected by irregularities and variations in the near surface geology. Statics corrections are applied to compensate for the effects of variations in elevation, weathering thickness, weathering velocity, or reference to a datum. A simple near surface model (Figure 4.7) outlines the basic geometry of the source-receiver relationship, with the surface / receiver elevation, source elevation, thickness and velocity variation of the weathering layer.

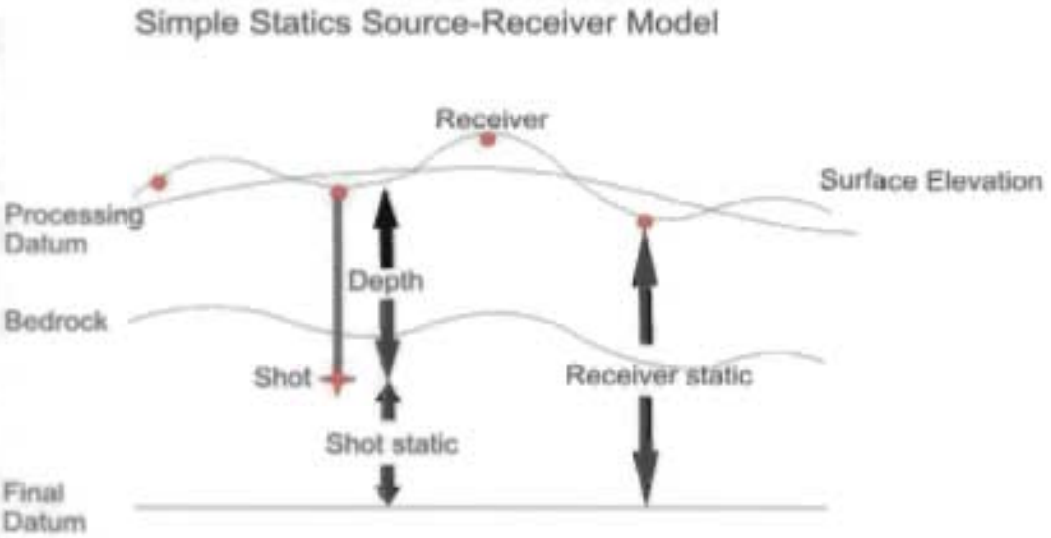

Figure 4.7. Diagram of statics attributes (ProMAX 2D Reference Guide, Volume 2, 1998 and Yilmaz, 2001).

Positioning of travel times to a new datum requires correction for the near surface weathering layer and differences in elevations of the source and receiver stations (Yilmaz, 2001). Calculation of the field static time shift by replacement of the weathering layer velocity with that of an average bedrock replacement velocity allows for transformation of source and receivers to a common datum.

The weathering velocity is usually calculated using uphole times recorded by the seismic operators during acquisition.

$$v=d/t \qquad (4.1)$$

- v = velocity
- d = source depth
- t = uphole travel time

Unfortunately during the acquisition of the Shoal Point landline no such times were recorded. Therefore discussion with the seismic operators and knowledge of the area allowed for estimation of the weathering layer as glacial till to boggy interval for which I've assigned an average velocity of 600m/s.

First break picks are generally the refracted energy associated with the base of the weathering layer / top of bedrock layer (Yilmaz, 2001). Normally seen as the first seismic energy on a shot record the first break times can be picked manually or automatically (Figure 4.8).

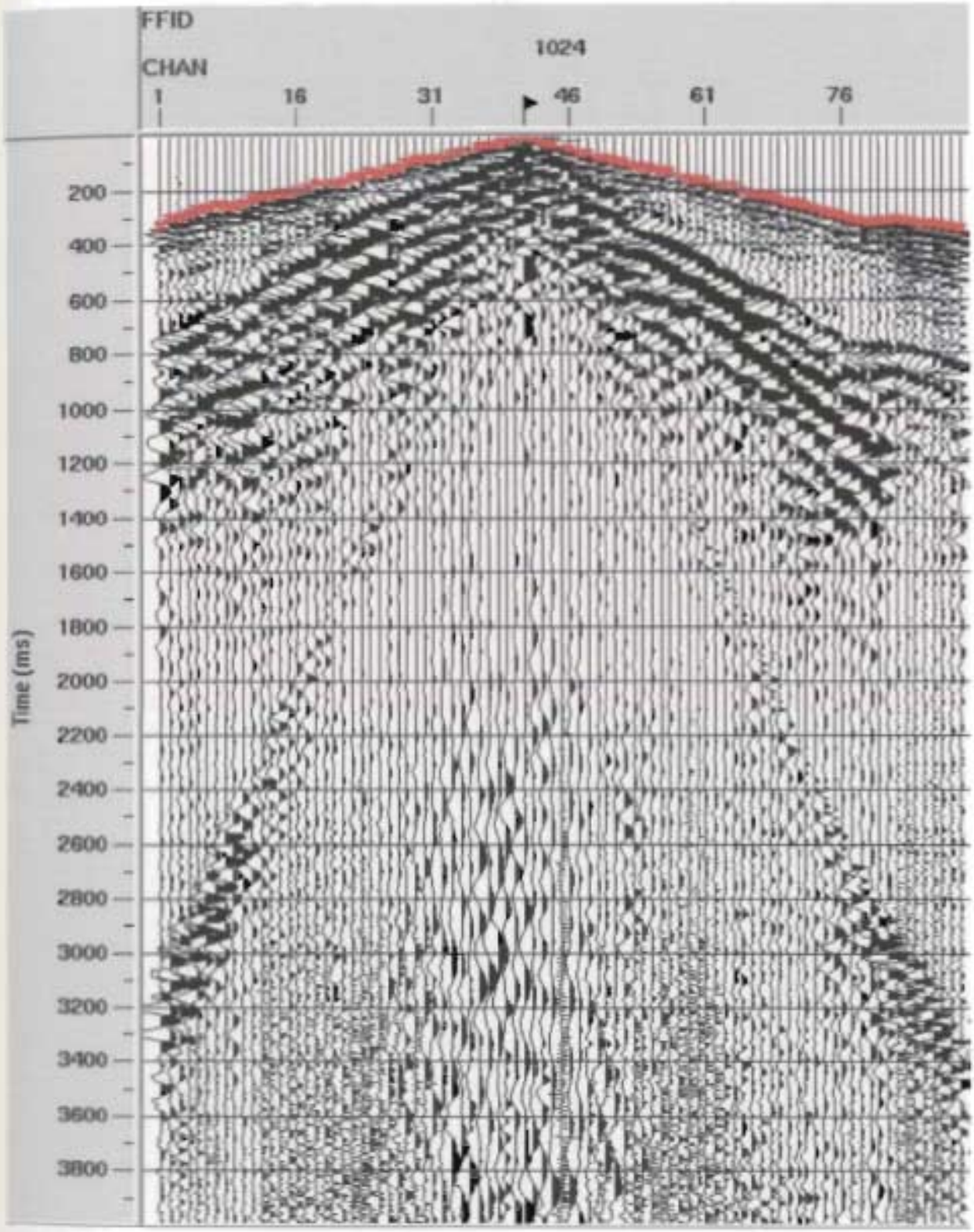

Figure 4.8. Field file 1024 with interactively picked first breaks high lighted in red.

First break times associated with the refracted arrival times are then used in an inversion scheme to estimate the near-surface model and calculate the overall statics.

Refraction statics analysis in ProMAX® enabled the automatic picking of first break arrival times, which when input into the Refraction Statics Analysis module allows for interactive adjustment and smoothing of pick times, layer thicknesses and velocities. ProMAX® refraction statics analysis contains several methods of refraction statics calculation, including:

- Diminishing residual matrices method (DRM).
- Generalized reciprocal method (GRM).

Comparative visual analysis of stacked data with each of the tested algorithms applied indicated that the diminishing residual method yields better results for the current seismic data. The overall difference that correct refraction statics analysis can make on a final stacked section is huge. The correct static shift results in a better alignment of the trace data and therefore increases the overall coherency of the reflectors dramatically. The following figures demonstrate key interactive steps followed for calculation of the final refraction statics. Figure 4.10 compares stacked data with and without refraction statics applied; the increased data quality and reflection resolution is clearly visible.

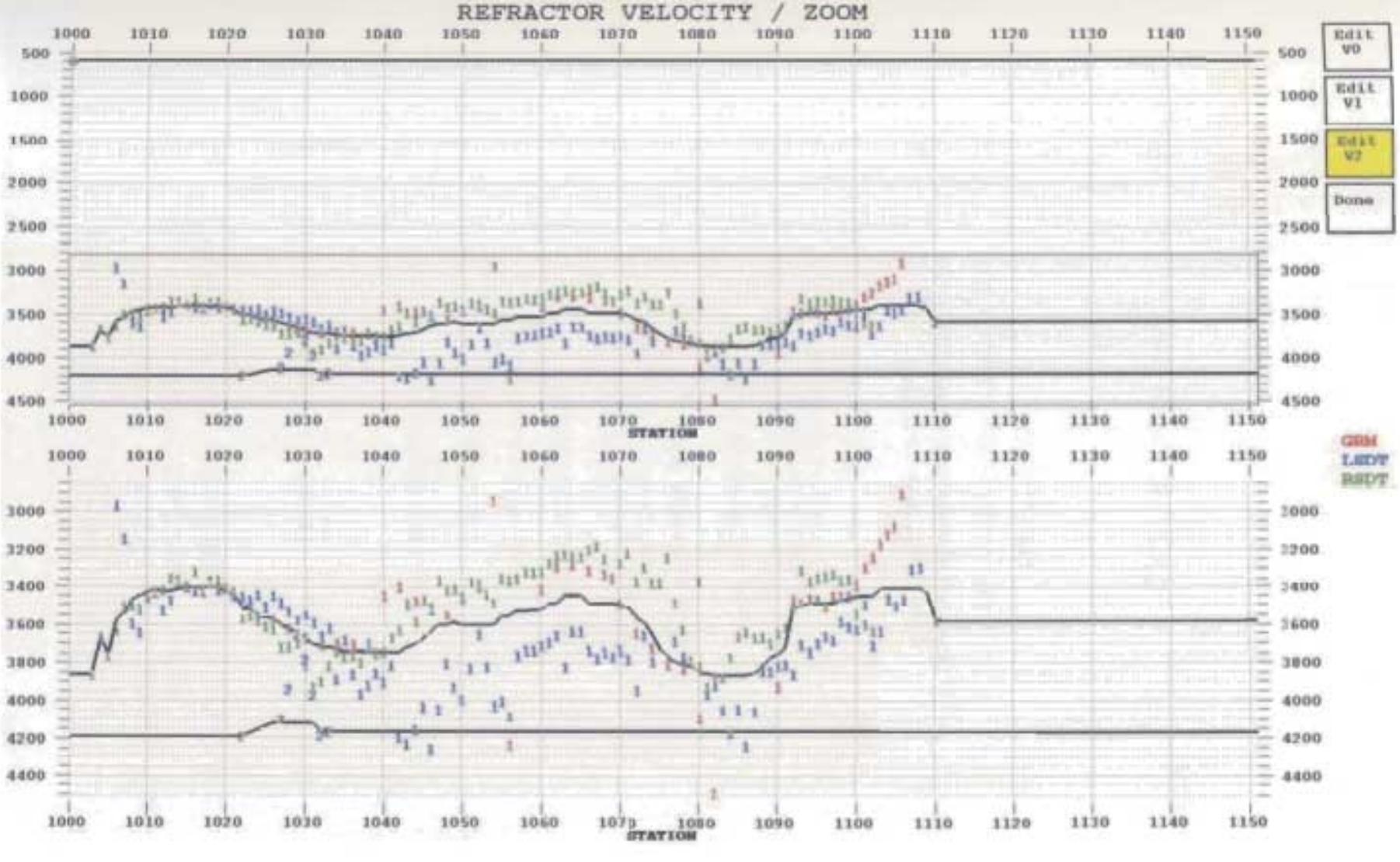

Figure 4.9a. Diagram of the velocity model generated from the first break picks for a 2 layer refraction statics model.

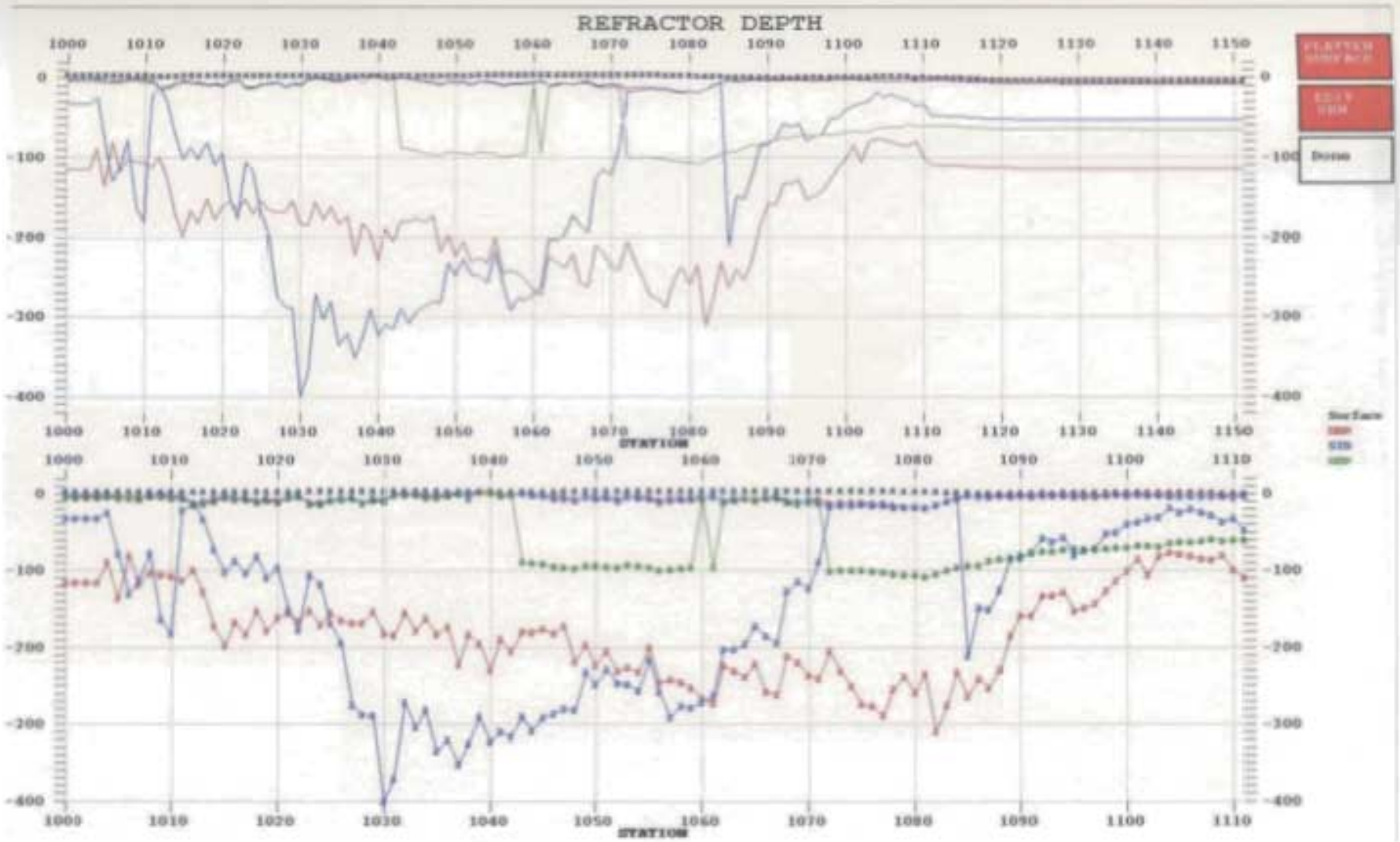

Figure 4.9b. Diagram of the depth model generated from the velocity model for 2 layer refraction statics analysis, note the DRM values (red) correspond to the refraction statics algorithm being used.

Figure 4.9c. Diagram of receiver static shifts generated from the velocity and depth models, again the DRM method is represented in red.

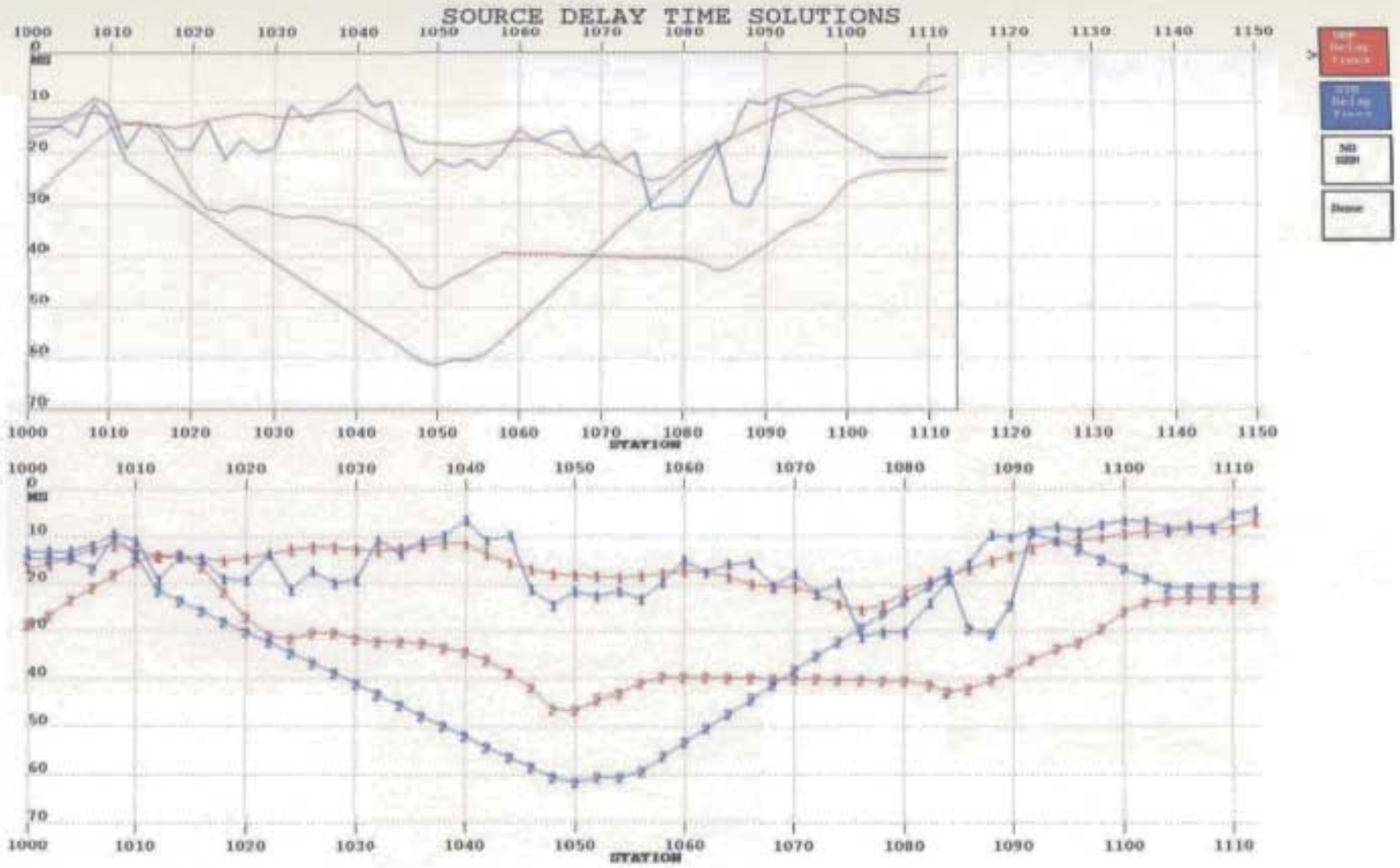

Figure 4.9d. Diagram of source static shifts calculated from the velocity and depth models, again the DRM values are in red.

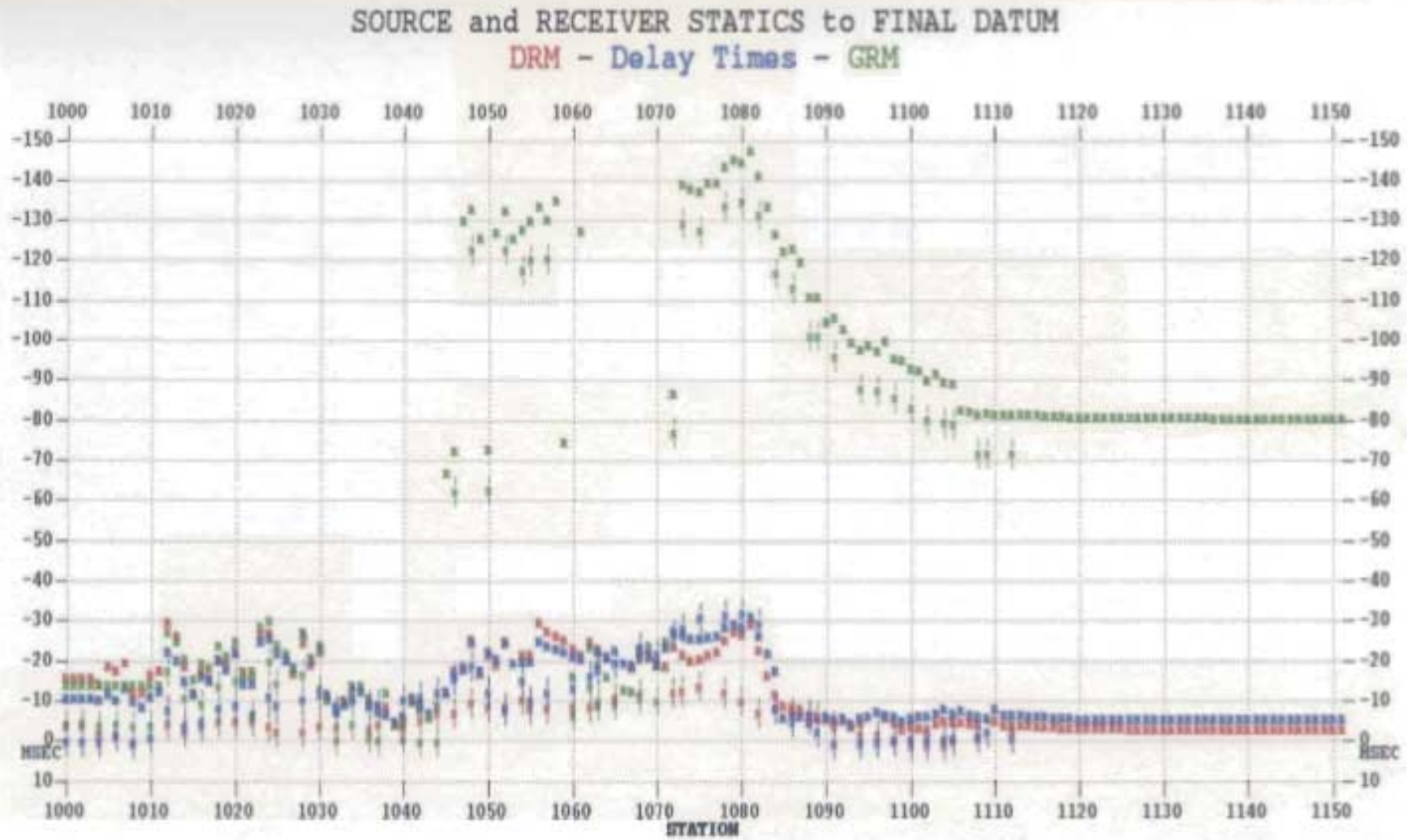

Figure 4.9e. Diagram of the final source-receiver static shifts.

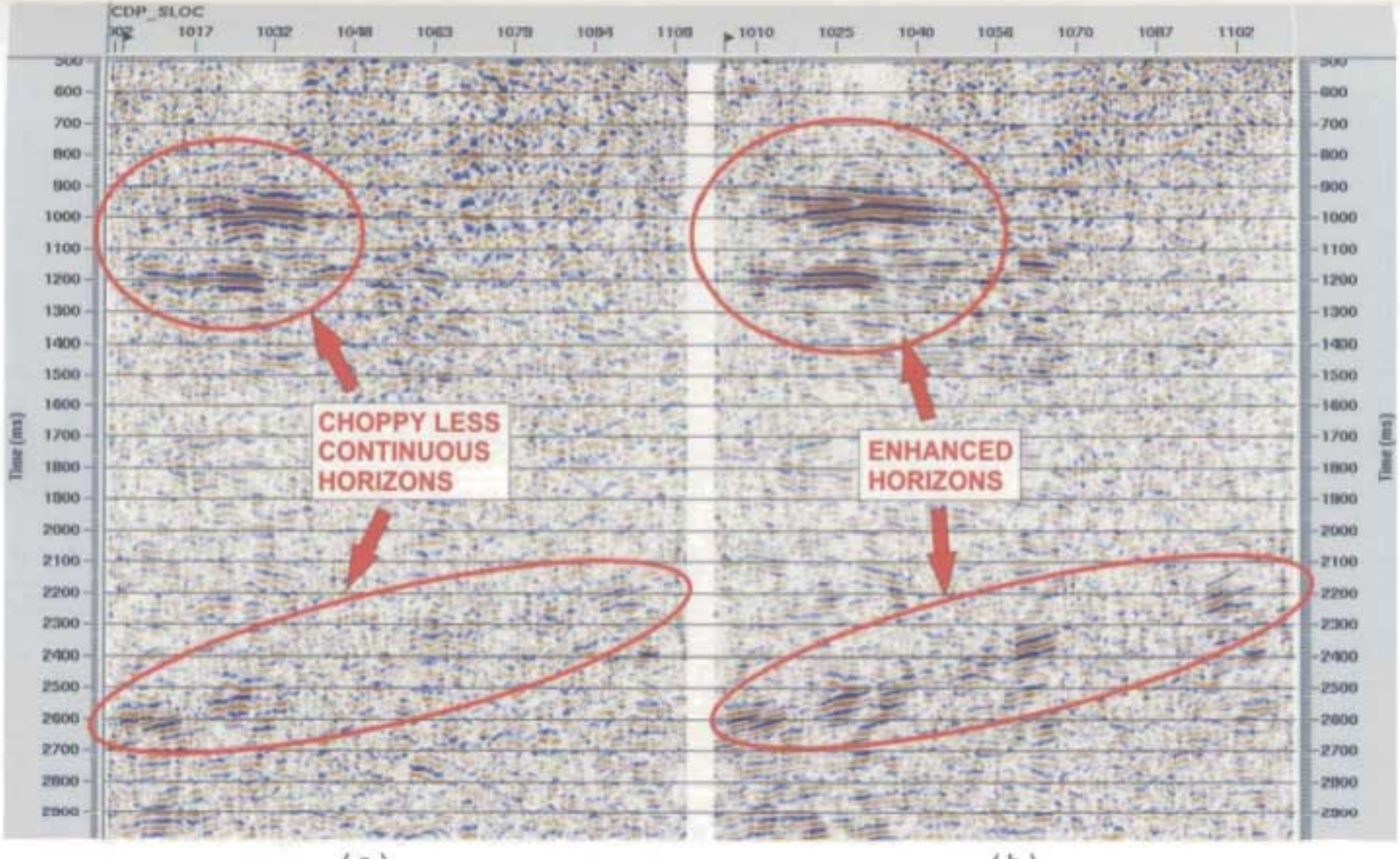

(a) (b)

Figure 4.10. (a) Structural stack without refraction statics. (b) Same structural stack with refraction statics applied.

4.3.5 Frequency – Wavenumber (FK) Analysis

The goal of FK analysis is to remove systematic noise signal from the seismic dataset. FK analysis allows the processor to simultaneously view both T-X domain data adjacent to F-K domain data for editing purposes. ProMAX® applies an FK filter which internally transforms the data to the F-K domain from the T-X domain using a two-dimensional Fourier Transform. FK filters are designed to either pass or reject the selected portion of the FK spectrum. Typical polygon filters can be interactively designed on a record to reject the specific area of noise in question.

For the current data interactive polygons were designed. Each record was viewed separately as the polygons were modified as needed to remove the low frequency noise and any aliased signal. The following figure (Figure 4.11) displays both the T-X and F-K spectrums for a representative gather, the figure is annotated showing the reject polygon area, aliased data, low frequency noise and seismic signal. Figure 4.12 is a shot record post FK filter, it is clear from the FK spectrum that the area within the reject polygon has been removed. The T-X domain shot record is visibly cleaner with less noise and more continuous signal.

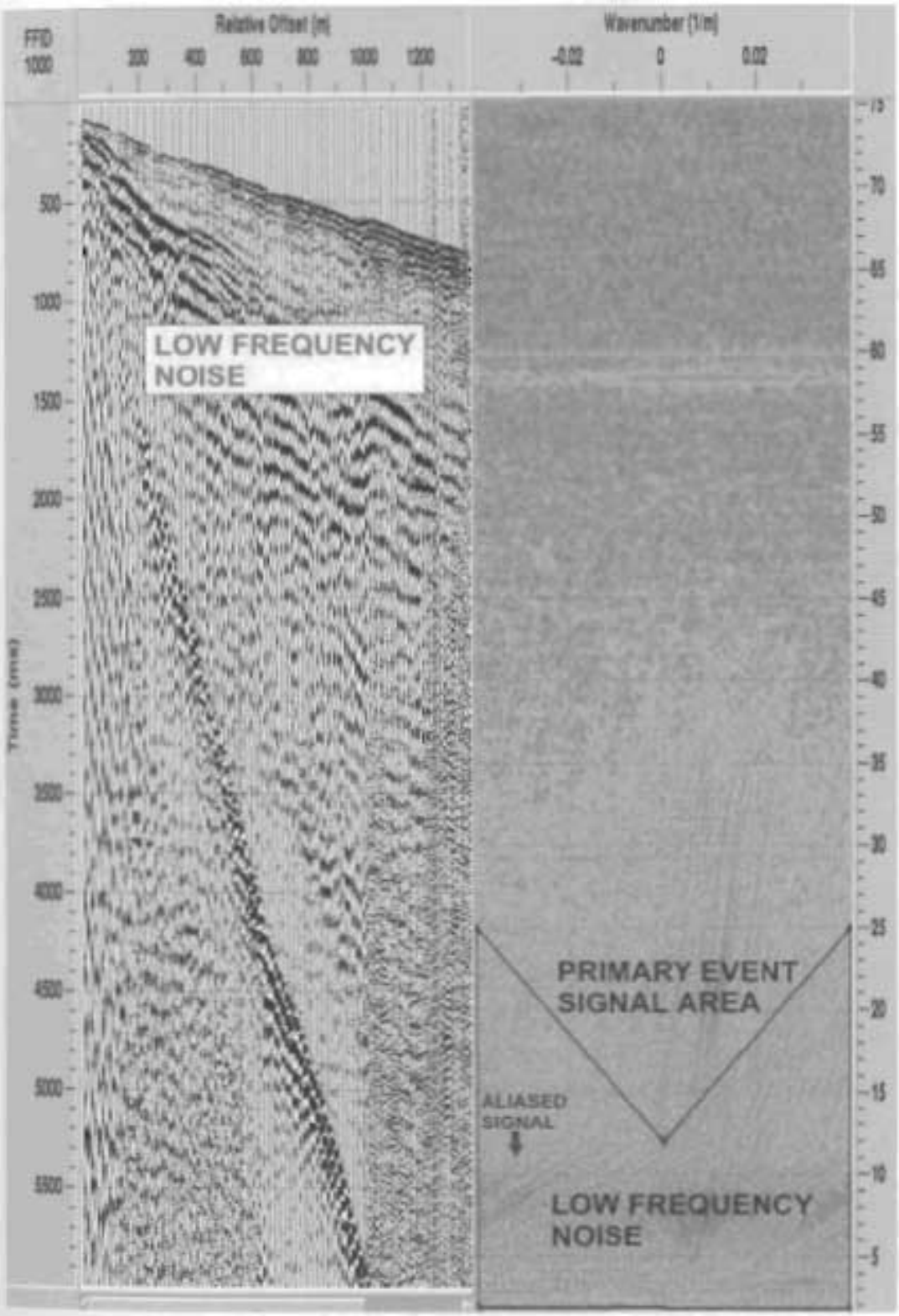

Figure 4.11. A typical land shot record with is corresponding FK spectrum, both prior to application of the FK filter.

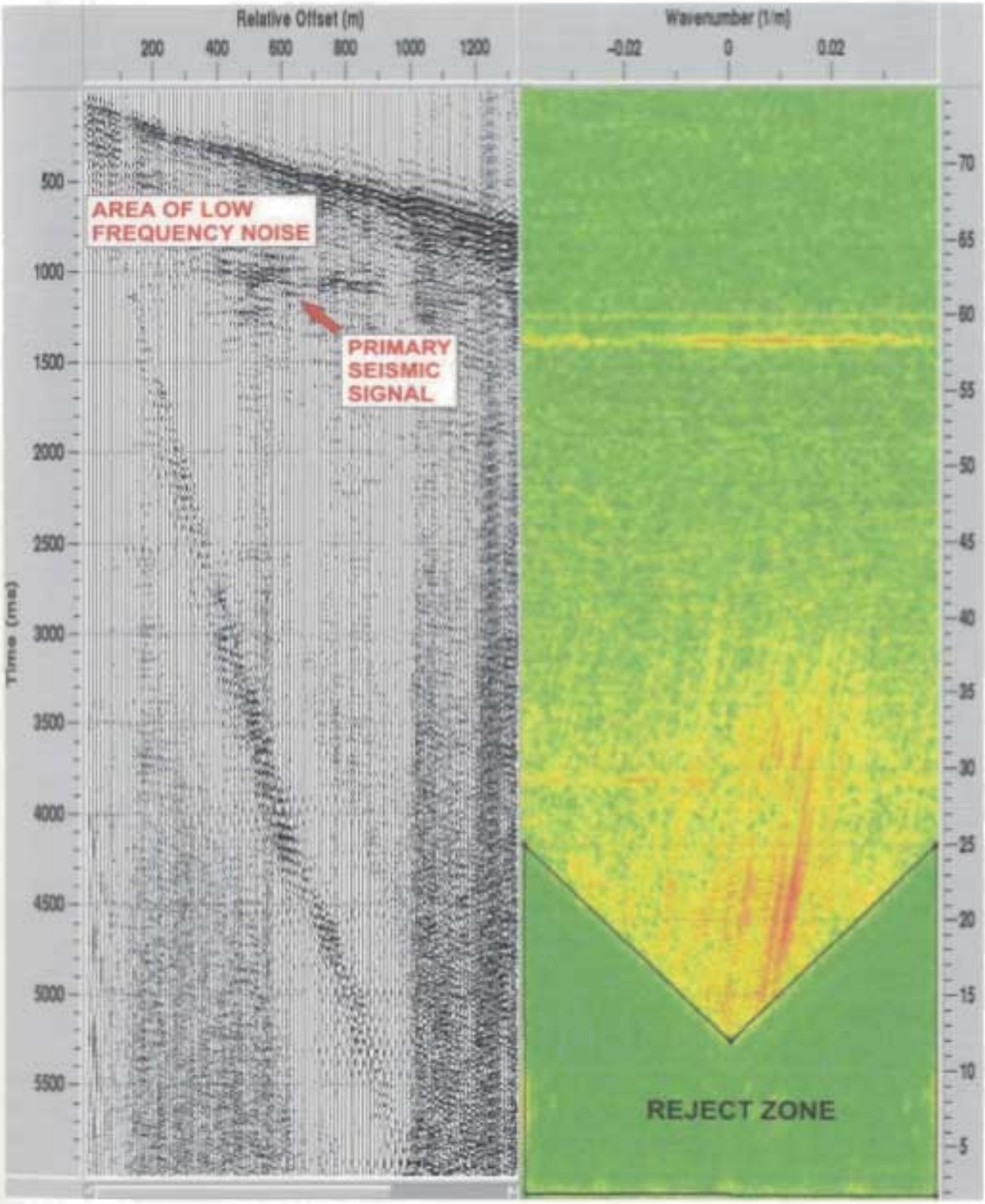

Figure 4.12. The same shot record as 4.11 but now the FK filter has been applied.

4.3.6 Pre-stack Top Mute / Surgical Muting

Muting can consist of various forms such as top muting, bottom muting and surgical muting to name the most common. Top mute design is focused on removal of the direct arrivals and any refracted events in the upper section of the record (Figure 4.13). Trace muting can be considered the exclusion of specific zones of seismic data selected on the traces in the time domain. Pre-stack top mute zones were defined interactively and applied to the dataset on a shot by shot basis. The use of surgical muting was primarily for the removal of high amplitude air blast in the lower portions of the shot data (Figure 4.13). Again this was designed interactively and picked individually for each shot record as required.

4.3.7 Scaling

The introduction of amplitude scaling to the data is crucial for compensation and gain adjustment of the seismic signal. As the signal spreads and travels through the earth, the wavefront expands and energy is dissipated. The implementation of a correct time-variant scaling technique helps improve the signal content in the lower half of the shot records, enhancing the overall signal levels.

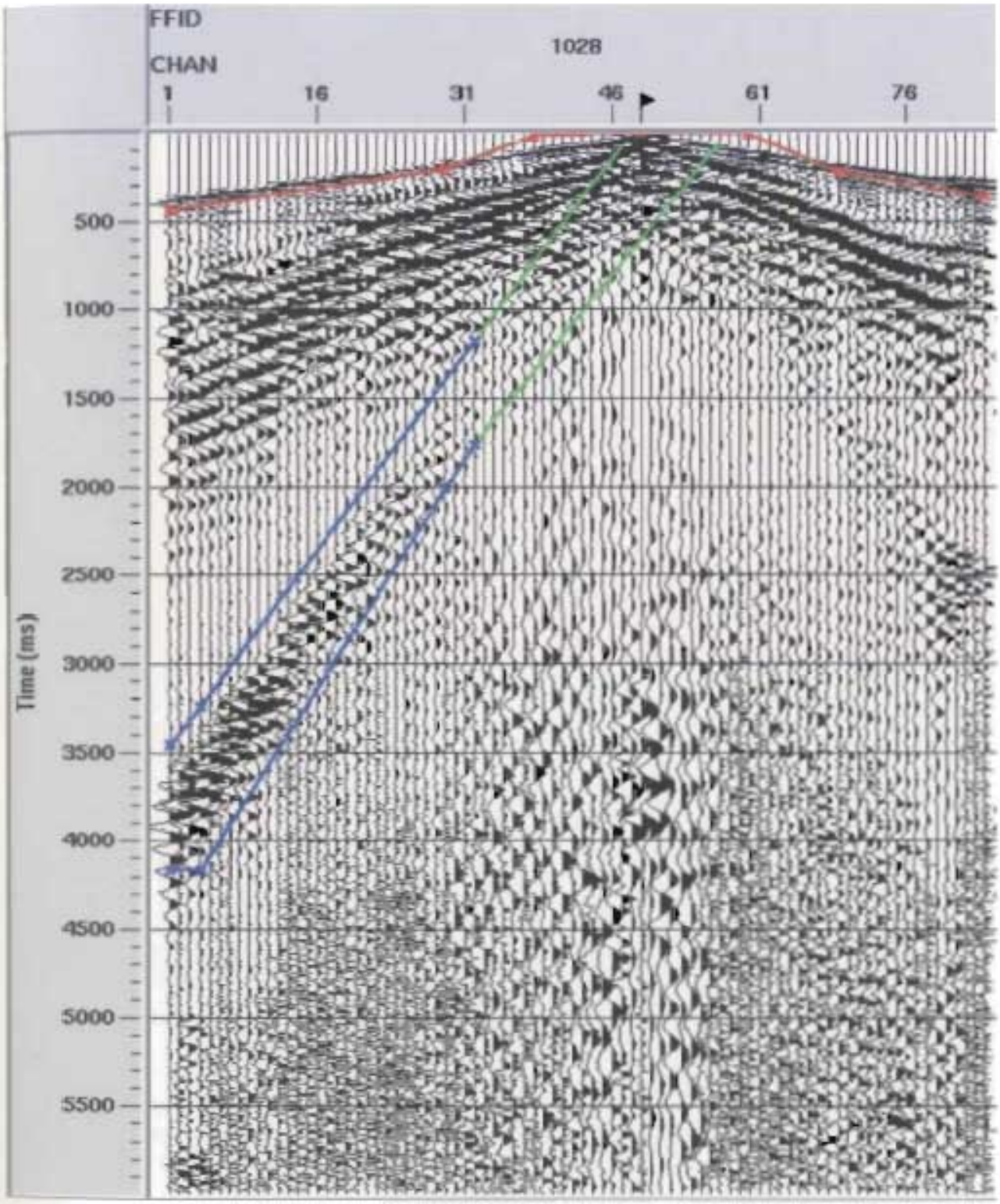

Figure 4.13. A typical land shot record showing the location of the pre-stack top mute (red) and surgical mute (green and blue).

Two dominant effects on a propagating wave field that account for the visible decrease in seismic signal characteristically seen with the increase of TWT on all shot records are:

1. In homogeneous media energy density decays proportionately to $1 / r^2$ (spherical divergence), where r is the radius of the wavefront (Yilmaz, 2001). i.e. deeper signal penetration equals an increase in r and a decrease in energy density.

2. Frequency content of the original signal changes in a time-variant manner such that high frequencies are absorbed more rapidly by the media than low frequencies (Yilmaz, 2001). This directly results in lowered resolution capabilities with time / depth.

The gain function for geometric spreading compensation is (Yilmaz, 2001):

- $g(t) = v^2(t)\, t / v_o^2\, t_o$ (4.2)
- v_o = the velocity at a specified time t_o

A correction for spherical divergence was applied as an amplitude equalization method. Figure 4.14 is an example of shot data before and after application of the scaling. This clearly demonstrates the effects of correct scaling on the overall signal character.

4.3.8 Trace Equalization

The primary effect of trace equalization is the removal of any spurious bursts of signal missed during editing and the overall adjustment of traces to a similar rms amplitude level (Yilmaz, 2001). Different from the gain scaling functions described above, trace-balancing functions are time-invariant typically using rms or mean amplitude criterion for correction.

4.3.9 Deconvolution

Conventionally applied pre-stack, the goal of deconvolution is to improve temporal resolution by collapsing the seismic wavelet to a spike and the suppression of signal reverberation (multiples). Spiking deconvolution is used predominantly for spectral whitening while predictive deconvolution compresses the seismic wavelet attenuating reverberations and short period multiples (Yilmaz, 2001). The presence of multiples in this data is questionable and difficult to identify due to data quality and noise levels. Therefore testing of the current data involved consideration of both spiking and predictive deconvolutions.

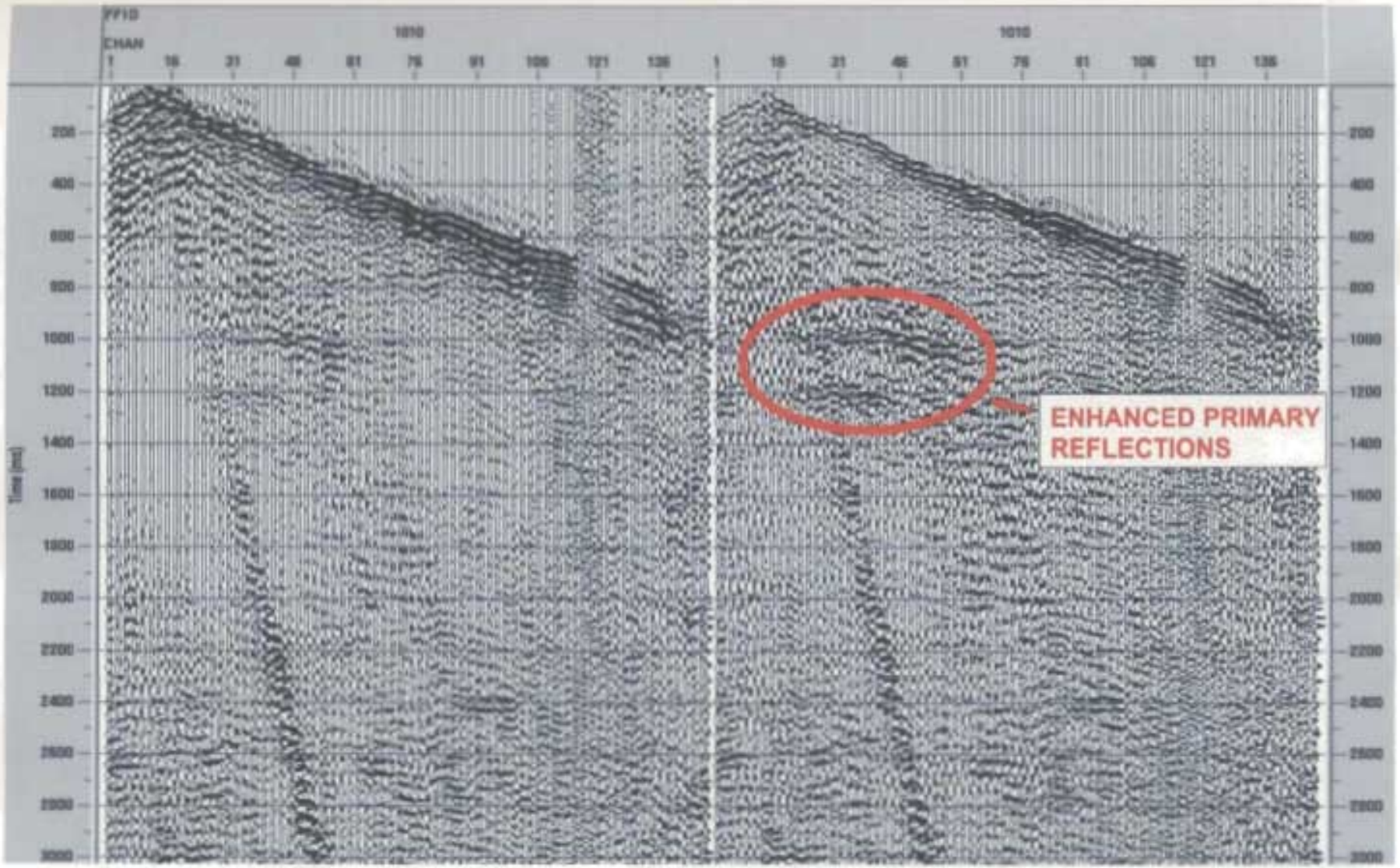

Figure 4.14. (a) A land shot record prior to correction for spherical divergence gain function. (b) Post gain the same shot is now more even in signal content and the carbonate platform reflections are enhanced.

Generally an autocorrelation function (ACF) display representing a zero-phase time series will indicate the location of coherent multiple reverberation while limiting the influence of random noise. Selection of a prediction lag / gap from the first or second ACF zero crossing followed by selection of the operator length defining the area selected for whitening is the rule of thumb. The following tables list gap and length times that were tested for both deconvolutions.

Table 4.1: Predictive deconvolution gap-testing parameters.

Type of Deconvolution	Operator Length (ms)	Gap Test Lengths (ms)
Predictive	128	8
		16
		32
		64

Table 4.2: Predictive deconvolution operator length testing parameters.

Type of Deconvolution	Operator Length (ms)	Gap Test Lengths (ms)
Predictive	64	64
	96	
	128	
	256	

Table 4.3: Spiking deconvolution operator length testing parameters.

Type of Deconvolution	Operator Length (ms)
Spiking	8
	16
	32
	64
	128

Figure 4.15 shows a series of deconvolved shot gathers used during processing for the testing of the above parameters. Attention was focused on the platform reflectors and the deconvolution operator's ability to enhance those reflectors while improving the appearance of the overall record. Careful comparison of both techniques indicated that the application of a predictive deconvolution with a gap of 32ms and an operator length of 128ms yielded the best results.

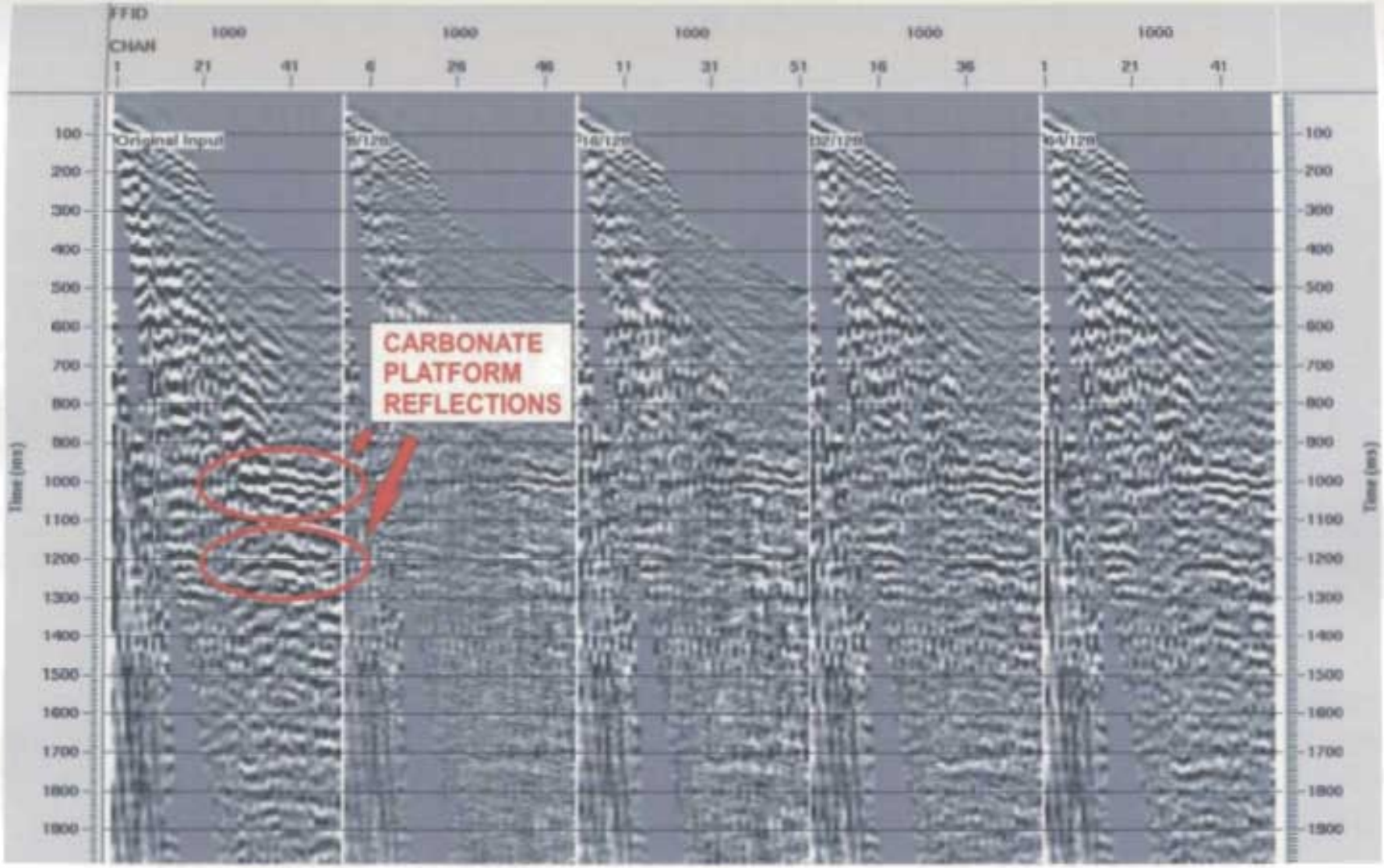

Figure 4.15. Deconvolution test panels demonstrating the effect of various gaps on shot record data. The annotated reflectors in the area of 1000ms and 1200ms are of primary interest.

4.3.10 Velocity Analysis / NMO Correction

In a true zero offset situation, the need for velocity analysis would be moot as there is no hyperbolic moveout (NMO) and traces will inherently stack constructively increasing the signal to noise (S/N) ratio. But, in most seismic exploration the increasing offset distances between the source and receivers generates a hyperbolic reflection pattern with increasing normal moveout at larger offsets. In this situation if stacking where attempted the traces would add in a deconstructive manner and reduce the S/N ratio. Testing to find the correct velocity is important as selecting too slow a velocity will generate an excessive amount of NMO correction pulling the event past horizontal into an upward curve (Figure 4.16c). Conversely too fast a velocity will leave the event hyperbolic (Figure 4.16d), either scenario will result in deconstructive stacking of the signal.

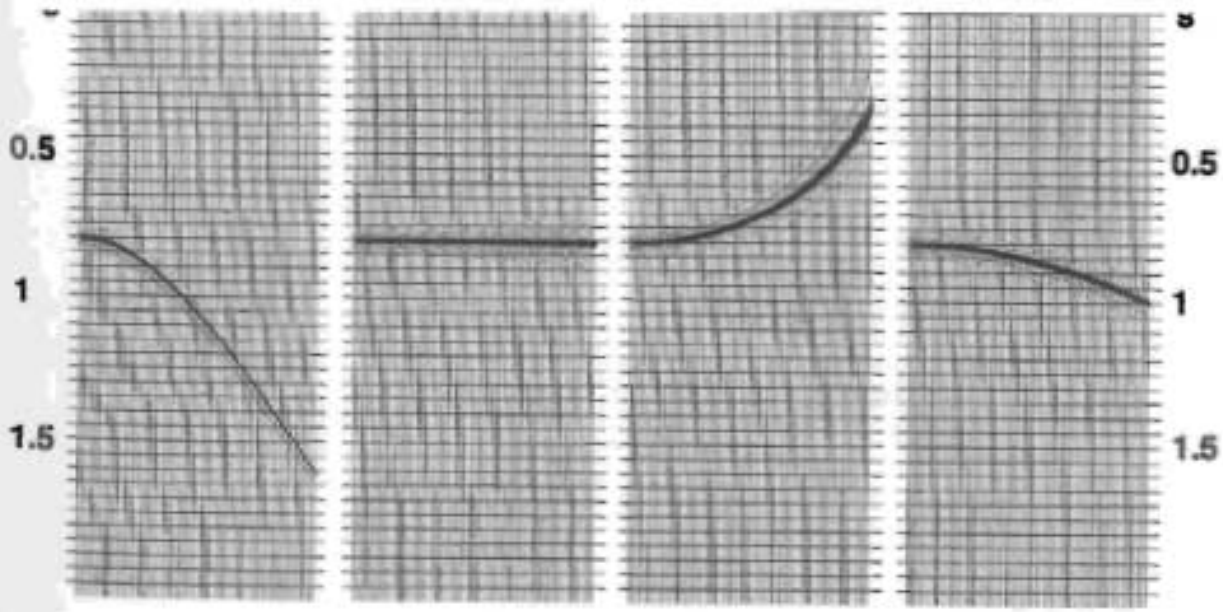

Figure 4.16. (a) (b) (c) (d)

Figure 4.16 shows different NMO results from slow, fast and correct velocity picks. (a) is an uncorrected hyperbolic reflection. (b) is the reflection NMO corrected using the proper velocity. (c) is the reflection NMO corrected using too slow a velocity. (d) is the reflection NMO corrected using too fast a velocity.

Velocity analysis followed by NMO correction is possibly the single most important step in the sequence of seismic data processing prior to stacking. Normal moveout is defined by Yilmaz (2001) as the difference between the two-way travel time for a specific reflector at a given offset and the two-way travel time at zero offset.

$$NMO = t - t_o \qquad (4.3)$$

Consider the travel time equation for a horizontal reflector as a function of offset.

$$t^2 = t_o^2 + x^2 / v^2 \qquad (4.4)$$

x = source-receiver offset

v = velocity (average velocity of the reflector)

t_o = zero offset time

t = travel time

Insertion of the correct velocity into equation 4.4 allows calculation of the normal moveout. This value can then be applied to the seismic data correcting the data to that for zero offset, thus allowing for constructive stacking and signal enhancement.

A conventional velocity analysis using semblance displays, offset gathers and velocity function stacks was used to interactively pick the subsurface velocities. The function of the semblance analysis is to measure the coherency of the signal along the hyperbolic trajectory of the reflection (Yilmaz, 2001), denoting the location of maximum coherency and ideal velocity on the velocity spectrum as an anomalous high "bulls eye".

Velocity analysis was performed along the Shoal Point line at 250m intervals using offset sorted super gathers created by summing 7 adjacent CDP's around the selected analysis location.

Figure 4.17 is a typical interactive velocity analysis display. The overall quality of the semblance spectrum is obviously not ideal, but using information from previous seismic exploration data (Hunt et al., 1996) combined with geological knowledge of the area appropriate velocity functions were picked.

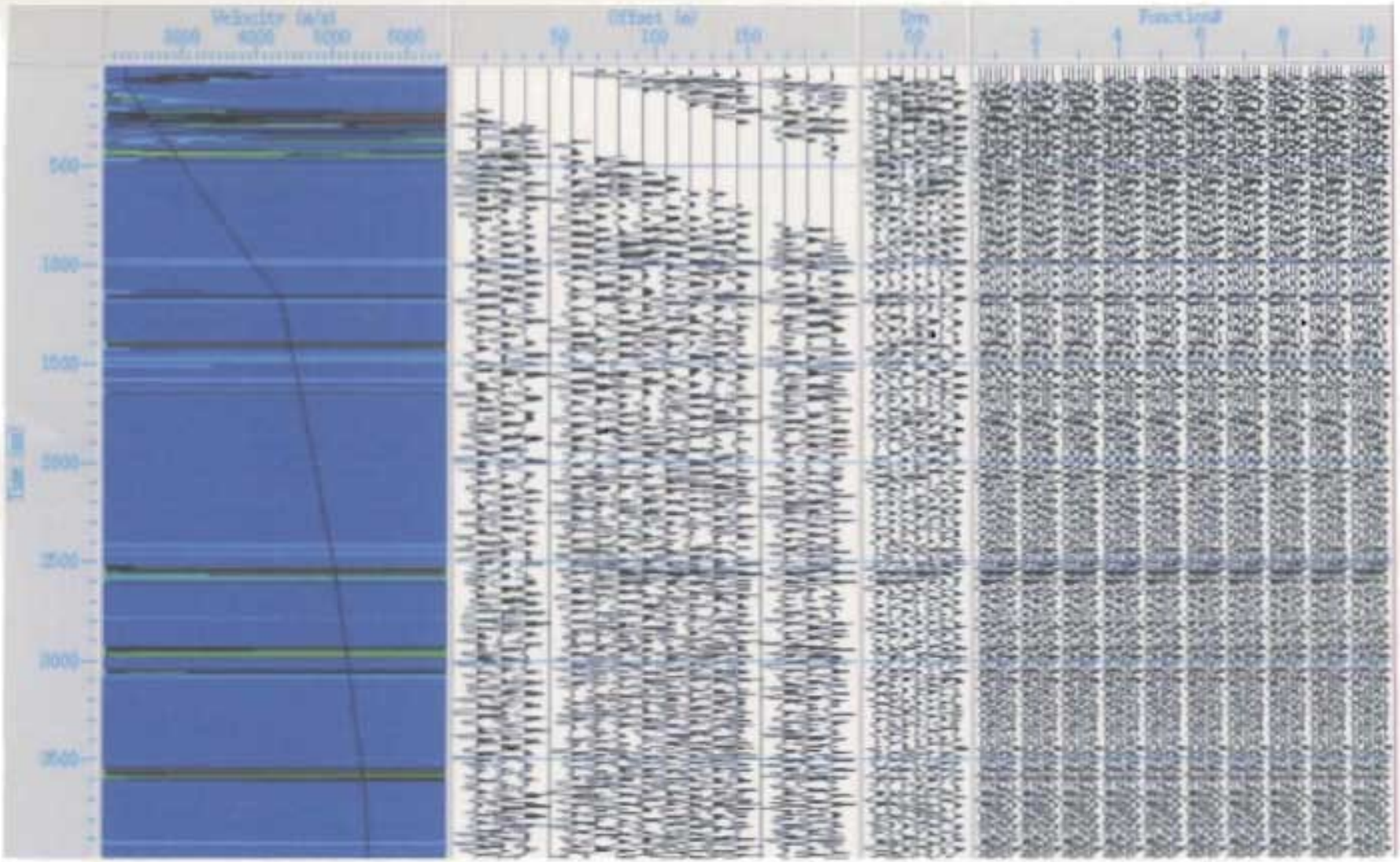

Figure 4.17. Typical semblance velocity analysis display containing the semblance plot, the super gather and velocity function stack panels. The picked velocity function is visible on the spectrum in black.

4.3.11 Post NMO Stretch Mute

Stretching of the seismic wavelet is unfortunately an unavoidable characteristic of correcting large-offset reflection signal for normal moveout. Particularly for shallow events with large-offsets the normal moveout correction may result in excessive wavelet stretching. This distortion of frequency characteristics then renders the signal inappropriate for addition in the stacking process. Yilmaz (2001) quantifies wavelet stretch as:

$$\Delta f / f = \Delta t_{nmo} / t_o \qquad (4.5)$$

f = dominant frequency

Δf = the change in frequency

Δt_{nmo} = NMO correction

t_o = zero offset time

Removal of this problem is accomplished by muting of the stretched zone in the CDP gathers. Stretch mutes can be applied both automatically and manually. Automatic muting uses equation 4.5 to numerically quantify the amount of wavelet stretch, which can then be expressed as a percentage of the overall possible limit. This allows the processer to then specify for the desired amount of wavelet stretch. In this case I have allowed for 30% NMO stretch to the data (Figure 4.18). Conversely the mute may be selected interactively by the

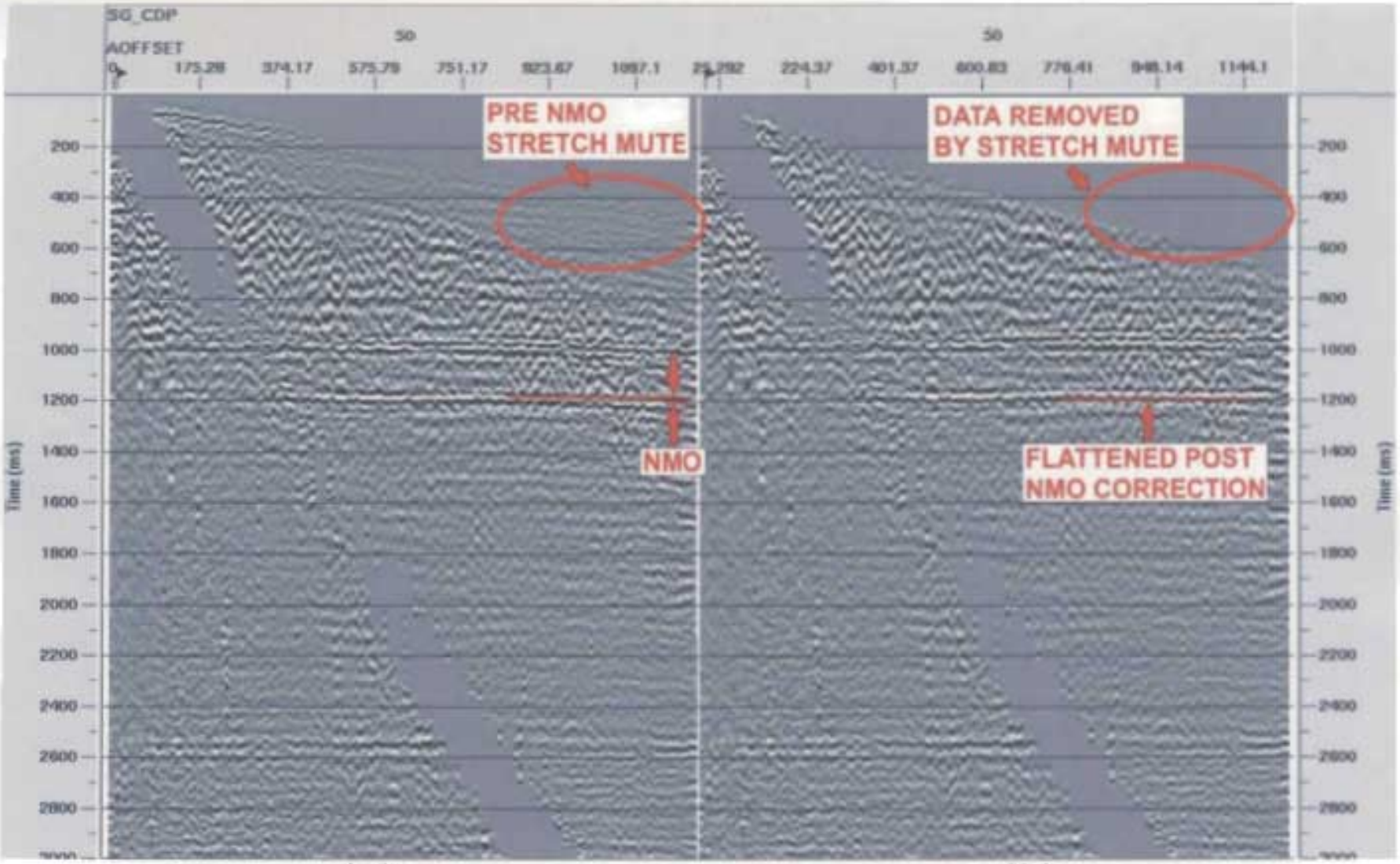

(a) (b)

Figure 4.18. (a) CDP supergather of the land data prior to NMO correction, note the slight hyperbolic moveout on the far offset channels of (a). (b) The same CDP supergather post NMO, note the reflectors are now flattened to horizontal.

processer allowing for a more reliable mute application in certain processing situations.

4.3.12 Residual Statics

Application of residual statics correction is one final alignment of the seismic trace data. Using the ProMAX 2D Maximum Power Autostatics, the residual static shift was calculated by maximizing the CDP stack power. Autostatics horizons were interactively picked on the stacked section (Figure 4.19). These picked locations are then used for the final calculation of residual statics. The effect of residual static trimming can be dramatic and generally is able to line up coherent reflections, making interpretation and correlation easy and more reliable. Figure 4.19 compares the 2D structural stack before and after application of the final residual statics. The carbonate platform reflectors show the most visible correction and shifting of the trace data after application of the residual static shift.

4.3.13 CDP Stacking

Following correction for normal moveout the seismic reflections are ready for CDP stacking. Stacking can be considered a summing of trace data at varying offsets to a single trace mimicking a zero-offset signal.

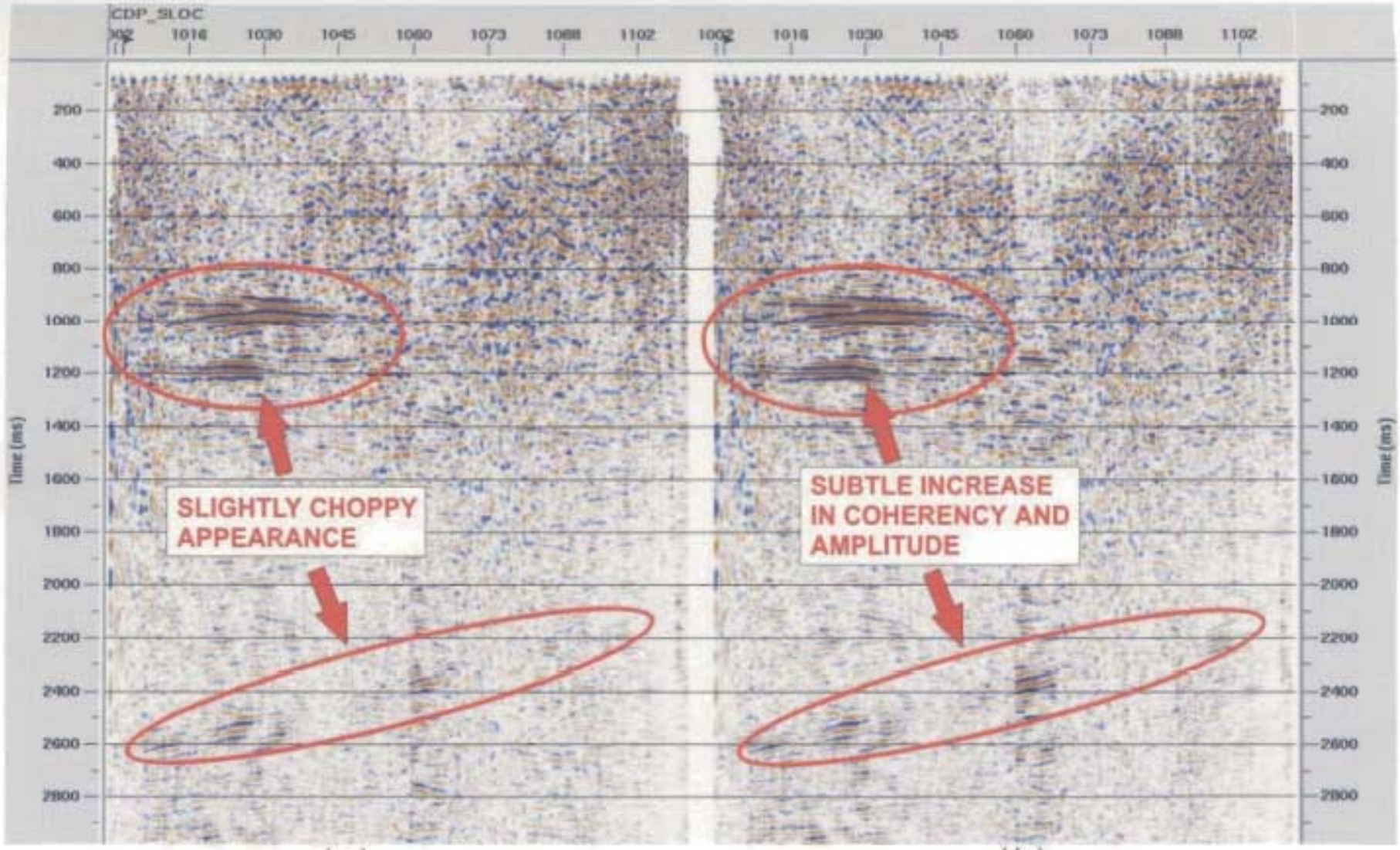

Figure 4.19. (a) the 2D stack prior to application of residual trim statics. (b) the 2D stack post application of residual trim statics. The overall enhancement of the product (b) is subtle but an improved stack is the result.

The effect of this process is primarily to increase the signal to noise ratio and render a true zero-offset section.

For the current dataset a max / min CDP stacking process was selected. This function searches and removes the samples with the highest and lowest amplitude from the stack; one final step in removing any spurious amplitude spikes or non-representative lows.

4.4 2D Processing Conclusion

Overall processing of the Shoal Point 2D landline went well considering the data quality and the structural complexity of the area, producing an acceptable seismic image of the subsurface geology. The final processing flow chart that was applied to the data is shown in figure 4.20. The Cambro-Ordovician carbonate platform (1000ms – 1200ms TWT) is properly imaged as a continuous north-dipping horizon corresponding to regional seismic and geological data. The deeper strong events I have interpreted as internal reflectors of the Grenvillian basement (Figure 4.21). A more detailed interpretation of the 2D landline will follow in Chapter 6, Interpretation.

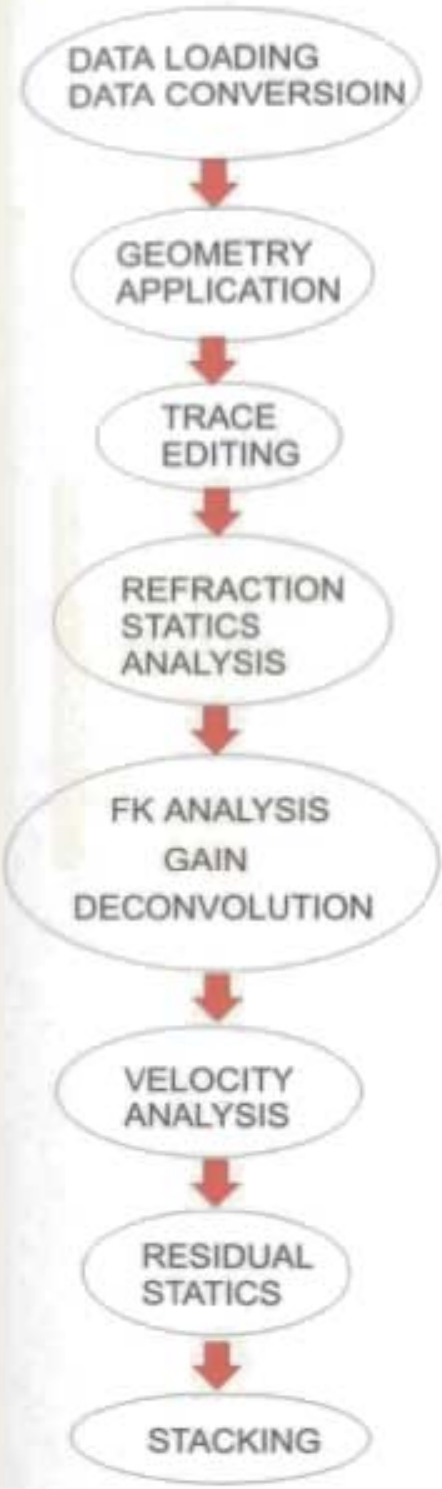

Figure 4.20. Flow diagram showing the processing steps used on the 2D data.

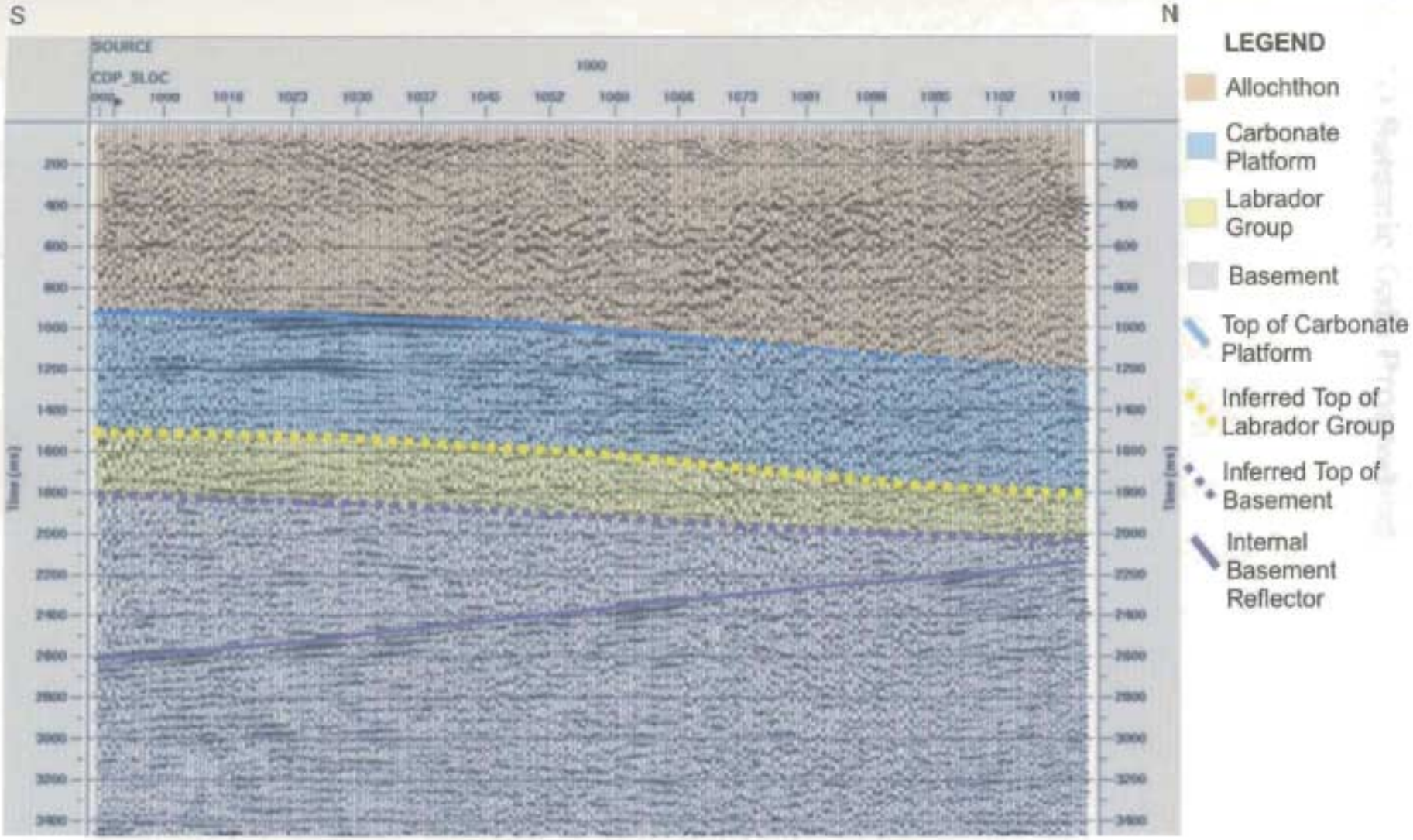

Figure 4.21. Shoal Point 2D structural seismic stack.

5.0 3D Seismic Data Processing

As discussed in Chapter 3, 3D acquisition generated a non-conventional 1591 record 3D seismic data volume. Again the following processing was completed with accomplishment of the initial project goals in mind.

- To demonstrate a novel and cost-effective technique to acquire, process and interpret 3D data in a shallow water transition zone.
- To develop a better understanding of the complex geology and tectonic history of the area.
- To provide a seismic image at the Shoal Point K-39 well location.
- Create a 3D mapped surface to the top of the Ordovician carbonate platform.

Correct processing is necessary to achieve the best dataset for interpretation and completion of the 3D surface maps.

5.1 Processing Overview

Three-dimensional (3D) seismic data processing is in many situations handled similarly to 2D seismic data processing, but overall 3D processing can be much more time consuming and computationally intensive resulting from the larger data volume. 3D data processing involves the consideration of various additional

techniques specific to the 3D realm. Processing considerations in areas such as binning and construction of a 3D velocity model for NMO correction are the processes requiring more extensive analysis during 3D parameter testing. Intuitively the data quality is paramount; it is the overall determining factor of the relevance / reliability of the final seismic product. As one would expect, working with data affected by various quality issues and data limitations increases the difficulty and length of the testing period and may limit the overall applicability of the output.

As discussed in the preceding chapters the Shoal Point 3D data quality is unfortunately very poor with no short offset information. Such information is key to shallow and near surface imaging of geological structures while maintaining a high level of data confidence. The following discussion will consider the handling of such limitations and how they were overcome to achieve the desired goals stated in the first chapter.

In many situations discussion of some parameters and techniques will be identical to those applied in chapter 4.0, therefore I will limit the discussion of theory for these processes previously discussed and refer the reader to the previous chapter for any further insight.

5.2 3D Data Testing and Processing Parameters

5.2.1 Data Loading

As in the 2D acquisition field file data was recorded in SEG-Y format to 8mm Exabyte tapes. Files were extracted at MUN facilities to UNIX workstations at which point the data was read into ProMAX® and converted to a Landmark proprietary format for data processing.

5.2.2 3D Geometry Assignment

From the start the acquisition of this seismic survey was considered non-conventional and "different". Completion of the acquisition phase resulted in a seismic data volume that cannot be classified as a truly land or marine seismic style and most easily resembles a transition zone survey. The resultant volume is oddly shaped and contains a large area with no data coverage corresponding to the location of Shoal Point. Consideration of the options directed the data geometry assignment to that of a 3D land data volume.

Marine shot positions were recorded in UTMs using a DGPS system onboard the seismic vessel which was time-synced with the onboard firing system for consistent timing. Both the marine source positions and the receiver geophone positions were converted to ASCII files and loaded in to the ProMAX geometry

spreadsheets where they were then merged with the seismic data. The following figure shows the positions for shot lines (black) and receivers (white), note that the layout corresponds well with the desired acquisition designed in the preliminary stages.

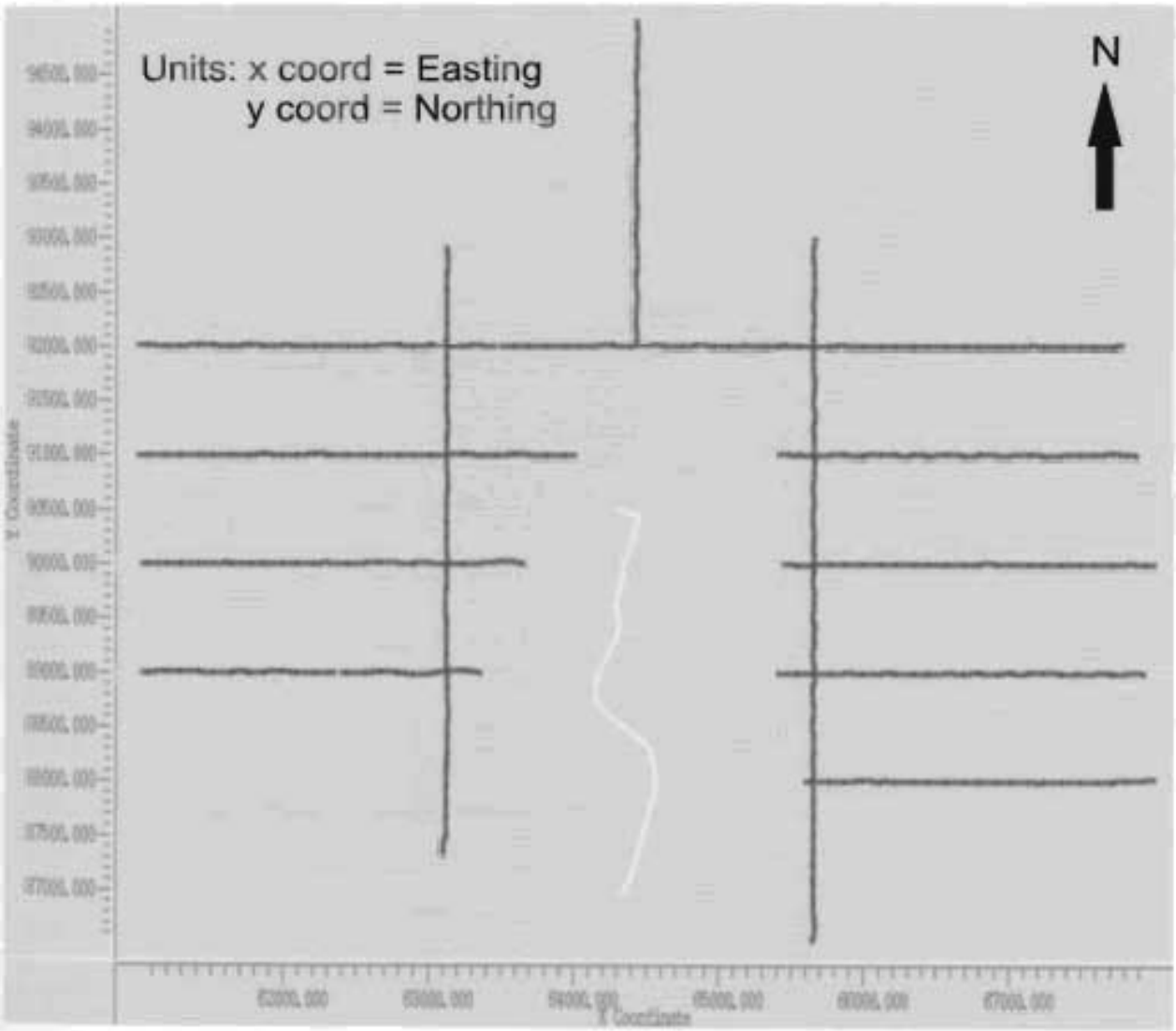

Figure 5.1. Shotpoint and receiver map for the Shoal Point 3D acquisition.

5.2.2.1 Binning

Unlike the 2D crooked line case, we are not working with one line of bins designed to follow the receiver spread. For 3D processing a parallelogram is generally designed to cover the entire area of data distribution such that all data points are included. This rectangular shape is then divided into CMP bins of specified dimensions that best fit the parameters and limitations of the data. In general the rule of thumb is that bin spacing is equal to half the receiver spacing in the inline direction and half the receiver line spacings in the crossline (xline) direction. Considering the non-conventionality of the survey these rules will not hold and a variety of binning strategies were tested:

E-W N-S

1. 50m x 50m
2. 25m x 25m
3. 50m x 25m
4. 50m x 12.5m

The binning selection is a direct trade off between seismic resolution and seismic smearing of the data. The determining factor when deciding on the size of CMP bins is the bin fold. Specifically what is the minimum fold and how is this fold pattern distributed across the dataset. Small bin sizes generate a more accurate representation of the seismic response at that specific location, but will generally

have low fold and therefore may display poor signal content degrading the resolution of the data. On the other hand large bin sizes will contain more CDP points and therefore more signal and possible higher resolution, but smearing of the data when the points are summed can result as they truly represent a wider range of different sub-surface locations and not one specific point.

Final binning parameters selected were 50m in the inline direction and 12.5m in the cross-line (xline) direction (Figure 5.2). These dimensions generated fold levels that varied dramatically across the dataset from low fold bins of 3 or 4 traces to high fold areas with 60 plus CDP traces per bin. On the average the survey bin fold level was on the order of 10. In figure 5.3 a plan view of the survey area shows data fold distribution colored to denote areas of minimum and maximum coverage, this shape was produced solely by the acquisition foot-print.

5.2.3 Trace Kills / Editing

The Shoal Point 3D seismic data was generally of poor quality, with very little signal and excessive amounts of extraneous noise in the gathers. Gathers typically consisted of the 111 land geophones, as use of the transition marsh hydrophones was limited during acquisition to seismic lines 4 west, 6 and 8. The fact that the extra receivers were not used for all lines does not matter because the marsh hydrophones display no signal with continuous noise at each location, consequently they were all killed.

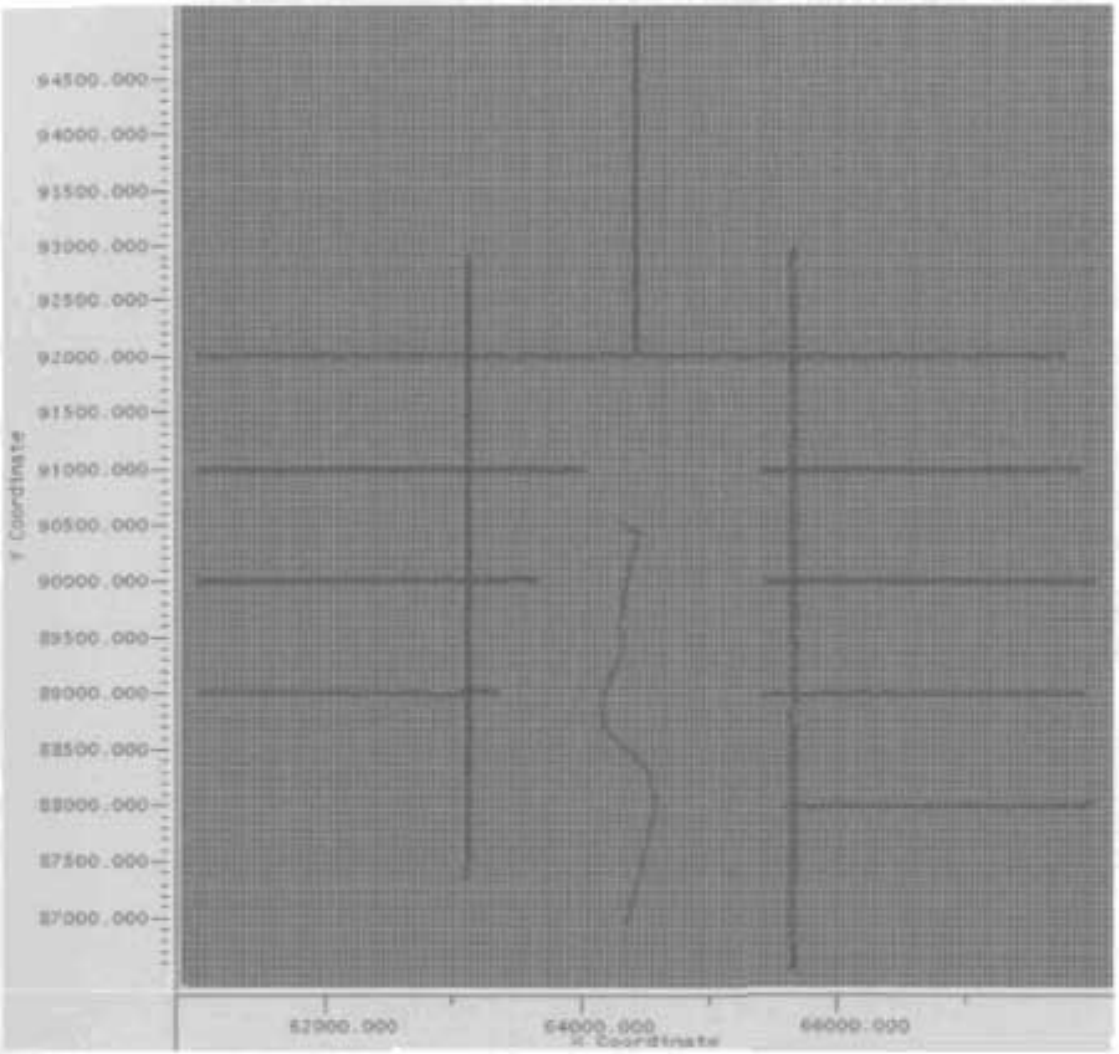

Figure 5.2. Survey shotpoint-receiver map overlain by the 3D binning diagram of 12.5m x 50m bin size.

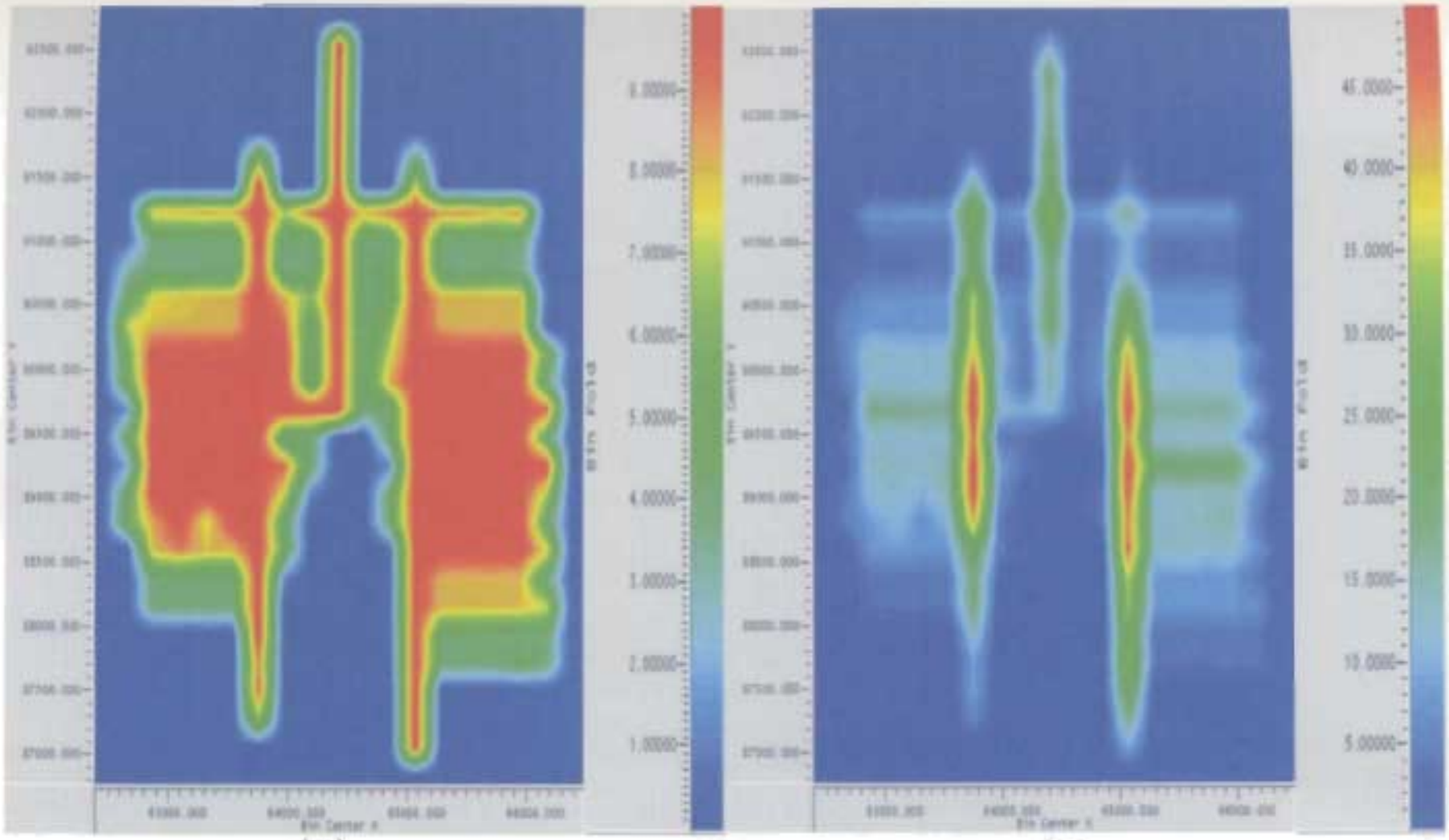

(a) (b)

Figure 5.3. Diagrams of bin fold distribution for the 3D Shoal Point seismic survey. (a) Fold coverage for a maximum display value of 10. (b) Fold coverage for a maximum display value of 50.

The following unfiltered / unscaled shot is representative of a typical marine record with the marsh phones still active. Annotated features include the reverberated first arrivals and various noise trains that are characteristic of the entire dataset.

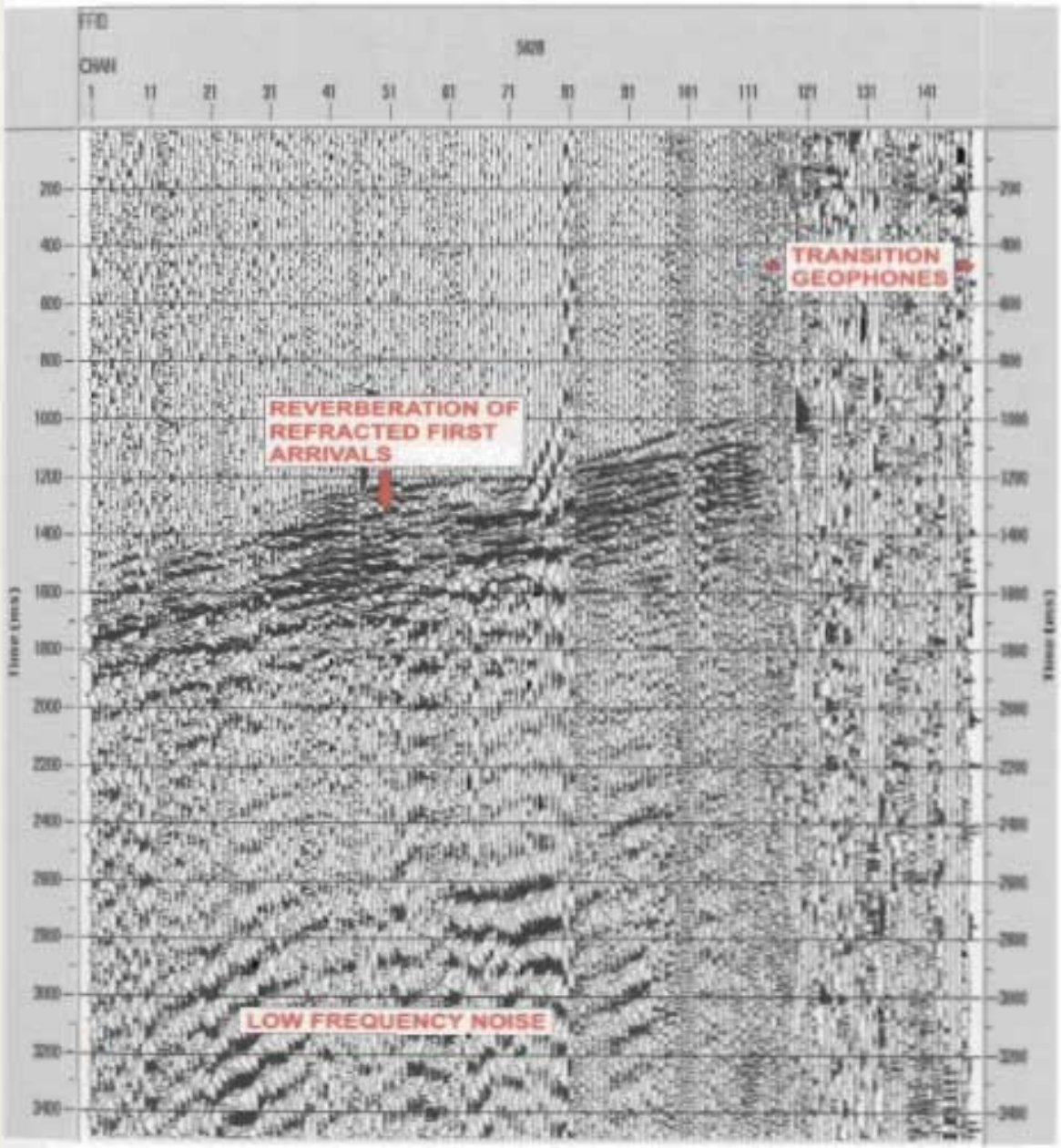

Figure 5.4. Marine shot annotated for characteristic seismic features.

Figure 5.5 is an example of what would be considered the best quality of shot record in the dataset; reflections corresponding to the carbonate platform can be clearly identified in the data.

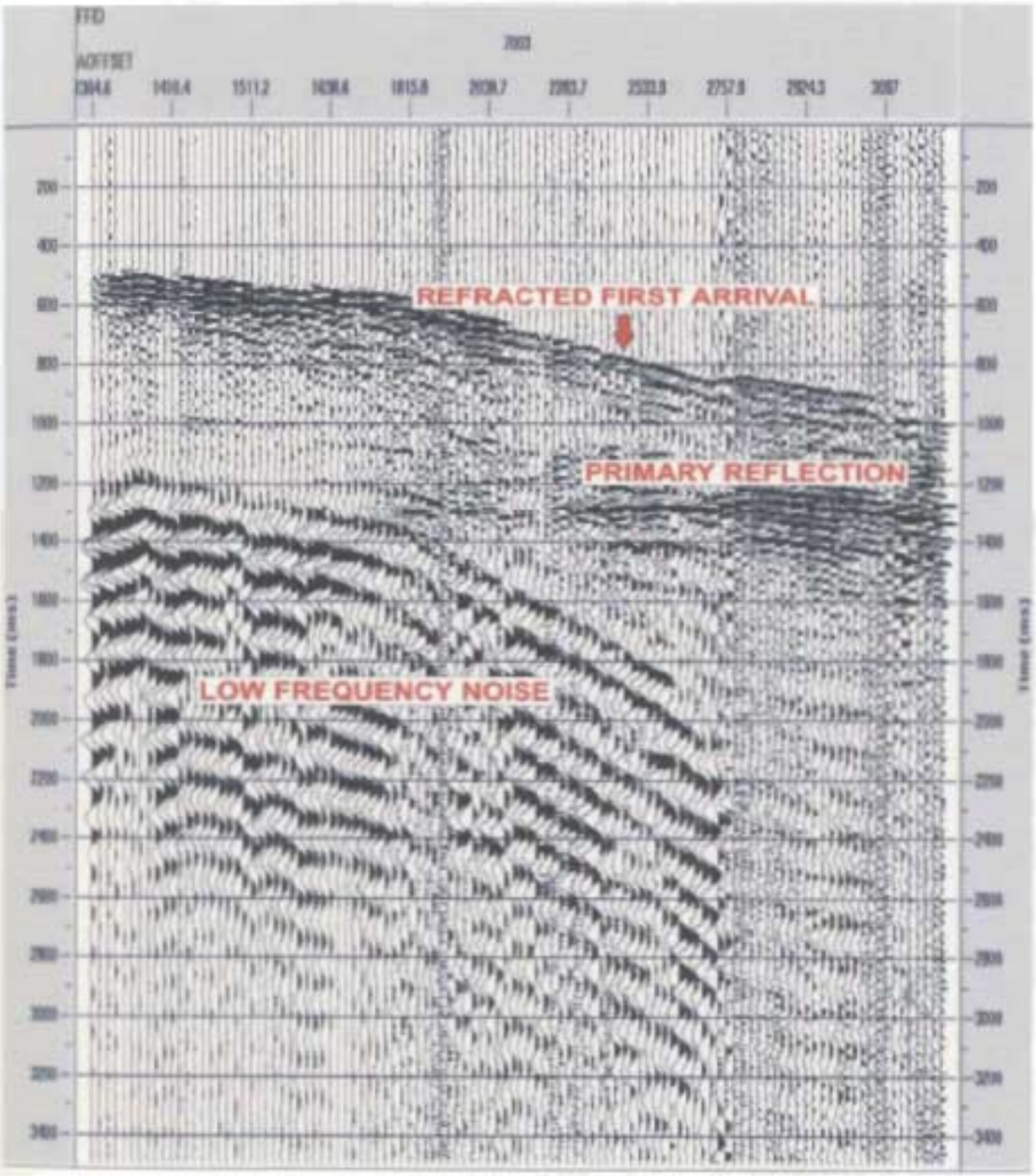

Figure 5.5. Example of the highest quality data recorded for the 3D acquisition.

Frequency content of the 3D marine data was consistent from line to line and was predominantly in the low frequency range. The following amplitude spectrum indicates that the high amplitude frequencies of the data are all lower then 50Hz.

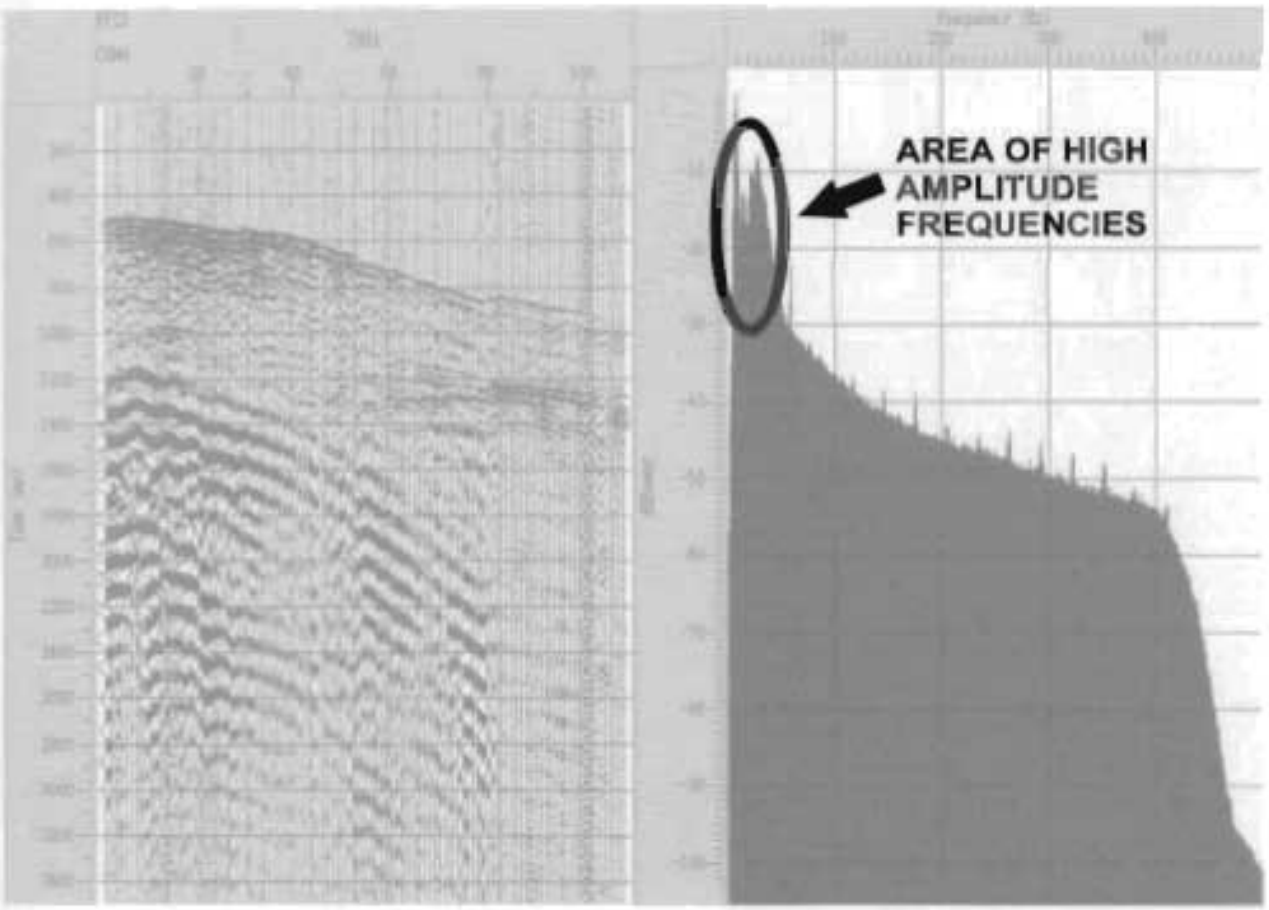

Figure 5.6. Conventional frequency-amplitude spectrum for the marine data.

Considering all of the above information each field file was individually edited to have all noisy traces, dead traces, misfires, signal bursts and noise trains edited. For each shot record channels 45, 101, 102 and 112 – 148 (marsh phones) were

killed along with various interactively picked channels that varied from clean to noisy on a shot by shot basis.

5.2.4 3D Statics Corrections

5.2.4.1 Bulk Shift

A bulk shift correction of -500ms was applied to the entire 3D seismic dataset. This large generic static shift was a correction due to a time delay entered into the ARAM 24 seismic acquisition system affecting all data during acquisition.

5.2.4.2 Hand Statics

The hand statics correction refers to a user defined static shift applied to individual channels correcting for some incorrect time offset. In this case there appears to be a random field time break problem resulting from some miscommunication between the marine firing system and the acquisition recording system. In follow up analysis, this time shift appears to have originated in the firing system. Using a series of random individual common receiver gathers the necessary shift needed for correction of the traces was calculated. I found that in situations where the channel was affected the time shift was always –10ms with respect to the surrounding data. In the following common receiver gather affected traces are annotated and the time shift is clearly discernable.

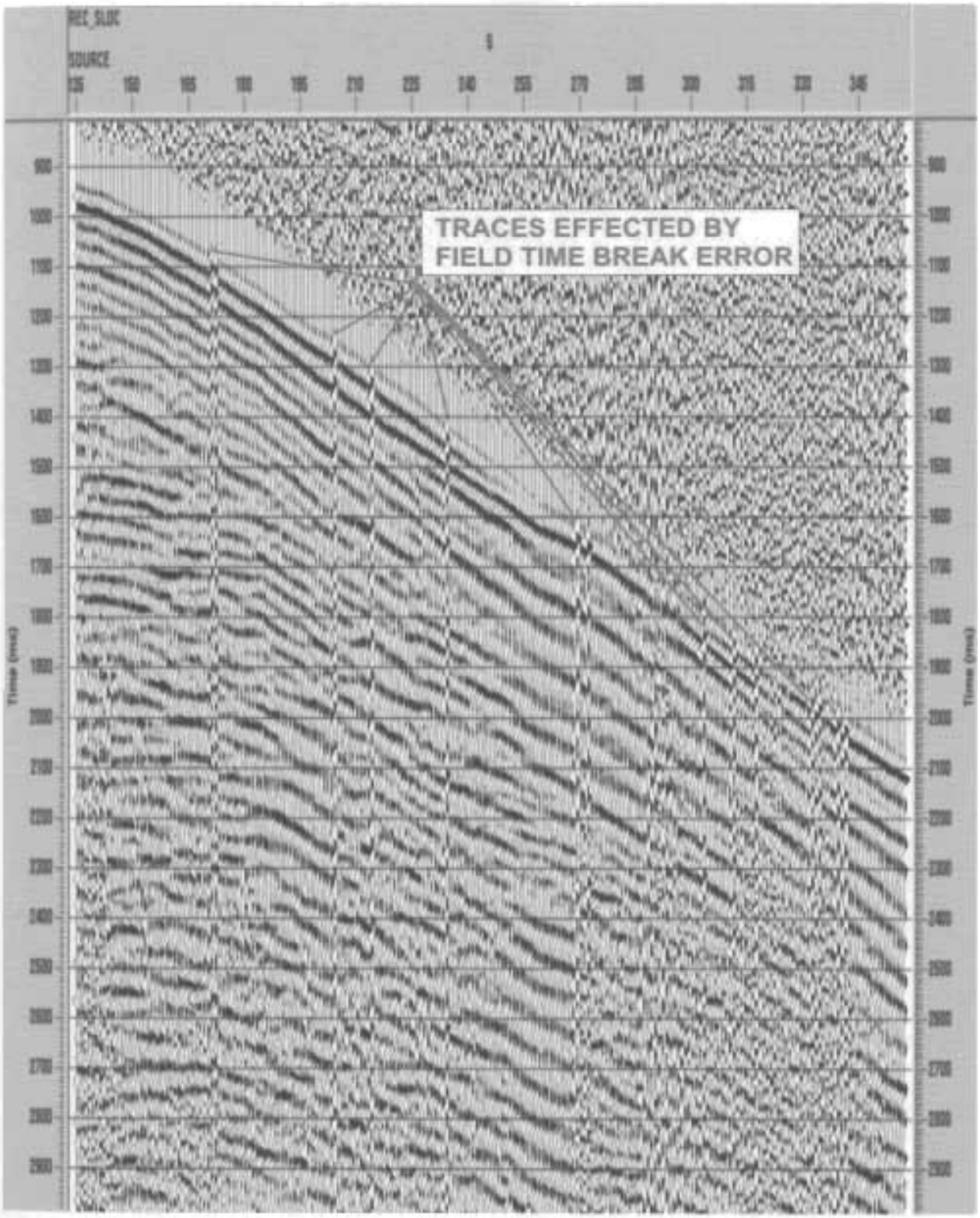

Figure 5.7. Common receiver gather 105, traces affected by the FTB errors are clearly visible.

5.2.4.3 3D Refraction Statics

3D refraction statics analysis is based on the same principles and theory previously discussed in chapter 4 for 2D refraction statics analysis. The desired outcome is to remove the statics effects of low velocity weathering layers and variations in source and receiver offset in the data correcting it to a new level reference datum. Figures 5.8 and 5.9 are simple cartoon diagrams detailing source and receiver relationships for the current statics scenario.

Unfortunately ProMAX's® automatic first break picking module was inconsistent and incapable of selecting the correct location for the first break pick with the noisy 3D data (Figure 5.10). Therefore FB picking was accomplished interactively by scrolling through each shot record of the 3D dataset (Figure 5.11). Refraction statics analysis was accomplished using the ProMAX® module similar to the one used for 2D refraction statics analysis. Again the FB picks, layer velocities and layer models were interactively adjusted and smoothed iteratively as to obtain the most realistic result and field static time shifts.

3D refraction statics analysis in ProMAX® uses the FB picks from interactively selected shotpoint locations for calculation of the refractor layer velocity (Figure 5.12). Using the DRM method ProMAX® created a single layer depth model and calculated necessary static time shifts to be applied to source and receiver for correction to the new datum.

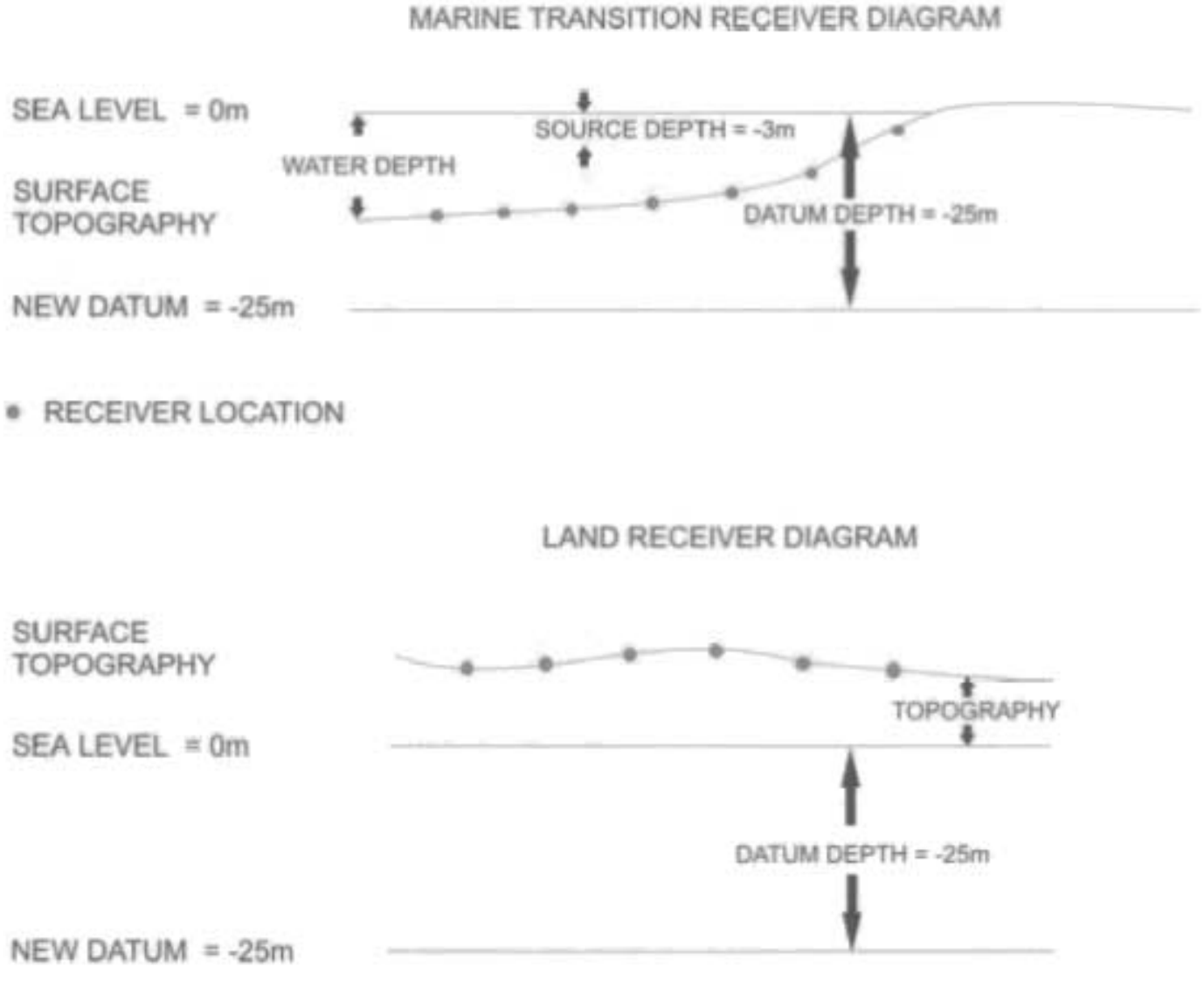

Figure 5.8. Simple geometric diagrams of marine and land receiver relationships for static shift calculations.

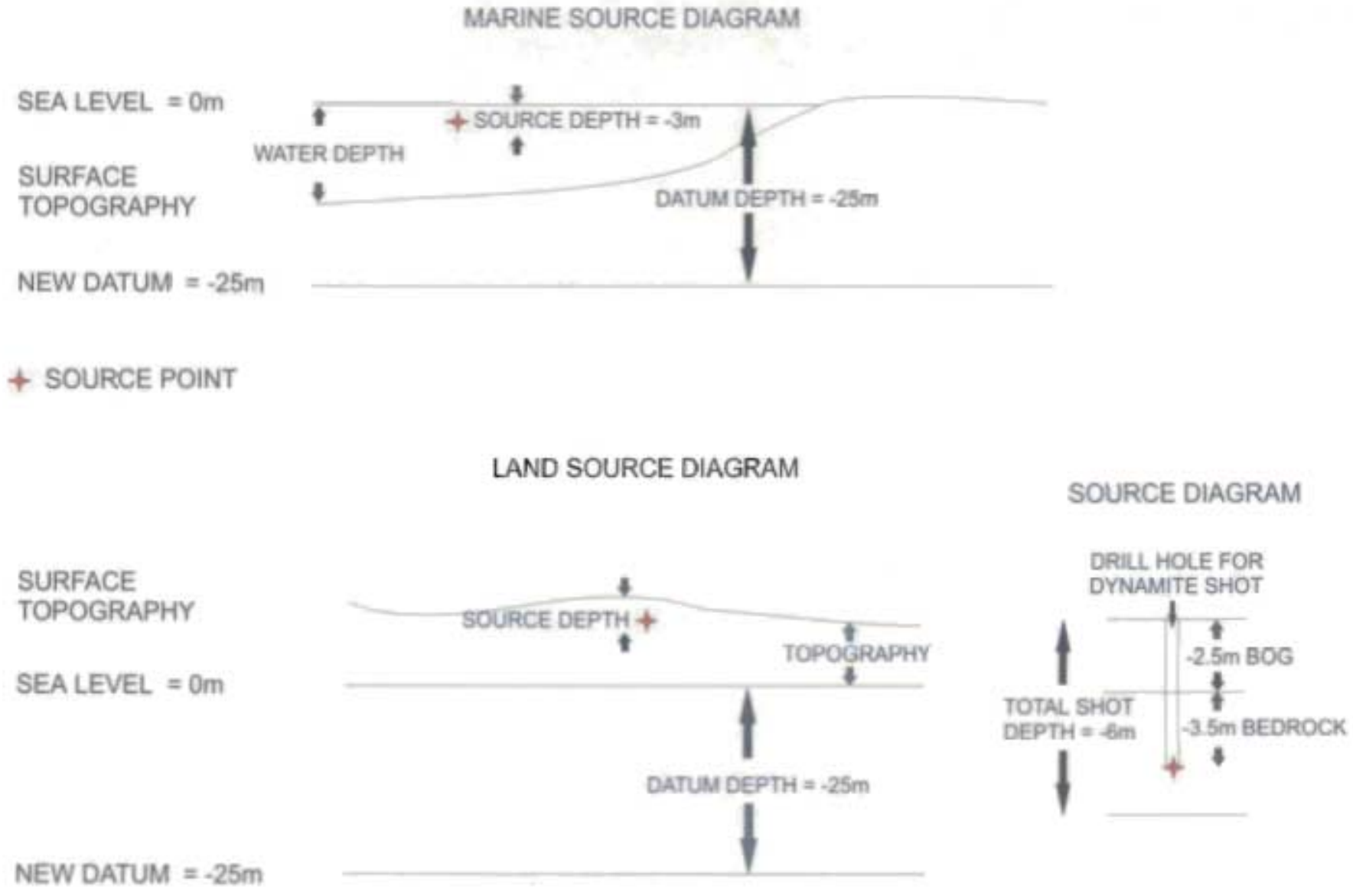

Figure 5.9. Simple geometric diagrams of marine and land source relationships for static shift calculations.

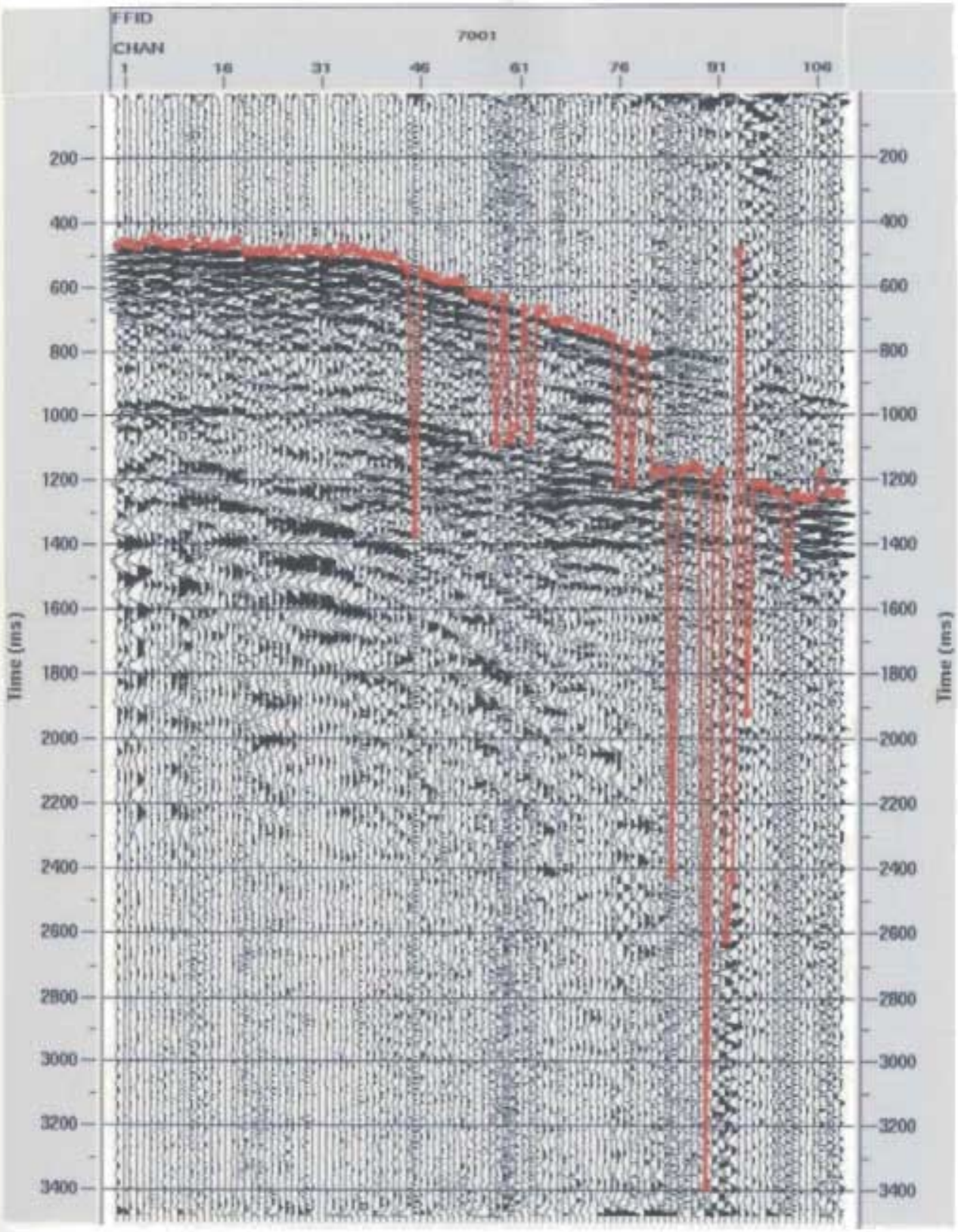

Figure 5.10. Shot record with ProMAX® automatic FB picks in red.

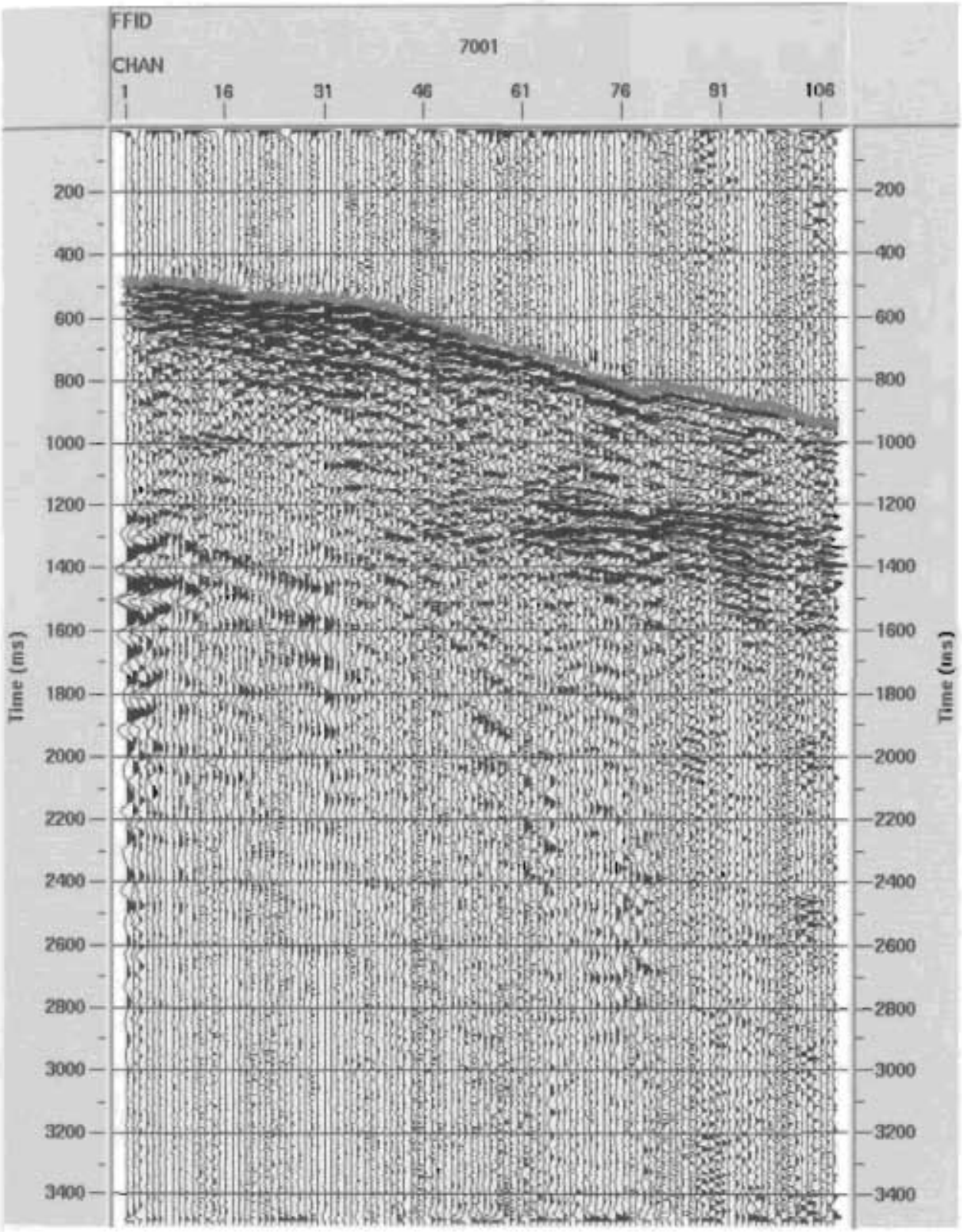

Figure 5.11. Shot record with interactively selected FB picks (red).

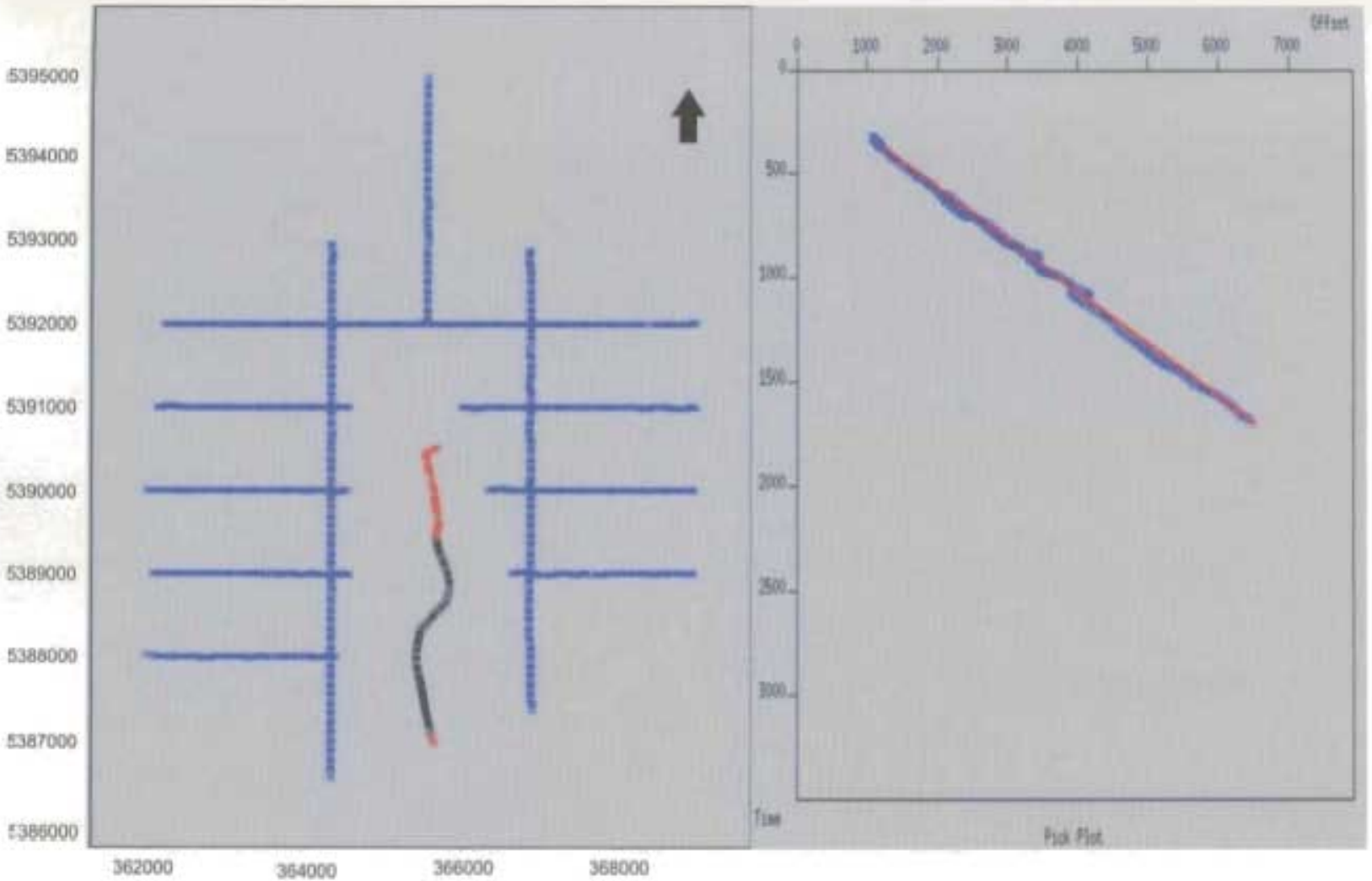

(a) (b)

Figure 5.12. (a) Diagram of source-rec layout used to select shot locations for automatic first break picking. (b) Diagram of first break picks used to select refractor velocity (red).

5.2.5 Frequency – Wavenumber (FK) analysis

FK analysis is an ideal tool for the precise removal of any identified noise seen in the shot gather domain. Conversion of the T-X domain data to the F-K domain spectrum creates a frequency versus wavenumber display that will clearly highlight all features such as aliasing, high / low frequency noise and electronic noise such as constant 60Hz signal. The FK spectrum display is also very useful for general analysis of primary and multiple seismic reflections. Coherent seismic signal will be mapped clearly in the FK spectrum as parabolic surfaces (Figure 5.13). Figure 5.13 is an example of a high quality shot gather and its FK spectrum, primary events are easily identified and have been annotated for clarity.

Comparison of the above FK spectrum from typical good seismic data to the following figure showing a good FK spectrum of a Shoal Point 3D shot gather clearly demonstrates the overall poor data quality. In the Shoal Point FK spectrum the frequency content is smeared throughout the entire low frequency range indicating wide spread noise distribution, with very slight hints of competent reflections being present. Note this is the best Shoal point data, an example of a more typical FK spectrum (Figure 5.15) shows no competent reflection signal and complete smearing of frequencies as noise.

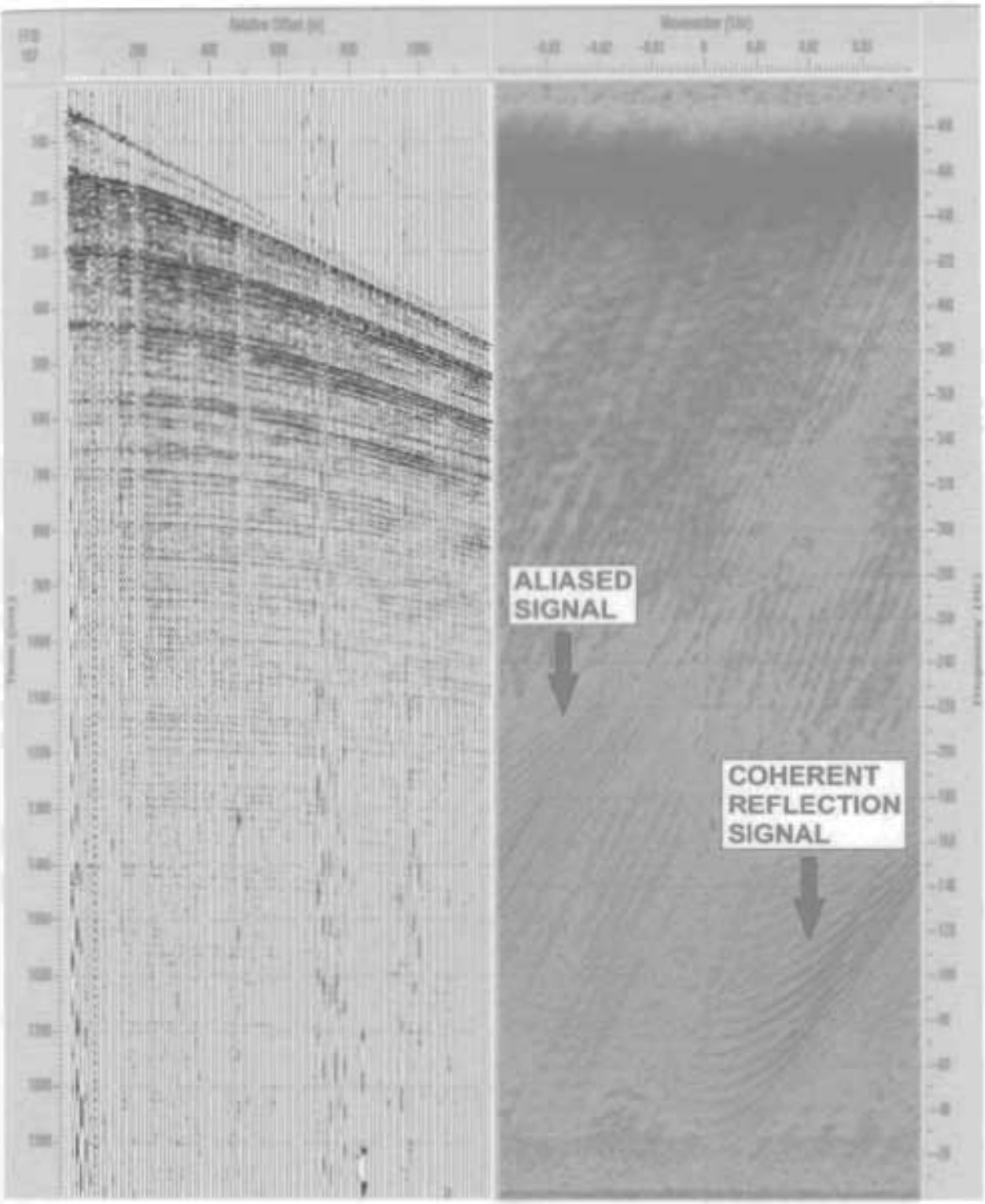

Figure 5.13. An FK spectrum taken from a conventional high-resolution marine seismic survey. (Courtesy of Shearwater Geophysical Corporation).

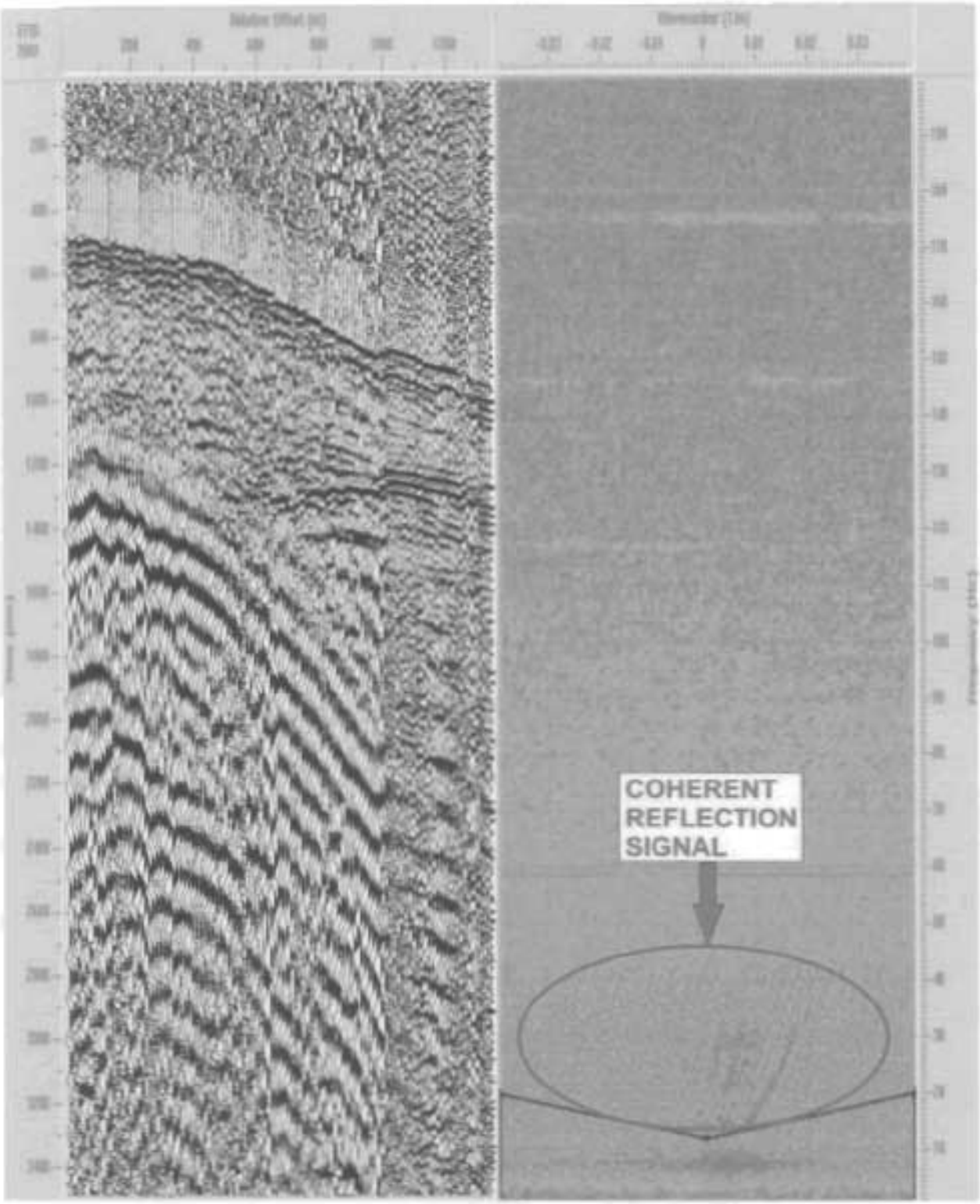

Figure 5.14. Typical "good" shot record and FK spectrum taken from the Shoal Point 3D survey. (Courtesy of Shearwater Geophysical Corporation).

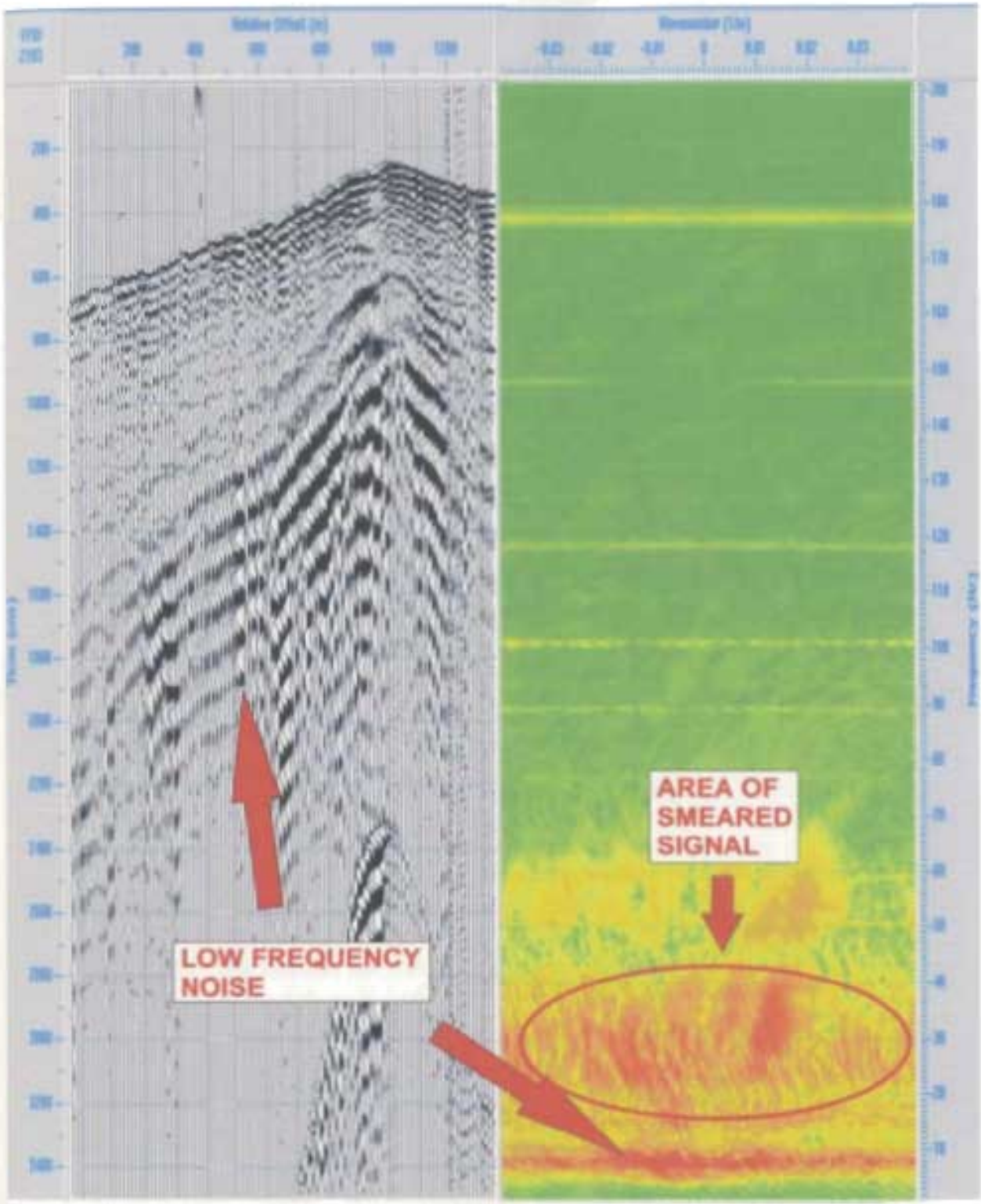

Figure 5.15. A typical shot record and FK spectrum from the current dataset.

The FK spectrum is smeared with no discernable signal.

Interactively I designed a general low frequency fan filter that was applied to each of the dataset records. It is designed specifically for the removal of low frequency noise and particularly the low frequency reverberation of the first arrivals. The rejection zone is easily identifiable as a black outlined polygon at the base of the FK spectrums. Comparison of the before and after T-X domain data demonstrates the success and ability of the FK filter to remove specific noise features. The post FK record is much cleaner in appearance with the dominant low frequency reverberation of the first arrival reflection being completely removed (Figure 5.16b).

5.2.6 Pre-stack Top Muting

Conventionally pre-stack top muting would be applied in the processing sequence at this stage of testing. Due to data offset limitations though, there must be more consideration given before applying this process. Conventional data will normally contain a distribution of both short and long offsets (Figure 5.17). The short offset data is used for the imaging of shallow and near surface reflections. The long offset data contains near surface information but is generally contaminated with the direct arrivals and accompanying reverberations. Conventionally, the long offset data is therefore muted out at early times. In the Shoal Point 3D dataset, unfortunately I do not have short offset near trace data as the unconventional survey design has generated all long offset data. Because of this, I need to limit the removal of the amount of long offset

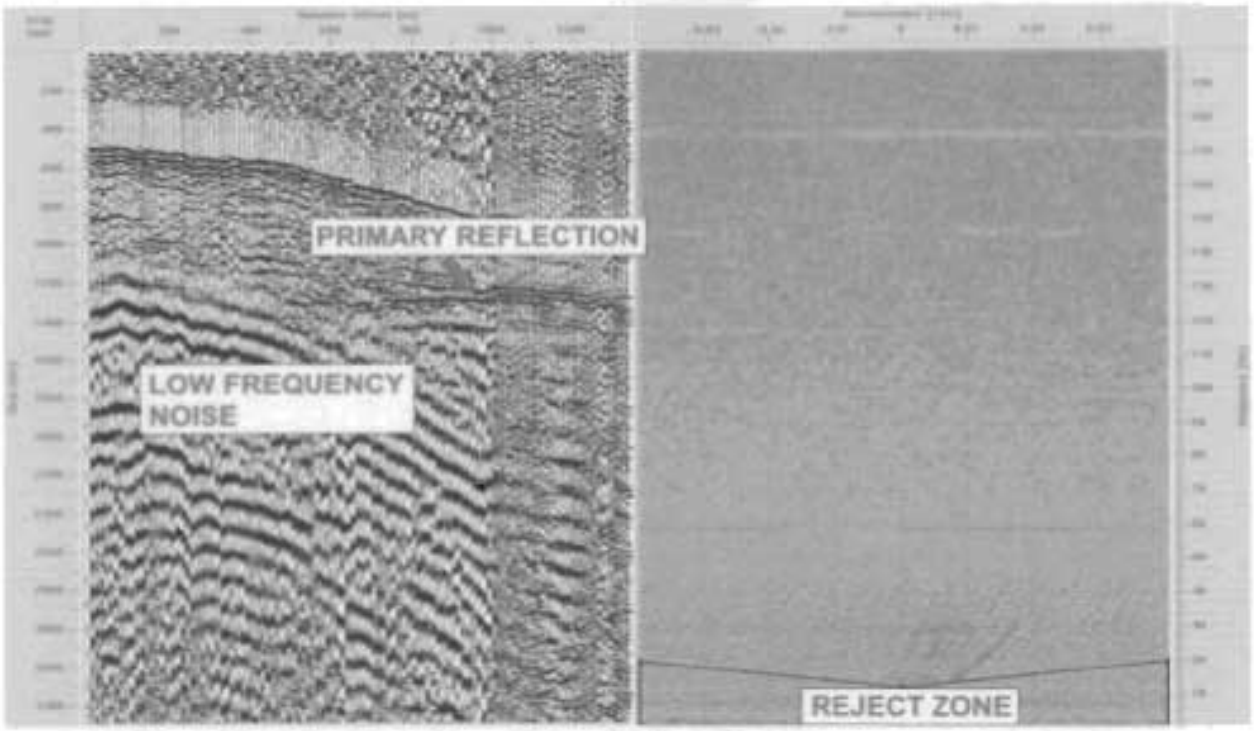

(a)

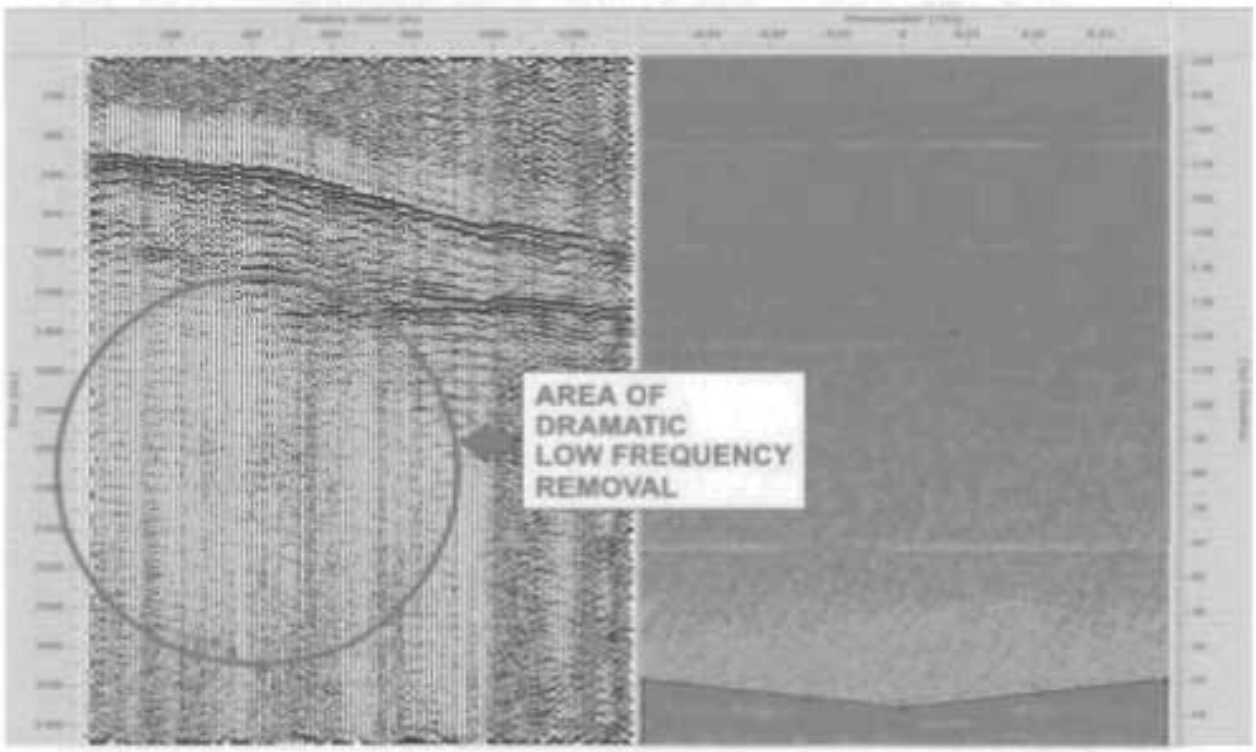

(b)

Figure 5.16. (a) Shot and FK data prior to application of the filter reject zone.

(b) The same data post FK filter application.

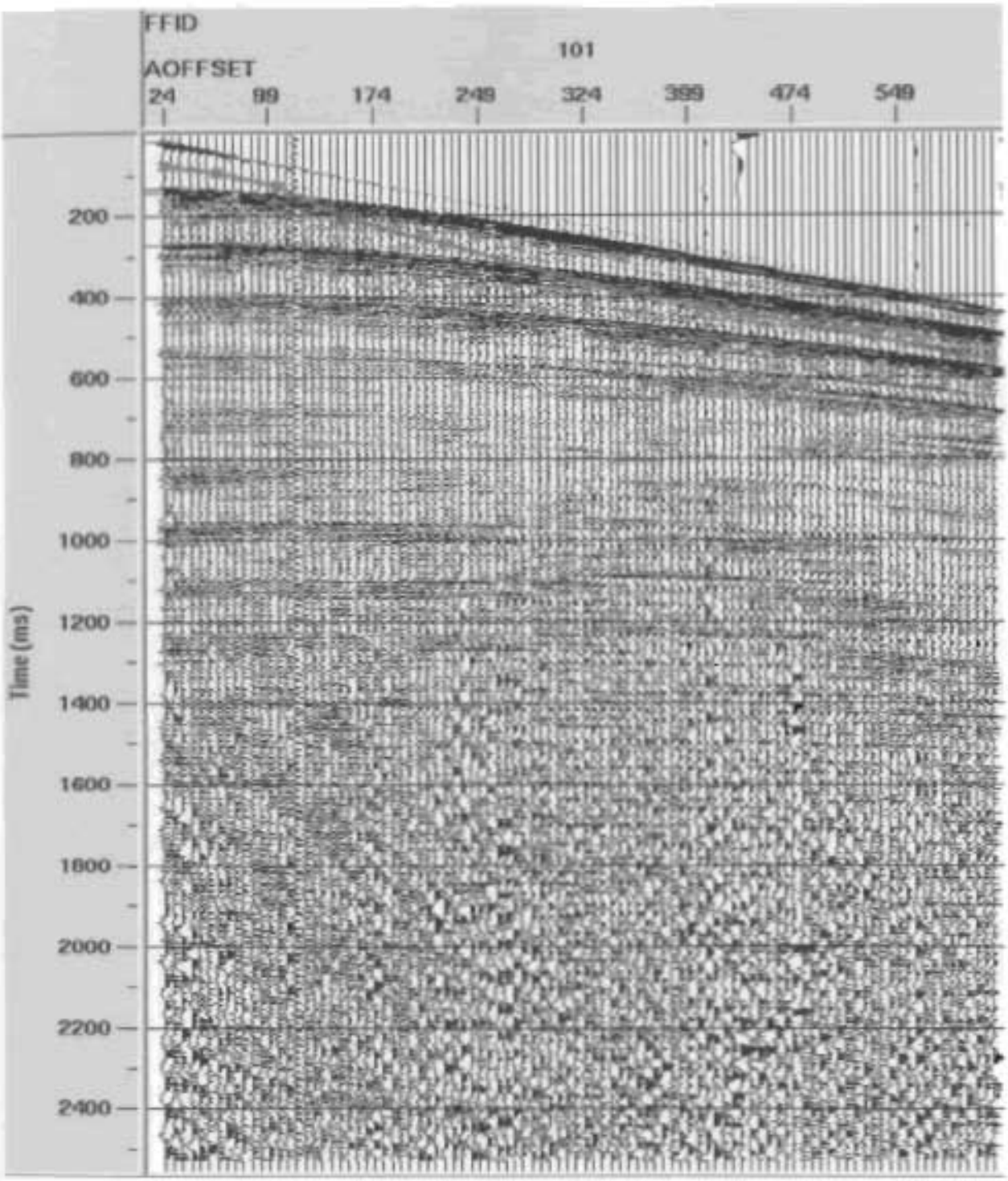

Figure 5.17. A typical high-resolution marine seismic shot record. The channels have been annotated for offset. (Courtesy of Shearwater Geophysical Corporation).

data that is typically clipped as it contains the only near surface seismic information available.

Testing for the application of a top mute involved the comparison of two mute designs with analysis of the results being performed on stacked seismic sections. The two designs compared were a conventional style top mute (Figure 5.17) and no mute at all. Figure 5.18 is of xline 70; first with no mute applied and secondly with the typical style of top mute applied. The effect of top muting is clearly visible on the stacked sections; the upper portion of data in the first 1000ms TWT is largely removed when the mute is applied. The implication of applying a conventional top mute would be removal of shallow seismic data that would be useful during the interpretation stage of the project. Because of this I have found it not to be in the best interest of the final product to apply any pre-stack top mute.

5.2.7 Scaling

As previously noted in Chapter 4, the introduction of amplitude scaling to the data is crucial for compensation and adjustment of the seismic signal. The implementation of a correct time-variant scaling technique will help improve the signal content in the lower half of the shot records and even the overall signal content.

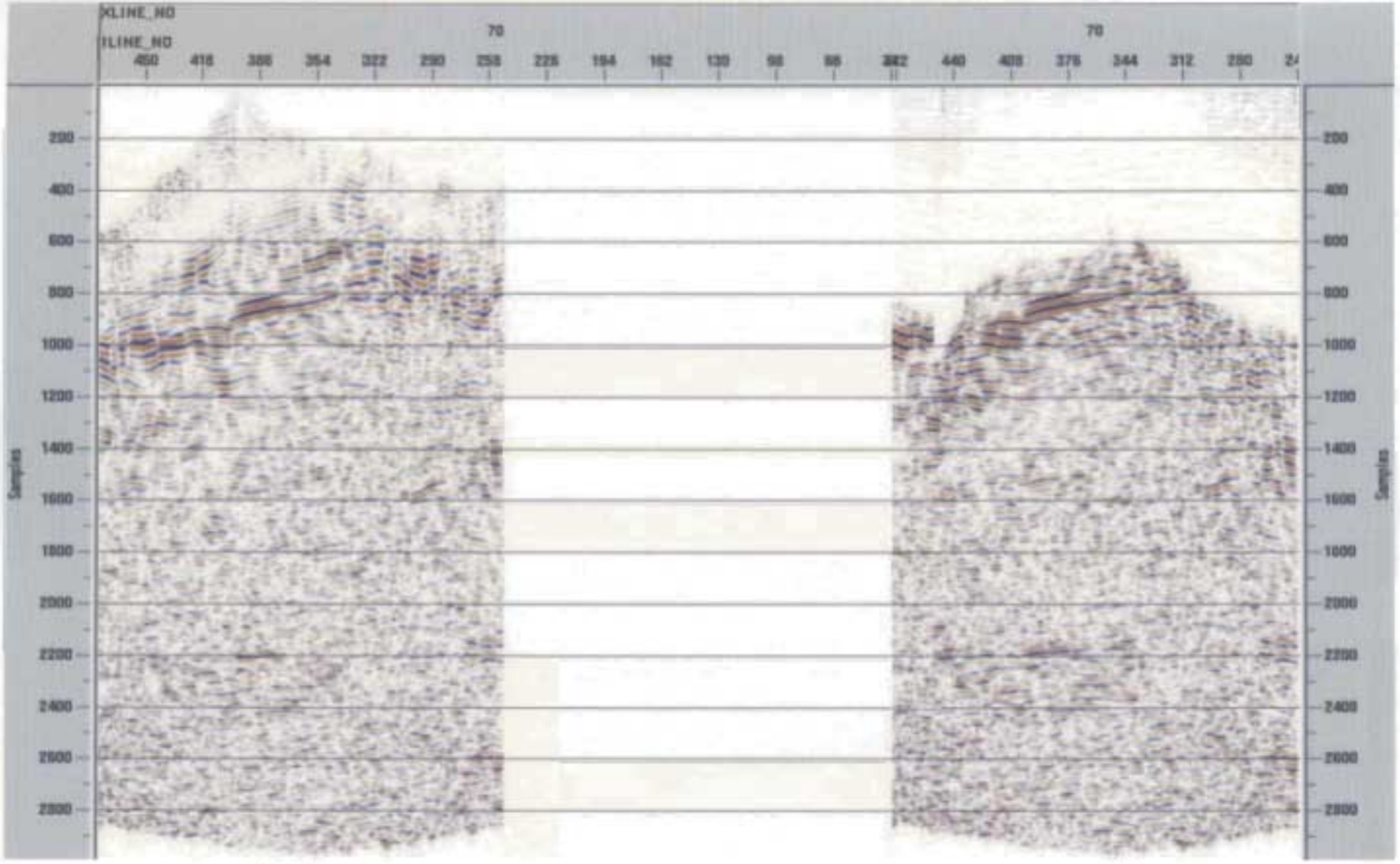

(a) (b)

Figure 5.18. (a) Xline 70 stacked with no pre-stack top mute applied. (b) Xline 70 with a conventional pre-stack top mute, note that the mute has a detrimental effect removing platform reflectors in the 600ms - 1000ms range.

Testing of scaling parameters for the Shoal Point 3D dataset included the following techniques:

1. Automatic gain control (AGC)
2. Offset amplitude recovery (correction for spherical divergence)

5.2.7.1 Automatic Gain Control (AGC)

Conventionally this would not be considered as a typical pre-stack scaling option. This procedure can have extremely detrimental effects to the true amplitude relationships of the data if used incorrectly. The key when applying AGC is to maintain an adequate time gate window. Application of AGC with a very small window will render the strong reflections indistinguishable from the weak reflections (Yilmaz, 2001). Yilmaz defines the scaling function for an instantaneous AGC as:

- $g(t) = desired\ RMS / {}^{1}/_{N} \sum_{i=1}^{N} |x_i|$ (5.1)
- x_i = trace amplitude
- N = number of samples

The goal of AGC as tested here is to enhance weak reflection signals to a more appropriate level corresponding to the surrounding data. The following figure

(5.19) compares a typical shot point before and after application of an AGC with a 1000ms time gate. The results indicate that modest signal enhancement is achieved, but I decided that the use of a more realistic and non-intrusive scaling would be best.

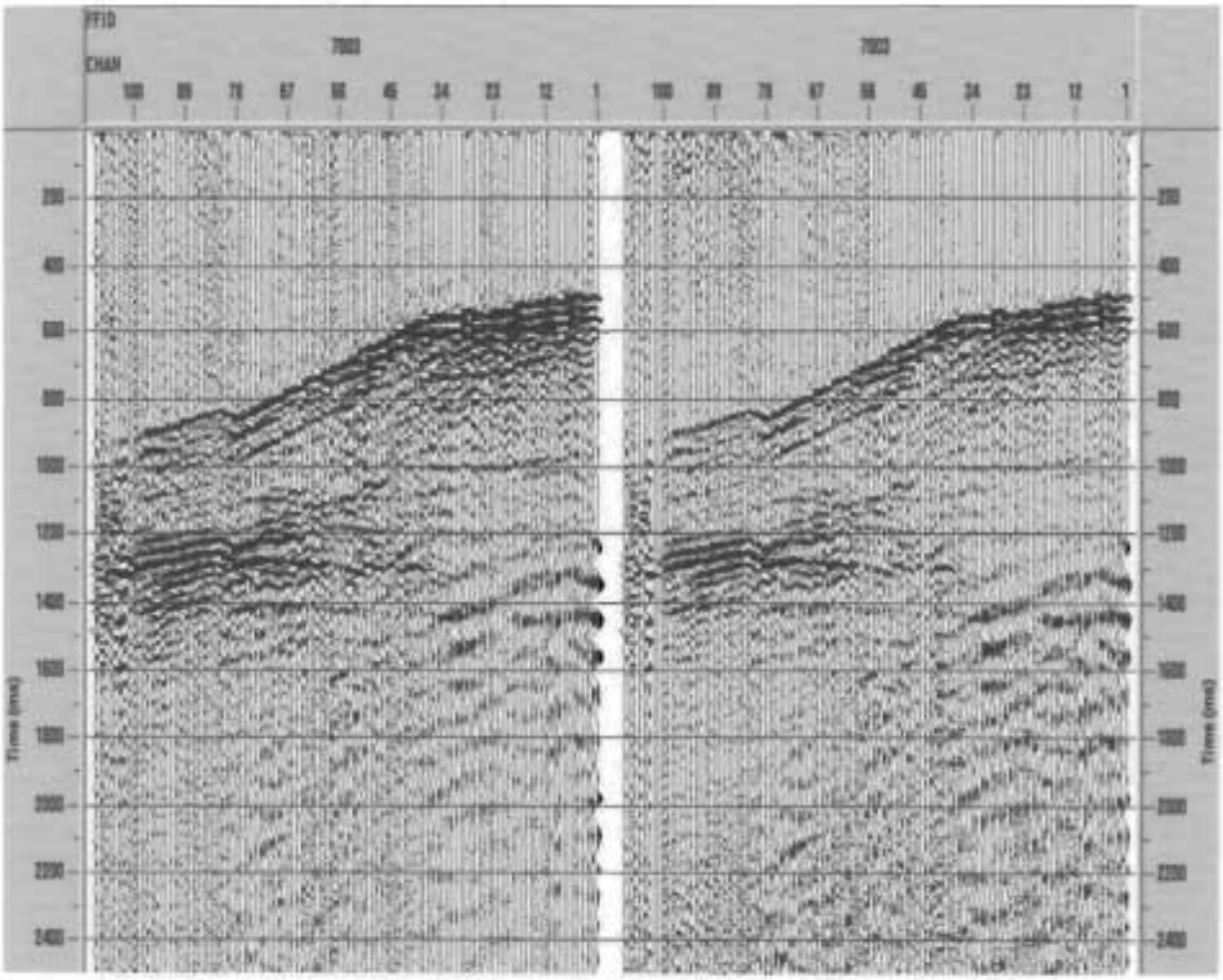

(a) (b)

Figure 5.19. (a) Shot 7003 prior to AGC. (b) Shot 7003 post application of the AGC scalar (1000ms time gate).

5.2.7.2 Offset Amplitude Recovery

Application of offset amplitude recovery helps correct both for geometric spreading and for frequency attenuation of the signal (section 4.3.7 provides a more in-depth look at offset amplitude recovery, the same process was used for the 3D data). Application of offset amplitude recovery using an RMS velocity function generated the most favorable results without the signal degradation found in AGC application. Figure 5.20 is an example of shot data before and after application of offset amplitude recovery. The reflection signal is enhanced and clarified as the first arrival amplitude is reduced to a less dominant level.

5.2.8 Deconvolution

Application of pre-stack deconvolution to any seismic data is generally attempting to improve the overall temporal resolution by manipulation of the seismic wavelet. As previously discussed in chapter 4 deconvolution will compress the seismic wavelet (spiking), and / or attenuate reverberations and short period multiples (predictive). Detail on pre-stack deconvolution using both spiking and predictive techniques is reviewed in section 4.2.9. The application of deconvolution to this dataset is focused primarily around attenuation of first arrival reverberations. The deconvolution parameters were chosen to best collapse the first arrival sequence to a single identifiable wavelet.

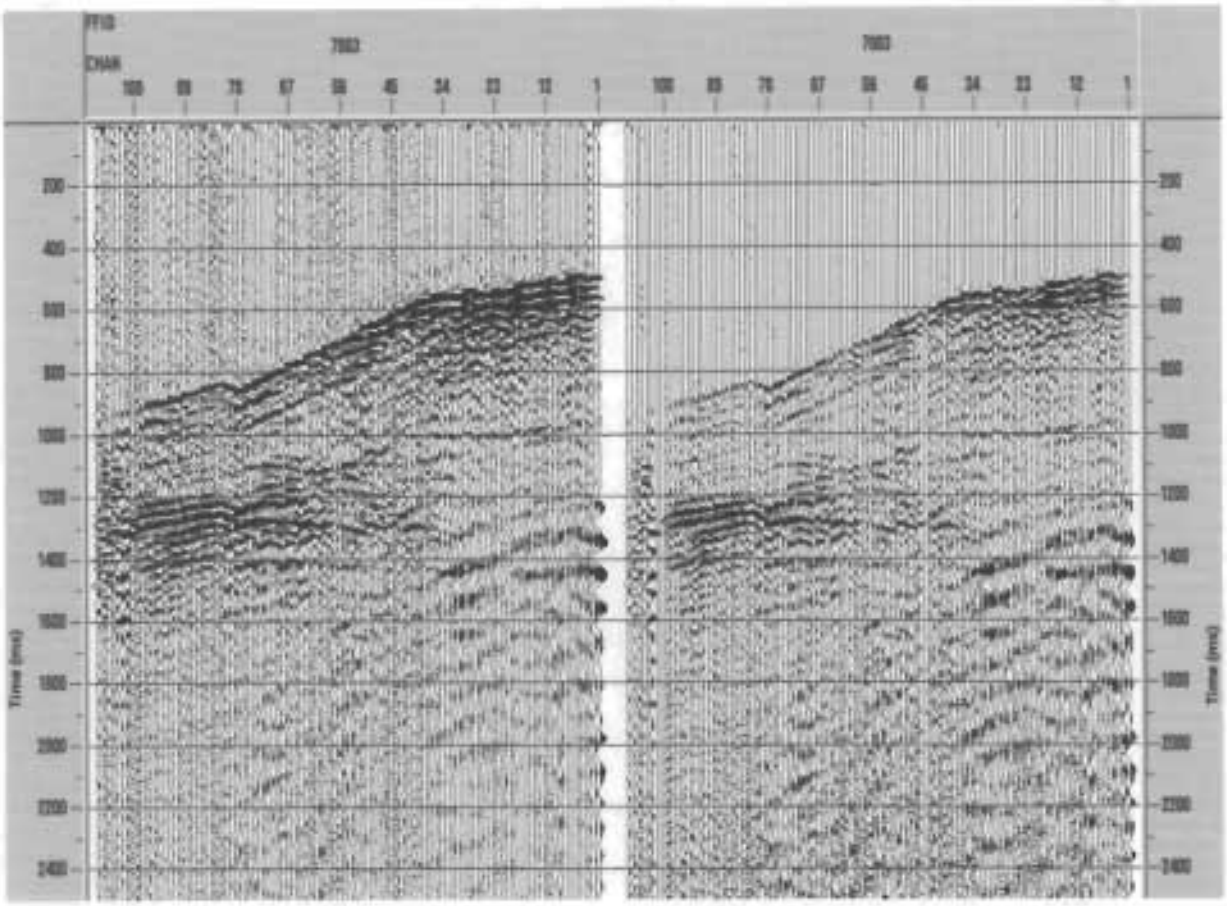

(a) (b)

Figure 5.20. (a) Shot 7003 prior to correction for spherical divergence. (b) Shot 7003 post application of correction for spherical divergence.

Testing for the current 3D data involved consideration of both spiking and predictive deconvolutions, gap and length times tested are as follows:

Table 5.1: Predictive deconvolution gap-testing parameters.

Type of Deconvolution	Operator Length (ms)	Gap Test Lengths (ms)
Predictive	120	10
		15
		20
		30
		40

Table 5.2: Predictive deconvolution operator length testing parameters.

Type of Deconvolution	Operator Length (ms)	Gap Test Lengths (ms)
Predictive	80	20
	100	
	120	
	160	
	240	

Table 5.3: Spiking deconvolution operator length testing parameters.

Type of Deconvolution	Operator Length (ms)
Spiking	8
	16
	32
	64
	128

Figure 5.21 compares a typical marine shot with no deconvolution, the final predictive deconvolution and a tested spiking deconvolution. The figure clearly demonstrates the effect of deconvolution on the pre-stack data and the difference in results depending on the technique selected. Analysis of displays similar to figure 5.21 and panels of stacked data indicated that a predictive deconvolution was much more successful then the spiking deconvolution at collapsing the first arrival reverberation to a single wavelet and thereby enhancing the key platform reflectors. Application of the spiking deconvolution resulted in excessive signal attenuation and was therefore deemed inappropriate. Careful consideration of the predictive deconvolution test panels indicated that application of a deconvolution with a 20ms gap and a 120ms operator generated the most desirable results.

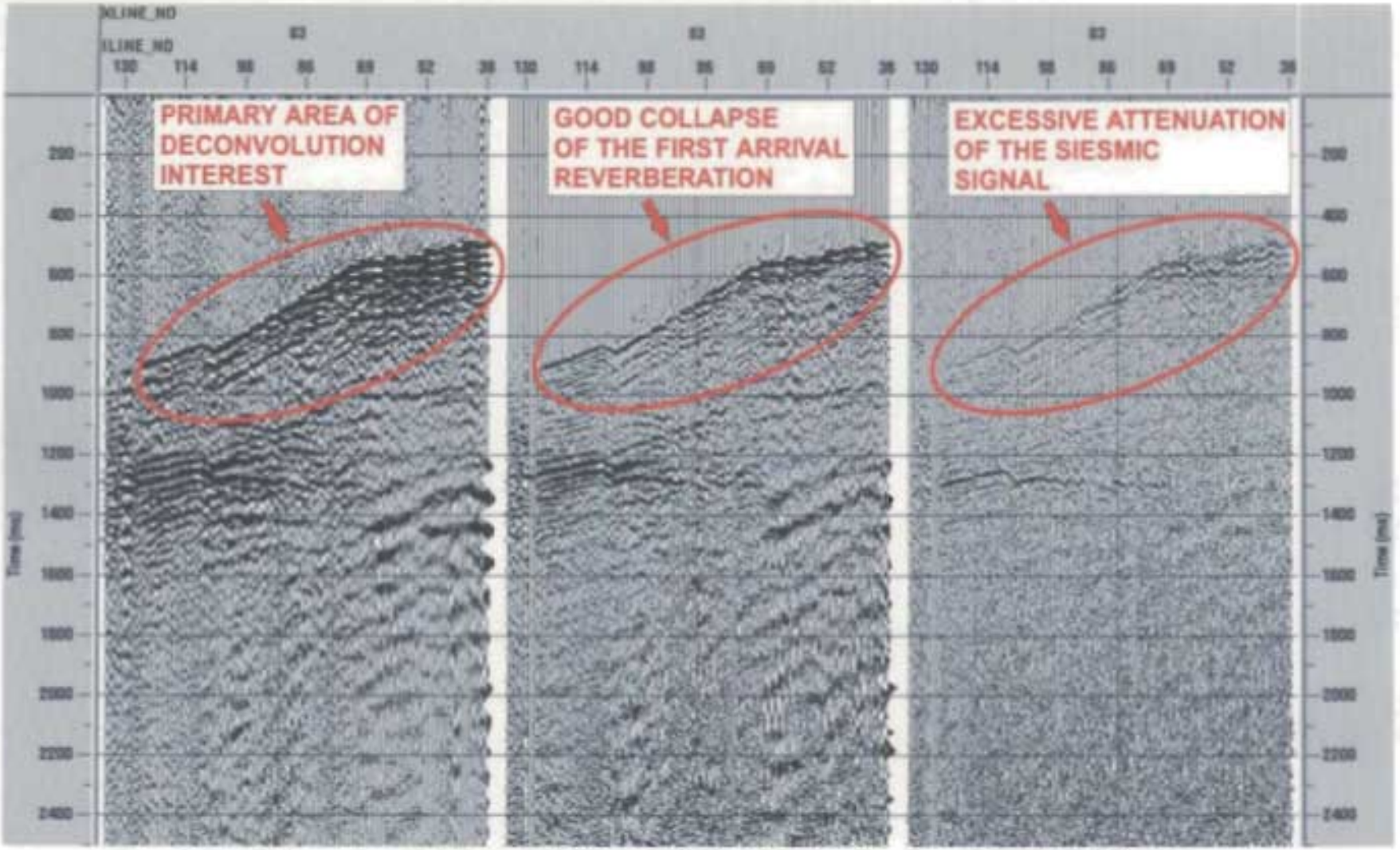

Figure 5.21. Decon testing (a) FFID 7003 with no decon. (b) FFID 7003 with a 20/120 predictive decon applied. (c) FFID 7003 with a 0/128 spiking decon applied.

5.2.9 Velocity Analysis / NMO Correction

Correct velocity selection is crucial for achievement of the proper normal moveout correction and subsequent stacking of the data. Poor data quality issues and lack of coherent signal from primary events made velocity analysis complex and lengthy. To complete this task an assessment of previous work and the application of numerous conventional velocity analysis techniques were required.

Initial consideration of a 3D velocity field involved study of the regional geology and the previous Hunt and EnCana (formerly PanCanadian) seismic lines around the survey area. Regionally the Port au Port peninsula is an area known to be seismically dominated by shallow high velocity Cambro-Ordovician carbonates (4000m/s – 5000m/s) of both allochthonous and autochthonous settings. Analysis of the released Port au Port bay seismic data clearly identifies the signature doublet expression of the top and internal reflectors of the carbonate platform characteristic of the area (Figure 5.22). This characteristic sequence was believed to be continuous within the bay and therefore the survey area for this study. This feature can generally be found in the 800ms to 1200ms TWT region. Therefore, using the released RMS seismic stacking velocities, I was able to gain a relatively precise definition of what stacking velocities should be applied at specific locations and TWT's within the study area.

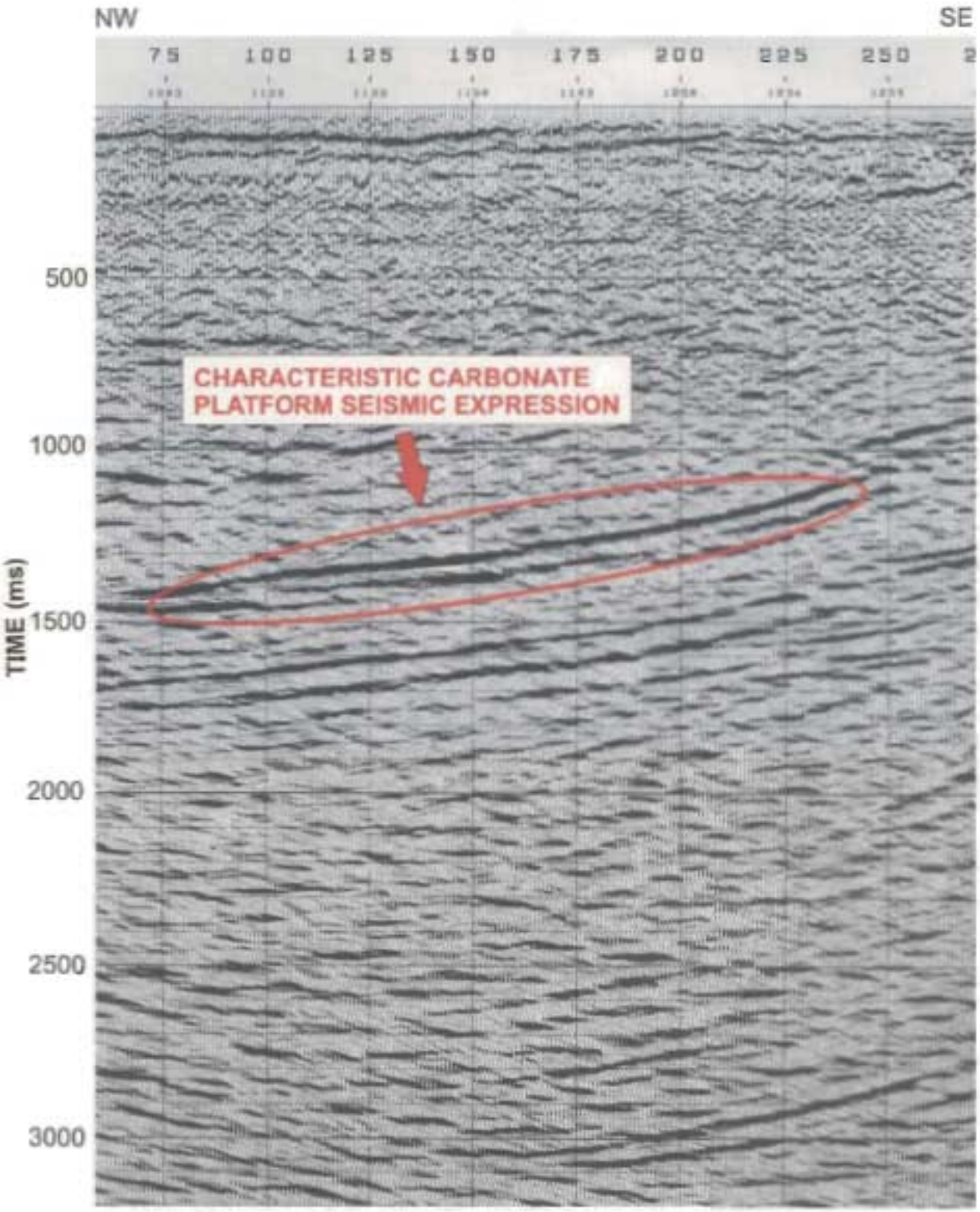

Figure 5.22. A transect taken from released PanCanadian 2D seismic acquired in Port au Port Bay.

The following figure (5.23a) is a typical Shoal Point semblance analysis display containing the semblance plot, the offset gather and the velocity function stacks. Compared to a semblance analysis example from a higher quality marine seismic dataset, the problem of poor data quality is clearly seen, notably the presence of clear reflections and the presence of high coherency velocity locations are not discernable on the Shoal Point velocity spectrum. Clearly velocity analysis would be difficult and unreliable if the semblance analysis technique alone was used for stacking velocity selection. Additional testing and consideration of possible options, led to the use of constant velocity stacks in conjunction with the semblance analysis for velocity field generation.

5.2.9.1 Constant Velocity Stacks

The use of constant velocity stacks typically involves the generation of panel displays showing either NMO corrected CDP gathers or paneled areas of the stacked data. Generation of constant velocity stacks over a range of incrementing velocities is typical for comparison relative to one another. A velocity function can be then composed by identification of the corresponding velocity-time pairs that facilitate the proper adjustment of normal moveout to flatten the horizons of the CDP gather or provide the best stacks. Due to the poor data quality and the limited offset ranges, constant velocity analysis on NMO'd CDP gathers is not viable. Instead constant velocity panels for a stacked xline were compared to one another.

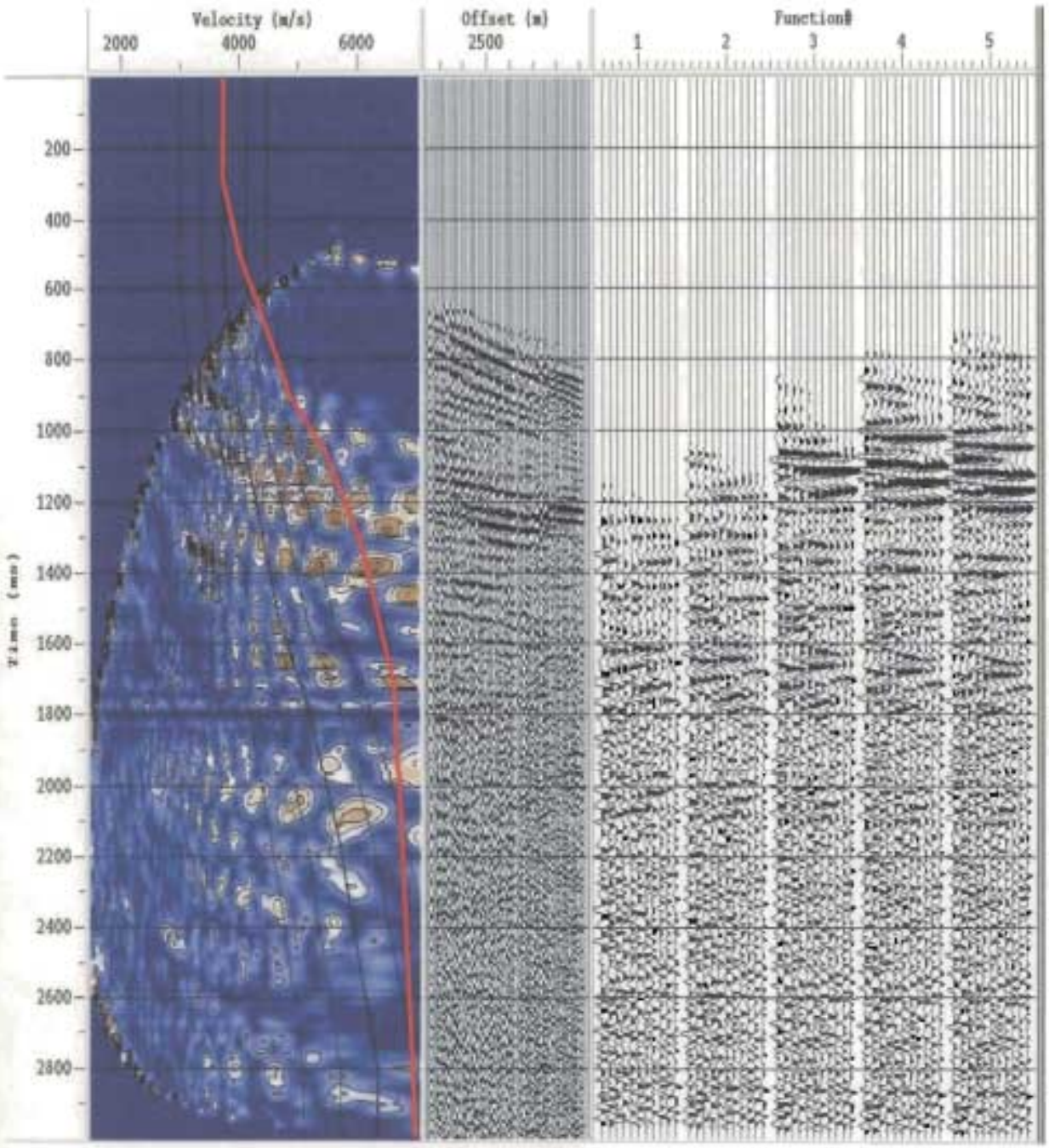

(a)

Figure 5.23a. A typical semblance analysis display from the Shoal Point 3D super gathers.

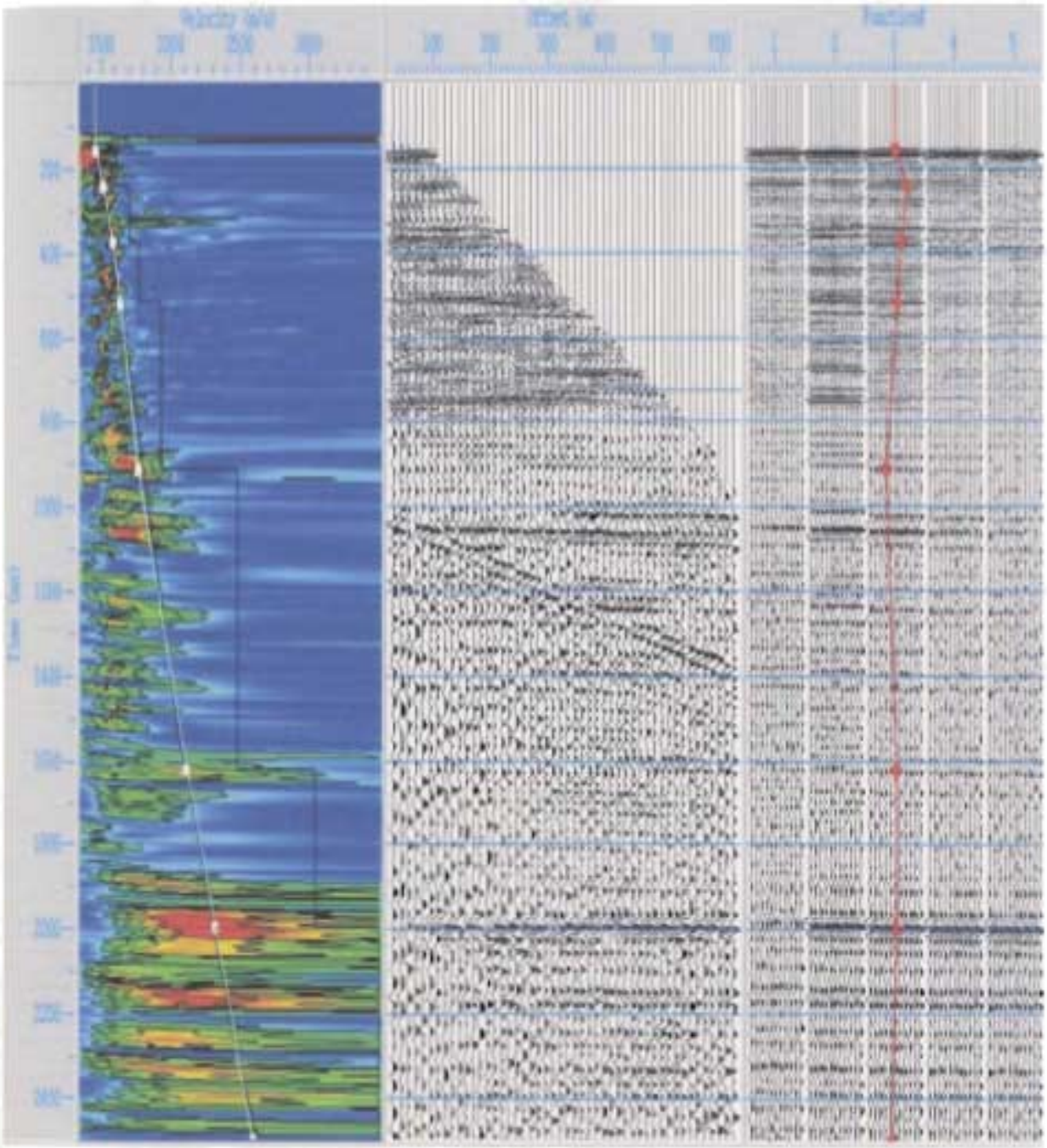

(b)

Figure 5.23b. A typical semblance analysis display from a high-resolution marine seismic survey. (Courtesy of Shearwater Geophysical Corporation).

Constant velocity stacks for each xline testing location were generated for the following range of velocities (m/s): 3000, 3500, 4000, 4500, 5000, 5500, and 6000. The following table lists each xline for which constant velocity stacks were generated and corresponding inline position at which the velocity function was picked, note a function was picked every 312.5m along each xline that was tested.

Table 5.4: Xline and Inline velocity analysis locations.

XLINE	INLINE
36	Every 25 inlines
48	Every 25 inlines
60	Every 25 inlines
67	Every 25 inlines
71	Every 25 inlines
81	Every 25 inlines
90	Every 25 inlines
96	Every 25 inlines

Therefore, the final technique for velocity analysis follows this scheme:

1. Generation of the CVS for the xline being tested.
2. Generation of the semblance display for the same xline, incrementing analysis locations at 312.5m intervals.
3. Keeping in mind the velocity information gained from the previous work, CVS were compared at the proper inline location in search of the velocity-time pair that generated the best coherency / stacking of the data. This velocity-

time pair was then picked on the semblance display and recorded to the velocity function.

The following figure displays the constant velocity stacks for xline 81 that were used for velocity testing. Figure 5.23(a) corresponds to the semblance display for inline position 109 along xline 81. The corresponding velocity function picked at that location is displayed on the velocity spectrum in red. Note that the inline analysis location is annotated on the constant velocity stacks where relevant.

Careful comparison of the constant velocity stacks allows for accurate selection of stacking velocities for optimal results. Considering 5.24(a) stacked with 3000m/s, the annotated platform area has not been imaged correctly. But when compared to the CVS for 4500m/s, one can easily see that a more accurate stacking velocity in this situation would be the higher 4500m/s. Key horizons were studied iteratively at each inline location using this technique to determine the best corresponding velocity values.

5.2.10 NMO Stretch Muting

Application of the correct NMO mute was a critical process that had to be treated more carefully in this current situation than would be needed in the processing of a conventional 3D dataset. As has been previously discussed stretching of the seismic wavelet is an unavoidable characteristic of correcting large-offset

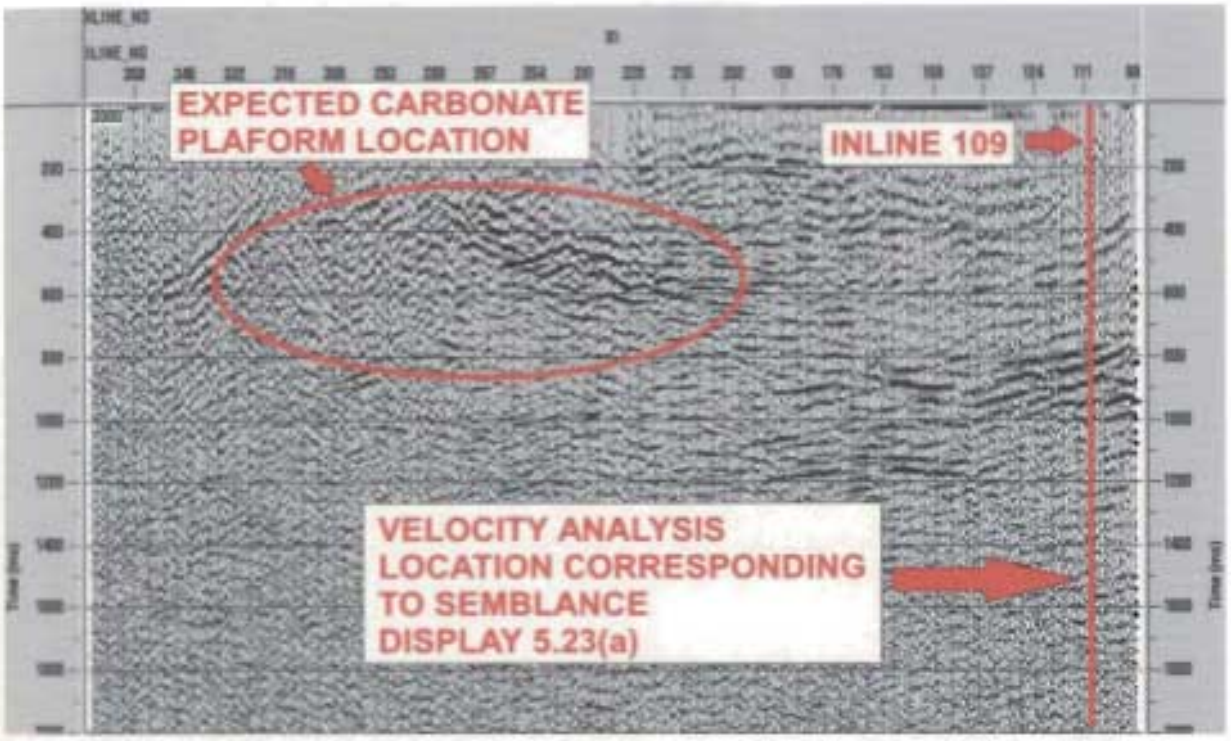

(a)

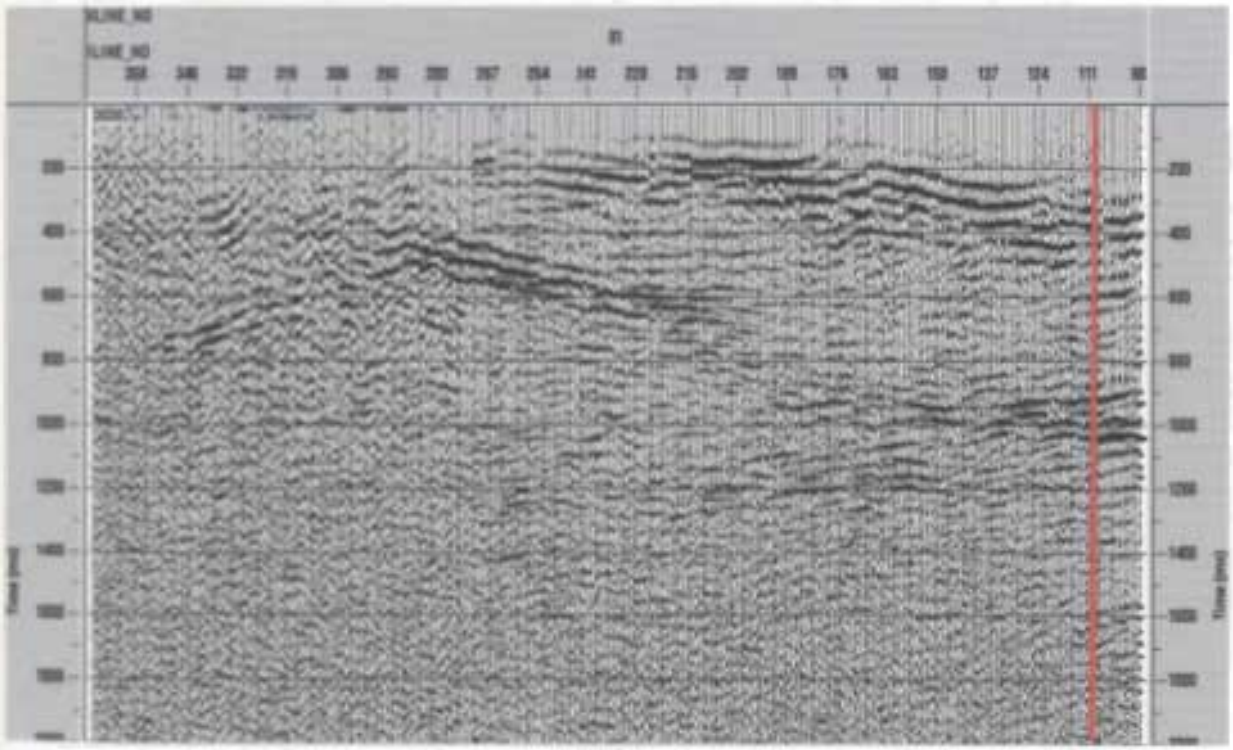

(b)

Figure 5.24. **Constant velocity stacks used for velocity analysis of the 3D volume. (a) xline 81 CVS for 3000m/s. (b) xline 81 CVS for 3500m/s.**

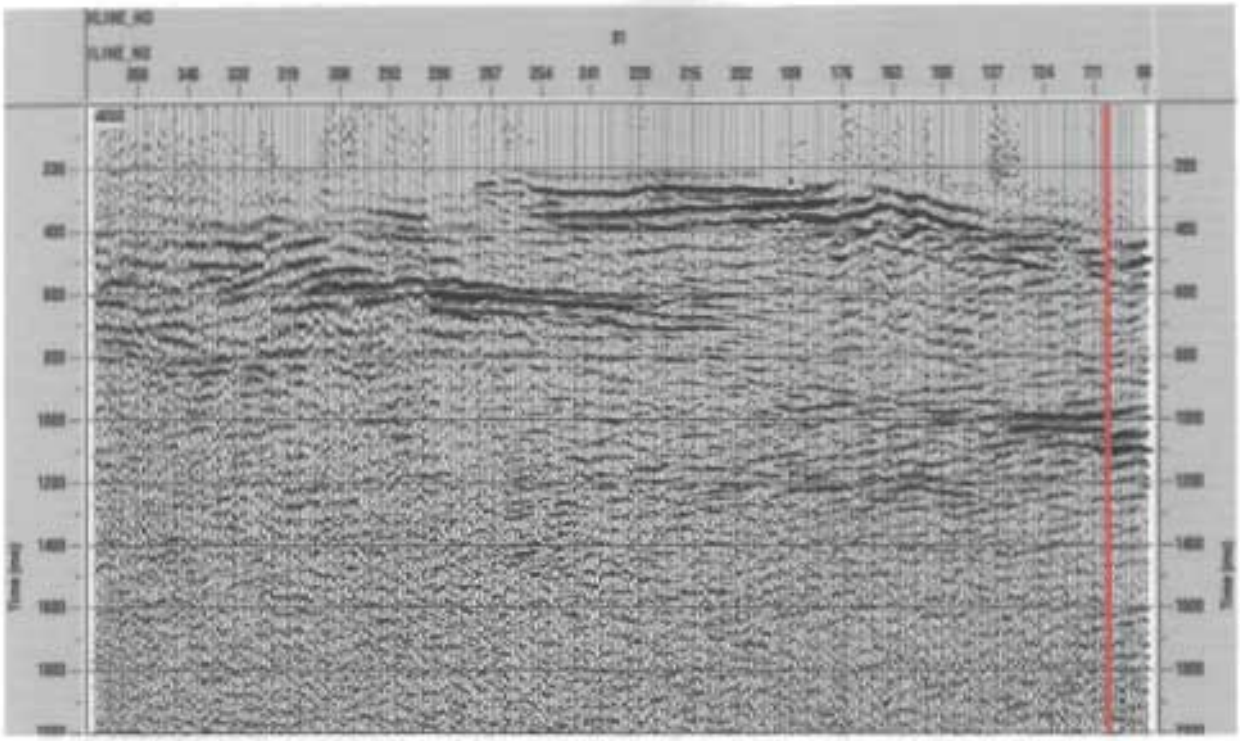

(c)

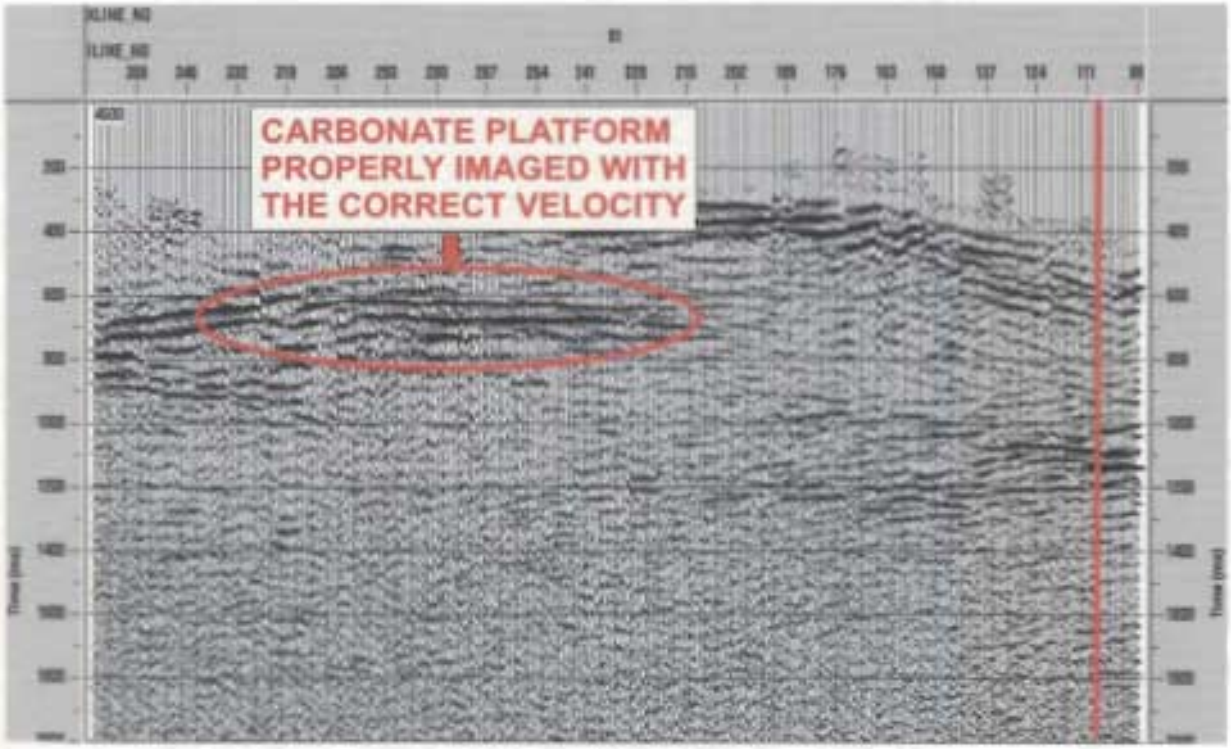

(d)

Figure 5.24. (c) xline 81 CVS for 4000m/s. (d) xline 81 CVS for 4500m/s.

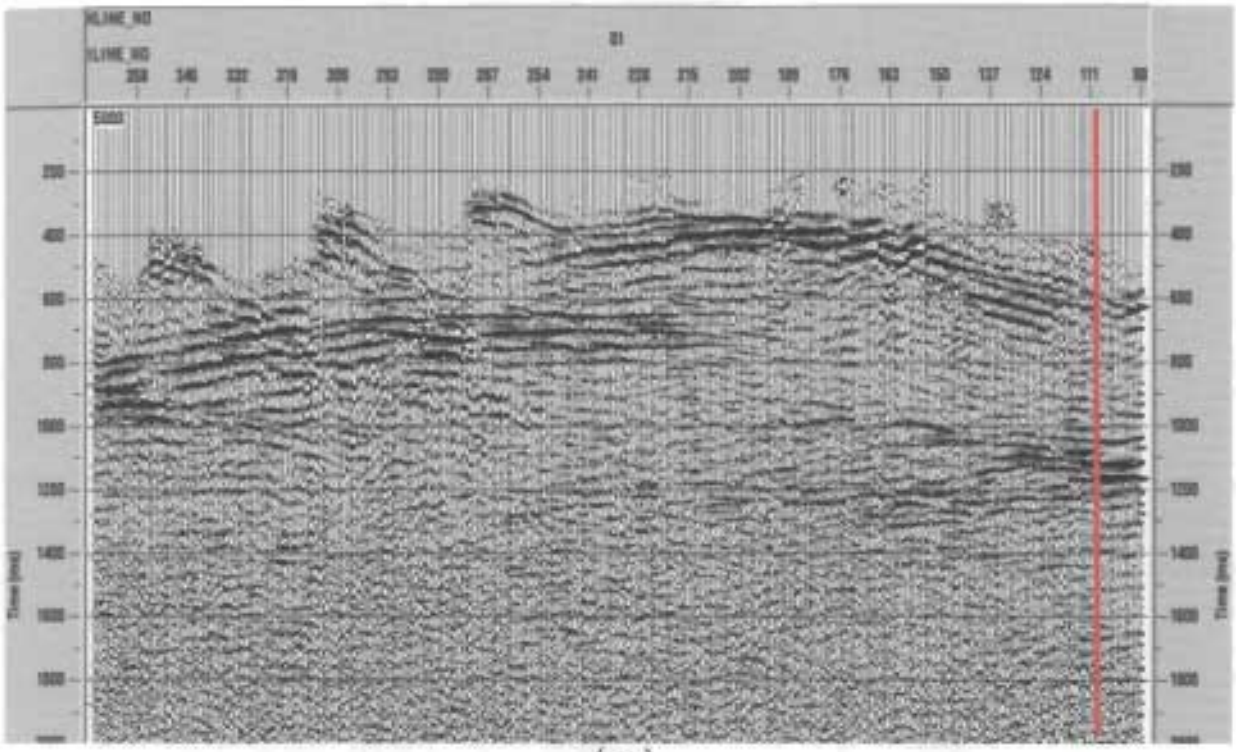

(e)

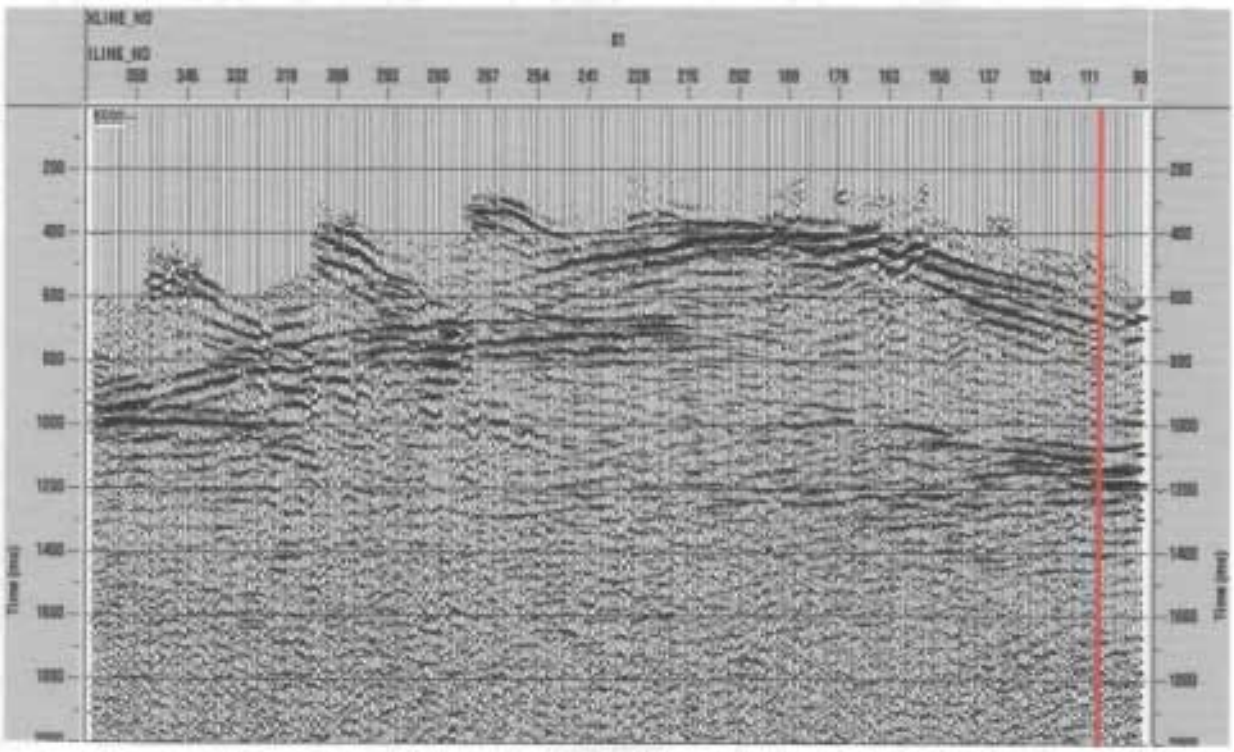

(f)

Figure 5.24. (e) **xline 81** CVS **for 5000m/s.** (f) xline **81 CVS** for **5500m/s.**

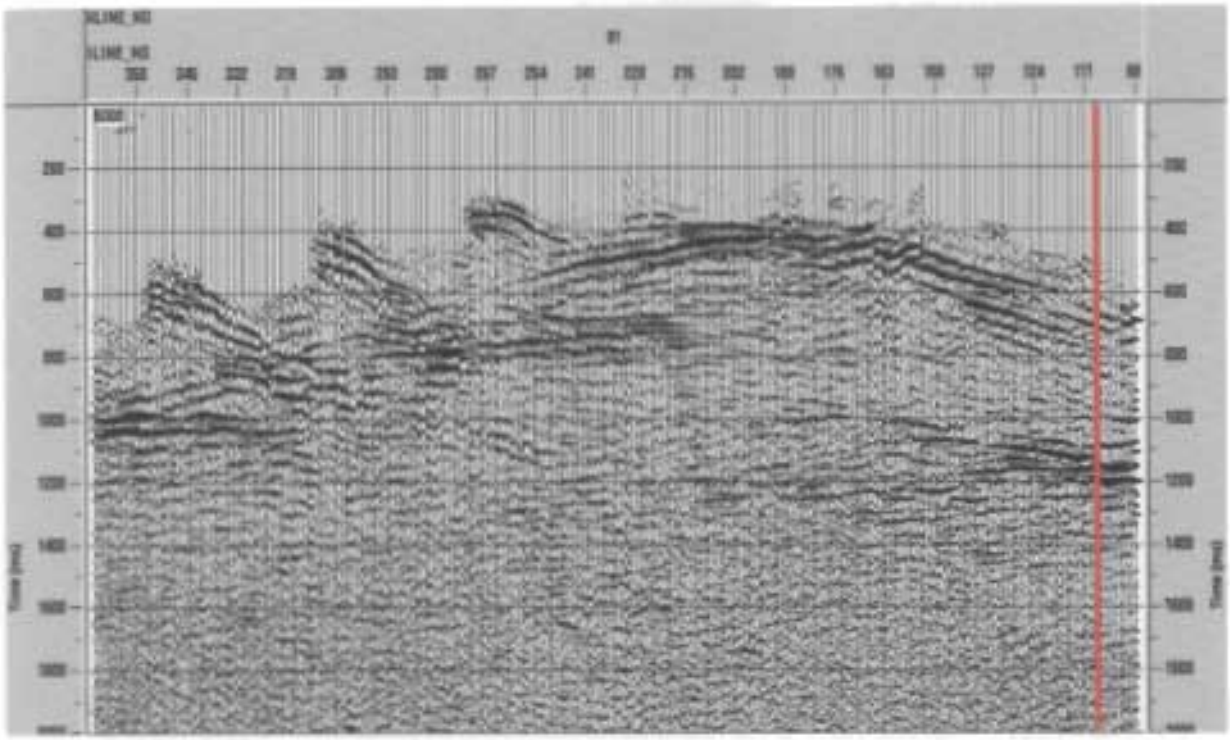

(g)

Figure 5.24. (g) xline 81 CVS for 6000m/s.

reflection signals for normal moveout. NMO stretch muting is normally applied either interactively or by setting a maximum stretch percentage of the wavelet to the data, thus removing the affected signal.

Unfortunately as the data is dominantly long-offset, the upper section of the gather will be the region affected by excessive wavelet stretching. It is this area that is removed during application of a conventional stretch mute. This problem has been previously discussed in pre-stack top muting. In short, the dataset contains no near offset trace data to image the shallow seismic reflectors. Therefore, signal in the long offset data corresponding to the shallow seismic

events needs to be retained to possibly image these events. But it is exactly these long offset shallow signals that are subjected to large NMO stretch that would normally constitute an area to be stretch muted.

Clearly the situation involves weighing how much wavelet stretching will be accepted relative to how much near surface data will be lost at specific percentages of NMO stretch muting. Testing involved comparison of the stacked data with no stretch mute (100%), a 75% stretch mute, a 50 % stretch mute and a 25% stretch mute. Remember the percentage corresponds to the allowed amount of wavelet stretch prior to application of the mute, so the larger the percentage the more stretching will be accepted.

The following sequence of figures shows xline 81 with the specified stretch parameters. The effect of the stretch mute is substantial and data is clipped far below the key area of interpretation representing the carbonate platform. Analysis of the data indicates that for this situation, the most relevant information will be obtained if no NMO stretch mute is applied to the dataset. One important thing to remember from this stage onward is that since the seismic wavelets have been allowed to stretch indiscriminately there is a point in the near surface of the data when wavelet stretch is so excessive that the resultant seismic record is incorrect and not a true representation of the subsurface geology. Events at less then 300ms – 500ms TWT in my opinion are not usable for interpretation, because of the NMO stretch issue.

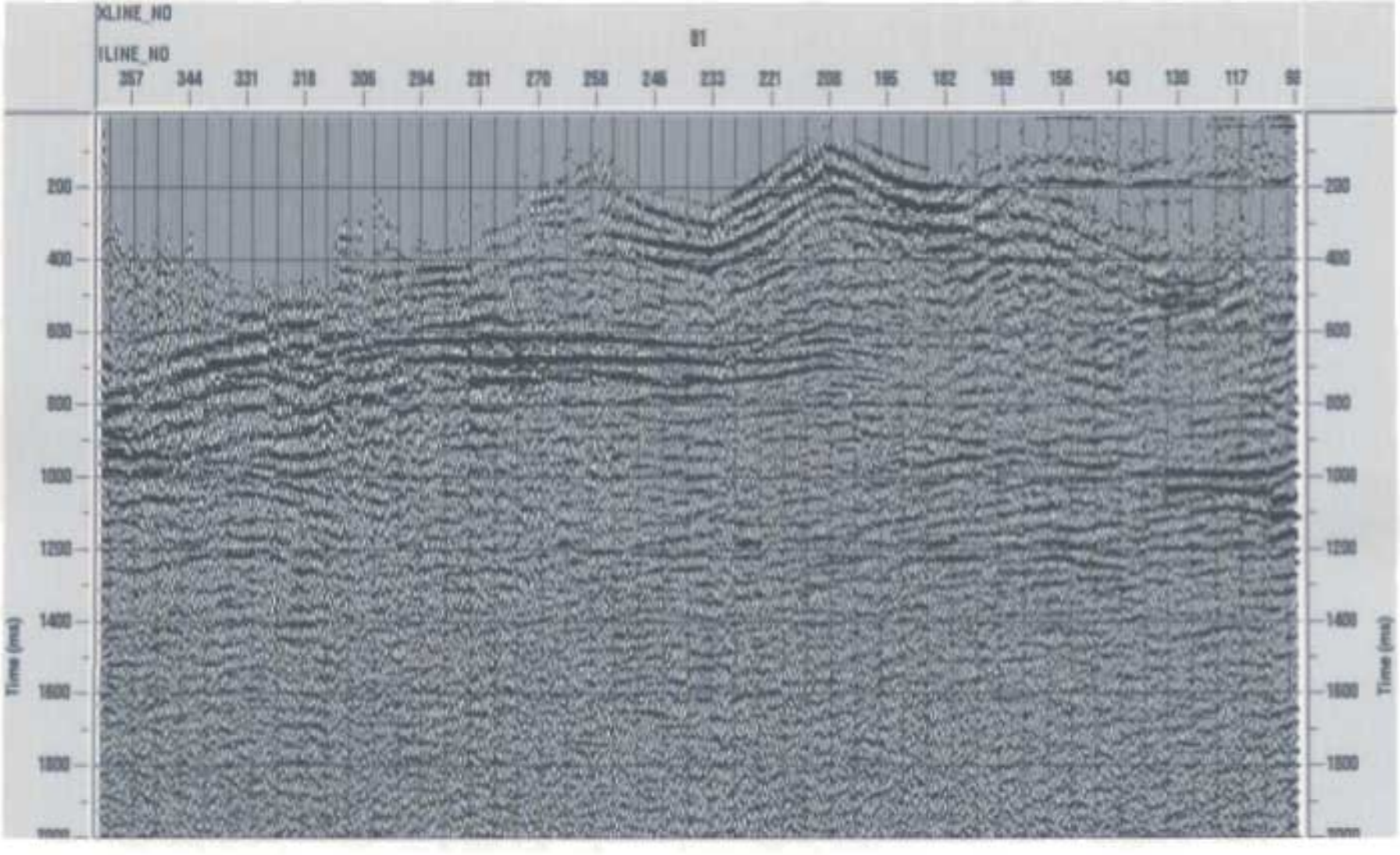

Figure 5.25(a). Xline 81 stacked with no post normal moveout correction stretch mute.

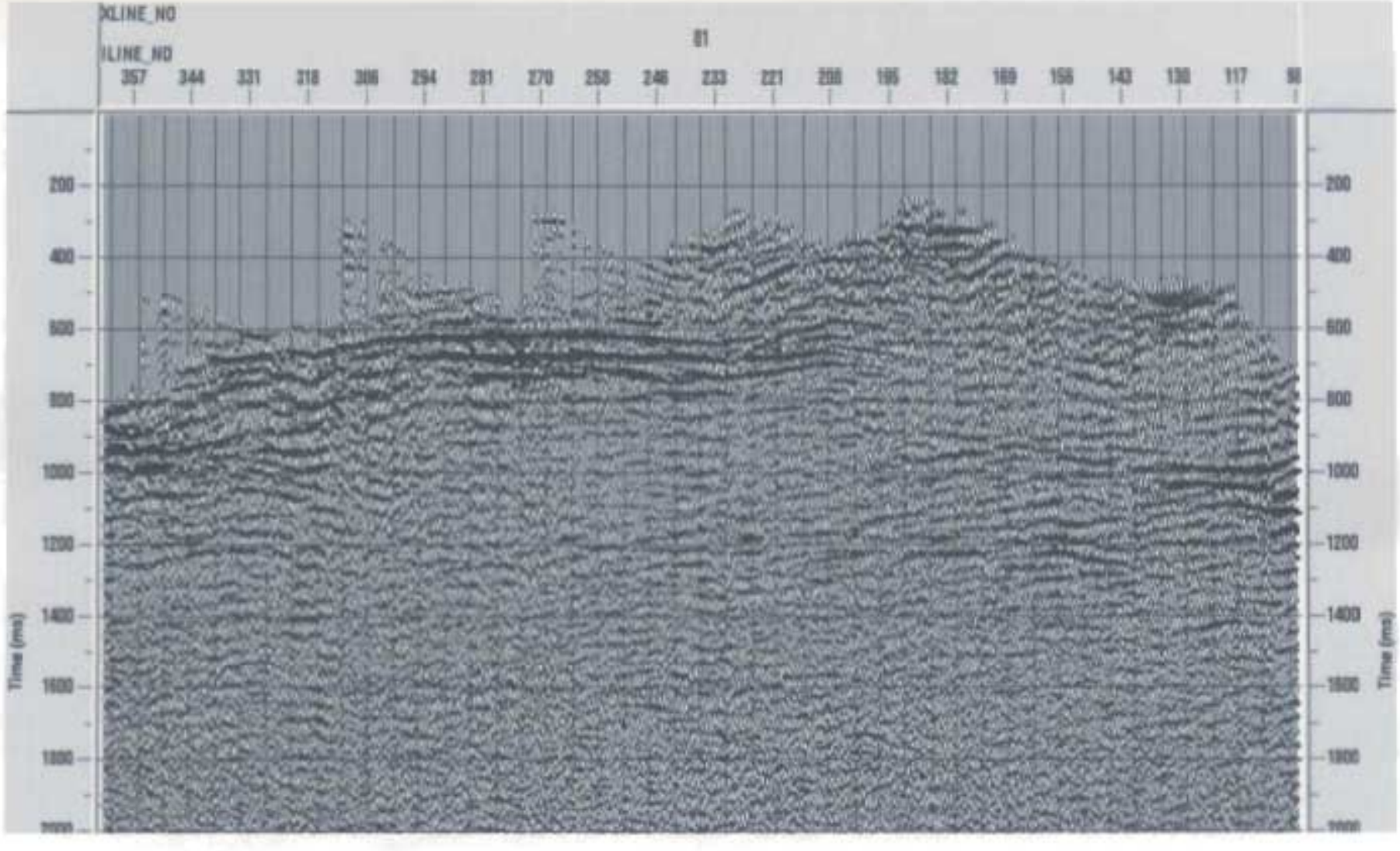

Figure 5.25(b). Xline 81 stacked with a post normal moveout correction stretch mute allowing 75% wavelet stretch.

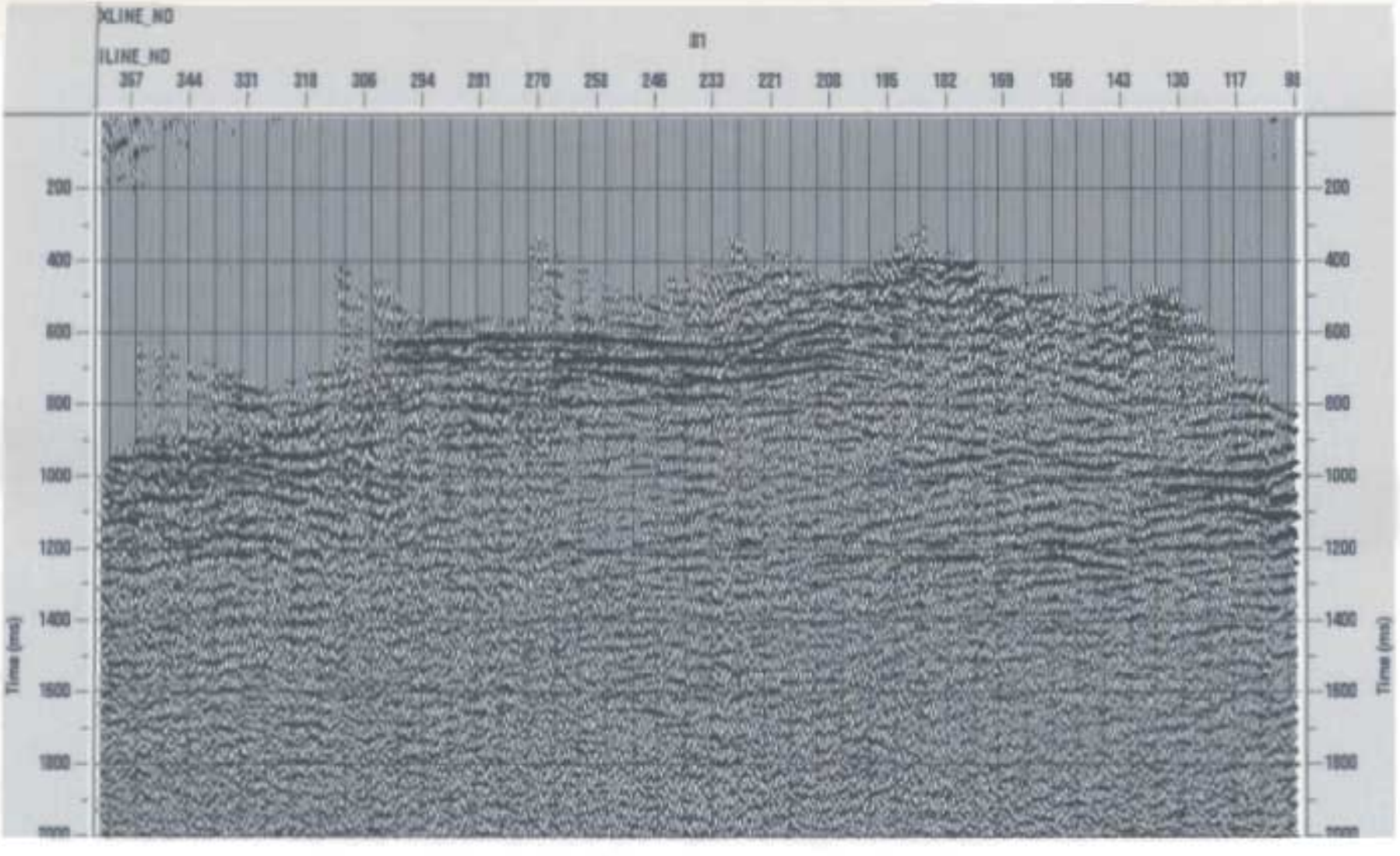

Figure 5.25(c). Xline 81 stacked with a post normal moveout correction stretch mute allowing 50% wavelet stretch.

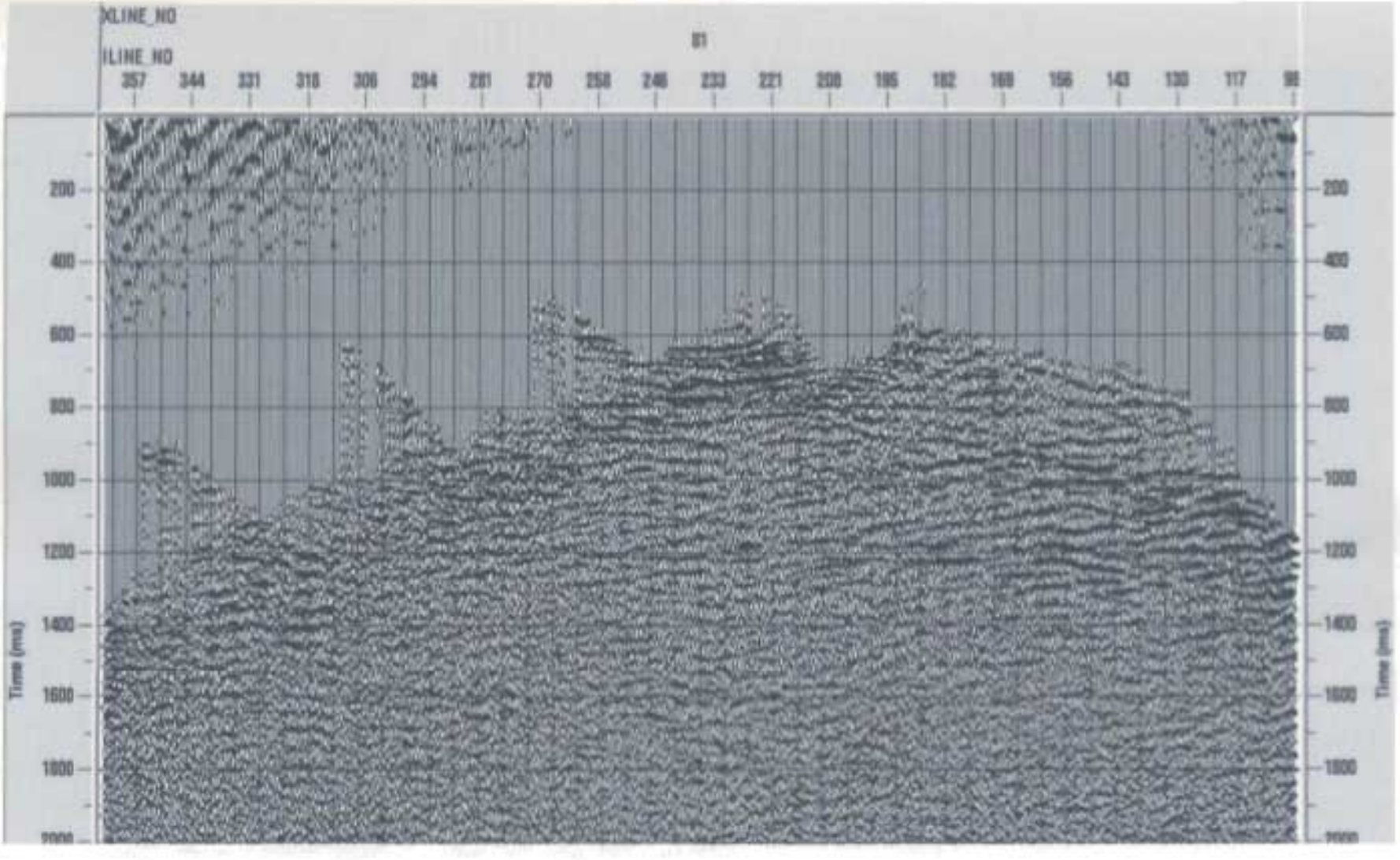

Figure 5.25(d). Xline 81 stacked with a post normal moveout correction stretch mute allowing 25% wavelet stretch.

5.2.11 Bandpass Filter

A conventional zero phase butterworth filter with the following frequency ramps and cutoffs was applied: 15Hz – 20Hz – 60Hz – 120Hz. In this situation it was clear that high frequency coherent signal would not be affected and any additional low frequency noise that passed through previous processes would be removed.

5.2.12 Trace Equalization

The primary objective of applying the trace equalization was the removal of any spurious bursts of signal missed during the editing sequence or previous scaling attempts. A time-invariant trace-balancing function using RMS amplitude criterion was applied to the dataset pre-stack.

5.2.13 Flex Binning

Flex binning is the manipulation and particularly the expansion of the pre-defined bin dimensions of a seismic survey, which in this case are 50m x 12.5m. Application of this technique is ideal for irregular datasets with irregular fold coverage and offset distributions as is seen in the Shoal Point 3D data. The desired effect of applying flex binning is to allow for more uniform fold coverage and offset distribution. It will also increase the actual fold in all individual bins,

important in situations like the current dataset where the fold coverage is considerably low and scarce in areas.

The application of flex binning involved testing of several expanded dimensions in the xline direction. Final expanded binning parameters decided on were 50m x 50m, such that the 12.5m xline dimension was increased by a factor of 4. The outcome of flex binning was an increase in average fold per bin from 8 traces to 20, therefore expanding the CDP footprint and broadening the CDP offset distribution.

5.2.14 CDP Stacking

A ProMAX® process called Stack 3D was used for CDP stacking of the 3D Shoal Point dataset. The function of the stack 3D process is vertically summing input ensembles of traces using a straight mean stack algorithm. The straight mean stack algorithm sums the sample values contributing to each CDP and divides by the number of samples summed raised to a supplied power. It is at this stage of the processing flow that a structural stack of the data is obtained (Figure 5.26), all future processes will be applied in the post-stack domain.

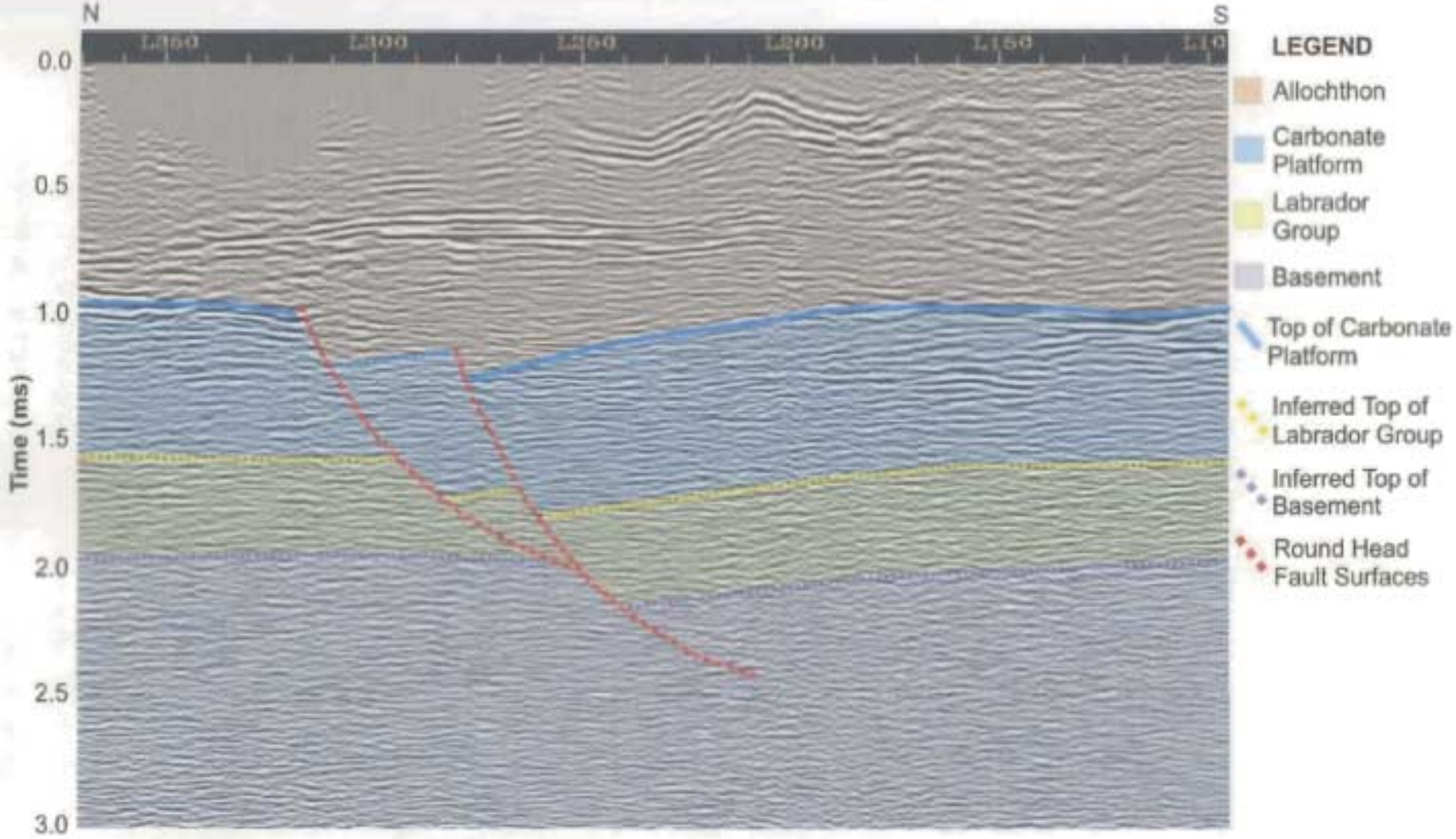

Figure 5.26. 3D xline 81, a typical example of stacked data from the 3D volume.

5.2.15 Post Stack Migration

The final step in the processing sequence is migration. Migration transforms the stacked seismic data so that it appears similar to a true geologic cross-section along the seismic traverse. There are two types of migration with slightly different goals. Time migration relocates dipping reflections to their true subsurface positions and collapses diffractions, thus increasing spatial resolution and yielding a better seismic image of the subsurface geology (Yilmaz, 2001). Depth migration accomplishes the same goal as time migration and in addition uses a user-provided velocity field to convert the sections to depth (from TWT).

The application of either form of migration is acceptable in a variety of different situations although the determining characteristic of the dataset that must be considered when selecting the migration format is lateral velocity variation. A time migration is appropriate as long as the lateral velocity variations within the subsurface geology are not too severe. In cases where the lateral velocity gradients are significant, a time migration will not correctly image the data producing a false subsurface picture. It is in this situation that the processer should consider the alternative of depth migration. It should further be noted that increasingly a full pre-stack depth migration is replacing post-stack migration processing. However in this instance the data are too noisy for an effective pre-stack migration to be applied.

Choice of the proper migration strategy is a key step during processing that should take into consideration the following points prior to selection (Yilmaz, 2001):

- A migration algorithm compatible with the strategy.
- Appropriate parameters for the algorithm.
- Migration velocities.

Possible migrations strategies include (Yilmaz, 2001):

- 2D vs. 3D
- post-stack vs. pre-stack
- time vs. depth

The choice between the options above ultimately comes down to what data quality will allow you to accomplish and how accurate a cross-section is necessary. When stepping into the realm of 3D pre-stack or depth migrations, the increased cost and time must be considered. Each of these processes generally adds extensive testing and computation time to the processing and therefore incurs an increased cost. In general 2D / 3D post-stack time migrations are most often used as they are the least sensitive to velocity errors while being able to generate acceptable results for reliable interpretations (Yilmaz, 2001).

Migration considerations and testing for the Shoal Point dataset involved migration the following techniques:

- A 3D post-stack Stolt time migration.
- A 3D post-stack explicit finite difference time migration.

5.2.15.1 Stolt Time Migration (FK)

The Stolt time migration is an F-K migration. Typically considered as one of the simpler migration methods the Stolt method is fast but limited in cases with vertically varying velocities. Originally designed for computation using a constant velocity situation, ProMAX® has been able to include vertical velocity variation by implementation of a Stolt stretch factor. This is a modification of the velocity field by the ratio of the local RMS velocity to the lowest RMS velocity on the data section.

The following seismic sections represent xline 81 with Stolt migration applied for the following percentages of the total RMS velocity field:

Table 5.5: Sample migration velocities.

Figure 5.26	Migration velocity	% of actual RMS stacking velocity
(a)	1000	~ 20%
(b)	2000	~ 30%
(c)	3000	~ 50%

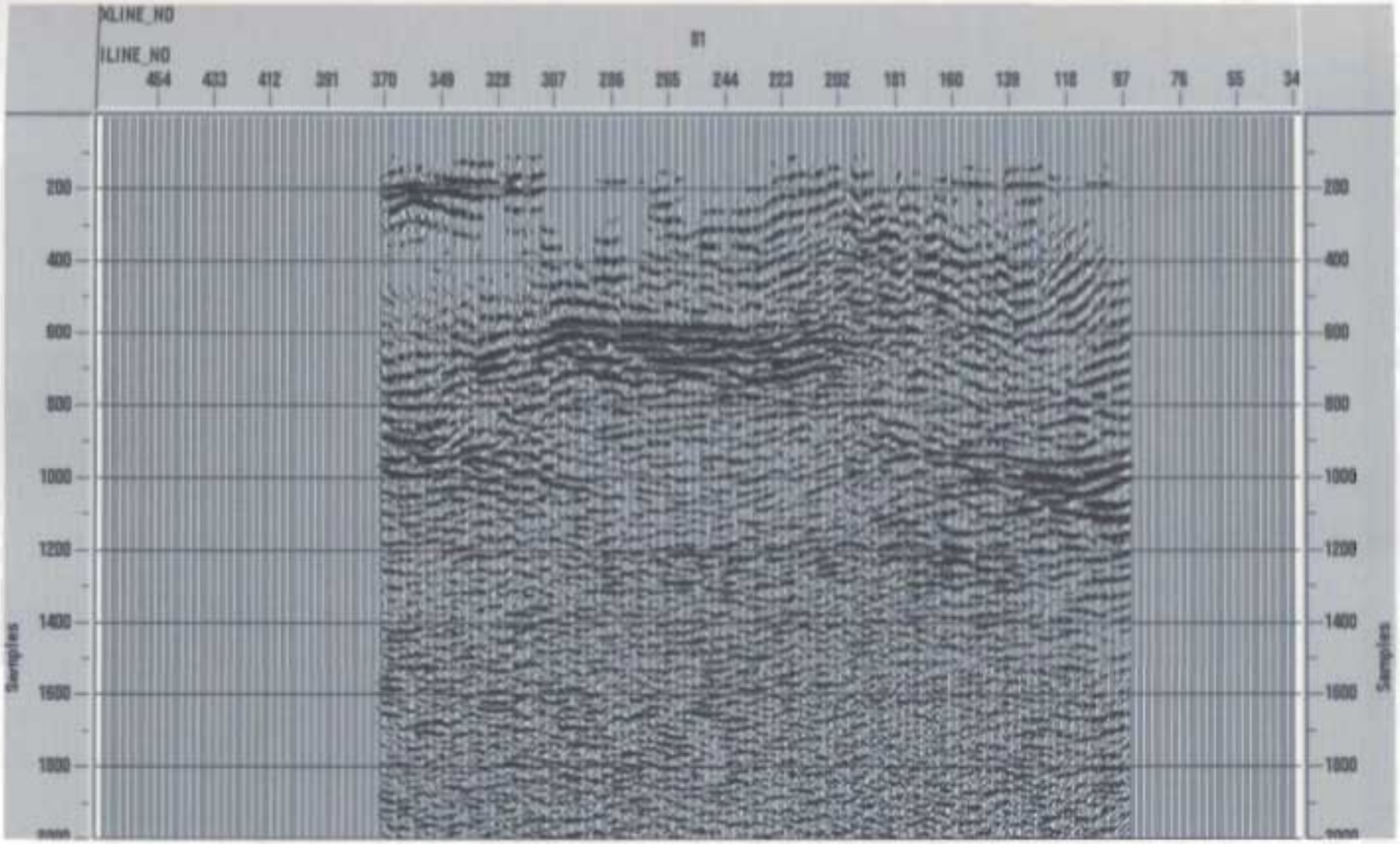

Figure 5.27a. Xline 81 Stolt migrated using a constant velocity of 1000m/s interval velocity function.

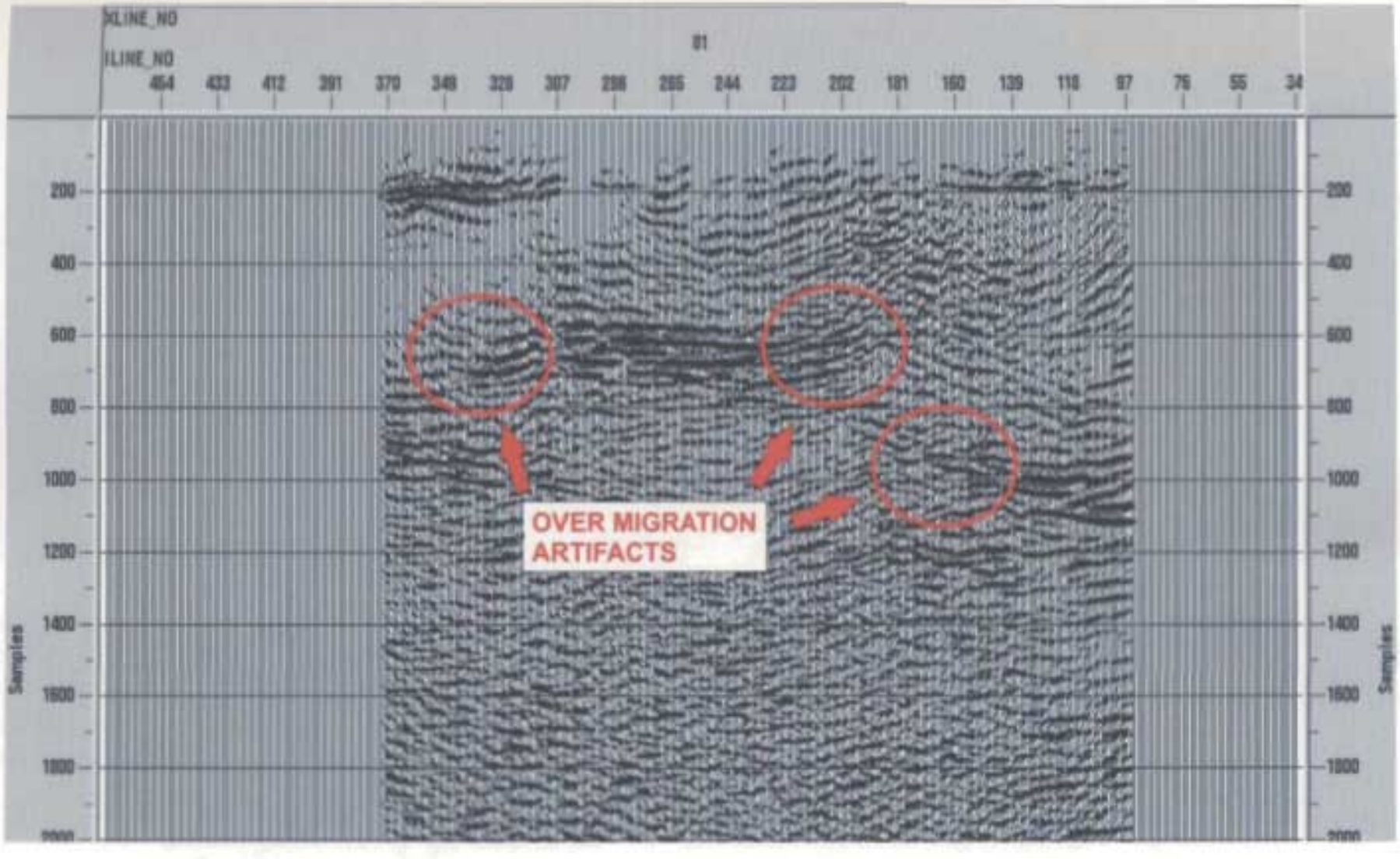

Figure 5.27b. Xline 81 Stolt migrated using a constant velocity of 2000m/s interval velocity function. Note the presence of overmigration artifacts that were not visible on 5.26a.

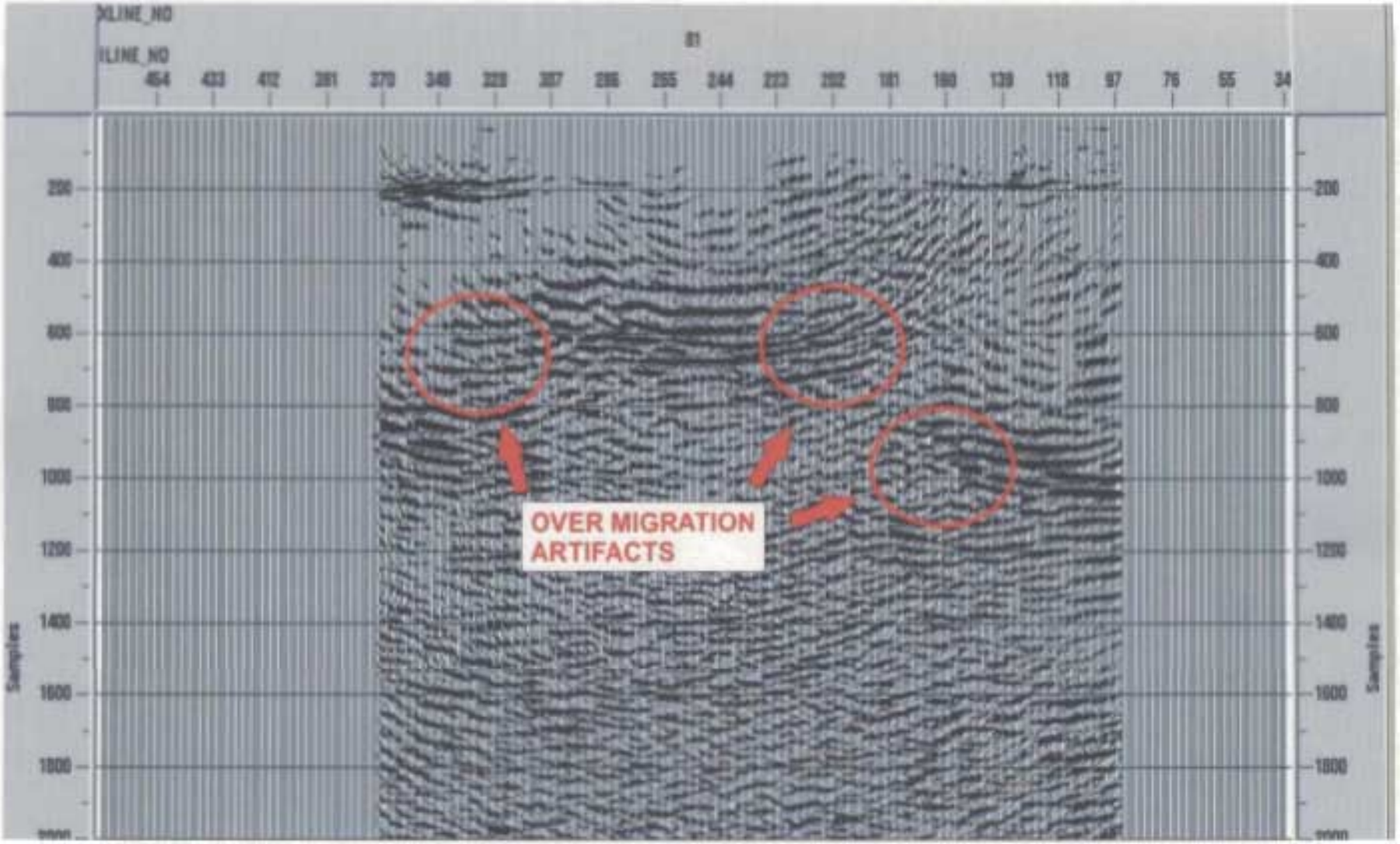

Figure 5.27c. Xline 81 Stolt migrated using a constant velocity of 3000m/s interval velocity function.

5.2.15.2 Finite Difference (FD) Migration

For 3D finite difference migration, ProMAX® applies an algorithm that uses F-X-Y spatially-variant convolution filters to provide explicit solutions to the scalar wave equation. A vertically and horizontally varying interval velocity function is necessary for operation of the finite difference migration. Testing involved a range of velocity functions. The following percentages of the RMS velocity function were tested, along with the following constant velocity functions:

Table 5.6: Sample FD migration velocities (% of RMS velocity function).

% of RMS stack velocity
45%
60%
75%

Table 5.7: Sample FD migration velocities (constant velocity function).

Figure 5.27	Migration velocity	% of RMS stack velocity
(a)	1000	~ 20%
(b)	2000	~ 30%
(c)	3000	~ 50%

The following seismic sections represent xline 81 with constant velocity FD migrations applied.

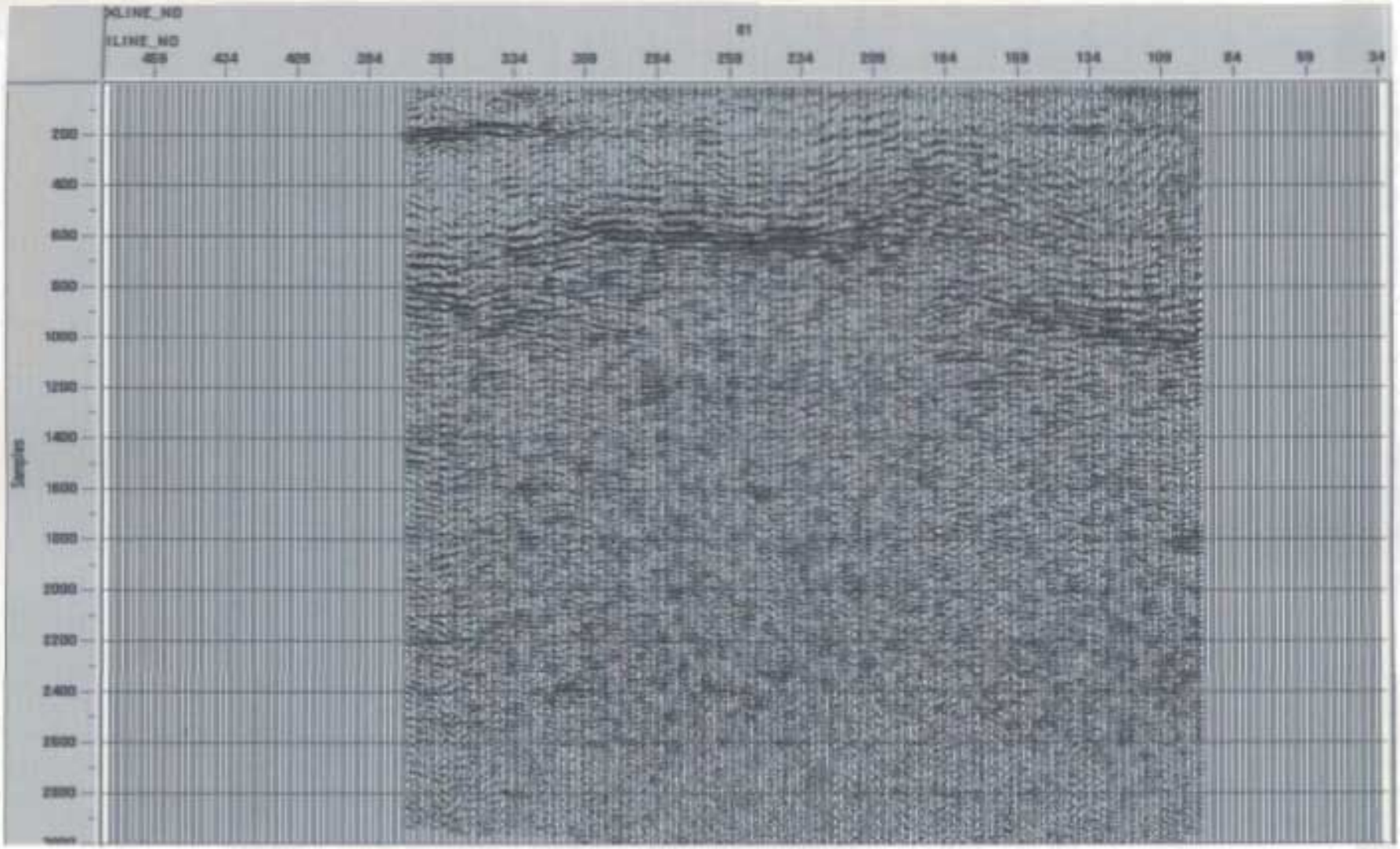

Figure 5.28a. Xline 81 Finite Difference migrated using a constant velocity of 1000m/s interval velocity function.

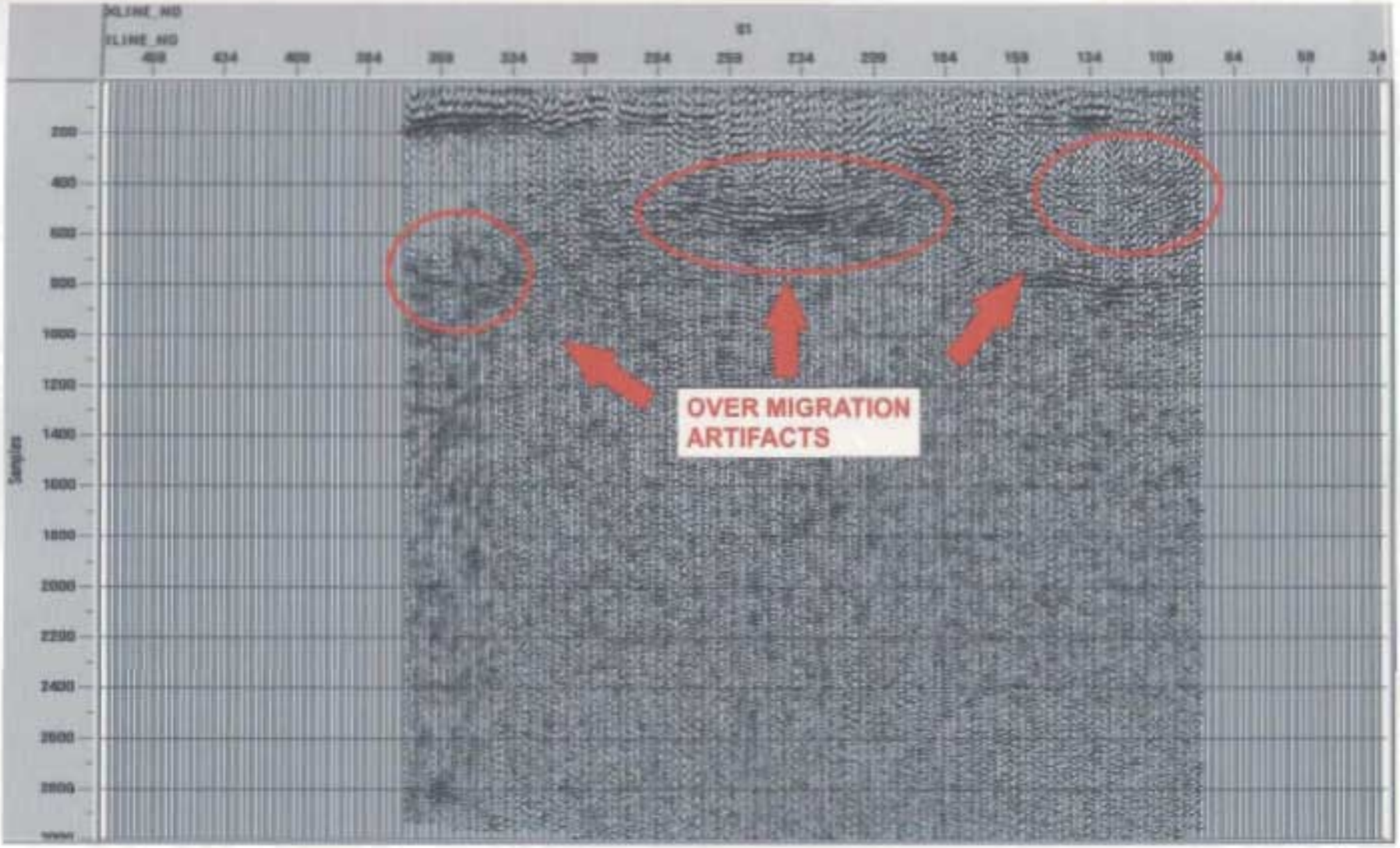

Figure 5.28b. Xline 81 Stolt migrated using a constant velocity of 2000m/s interval velocity function. Note the presence of excessive overmigration artifacts.

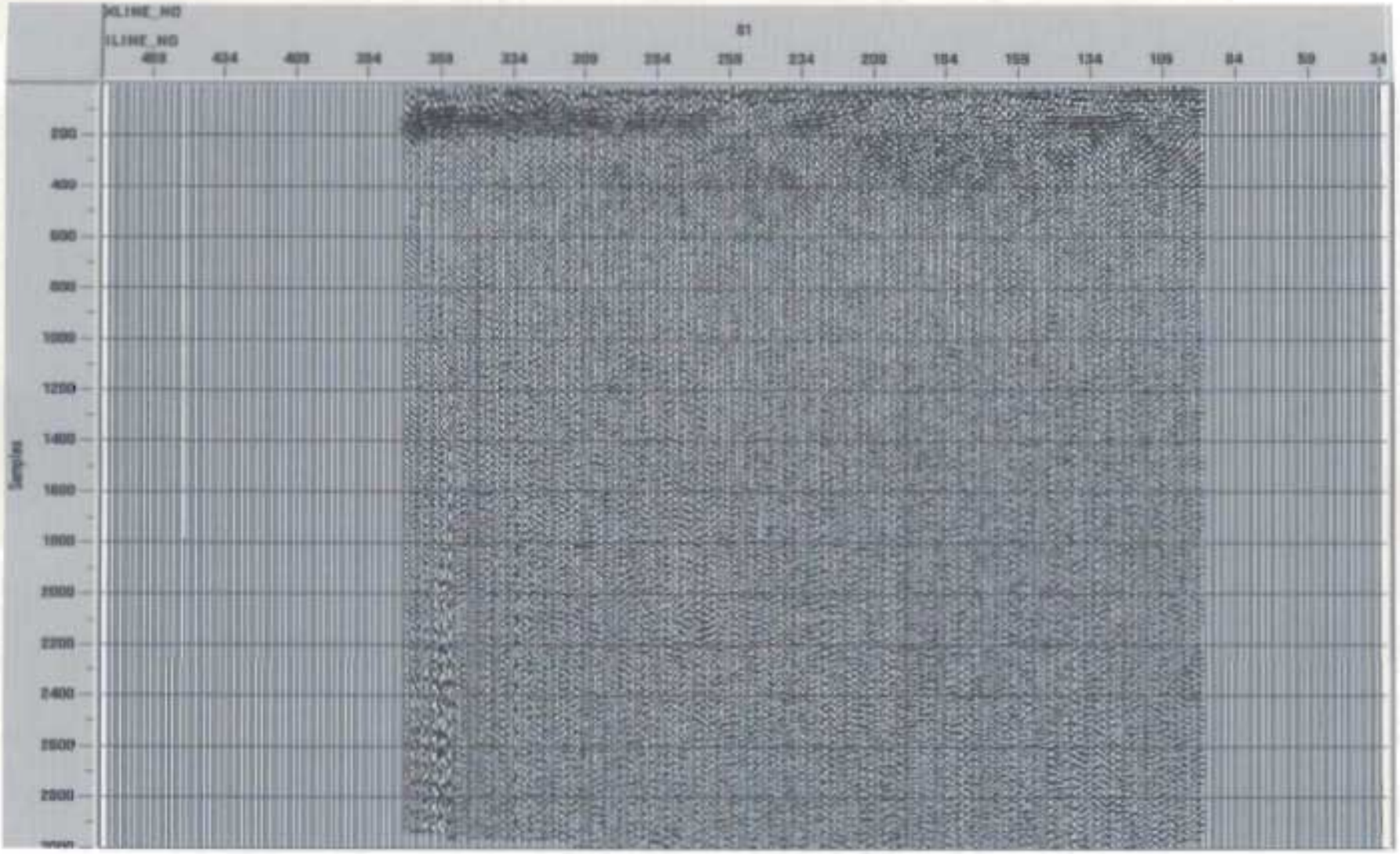

Figure 5.28c. Xline 81 Finite Difference migrated using a constant velocity of 3000m/s interval velocity function.

5.2.15.3 Migration Conclusion

Consideration of the above migration displays clearly indicates that the application of a correct post-stack migration will be difficult. The dominant characteristic of the migrated sections is over migration represented in the form of excessive migration smiles. Typically this feature would indicate the application of too high a velocity function, but it is clear in figures 5.26b, 5.27b where only 30% of the interval velocity function is used there are still over migration smiles. Realistically the migration values should be more in the range of 80% – 90% of the interval velocities. From existing seismic in the bay, it is clear that for a higher quality dataset migration can be correctly applied using realistic interval velocities.

In my opinion this artifact problem and inability to migrate is not due to incorrect velocities but is more a combination of issues including the following:

- Low signal / noise ratio
- Poor distribution of offsets
- NMO stretch issues
- Complex geological setting

Necessary steps such as no NMO stretch muting, combined with the poor signal / high noise, and a complex geology from an extremely fragmented allochthon

caused the migration to focus on these features and therefore generate the inaccurate seismic response. Because of this difficulty, a migration was not retained in the final processing sequence and all interpretation was completed using structurally stacked, unmigrated sections.

5.3 Processing Conclusion

Overall the 3D data processing was lengthy and iterative due to the poor quality and data limitation problems. The stacked data is generally only fair with sporadic xlines displaying quite good imaging of the Cambro-Ordovician carbonate platform. This is exacerbated by the faulted nature of the top of the platform. Appendix A contains the complete volume of stacked xlines for the 3D dataset. Examples of the higher quality lines with imaging comparable to industry seismic data include xlines 60, 81, 82, 83, 84 and 95. The final 3D seismic product was not migrated and therefore the geological interpretation was completed using structurally stacked sections. In the following Chapter I successfully use the stacked sections to interpret the top of the carbonate platform and major fault surfaces.

6.0 Interpretation

The ultimate goal of the Shoal Point project is the successful mapping of the top of the Ordovician carbonate platform and the Round Head fault system in the Shoal Bay area. The 3D seismic interpretation will be used to produce 3D maps in TWT of the top of the platform, allochthonous thrust sheets and internal carbonate platform horizon. The successful completion of this task will be the measure of the overall project goal achievement.

As has been previously discussed in Chapter 5, the interpretation was completed using structurally stacked seismic data. The following analysis will show that areas of the stacked 3D volume clearly display an image of the carbonate platform that corresponds to the seismic interpretations I have picked for the 2D Shoal Point landline and the surrounding Hunt / PanCanadian 2D marine seismic lines. Established correlation between these two seismic surveys allows the interpolation of the platform reflector into areas of the 3D survey volume where the data quality is poor. It is important to note that picking of the carbonate platform along the northern end on many lines is difficult. In areas of the 3D data where the picks are ghosted through there is a higher level of uncertainty relative to that pick location. To lower pick uncertainty iterative interpretation using all three datasets was employed, this process therefore enabled the production of a final 3D map that is self-consistent, accurate and geologically realistic.

Interpretation and mapping of the Shoal Point 2D and 3D seismic was completed at Memorial University on Unix based Silicon Graphics work stations. The Landmark Graphics Corporation interpretation package Seisworks® 2D / 3D, was used for selection of all relevant horizons and fault surfaces. Conversion of geological horizons from Seisworks® into 3D maps was accomplished using Gocad®, a geoscience-modeling program by Earth Decision Sciences. My interpretation of the 1997 Hunt seismic data was completed on un-interpreted paper seismic sections obtained as public record at the Canada Newfoundland Offshore Petroleum Board library.

As previously discussed in Chapter 2 (Geology) I will describe the seismic stratigraphy by subdivision of the basin geology into four dominant geological and stratigraphic units, which are as follows:

1. Taconic Allochthon sequence (Carbonates and basinal shales from the Ordovician platform sequence)
2. Ordovician Carbonate platform sequence (Port au Port Group, St. George Group, Table Head Group, Goose Tickle Group)
3. Pre-Ordovician Labrador Group (Primarily clastics of the Hawke Bay, Forteau and Bradore Formations)
4. Grenvillian Basement

6.1 Interpretation of the 2D Hunt / PanCanadian Seismic Data

The 1997 Hunt seismic exploration program acquired within Shoal Bay was instrumental in aiding the overall interpretation of the 3D seismic volume. The seven-line OBC seismic survey contained three lines in particular that provided extensive aid in correlation of the platform throughout the study area. Line PAP-1 is located due west of the current area trending almost N-S. Line PAP-2 runs on the diagonal NW-SE through the NE corner of the 3D area and line PAP-7, which trends N-S, is located on the eastern edge of the new 3D seismic volume (Figure 6.1).

All seven of the Hunt PAP series seismic lines were interpreted during this stage, with special attention paid to the location of the Round Head fault and the hanging-wall / footwall relationship. For the purpose of this study, only the specific common midpoint ranges directly comparable to the current data are discussed. Line PAP-1 is approximately 20km long running from the south of West Bay to Long Point. The common midpoint (CMP) range of specific interest corresponding to seismic data situated less then 1km west of the 3D data volume is CMP 300 – 550. Line PAP-7 was acquired at the eastern edge of the current 3D survey and is also in excess of 20km length. In this case, the relevant CMP range is 150-250. Finally line PAP-2 trends NW-SE through the northeastern corner of the current area with CMP's 300-500 of direct interest in this study.

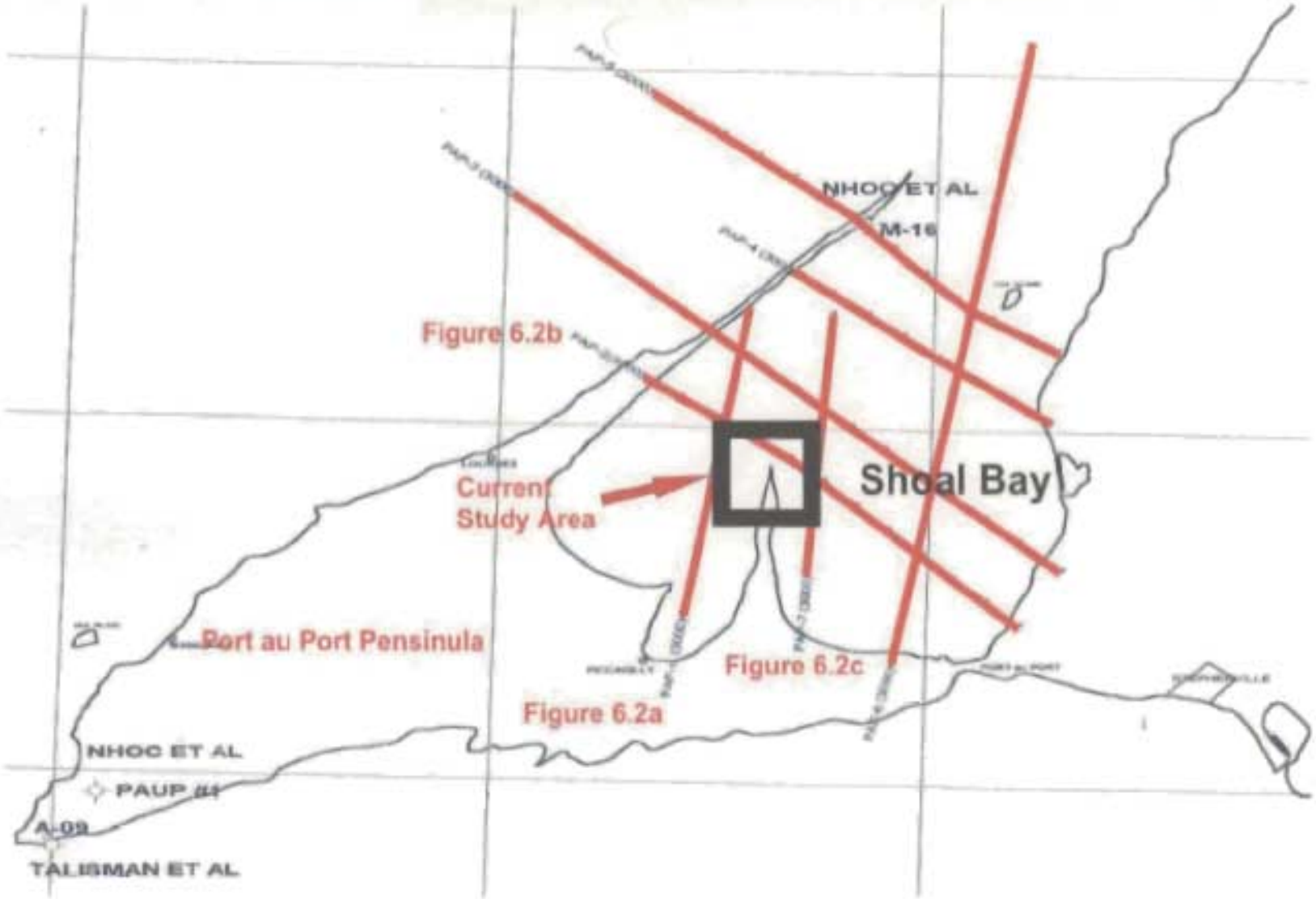

Figure 6.1. Seismic line locations acquired by Hunt and partners in 1996 for the Shoal Bay exploration program. Overlain is the current project area and following figure locations..

6.1.1 Taconic Allochthon Sequence

The shallow-most sediments within the bay, the allochthon covers the entire area with dramatic variations in thickness throughout. Thickest in the north, the allochthonous sequence thins consistently towards the south as the carbonate platform, upon which it was emplaced, steps to the surface (Figures 6.2a, b, c). At the southern tip of all three lines the seafloor surface of the allochthon meets the basal detachment surface, such that the allochthon sediment package is not present in the area south of this point.

The internal geology of the allochthon consists of fragmented thrust slices of carbonate and clastic sediments from the lower shelf sequence (Cooper et al., 1998). Generally a poorly imaged sequence, the allochthon within the bay does not exhibit continuous competent seismic reflectors that can be mapped on a regional scale. However, in some areas thrust slices similar to those imaged in the Triangle zone (Figure 2.3b) are present. (Figure 6.2c has been annotated for an allochthonous slice in the area of the Round Head thrust). Carbonate thrust surfaces range in size as we can see in this example where the sheet is in excess of 1500m long within the plane of the seismic line. The thrust faults themselves are difficult to interpret and are not clearly imaged on any of the seismic lines within Shoal Bay.

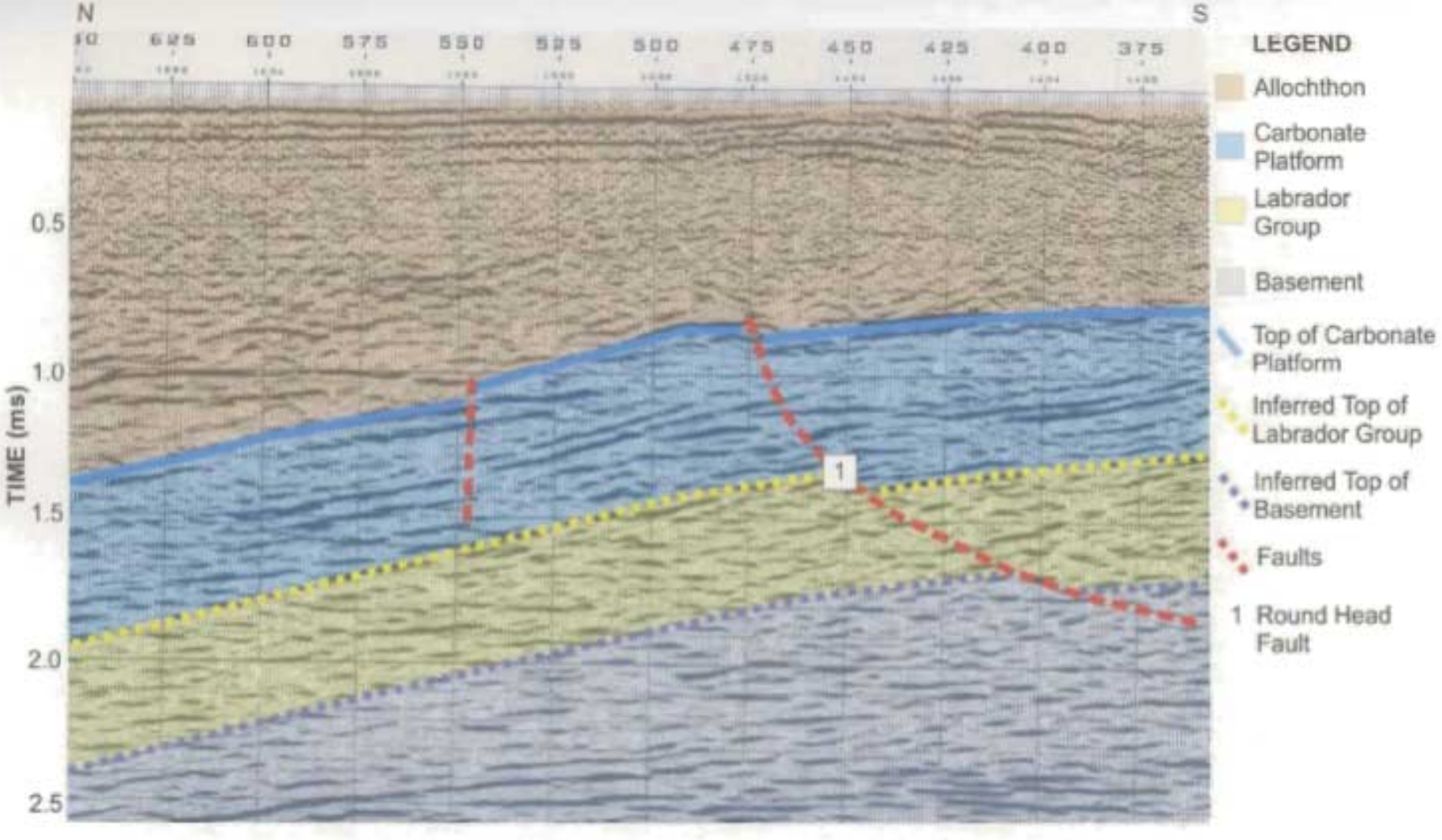

Figure 6.2a. Hunt seismic line PAP-1 acquired on the western edge of the current study area, note there is only minor extension on the Round Head fault system (See figure 6.1 for exact location).

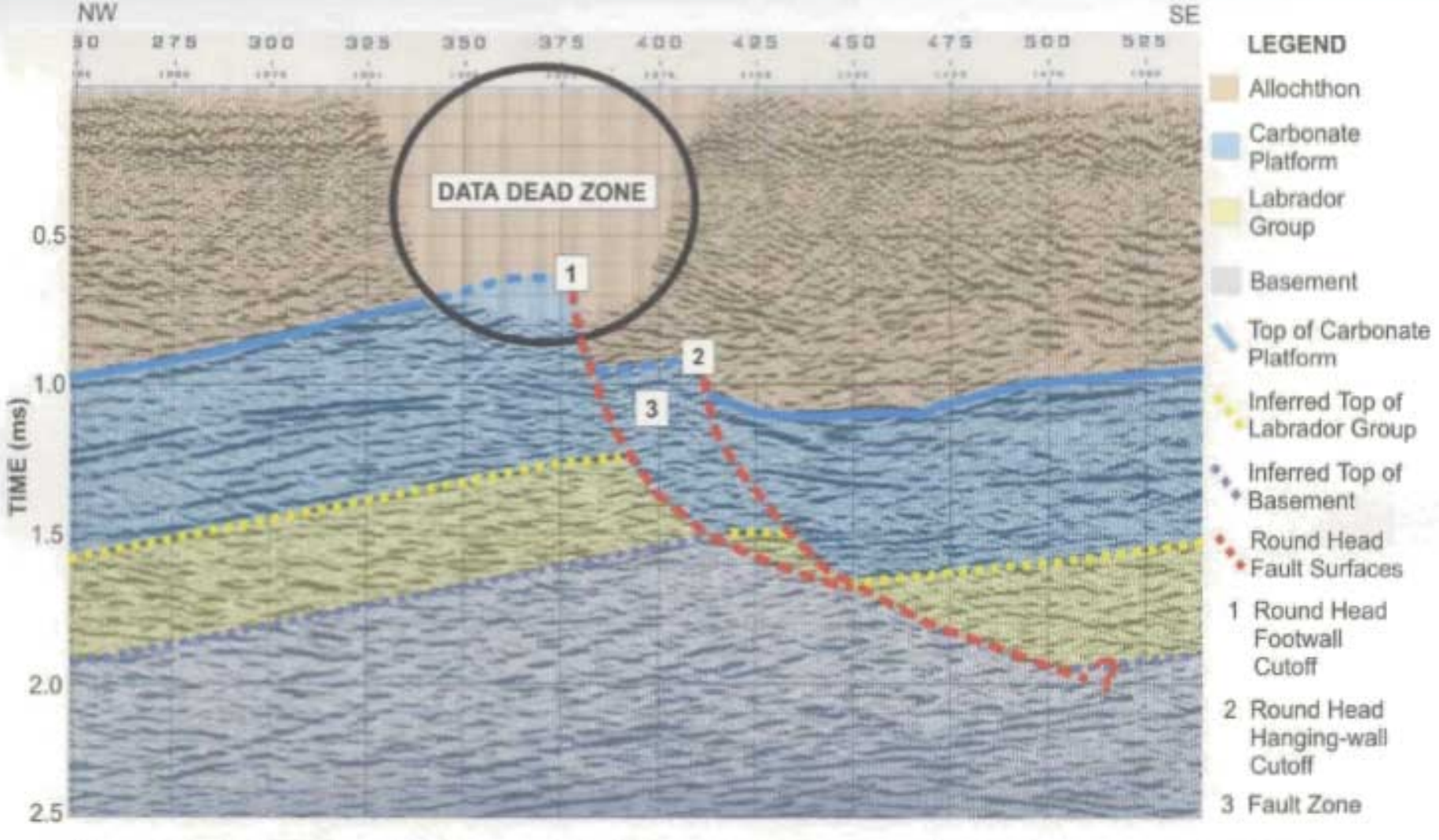

Figure 6.2b. Hunt seismic line PAP-2 acquired NW-SE through Shoal Bay. The data dead zone corresponds to Shoal Point and therefore waters too shallow for the source boats. Note the extension of the Round Head fault system.

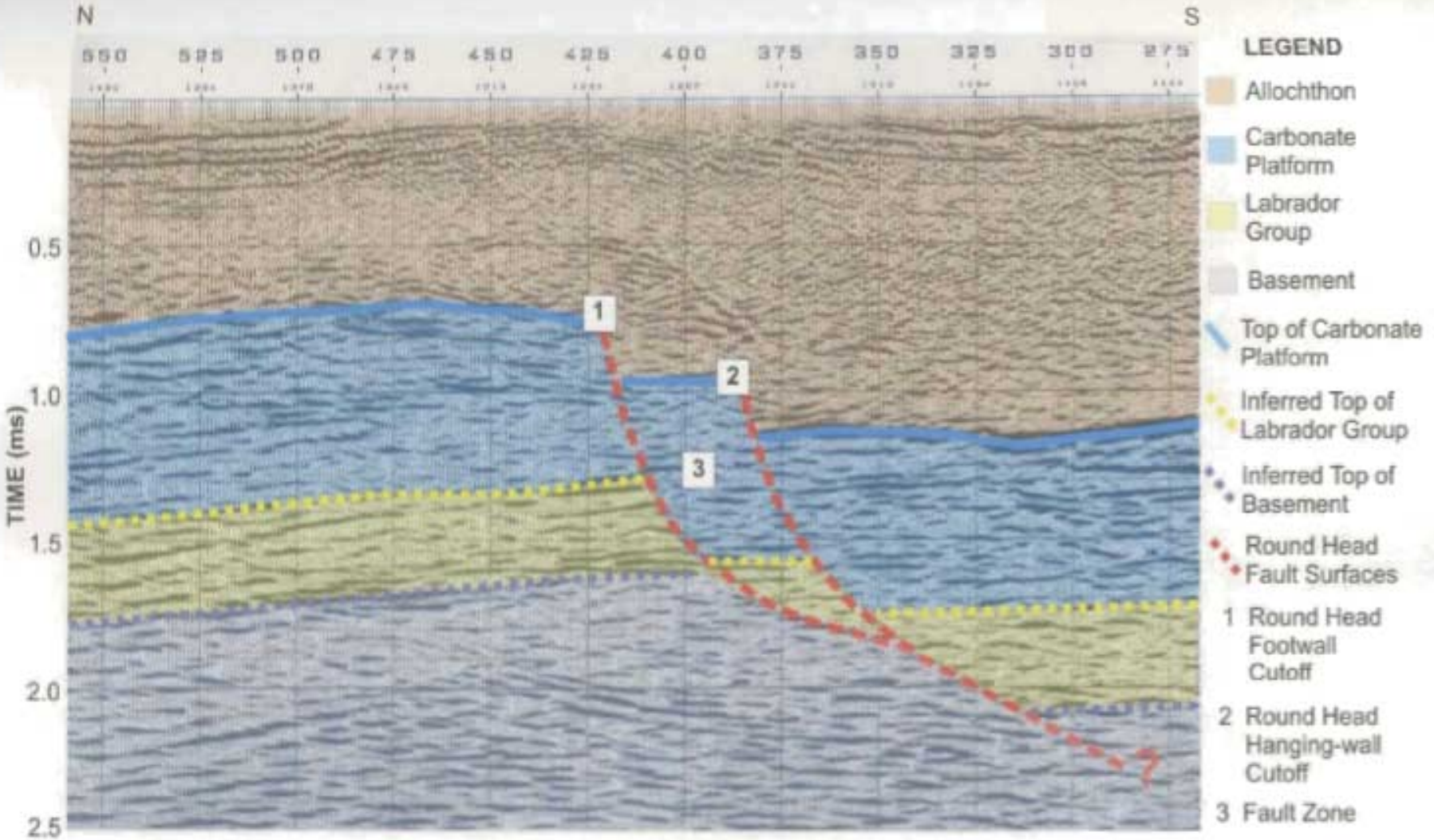

Figure 6.2c. Hunt seismic line PAP-7 acquired on the eastern edge of the current study area, note the net extension of the Round Head fault system (See figure 6.1 for exact location).

6.1.2 Ordovician Carbonate Platform Sequence

The top of the Ordovician carbonate platform seismic expression is the characteristic seismic marker of the Port au Port peninsula. The continuous platformal reflectors are characterized by a top platform doublet seismic expression followed by a package of extremely reflective horizons. Platform thickness does not vary dramatically within the bay and the sequence is imaged as a parallel package ranging from 500ms – 700ms TWT in overall thickness (approximate average of 1250m thickness).

Deepest in the north, the top of the carbonate platform consistently shallows towards the south and outcrops on land at the southern edge of Shoal Bay. The carbonate platform is most discontinuous and difficult to image in the area corresponding to the 3D seismic survey. Again, this situation is a result of the Round Head fault expression, which is believed to be an inverted fault system from an earlier Taconic extensional fairway. Mapped on land as a large thrust fault, it appears that the compressional forces within the bay were insufficient to completely invert it to a thrust association and therefore it remains in net extension.

The expression of the Round Head fault varies dramatically between the three Hunt lines surrounding the current study area. On each line the same structural association is being imaged to show different degrees of extension. Figure 6.2a

(PAP-1) images the null point of the Round Head fault geometry: here it can be seen that a fault plane is present, but the net extension is small. Moving east to the N-S trending line PAP-7, the Round Head fault seismic expression is now clearly in net extension (Figures 6.2a, b, c). The obvious effect of this on the carbonate platform is that geology is truncated and offset across the fault zone. The change in fault geometry as one steps east from line PAP-1 is that instead of a single major fault plane, the system now is comprised of multiple large faults / fault splays. These splays define separate hanging-wall and footwall cutoff points (Figures 6.2a, b, c) with a fault zone between them.

Fault offset between the carbonate platform hanging-wall and footwall surfaces increases consistently from west to east across the 3D survey area. Figure 6.2a from the western edge exhibits a small net extension in the platform of about 50ms TWT, approximately 100m of extensional offset. Traveling east to line PAP-7 (Figure 6.2c) on the eastern edge, the Round Head fault net extension has increased and the hanging-wall and footwall cutoff points are now offset 400ms TWT or 900m in overall extension. This overall trend is consistent and will be discussed further and clearly displayed in the following 3D maps of the platform surfaces.

6.1.3 Pre-Ordovician Labrador Group

The oldest sediments of the basin, the Labrador Group, consist of varying reefal limestones, marine shales and shallow marine sands (Cooper et al., 1998). Seismically there is no dominant top Labrador Group reflector comparable to the doublet expression of the Ordovician carbonate platform. It is difficult to pick the exact top of the Labrador Group; but, from consideration of previous drill information and seismic land data from the Port au Port peninsula, it is possible to infer an accurate base platform and therefore top Labrador Group sequence. Overall sediment thickness variation of the Group within the survey area appears to be minimal. The Labrador Group exhibits the same geographic dips and trends seen in the overlying stratigraphy of the carbonate platform. Exact thickness is difficult to quantify, as the top, and especially the basal contact with the Grenvillian basement are not easily distinguishable.

The effect of the Round Head fault on the Labrador Group is substantial and fault movement has generated extensional offset of Labrador Group geology that is comparable to the previous values discussed for the platform in figures 6.2a-c. The major fault planes of the Round Head system appear to merge together at the base of the Group near the basement contact, continuing to travel deeper to a basal detachment surface within the Grenvillian basement.

6.1.4 Grenvillian Basement

The basement sequence consists of Grenvillian age crystalline igneous rock. Seismically imaged on all of the current Shoal Point project seismic data and the adjacent Hunt / PanCanadian seismic lines, the basement is consistent throughout the entire study area and the Port au Port peninsula. The inferred top of basement horizon (Figures 6.2a-c, 6.3, 6.5a-d) corresponds to the overall trends of the carbonate platform shallowing to the south. In the area of the Round Head fault the basement is uplifted to its shallowest levels, equivalent to an average maximum of 1500ms TWT and a depth of approximately 3000m-3500m.

Internally the igneous basement contains a package of strong seismic reflectors dipping to the south. Continuous within the plane of the seismic lines, I interpret the highly reflective horizons as layering of the igneous fabric corresponding to previous deformation. These results correspond to previous independent Lithoprobe studies conducted during the early1990's. Quinlan et al., (1992) concluded that the strong basement reflectors dipping toward the southeast correspond to internal reflection fabrics that are indicators of Mid-Ordovician to Mid-Silurian strain.

6.2 2D Shoal Point Landline

An extremely important piece of the final 3D interpretation, the 2D land seismic data provides a conventional seismic image of the subsurface geology below the Shoal Point peninsula. This dataset provides an excellent check on the validity of the 3D seismic data and an additional source for interpretation of the carbonate platform within the study area.

The Shoal Point 2D landline is approximately 2km in length and covers the northern tip of the point. The data (6s TWT) will penetrate as deep as basement if any coherent seismic energy is returned from that depth. From previous work and the Hunt / PanCanadian seismic, it is known that the Round Head fault traverses across the bay somewhere in the area of the tip of Shoal Point. The key questions to be answered regarding the interpretation of the 2D line are:

1. Where is the platform under Shoal Point?
2. Is the Round Head fault imaged on land?

6.2.1 Taconic Allochthon Sequence

The Taconic Allochthon in the area of the Shoal Point landline is identical to that previously discussed for the Hunt seismic data. The seismic expression of this sequence is discontinuous with no interpretable horizons present at this location.

The overall thickness of the allochthon changes little along this short line with some slight thinning of the sequence to the south. At the north end of the line, the base of the allochthon is imaged at 1100ms TWT stepping up to 900ms TWT at its southern edge (Figure 6.3).

6.2.2 Ordovician Carbonate Platform Sequence

The landline displays the typical carbonate platform doublet and strong internal seismic reflectors discussed above (Figure 6.3). Again we see a gentle dipping in the platform horizons toward the north corresponding exactly to the seismic expressions interpreted on the Hunt seismic data. On the following interpreted seismic section, the top of the platform is easily identifiable at the southern end but becomes choppy in the middle of the line (SP 1052) and non-existent in the north (SP 1070-1112) (Figure 6.3).

The lack of seismic reflectors in the north could possibly be attributed to either poor data quality or absence of competent carbonate platform due to proximity to the Round Head fault. In this situation the resultant poor seismic image in the north is, in my opinion related to an increase in geological complexity on approach to the Round Head fault zone.

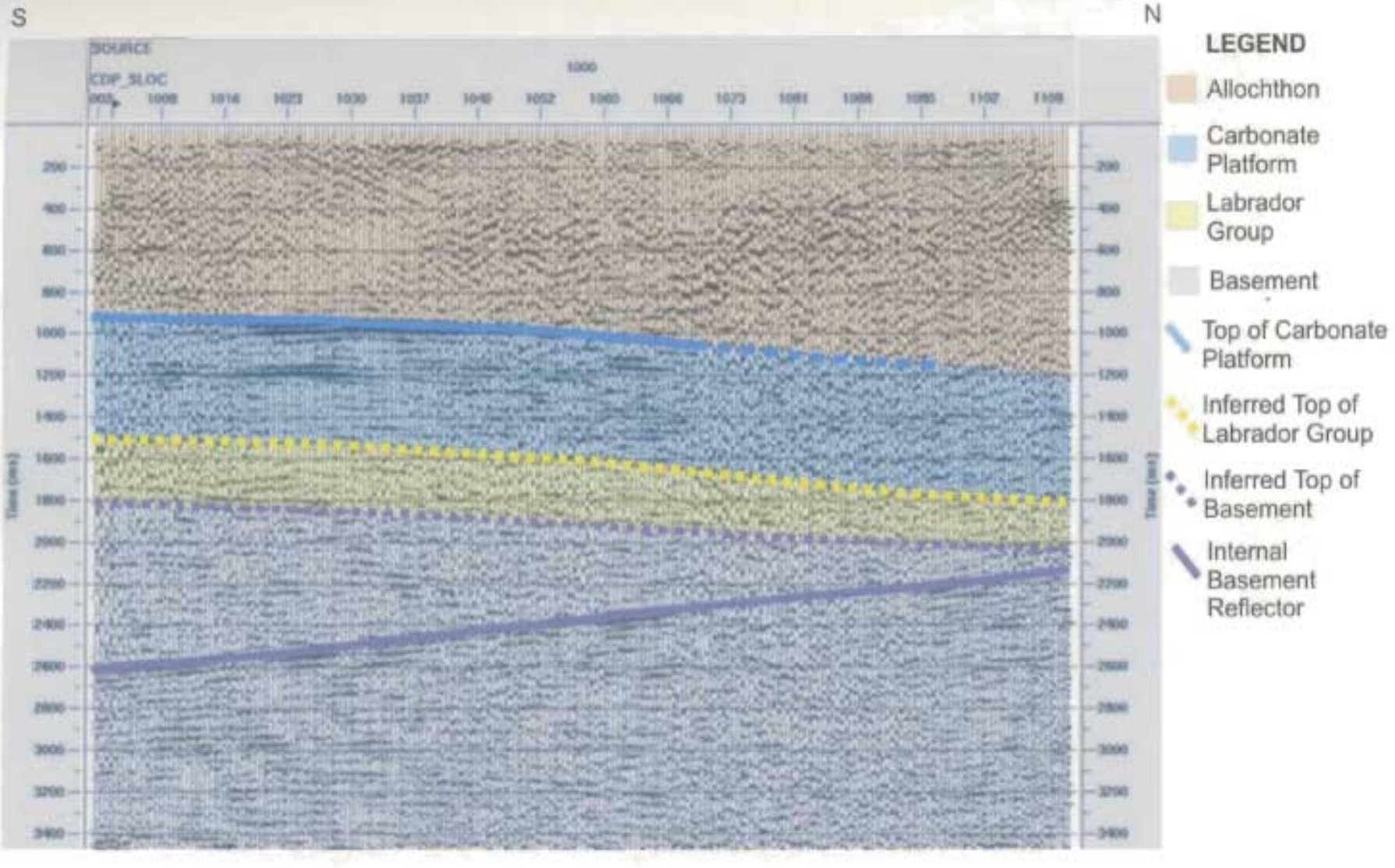

Figure 6.3. Shoal Point 2D dynamite landline interpreted for major geological horizons. The seismic discontinuity of the platform towards the north corresponds to encroachment of the Round Head fault system.

Unfortunately, the data quality is not ideal and when combined with the above situation the data does not image the hanging-wall cutoff point or fault surfaces. At this stage it is difficult to conclude if the fault system is present directly on the peninsula or located just slightly offshore. The following interpretation of the 3D seismic will address this question and define the interpreted location of the hanging-wall and footwall cutoffs.

6.2.3 Pre-Ordovician Labrador Group

The Labrador Group seismic expression displayed on the Shoal Point landline is comparable to the horizons interpreted on the Hunt data. Again the package trends parallel to the carbonate platform with little variation in overall thickness, in the northern section of the line the Labrador Group exhibits increased discontinuity similar to that seen in the platform package. The Labrador Group of the Shoal Point landline is limited in the information that it adds to the study but it is consistent with the expressions identified on surrounding seismic data.

6.2.4 Grenvillian Basement

Figure 6.3, the Shoal Point landline is displayed to 3.5s TWT imaging a thick section of basement geology. The seismic expression of the sequence is similar to the Hunt data and most importantly images the north dipping internal package of reflectors. Imaged at 2600ms TWT at SP 1001, the reflector is seismically

continuous up to SP 1066 at which point it becomes intermittent and best imaged in the north end at SP1100. I interpret this horizon as a single continuous event that, due to quality issues, was not properly imaged at the northern end of the line. This horizon corresponds to the similarly dipping reflective sequence of events that were previously identified as basement igneous fabric (Figure 6.3), again correlating to the Lithoprobe data of Quinlan et al., (1992).

In summary, the interpretation of the Shoal Point landline does enable completion of the two goals defined at the outset of this section. Most importantly, the hanging wall section of the carbonate platform was imaged properly and can be correlated to the carbonate platform structure on all of the Hunt lines. It appears that the platform remains a continuous structure in the south with an apparent encroachment towards a rubble zone in the north related to the Round Head fault. From the data I have inferred that the fault system is at the tip or just north of the tip of Shoal Point although the locations of the cutoff point have not been imaged on this line.

6.3 3D Shoal Point Seismic Dataset

The interpretation of the 3D seismic volume is the culmination of the Shoal Point seismic project. Interpretation will enable the generation of contoured maps detailing the surface topography of the Ordovician carbonate platform. Covering an unconventionally shaped surface distribution due to acquisition geometry

(fold), the final interpreted horizons are interpolated through the data gaps allowing for consistent map coverage over a rectangular surface of 4km X 6km. The interactive picking of the 3D volume involved careful consideration of the previous interpretations of both the Hunt and Shoal Point land data.

The following discussion will include stacked 3D x-lines interpreted for the characteristic horizons of the local geology such as allochthonous structures, the Ordovician carbonate sequence, the Labrador Group, Grenvillian basement and the Round Head fault. Due to the variation in the quality of seismic imaging throughout the 3D volume, horizon picking in areas of poor data quality was interactively accomplished via interpolation between good 3D x-lines and the Hunt and Shoal Point land data.

The Round Head fault expression imaged in the current study area defines a southern net extension throughout and therefore places the hanging-wall side of the fault geometry deeper than its counterpart footwall side. The interpretation covers a rectangular area oriented north-south that is roughly cut in half in the east-west direction by the Round Head fault. Due to the net southern extension, the hanging-wall defines the southern half of the area while the footwall defines the northern half.

Interpretation of the 3D seismic volume is also completed as above by separation of the four main geological sequences:

1. Taconic Allochthon sequence (Carbonates and basinal shales from the Ordovician platform sequence)
2. Ordovician Carbonate platform sequence (Port au Port Group, St. George Group, Table Head Group, Goose Tickle Group)
3. Pre-Ordovician Labrador Group (Primarily clastics of the Hawke Bay, Forteau and Bradore Formations)
4. Grenvillian Basement

The following figure is a basemap of the area taken from the interpretation stage of the study. The annotated 3D xlines correspond to the line locations for the following series of seismic figures related to the 3D volume (Figure 6.4).

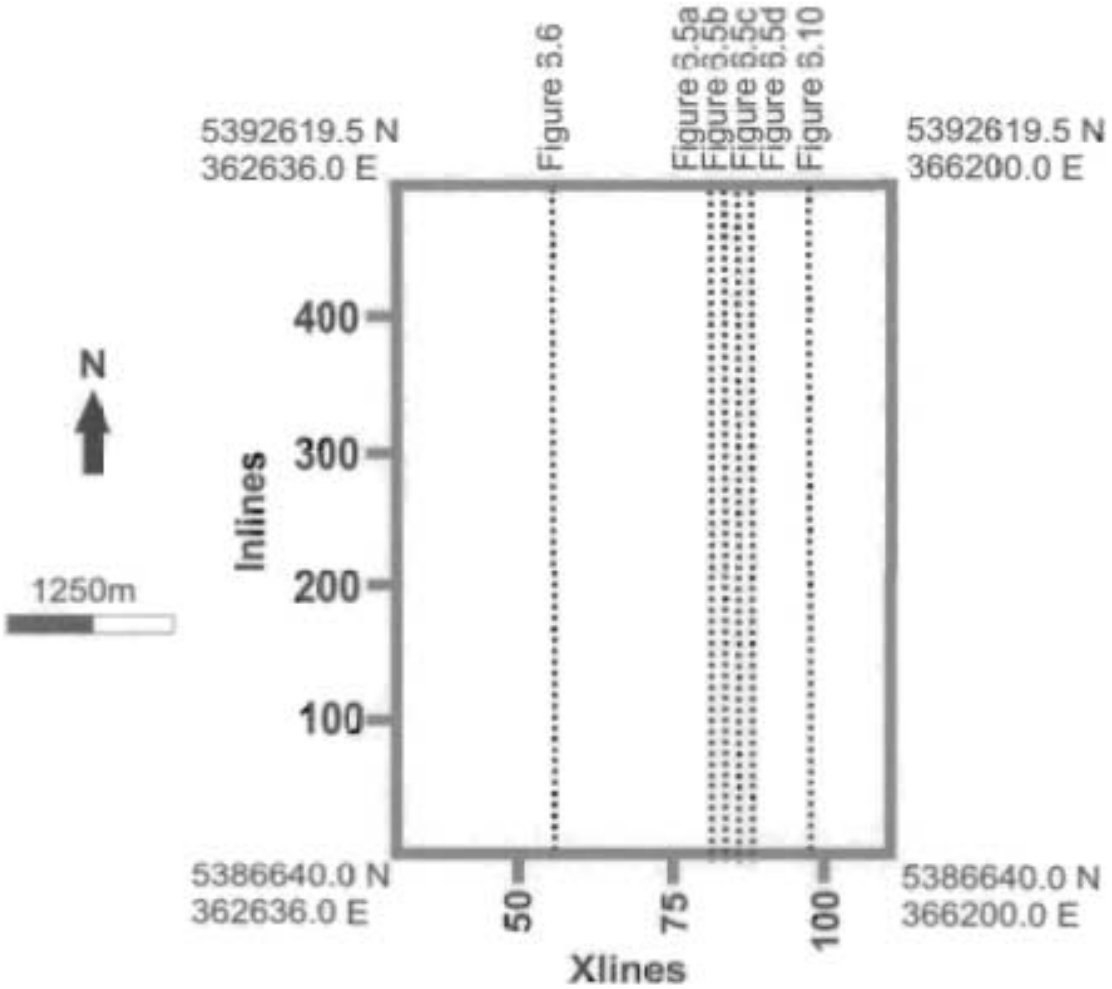

Figure 6.4. Line location map for the 3D interpreted seismic volume.

6.3.1 Taconic Allochthon Sequence

Imaging of the Taconic allochthon by the 3D seismic yields results very similar to those discussed previously for the Hunt and Shoal Point data. The discontinuous seismic image of the allochthon is easily identifiable in the following series of figures showing various interpreted 3D xlines from Seisworks®. The top of the allochthonous sequence corresponds to the seafloor surface, while the basal detachment surface and base of the sequence is easily picked at the top of the carbonate platform. The allochthonous package within the study area thins substantially towards the south and is thickest (1200ms) on the hanging-wall at the Round Head fault platform hanging-wall cutoff point (Figures 6.5a, b, c, d). Moving north and passing over the fault, the allochthon steps up to remain on top of the footwall carbonate platform. The variation of thickness in the allochthon clearly corresponds to the offset in the Round Head fault and the dip and depth of the carbonate platform (hanging-wall and footwall); both of these expressions will be discussed and displayed in more detail in upcoming sections.

Seismic velocities of the allochthon are extremely high for shallow sediments (~3500m/s – 4000m/s), corresponding to the interpreted geological framework of over thrust carbonate sheets. The imaging of these thrust structures is intermittent on all of the seismic programs, but adequate enough in some locations to confirm the interpretation.

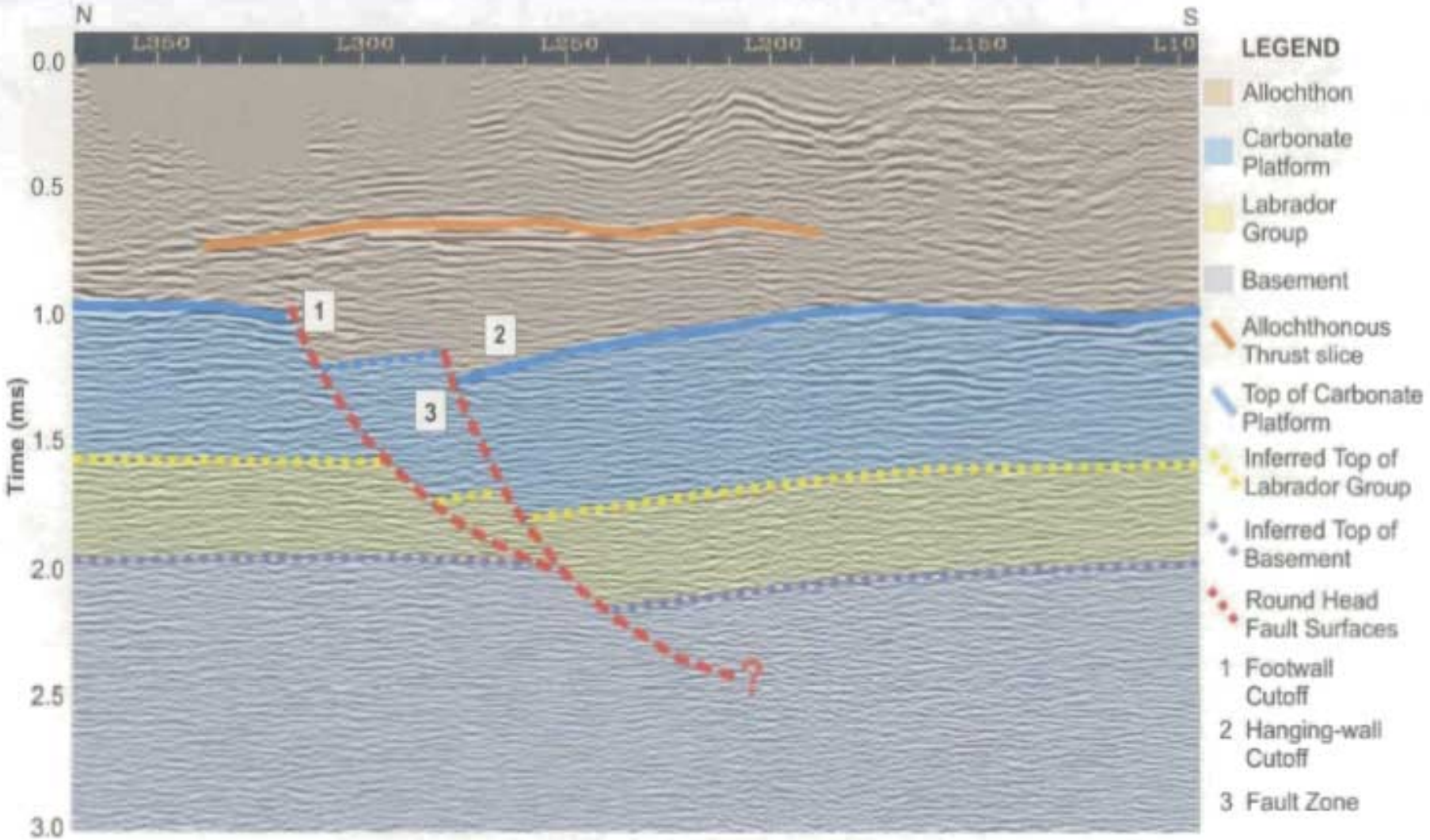

Figure 6.5a. 3D xline 81 interpreted and annotated for characteristic structure and geological sequences (See figure 6.4 for location).

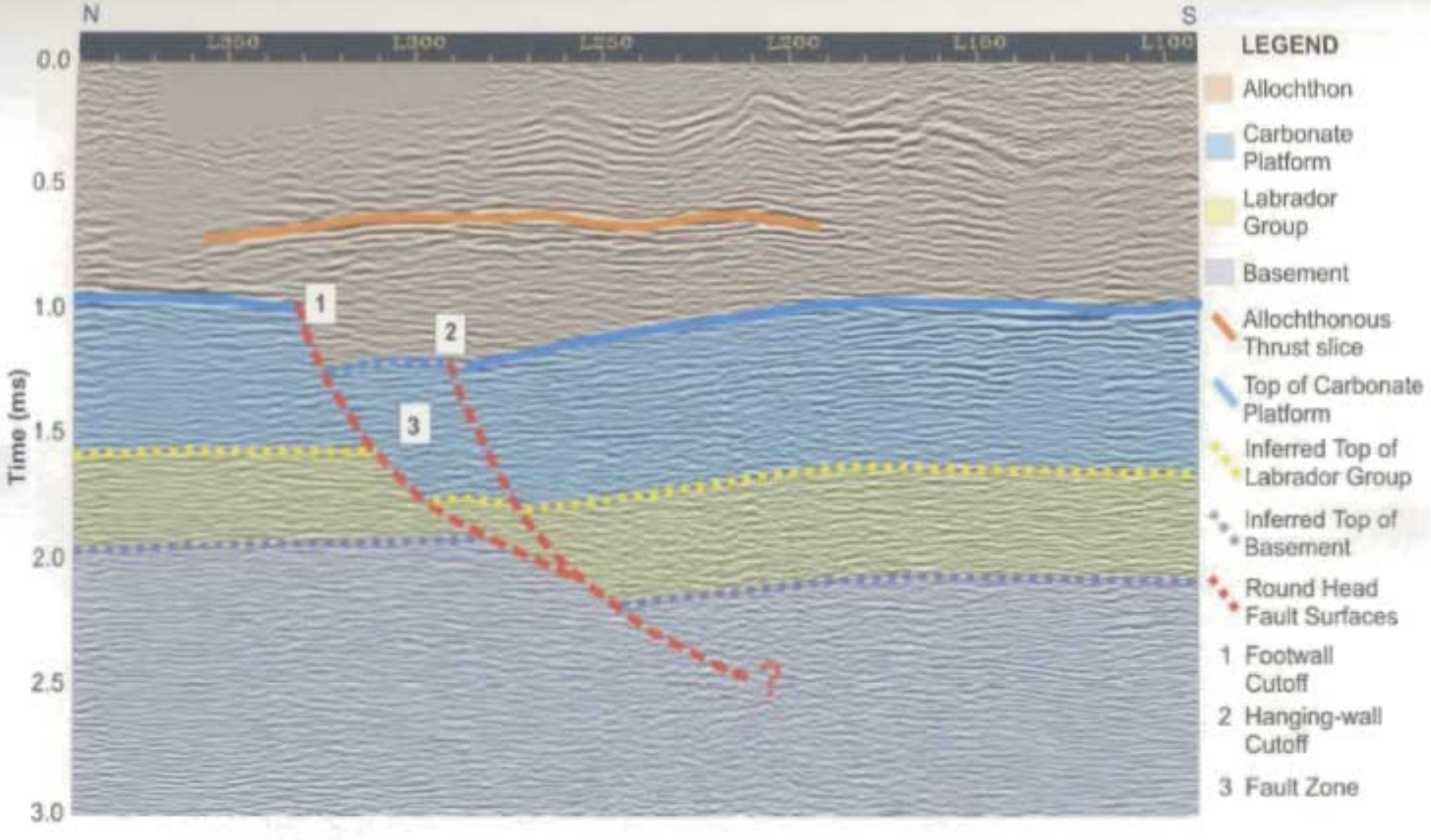

Figure 6.5b. 3D xline 82 interpreted and annotated for characteristic structure and geological sequences (See figure 6.4 for location).

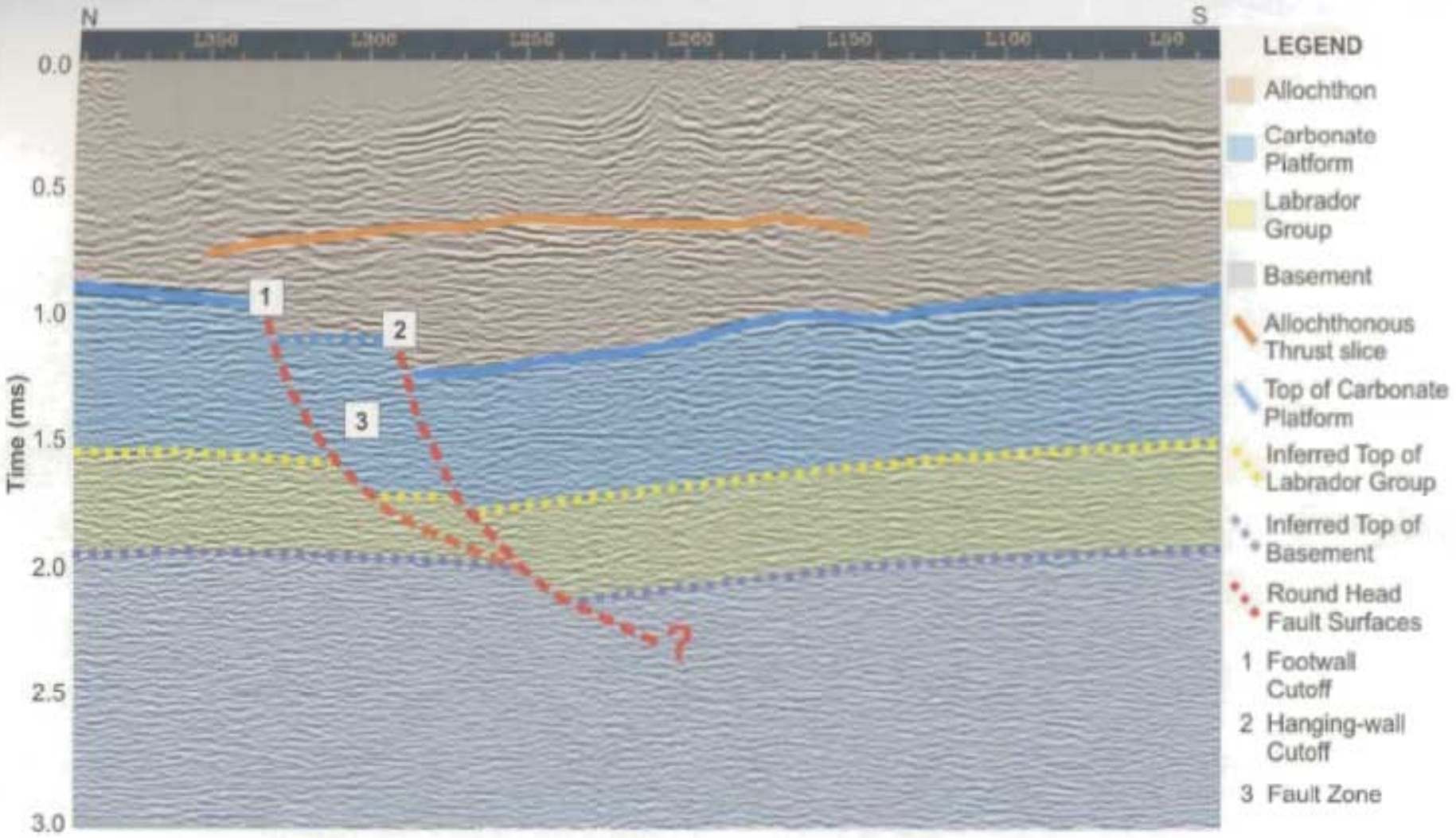

Figure 6.5c. 3D xline 83 interpreted and annotated for characteristic structure and geological sequences (See figure 6.4 for location).

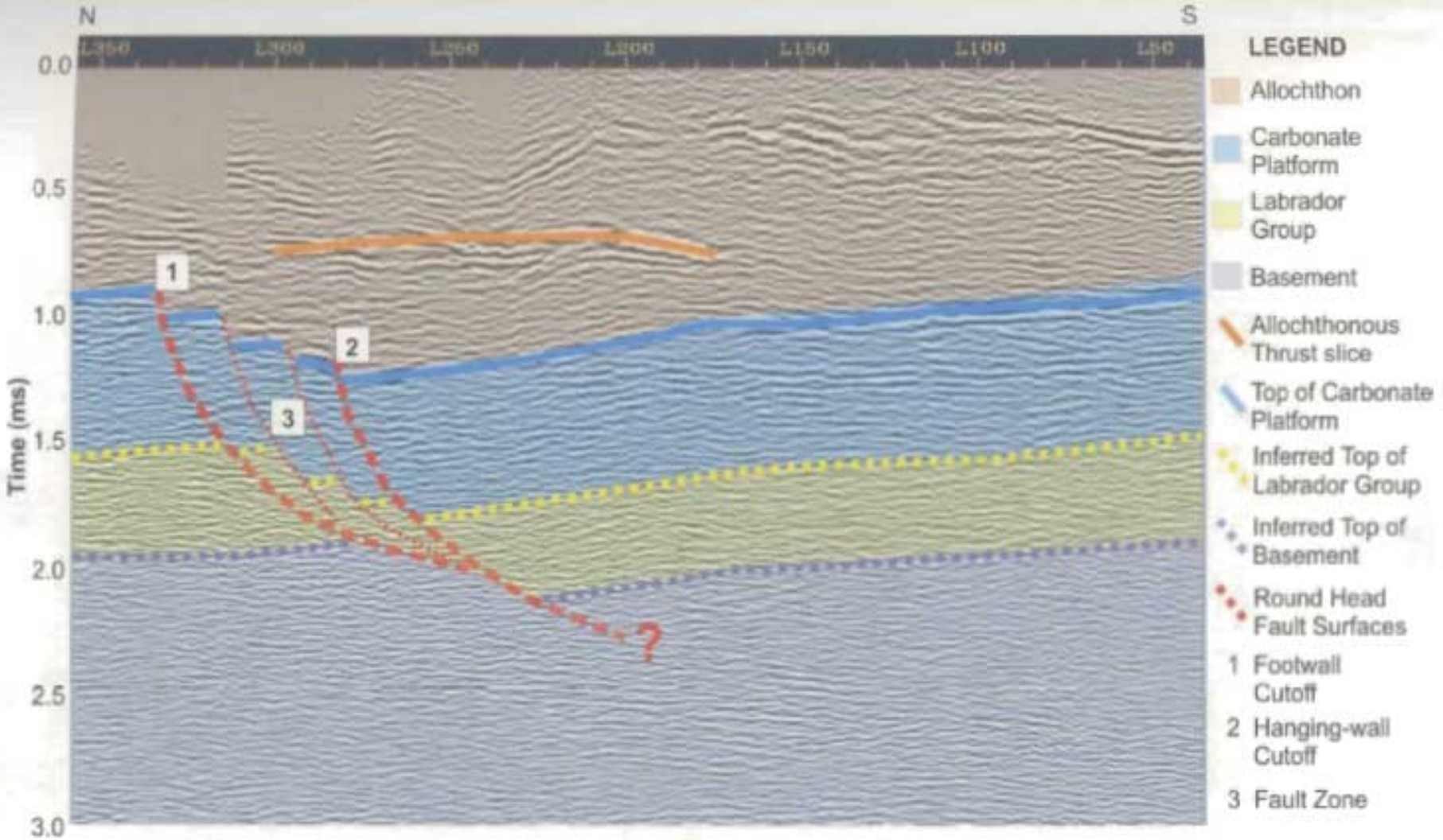

Figure 6.5d. 3D xline 84 interpreted and annotated for characteristic structure and geological sequences (See figure 6.4 for location).

The previous xlines from the eastern edge of the survey area are annotated for shallow highly reflective events that I have interpreted as a slice of the carbonate shelf corresponding to a Taconic thrust sheet (Figures 6.5a, b).

6.3.2 Ordovician Carbonate Platform Sequence

Due to the Round Head fault, the carbonate platform hanging-wall and footwall surfaces are offset and vary substantially with respect to structure and surface topography. For ease of interpretation I will therefore discuss the platform hanging-wall and footwall separately, combining the mapped surfaces together in the summary to give a complete picture of the top of the platform as seismically imaged in the current study area.

6.3.2.1 Carbonate Platform Hanging Wall

In areas where the 3D data images the carbonate platform, the seismic expression is identical to that seen on the Hunt and Shoal Point seismic lines. Seismic velocities of the carbonate platforms dolomites and limestones are high ranging from 4500m/s to 5500m/s on average, while thickness variation of the platform is minimal, consistent with the previous studies (Hunt / PanCanadian, 1996). The platform is consistently imaged as a package of parallel horizons containing internal reflectors with high seismic reflectivity (Figures 6.5c, d).

Xline 83 is a typical seismic line from the eastern edge of the data volume that properly images the platform package of reflectors (Figures 6.5c). In figure 6.5c the interpreted platform horizon displays the characteristic shallowing of the boundary towards the south. The northern hanging-wall cutoff for the platform is at 1200ms TWT, shallowing in time towards the south to a TWT of 850ms at the edge of the line. When we compare this to xline 60 from the western edge of the survey, the hanging-wall cutoff is now at 1050ms TWT decreasing towards the south to a minimum of 800ms at the southern edge (Figure 6.6). The resultant interpretation when comparing seismic from the western and eastern edges of the area is that overall the platform surface is dipping northward with an increase in dip to the east. Studying this eastward dip further it is clear from the mapped 3D surface that the platform hanging-wall is plunging with a northeastern trend that increases in dip consistently to the northeast. This orientation results in a substantially deeper platform at the northeast corner of the hanging-wall surface.

The northern edge of the platform hanging-wall is cutoff and controlled by the Round Head fault. In figure 6.7, the Round Head fault zone corresponds to the cross hatched area. I have interpreted this region as the geology between the hanging-wall and footwall cutoff faults. In general this zone is heavily faulted and fragmented and therefore is not well imaged seismically. On the northwest side of the hanging-wall a visible step up in the surface corresponds to an interpretable surface of the fault zone (Figure 6.7). As the western edge of the platform begins to approach the null point, the offset and

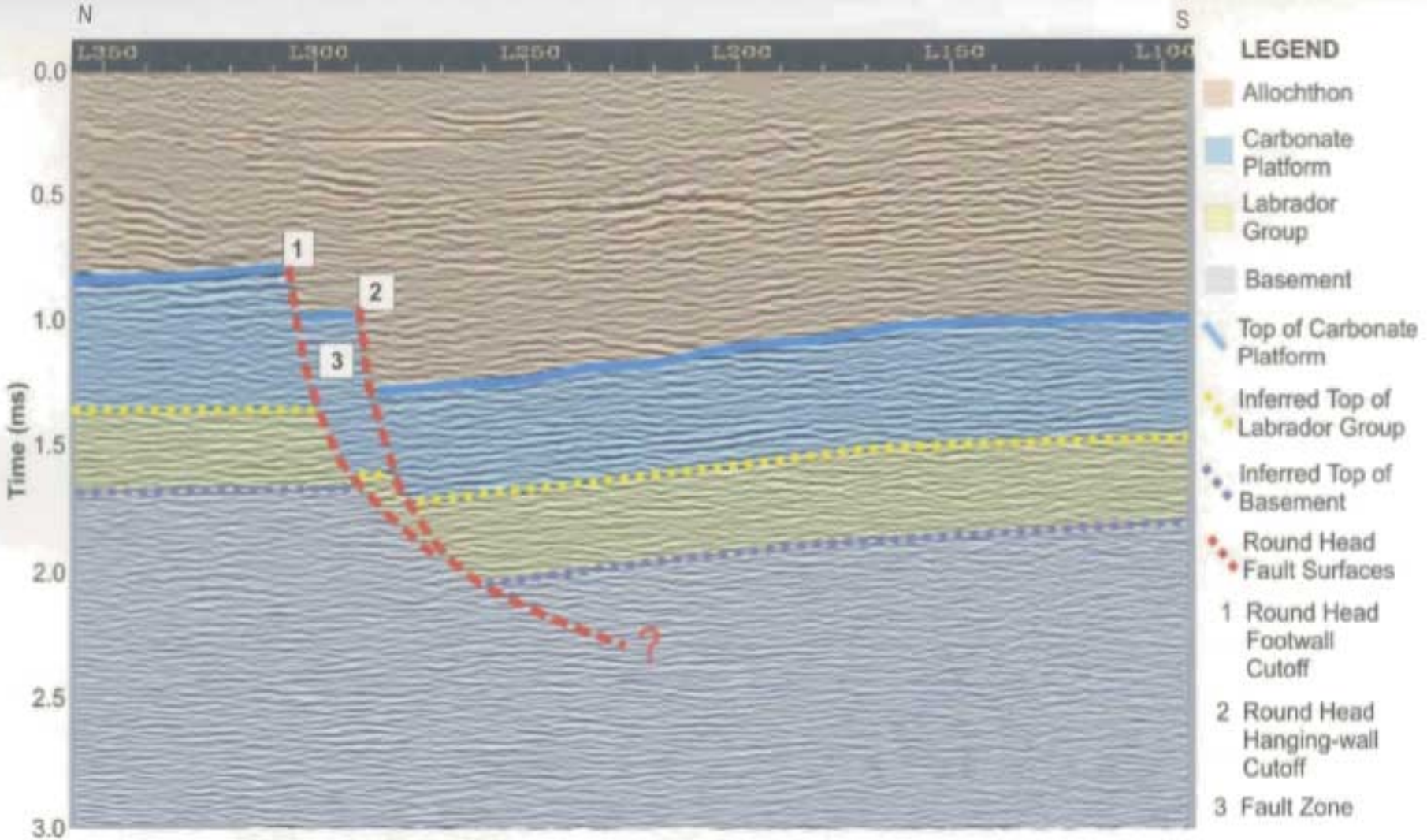

Figure 6.6. 3D xline 60 interpreted and annotated for characteristic structure and geological sequences (See figure 6.4 for location).

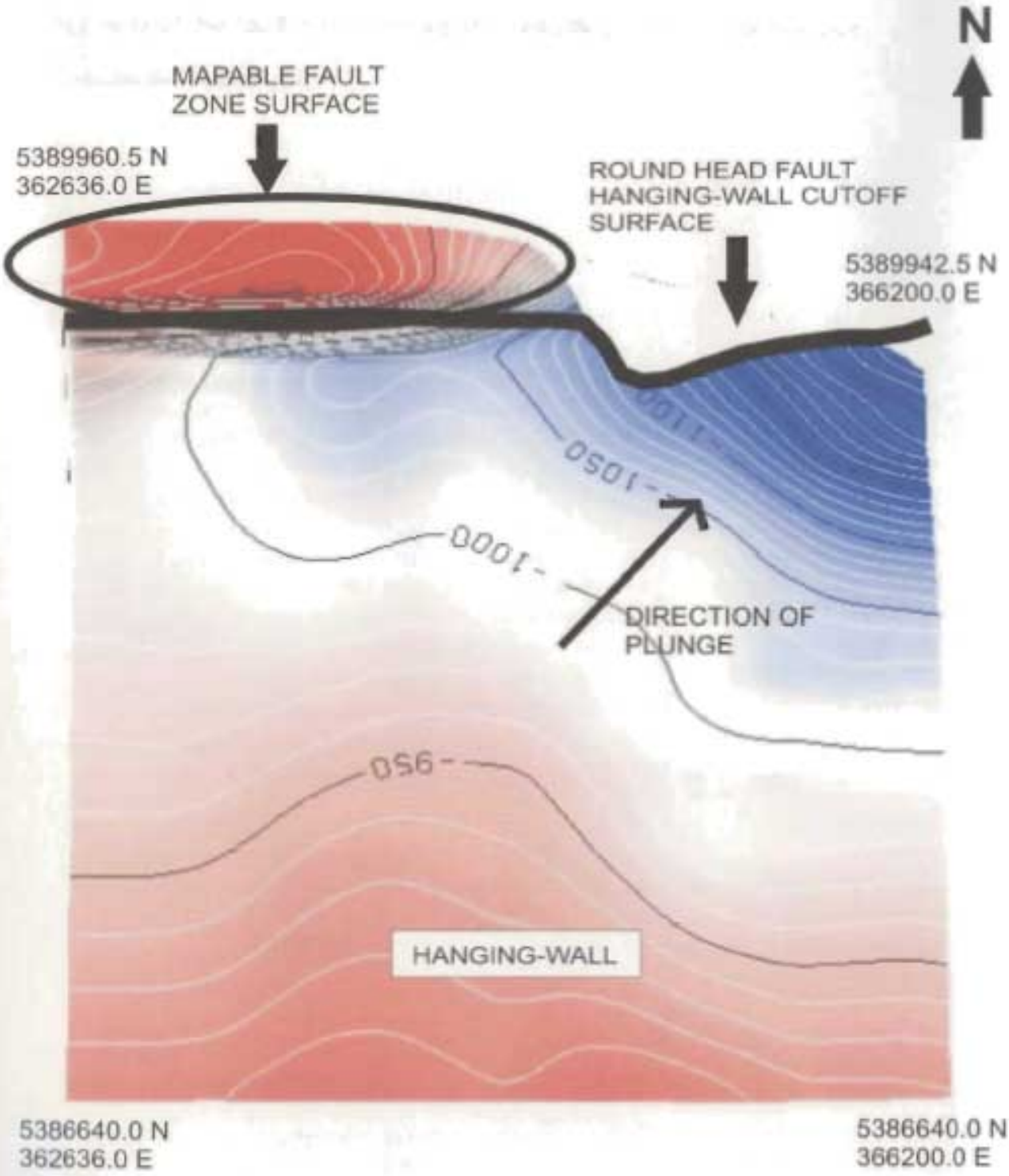

Figure 6.7. Map view of the 3D surface for the top of the carbonate platform hanging-wall.

complexity of the fault zone decreases, resulting in more continuous, interpretable reflectors.

The following figures (Figures 6.8a, b, c) are the smoothed and contoured hanging-wall platform surfaces modeled from the interpreted seismic. Note the contours indicating the increase in TWT to the surface from south to north. The synclinal surface structure along with the mapped area of the fault zone has also been annotated and is clearly distinguishable (Figures 6.8a, b, c).

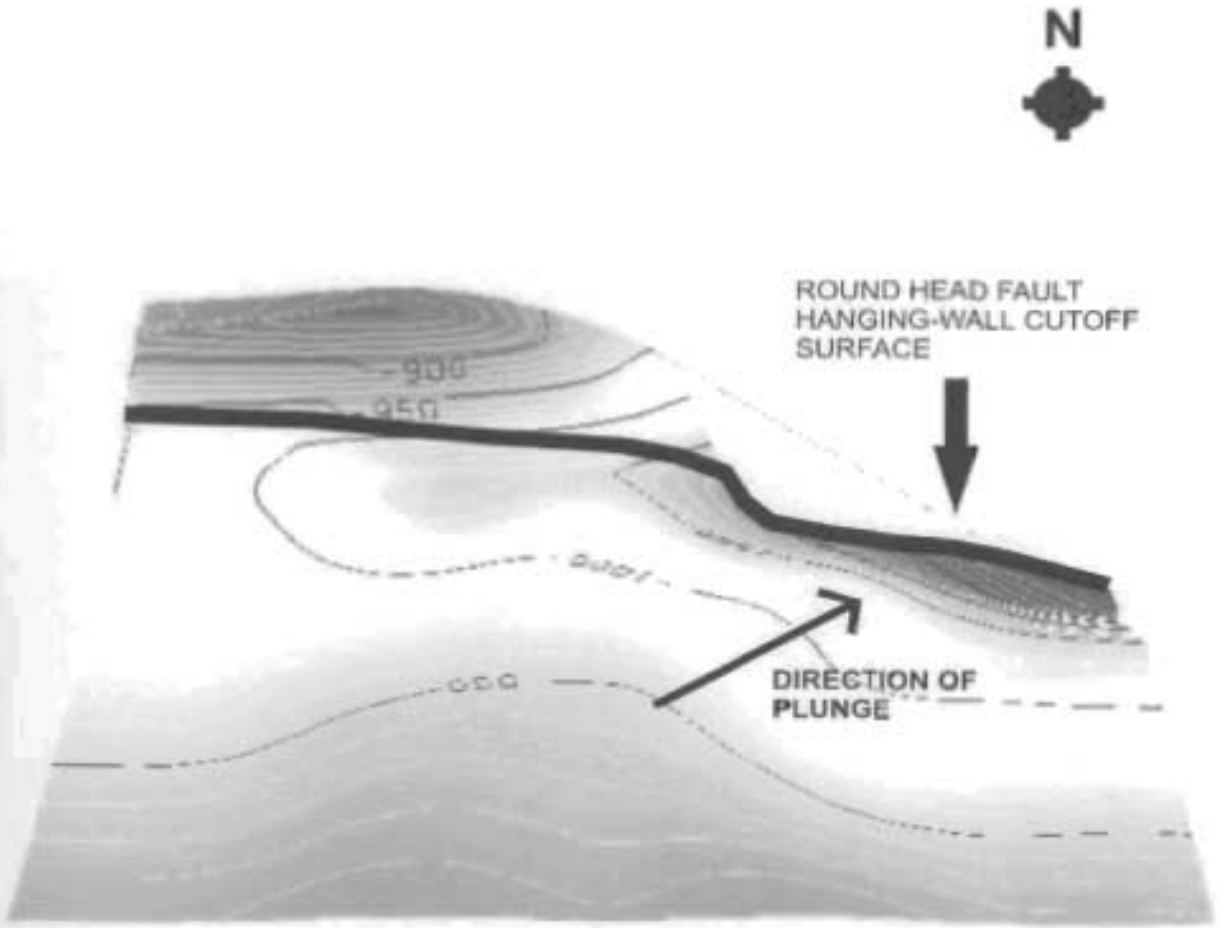

Figure 6.8a. 3D surface to top of the carbonate platform hanging-wall, view is looking into the page.

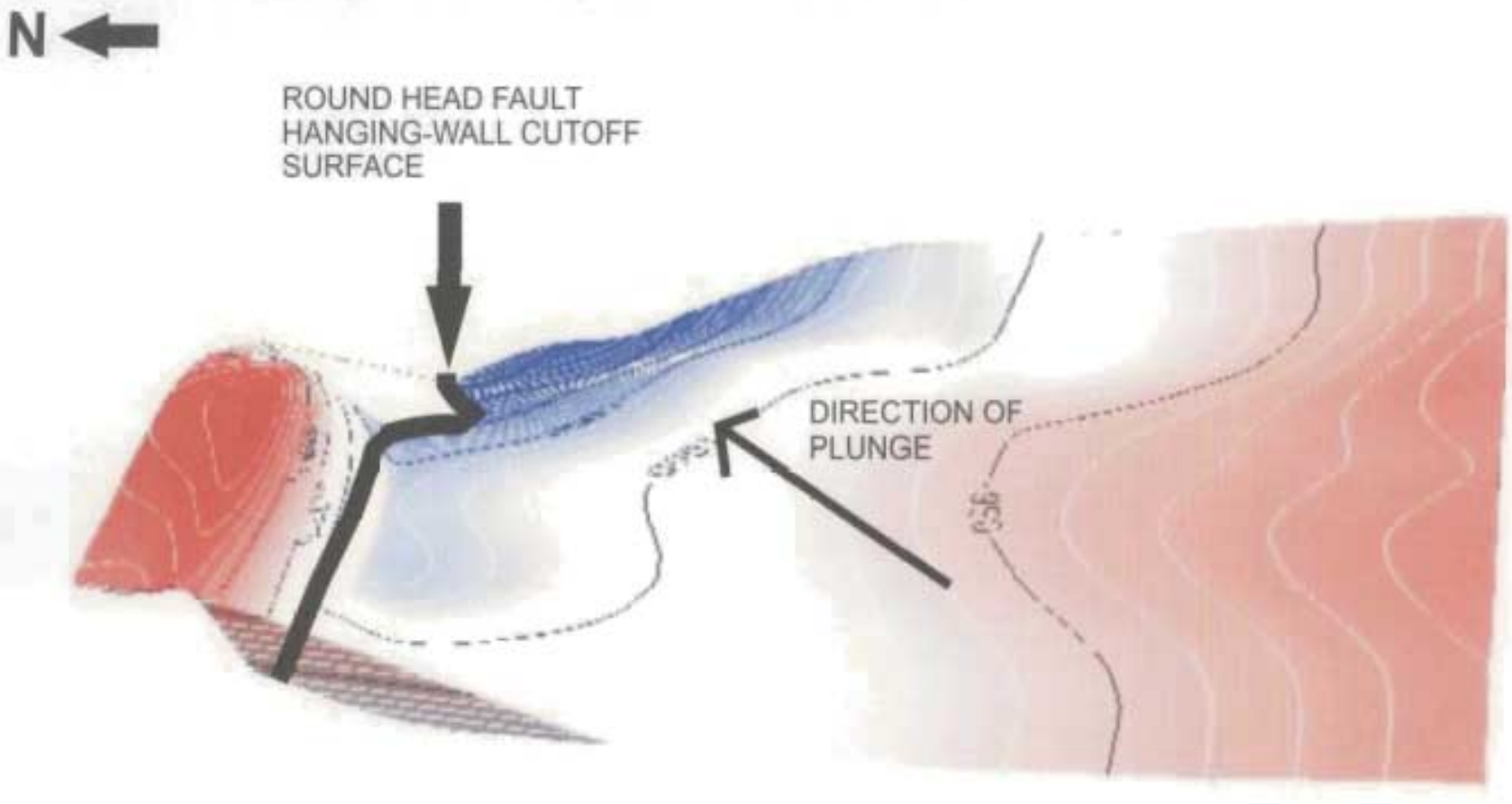

Figure 6.8b. 3D surface of the top of the carbonate platform hanging-wall, view is from the west looking east into the page.

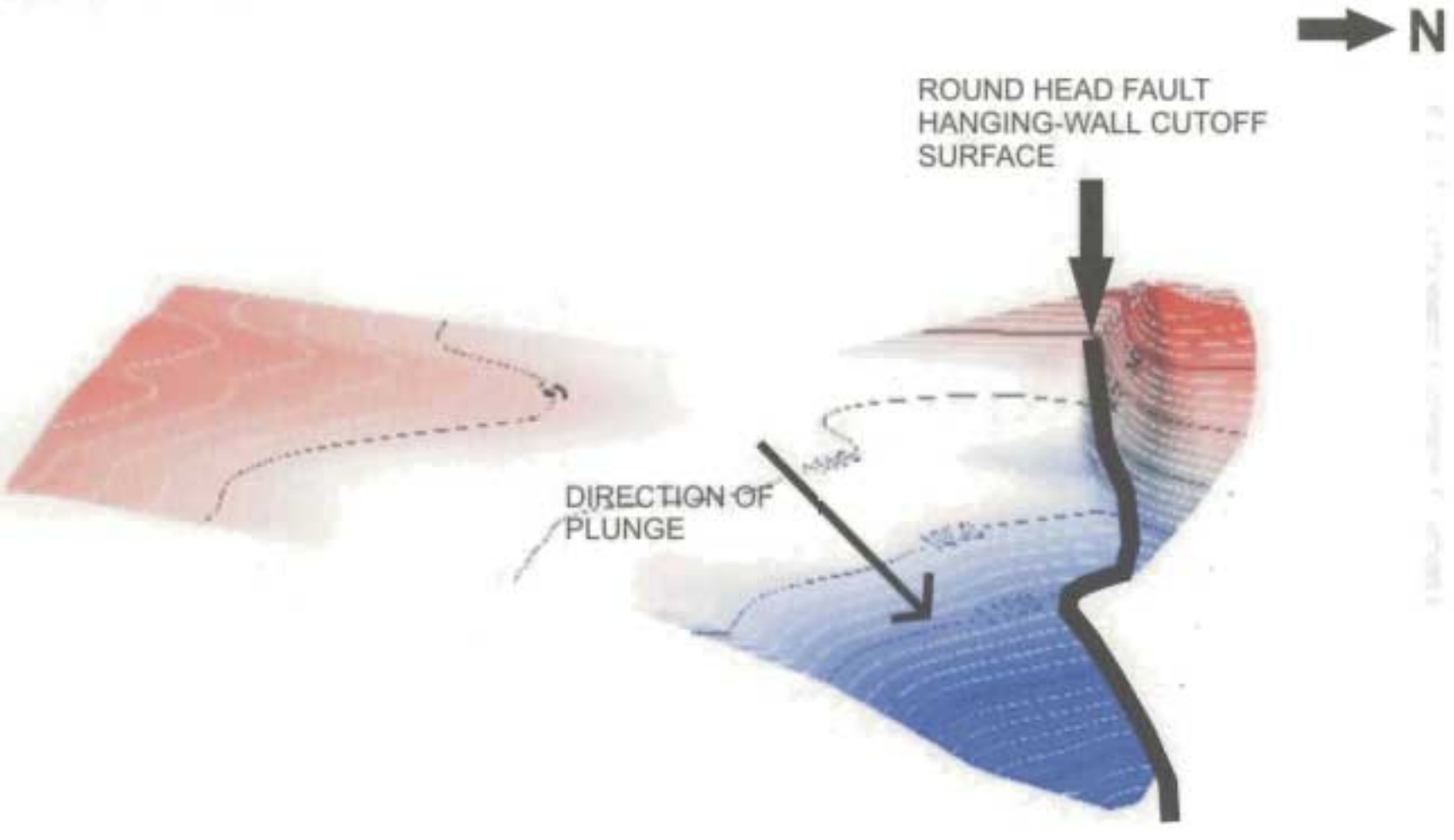

Figure 6.8c. 3D surface of the top of the carbonate platform hanging-wall, view is from the east looking west into the page.

6.3.2.2 Carbonate Platform Footwall

The carbonate platform footwall is very different from the hanging-wall portion of the fault geometry. Foremost the footwall is offset above the hanging wall as the Round Head fault is in net extension within the survey area. The footwall section of the study area covers approximately the northern one-third of the overall space. Stratigraphically identical to the hanging-wall, the seismic expression of the footwall is characteristic of the top platform event throughout the bay. The seismic data coverage of the northern footwall area is sparse in comparison to the hanging-wall portion and therefore interpretation relied more heavily on the surrounding lines of the Hunt survey.

Overall the platform footwall surface can be described as a structural high with the apex of an anticlinal structure being juxtaposed against the Round Head fault slightly north-northwest of the tip of Shoal Point (Figures 6.9a, b, c, d). At its shallowest the footwall structural high is about 750ms TWT. This depth increases in time on its flanks to greater then 900ms TWT. It is this structure that Hunt and PanCanadian probably attempted to test through the drilling of the Shoal Point K-39 well.

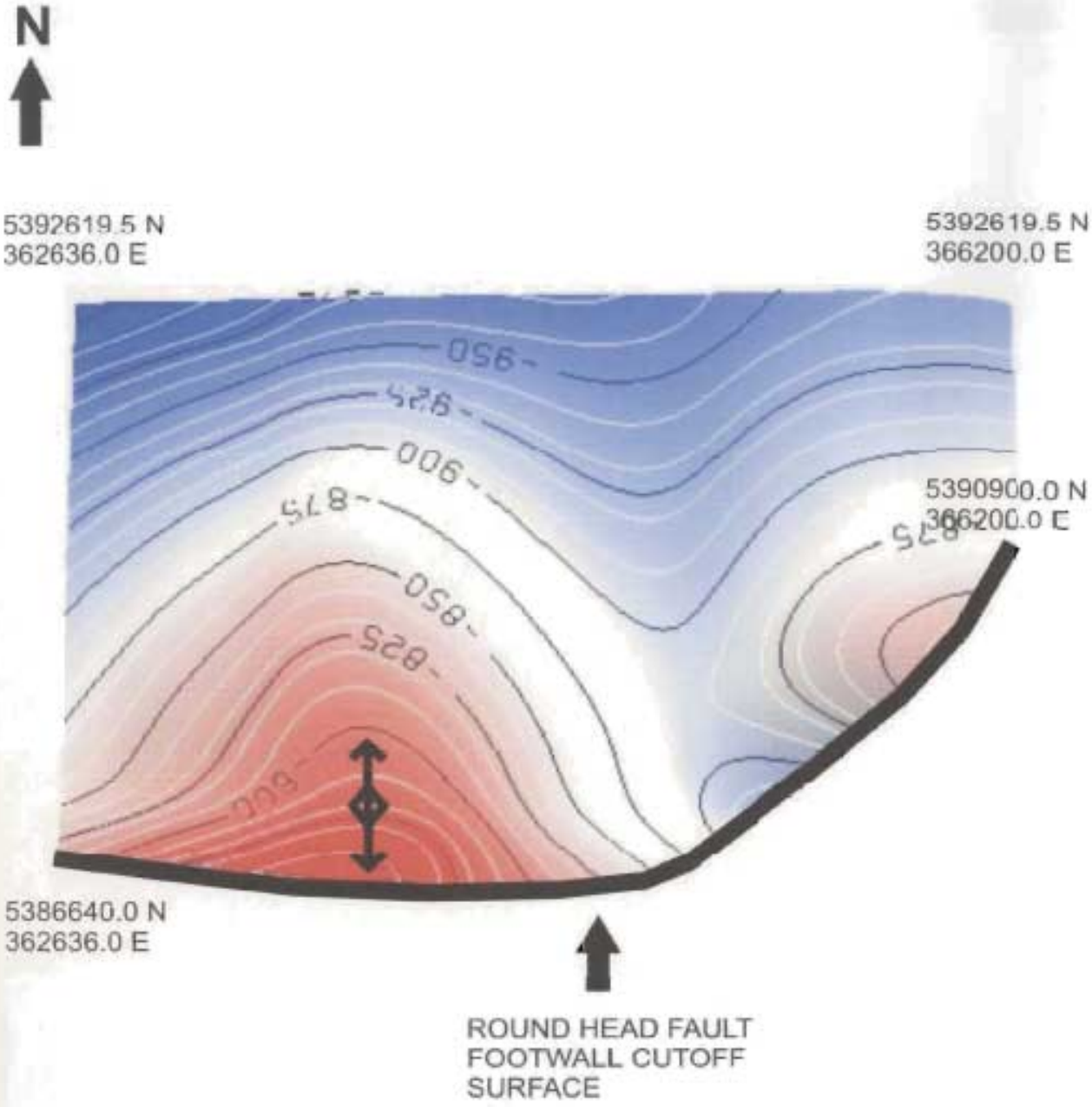

(a)

Figure 6.9a. Map view of the 3D footwall surface for the top of the carbonate platform annotated for the dominant structural expressions. Again contouring is for the seismic travel time (ms) to the platform horizon.

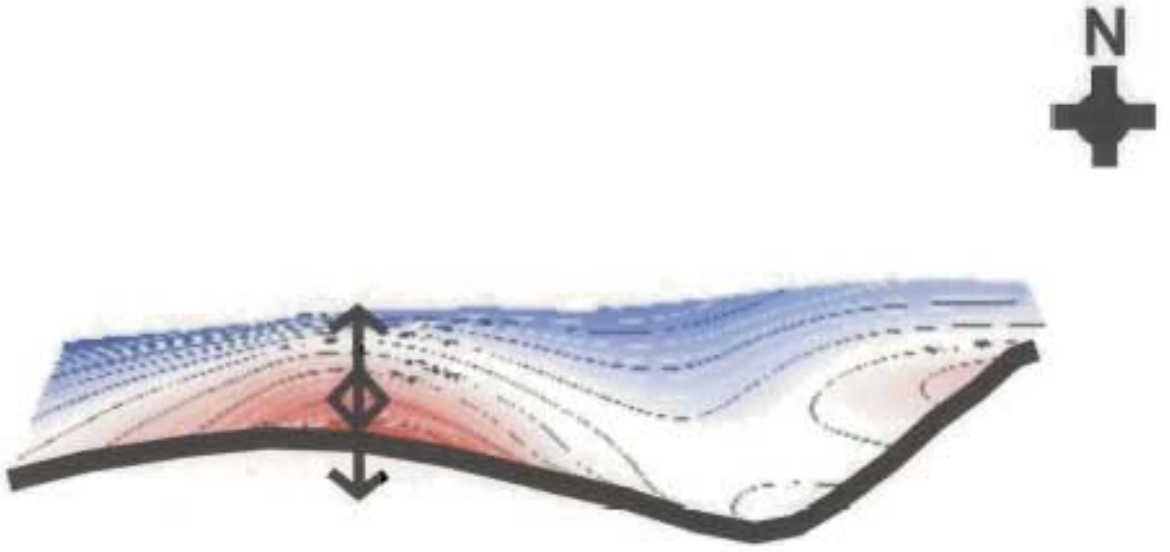

(b)

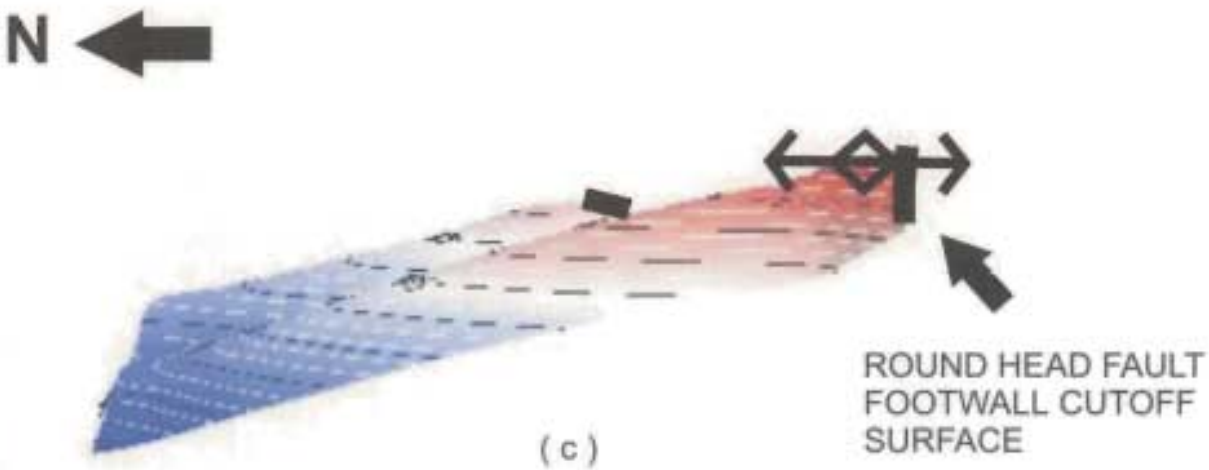

(c)

Figure 6.9 (b) 3D surface of the carbonate platform footwall looking north into the page, the anticline is identified as the large structural high in the SW corner. (c) 3D surface of the carbonate platform footwall from the west looking east.

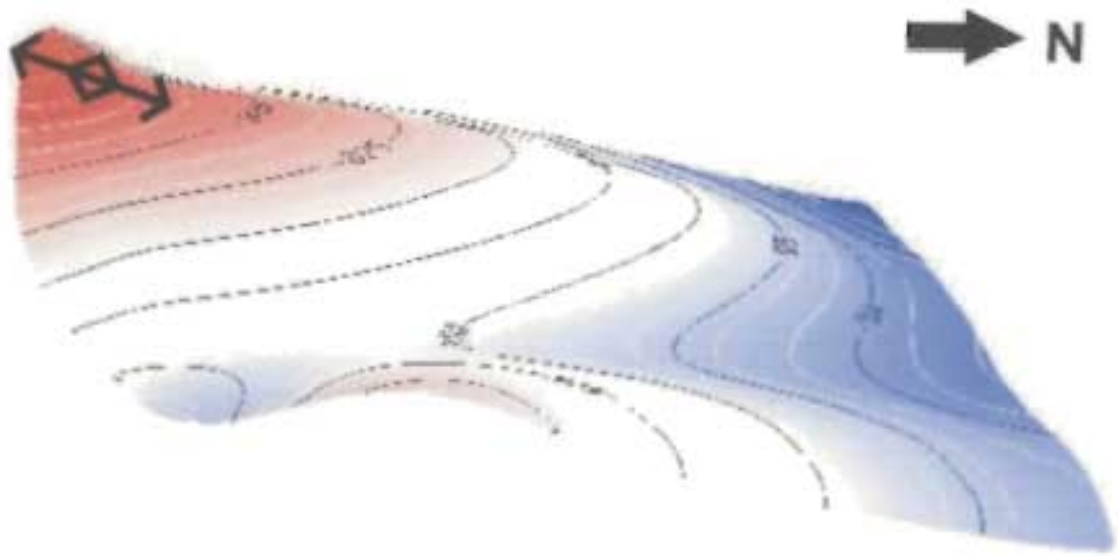

(d)

Figure 6.9 (d) 3D surface of the carbonate platform footwall looking east into the page.

6.3.3 Pre-Ordovician Labrador Group

Imaging of the Labrador Group within the 3D volume is generally poor with some areas of deeper penetration and resolution on the eastern side of the point. When the geology is imaged the horizons correspond perfectly with the Labrador Group expression imaged on the Shoal Point landline (Figure 6.10). A geologic package with extremely high seismic velocities from 6000m/s to 6500m/s the Labrador Group is relatively shallow. Overall, its thickness appears to be constant. This is approximate, as the basal contact with the underlying basement is not clearly imaged.

6.3.4 Grenvillian Basement

The 3D seismic volume does a fair job of imaging the basement and in particular the southerly dipping basement fabric. Figures 6.10 is annotated for the characteristic basement horizon imaged on all three of the interpreted datasets, seismically the reflector is identical with the same attributes of the basement horizon discussed in the previous interpretations. Both the 2D landline and the 3D volume correlate with the results expressed by Quinlan et al., (1992) in the onshore Newfoundland Lithoprobe studies, presenting the southeast dipping horizons as the internal fabric resultant from the Mid-Ordovician to Mid-Silurian strain. In all of the interpreted datasets, including the 3D volume I have interpreted, the Round Head fault appears to sole at basement depths in a surface that is not seismically imaged.

Overall basement depth variation within the 3D dataset is identical to that of the Hunt data. In figures 6.5a-d it is obvious that the basement is shallowest at the Round Head fault zone. The inferred top of basement horizon trends with the dip and orientation of the platform, stepping up to a maximum shallow depth of 1500ms / 3500m at the intersection of the top basement and the Round Head fault surface.

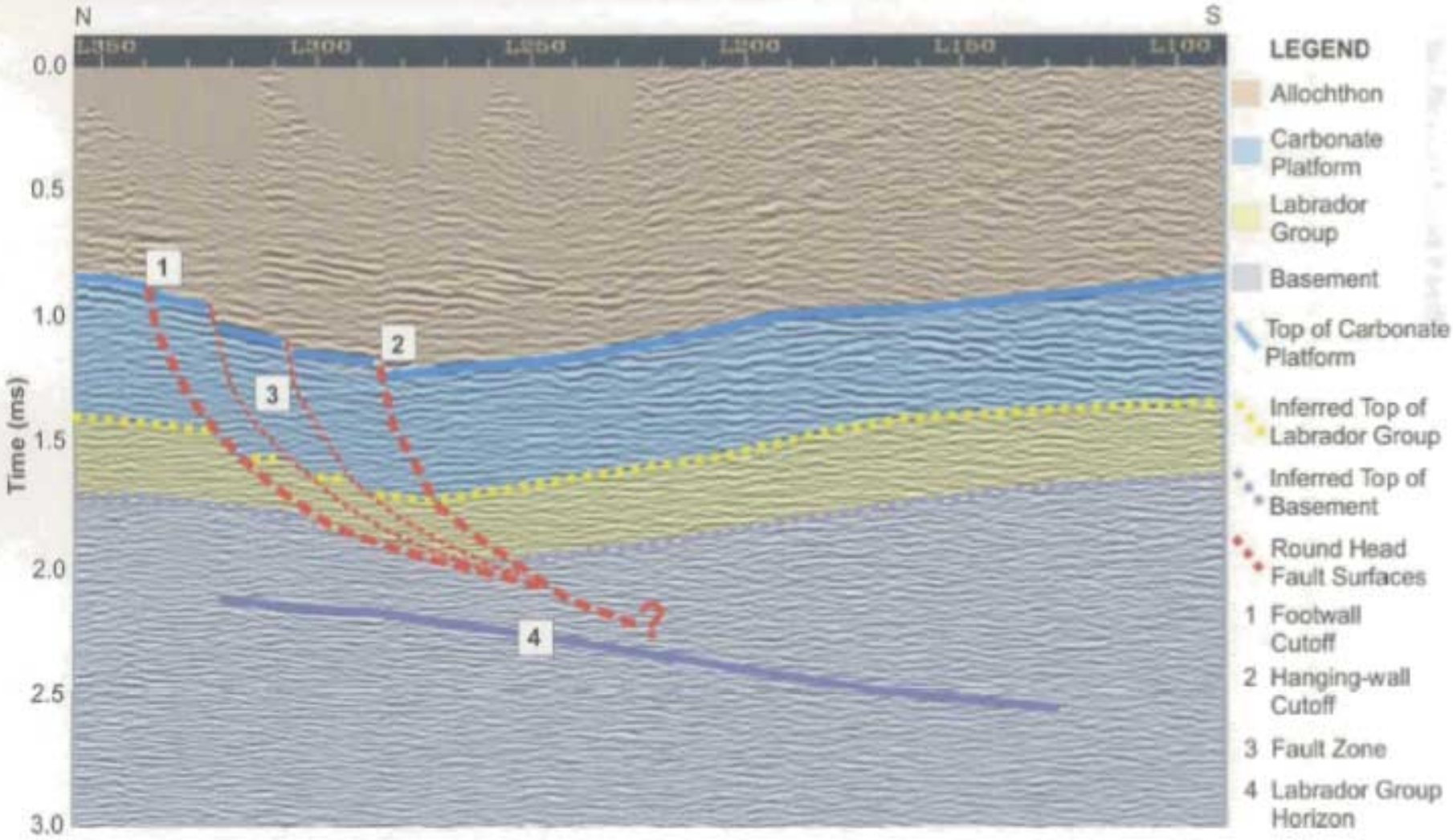

Figure 6.10. 3D xline 95 interpreted and annotated for characteristic structure and geological sequences (See figure 6.4 for location).

6.3.4 Round Head Fault

A general expression of the Round Head fault is already clear based on the previous interpretation and discussion of the carbonate platform surfaces. The Round Head fault varies from net compression on land on the Port au Port peninsula to net extension in Shoal Bay. Mapping of the interpreted horizons from the current study area has allowed for a detailed image of the fault expression as it traverses the center of the bay past Shoal Point.

In the following figure, the hanging-wall and footwall cutoff fault points have been clearly annotated. It is obvious that the fault tracks east-west towards the midpoint of the study area at which point they begin to diverge (Figure 6.11). Figure 6.11, a map view of the area demonstrates that past the midpoint of the bay, the fault system begins a north-eastern transgression and the footwall cutoff fault begins to migrate to the northeast with a continuous azimuth change towards the north for more easterly locations. The hanging-wall fault expression is slightly different; as the fault plane migrates past the midpoint of the bay, it begins to gently turn south for a distance of 1km before it again changes direction and arcs northeastward (Figure 6.11). Both the footwall fault surface and hanging wall fault surface beyond the midpoint can be described as arcuate stepping north the further east the location.

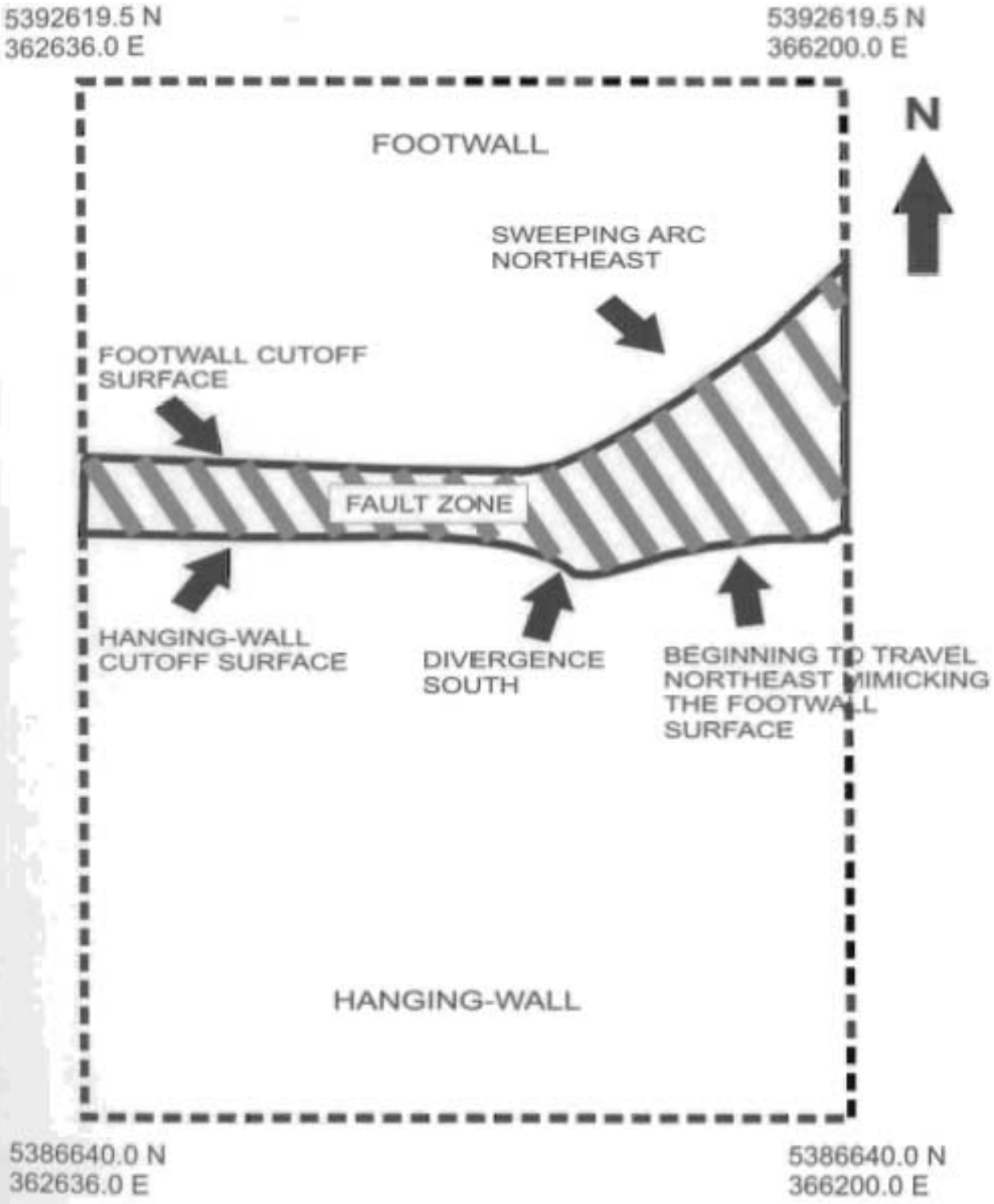

Figure 6.11. Display of the Round Head fault zone annotated for the variation and expressions in each of the fault surfaces.

6.4 Correlation of Drilling Data

PanCanadian et al. drilled the Shoal Point K-39 well in 1999. Spudded at the very tip of Shoal Point the well was drilled directionally north apparently in an attempt to test the structural high of the footwall carbonate platform. K-39 was abandoned as a dry hole and PanCanadian and partners have since dropped the licence containing the Port au Port peninsula.

The goal of this section is to correlate K-39 geological tops and the Round Head fault location in time to the 3D seismic data using an interactively selected seismic line from the 3D volume. The 3D seismic line was picked so that the true K-39 well trajectory lies in the section (Figure 6.12). This will confirm the validity of the 3D data, as well as provide a better understanding of the unsuccessful K-39 well. The subsurface well track was derived using the known surface and bottom hole UTM locations, along with the well report survey information and the VSP. Using this survey information, surface location along with its corresponding subsurface true vertical depth can be correlated to its correct seismic travel time. All seismic travel times to key geological horizons and faults were obtained via correlation of the geological strip log to well VSP information (Table 6.3). The following tables contain the relevant information used to project the K-39 well track over the current 3D seismic data.

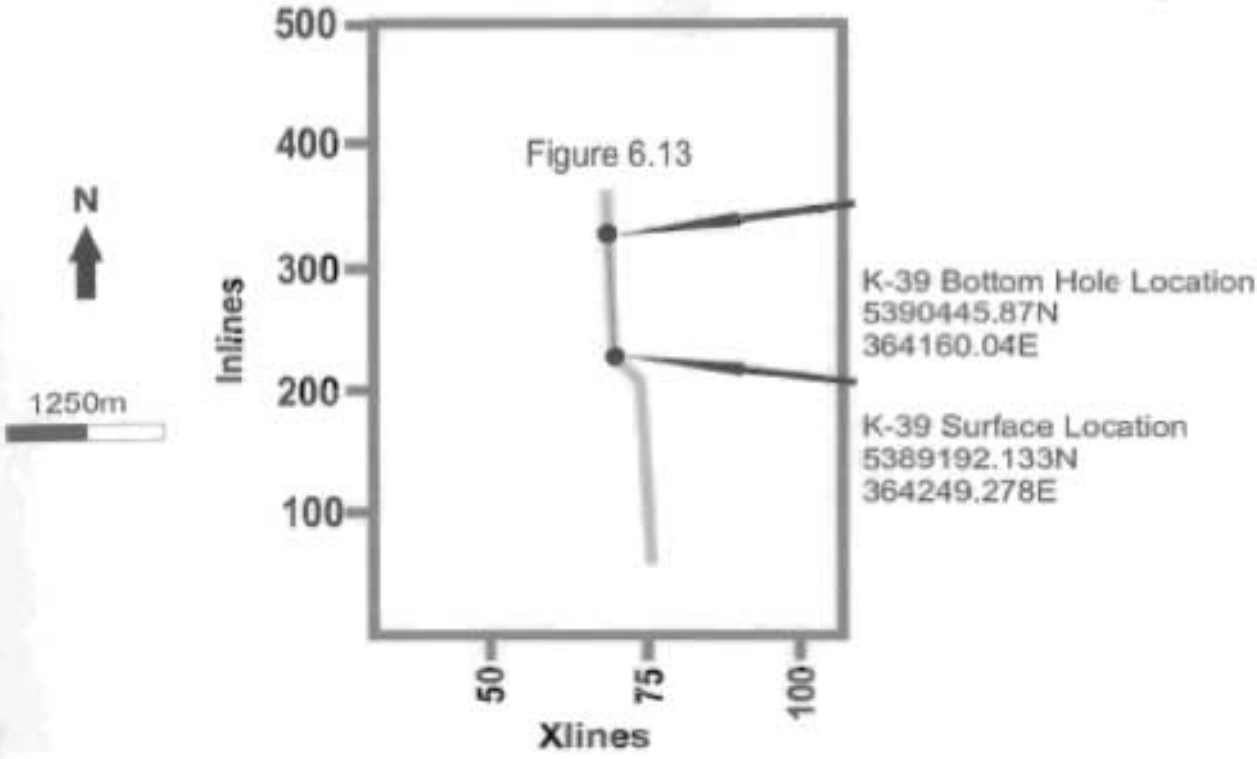

6.12. Basemap of 3D inlines / xlines showing figure 6.13 location and the K-39 well surface expression.

Table 6.1: Well information for well trajectory reconstruction.

Surface	True Vertical Depth (m)	Two-way seismic travel-time (ms)	Northing (UTM)	Offset from surface well location(m)	# of inlines corresponding to offset
1.0	500	290	5389192	0	0
2.0	750	420	5389421	229	18
3.0	1000	580	5389656	464	37
4.0	1500	770	5390052	860	69
5.0 Round Head fault / Catoche	1890	900	5390266	1074	86
6.0 Top of Labrador Group	2590	1100	5390446	1254	100

Table 6.2: K-39 Well Location.

Well Location	X	Y	3D Inline	3D Xline
Surface	5389192.133 N	364249.278 E	224	68
Bottom hole	5390445.87 N	364160.04 E	325	66

Table 6.3: K-39 Geological tops with corresponding seismic travel times.

FORMATION	LOG TOPS (m)	TVD (m)	Seismic TWT (s)
KB		10.56	
Humber Arm Allochthon Carbonates	1031.5	943	530
Round Head Fault	2207	1899	900
Catoche	2207	1899	900
Fault 1	2251	1940	
Fault 2	2296	1980	
Boat Harbour 1	2341	2021	
Boat Harbour Discon. 1	2369	2047	
Fault 3	2452	2122	
Boat Harbour 2	2461	2131	
Boat Harbour Discon 2	2490	2158	
Fault 4	2535	2200	
Fault 5	2570	2234	
Petit Jardin			1020
VSP bottom	2897	2556	1120

Figure 6.13 displays the resultant correlation of the K-39 well path with the 3D seismic data. There are two key locations of specific interest annotated on figure 6.13 as points 5 and 6 that should be discussed. These positions are important

because they mark a major fault and geological sequence boundaries. It was crucial that these main boundary points recorded from the well data correspond to the 3D seismic to have a positive correlation.

Position 5 defines the location in the well information corresponding to the Round Head fault and the transition from Allochthonous carbonates to the Ordovician carbonate platform. The well site geologist recorded the first platform formation encountered by the drill as the Catoche (Table 6.3), corresponding to an internal platform formation, i.e. the drill did not enter into the top of the platform but lower into the stratigraphic sequence (Figure 2.2). Comparing this information to the interpreted seismic, it is clear that the top of the carbonate platform is above the well track, and that the well travels into what is seismically imaged as the face of the Round Head fault footwall surface.

Position 6 defines the location of the Carbonate platform / Labrador Group boundary as stated in the well report. Again the interpreted seismic corresponds to the well trajectory and geological information. Therefore I can state that the 3D seismic section corresponding to the true well trajectory correlates perfectly to the K-39 well geological summary, well location survey, strip log and VSP data. This independent data further substantiates the interpretation in the foregoing sections.

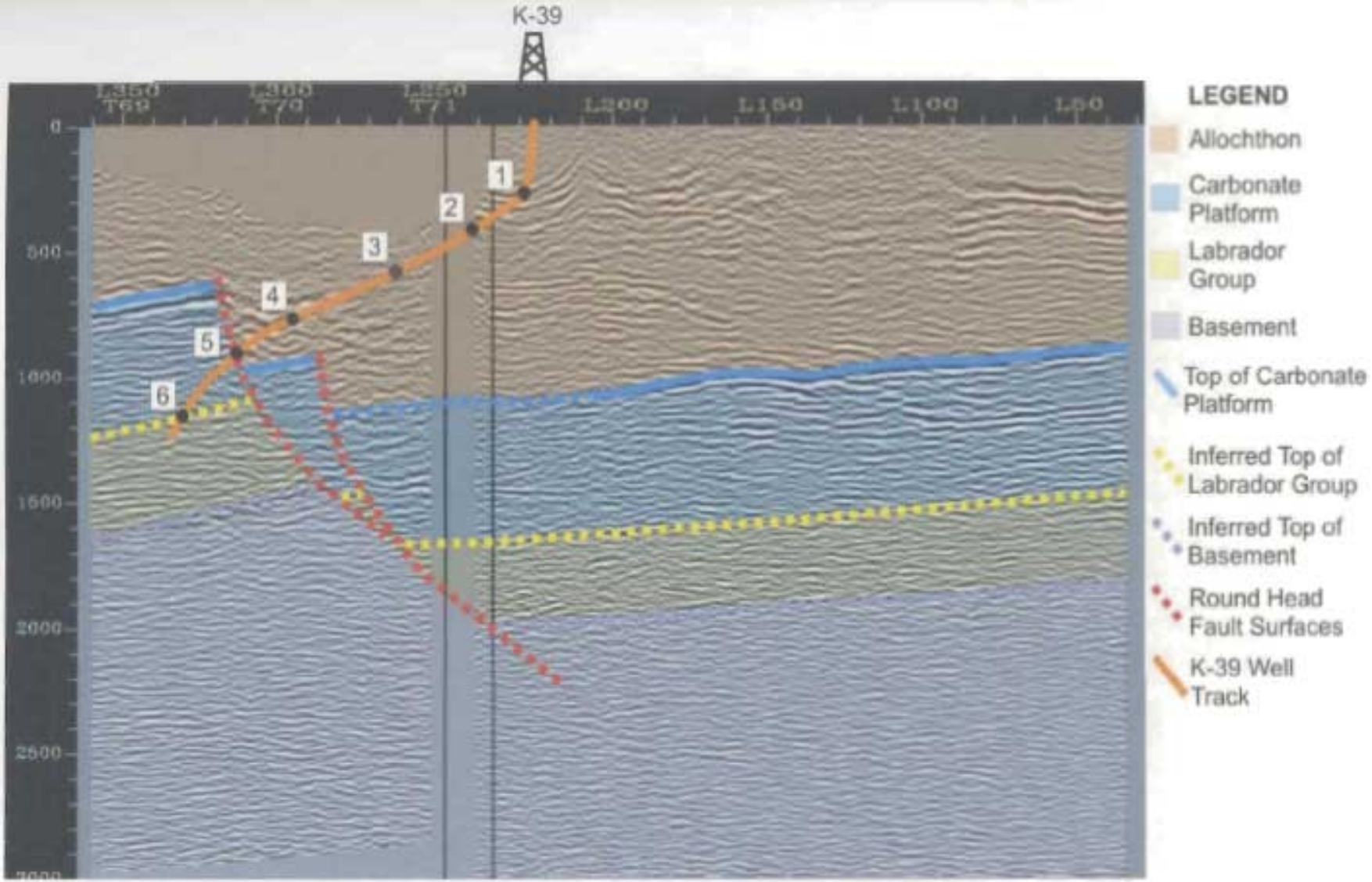

Figure 6.13. 3D seismic line corresponding to the K-39 surface well trajectory. Overlain by the K-39 well track, interpreted for geological sequences and characteristic structure; line location in figure 6.12, well track number legend in table 6.1.

6.5 Interpretation Summary

The interpretation of the 3D dataset proved difficult but ultimately was accomplished through close consideration of all available surrounding seismic. By mapping the carbonate platform footwall and hanging-wall surfaces the primary goal of the project was accomplished. Correlation of the K-39 well to the 3D data provided an additional check to overall data quality and interpretation validity, given the processing difficulties and non-conventional methods applied to the data in order to achieve a final product. In short, from the 3D data we are able to achieve a better understanding of the dominant geological formations and processes of the Port au Port peninsula along with a more detailed description of the Round Head fault within the bay.

The following figures (6.14a, b, c, d) are various viewing orientations of the carbonate platform surface, both the hanging-wall and footwall. Features such as the structural highs, the hanging-wall synclinal feature and the expression of the Round Head fault hanging-wall and footwall fault cutoff surfaces much more visible in orientation and positional relationship to one another in these figures.

Combination of all of the interpreted horizons into mapped surfaces generates the final 3D view; this figure gives an excellent overall picture of all of the interpreted geological sequences and how they are positioned together within Shoal Bay (Figure 6.15).

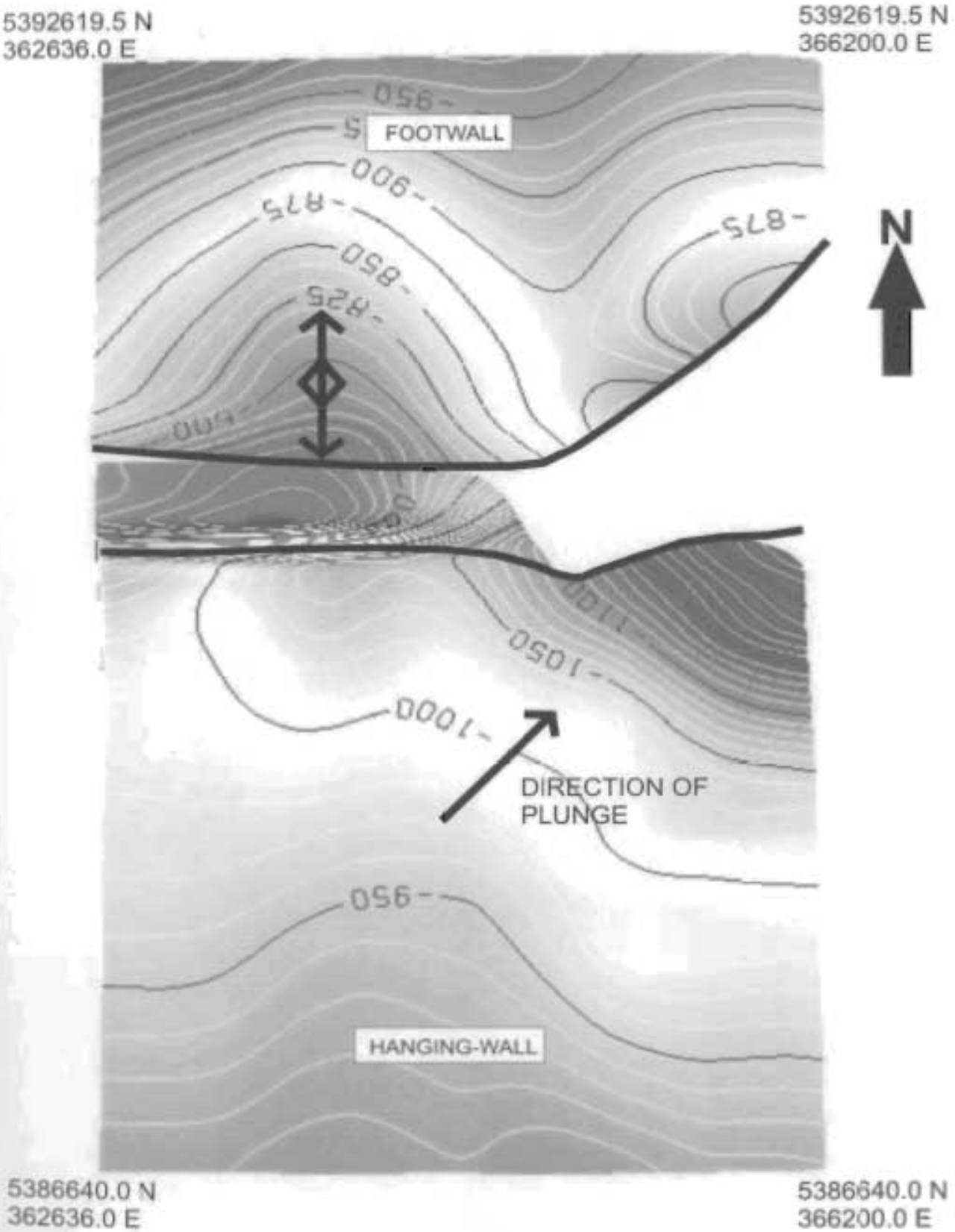

Figure 6.14a. 3D map view of complete top carbonate platform surface.

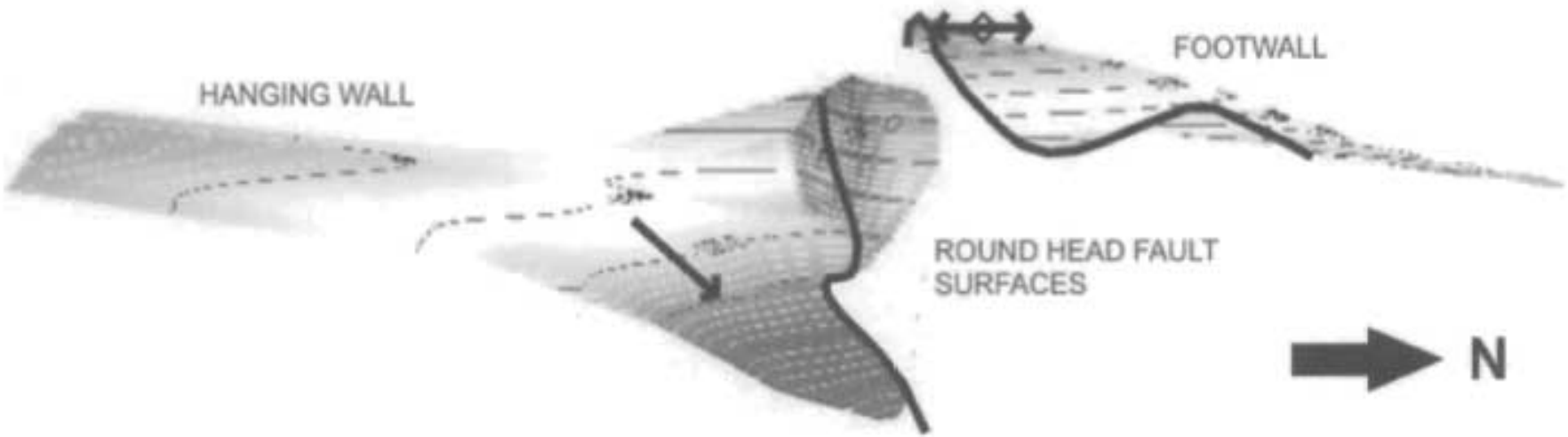

Figure 6.14b. Mapped hanging-wall and footwall 3D surfaces for the top of the Carbonate platform. View is from the east looking west across the platform.

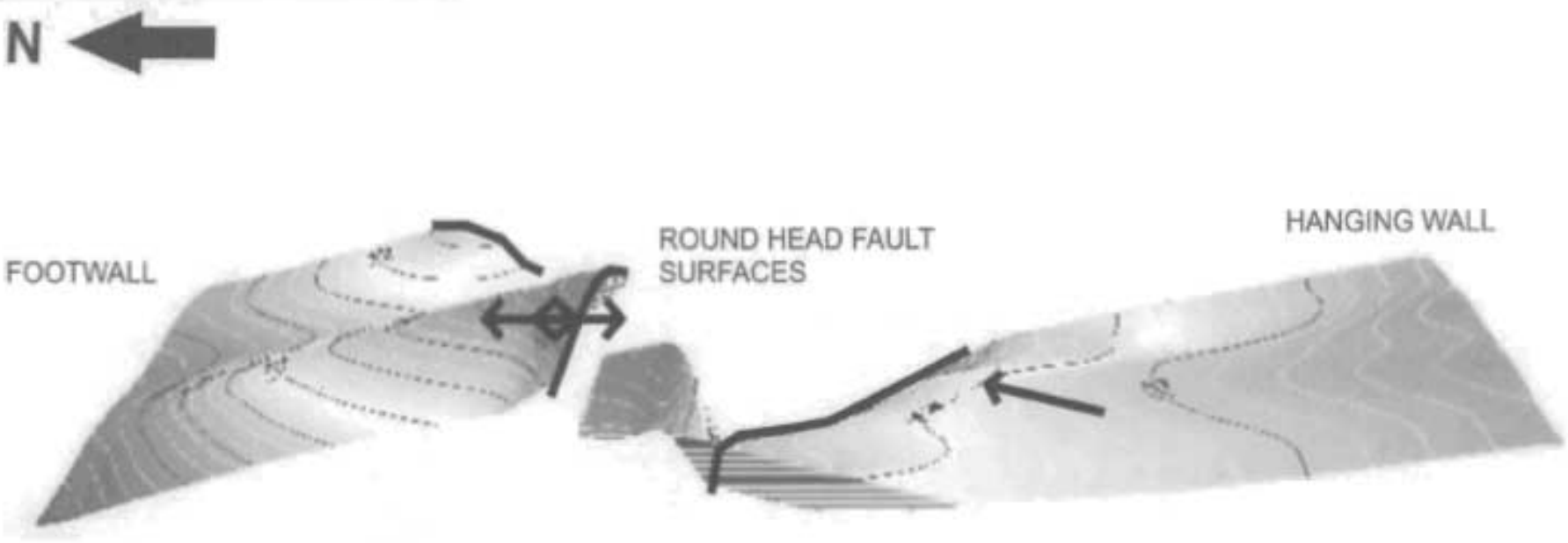

Figure 6.14c. Mapped hanging-wall and footwall 3D surfaces for the top of the Carbonate platform. View is from the west looking east across the platform.

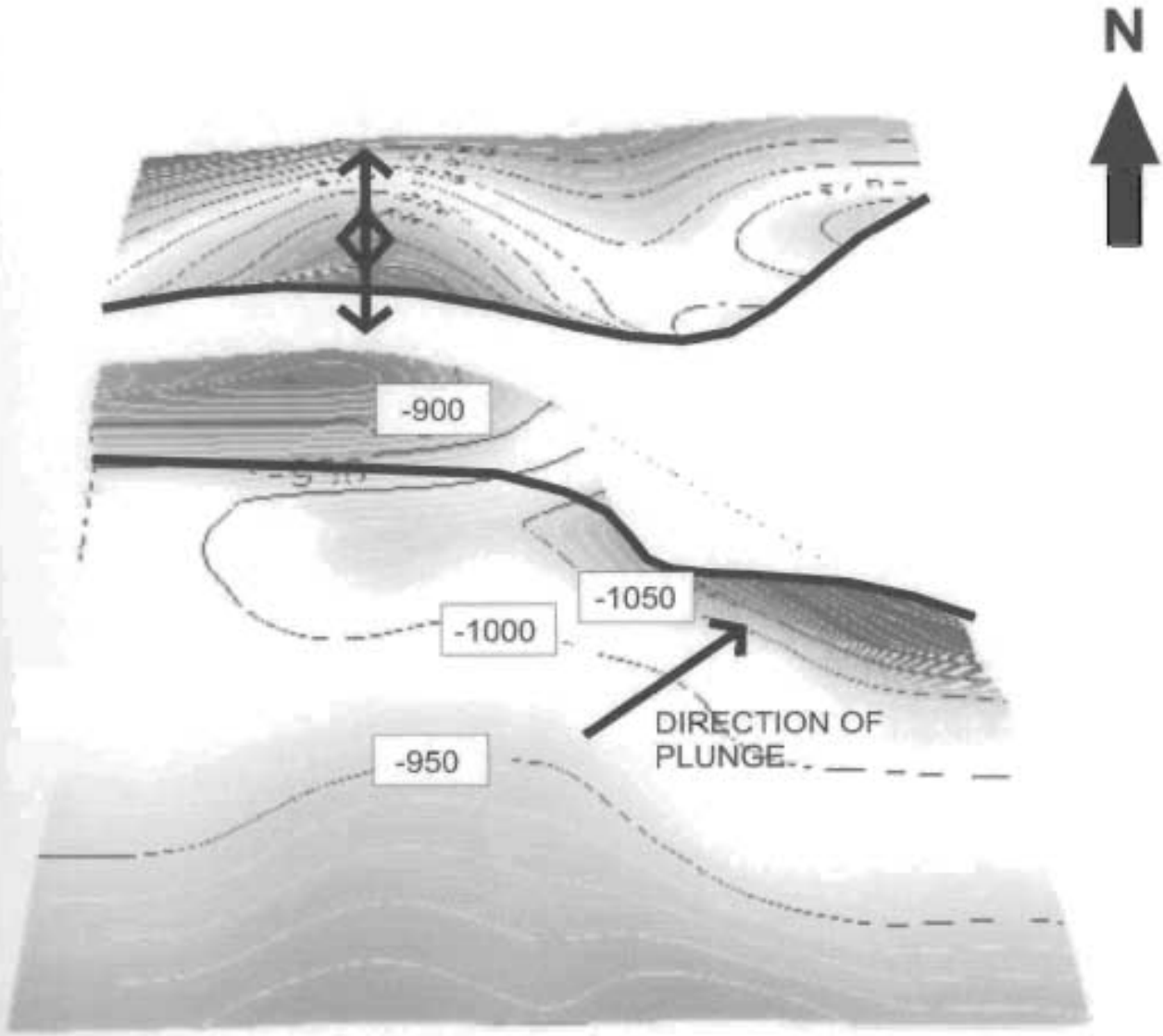

Figure 6.14d. Complete footwall / hanging-wall 3D carbonate platform surface oriented into the page, note the fault offset between the two surfaces.

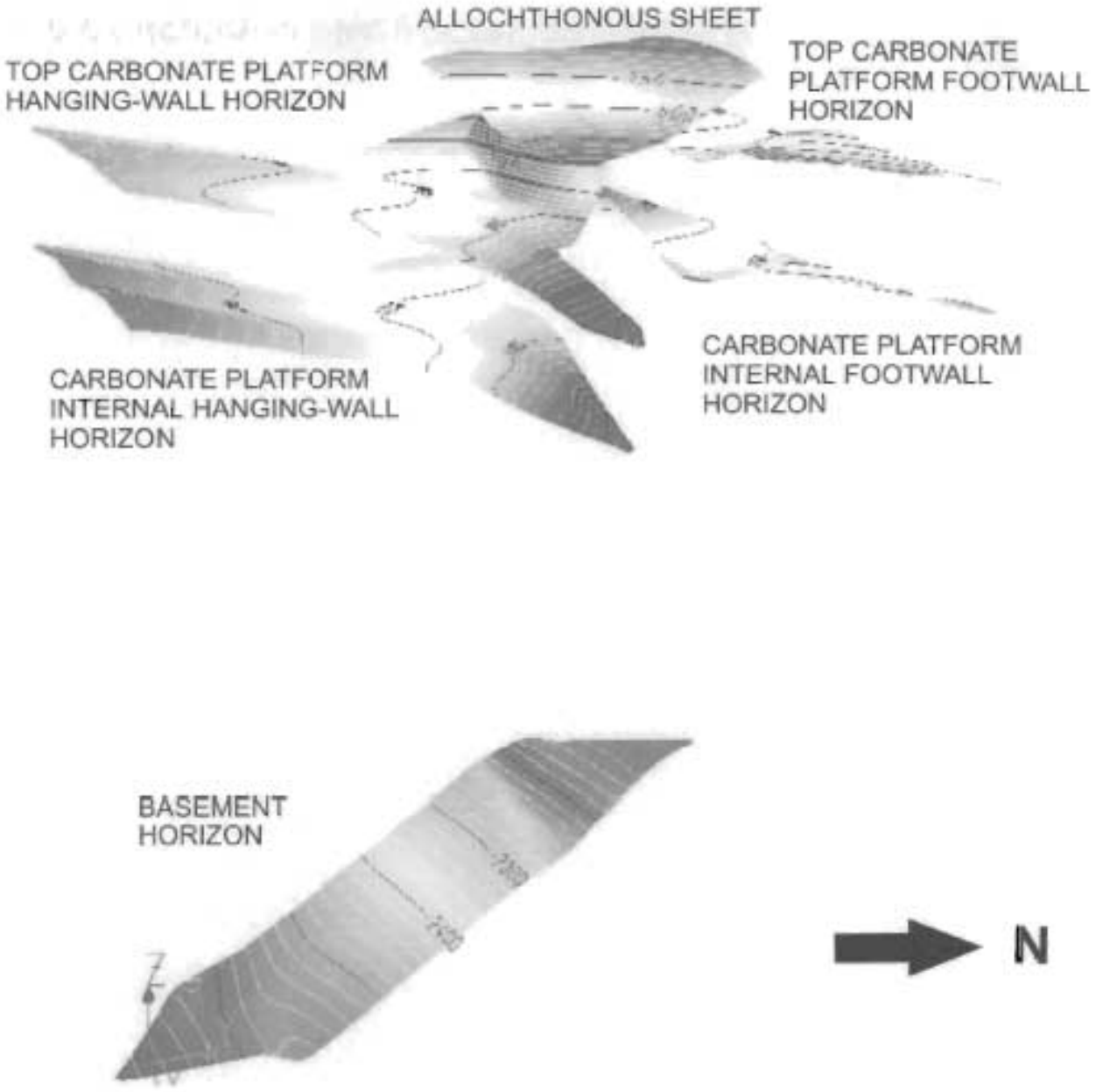

Figure 6.15. 3D image of all previously discussed geological sequences of the study area.

7.0 Conclusion and Recommendations

The primary objectives of the Shoal Point seismic project initially discussed in Chapter 1, were established as the following:

- To demonstrate a novel and cost-effective technique to acquire, process and interpret 3D data in a shallow water transition zone.
- To develop a better understanding of the complex geology and tectonic history of the area.
- To provide a seismic image at the Shoal Point K-39 well location.
- Create a 3D mapped surface to the top of the Ordovician carbonate platform.

The entire project was designed, acquired and interpreted with these four main goals in mind. The acquisition, though not part of this thesis was completed as designed in a precise manner within a strict timetable and budget, meeting the initial aspects of the first goal. Processing and interpretation of both the 2D and 3D datasets resulted in the successful completion of the second half of the first goal. The results of this work led to a successful accomplishing of the remaining objectives.

The final two objectives above can be considered the ultimate in the successful completion of the project. By correctly acquiring and processing a dataset that

could be interpreted to correlate perfectly with exploration seismic and drill data it is possible make several points with respect to the previous petroleum exploration of the area, and therefore the continued petroleum potential of the area.

The correlation of the K-39 well with the 3D seismic shows that PanCanadian et al. missed their target, stated in the drilling report as "Ordovician age carbonates of the Table Head and St. Georges Group". As was previously discussed the drill passed through the Round Head fault entering directly into the Catoche Formation of the Port au Port Group (Figure 2.2) missing the top platform Table Head Group completely, drilling into the face of the fault below the desired target. Therefore, it can be concluded that the desired target was missed and that the structural high footwall play concept was not successfully tested.

Presentation of the 3D maps in Chapter 6 meets the requirements of the fourth and the final project goal. The successful interpretation of the 3D volume allowed the mapping of the top of the Ordovician carbonate platform, the Round Head fault, allochthonous thrust slices and other geological boundaries. From the 3D mapped surface, we obtain an increased level of accuracy for the platform orientation and geological features, (i.e. the footwall anticline) along with a better understanding of the Round Head fault expression.

Consideration of all of the current study data does add to the overall understanding of the complex geology and tectonic history of the area. It provides a better picture of possible petroleum targets, also allowing the analysis of previous drilling and seismic exploration within the area. In closing I think the project clearly indicates that petroleum potential for the area still exists and that using the 3D maps and the increased knowledge of the geological setting the footwall anticline is a viable target that can be tested correctly.

References

Cooper, M., Weissenberger, J., Knight, I., Hostad, D., Gillespie, D., Williams, H., Burden, E., Porter-Chaudry, J., Rae, D., and Clark, E., 1998. Basin evolution in western Newfoundland: New insights form hydrocarbon exploration. The American Association of Petroleum Geologists Bulletin, v. 85, No.3, p. 393-418.

Cawood, P. A., and Williams, H., 1988. Acadian basement thrusting, crustal delamination and structural styles in and around the Humber Arm allochthon, western Newfoundland. Geology, v. 16, p. 370-373.

ProMAX® 2D Reference Guide, 1998. A reference guide for the ProMAX® geophysical processing software. v. 1 and 2.

Quinlan, G. M., Hall, J., Williams, H., Wright, J. A., Colmen-Sadd, S. P., O'Brien, S. J., Stockmal, G. S., Marillier, F., 1992. Lithoprobe onshore seismic reflection transects across the Newfoundland Appalachians. Canadian Journal of Earth Sciences, v. 29, p. 1865-1877.

Stenzel, S. R., Knight, I., and James, N. P., 1990. Carbonate platform to foreland basin: revised stratigraphy of the Table Head Group (Middle Ordovician), western Newfoundland. Canadian Journal of Earth Sciences, v. 27, p. 14-26.

Stockmal, G. S., and Waldron, J. W. F., 1990. Structure of the Appalachian deformation front in western Newfoundland: Implications of multichannel seismic reflection data. Geology, v.18, p. 765-768.

Stockmal, G. S., Slingsby, A., and Waldron, J. W. F., 1998. Deformation styles at the Appalachian structural front, western Newfoundland: Implications of new industry seismic reflection data. Canadian Journal of Earth Sciences, v. 35, p. 1288-1306.

Waldron, J. W. F., and Stockmal, G. S., 1991. Mid-Paleozoic thrusting at the Appalachian deformation front: Port au Port Peninsula, western Newfoundland. Canadian Journal of Earth Sciences, v. 28, p. 1992-2002.

Waldron, J. W. F., and Stockmal, G. S., 1994. Structural and tectonic evolution of the Humber Zone, western Newfoundland, 2: A regional model for Acadian thrust tectonics. Tectonics, v. 13, p. 1498-1513.

Waldron, J. W. F., Stockmal, G. S., Corney, R. E., and Stenzel, S. R., 1993. Basin development and inversion at the Appalachian structural front, Port au Port Peninsula, western Newfoundland Appalachians. Canadian Journal of Earth Sciences, v. 30, p. 1759-1772.

Williams, H., 1979. Appalachian orogen in Canada. Canadian Journal of Earth Sciences, v. 16, p. 792-807.

Yilmaz, Ö., 2001. Seismic Data Analysis: Processing, Inversion, and Interpretation of Seismic Data. Society of Exploration Geophysicists, v. 1 and 2.

Appendix A

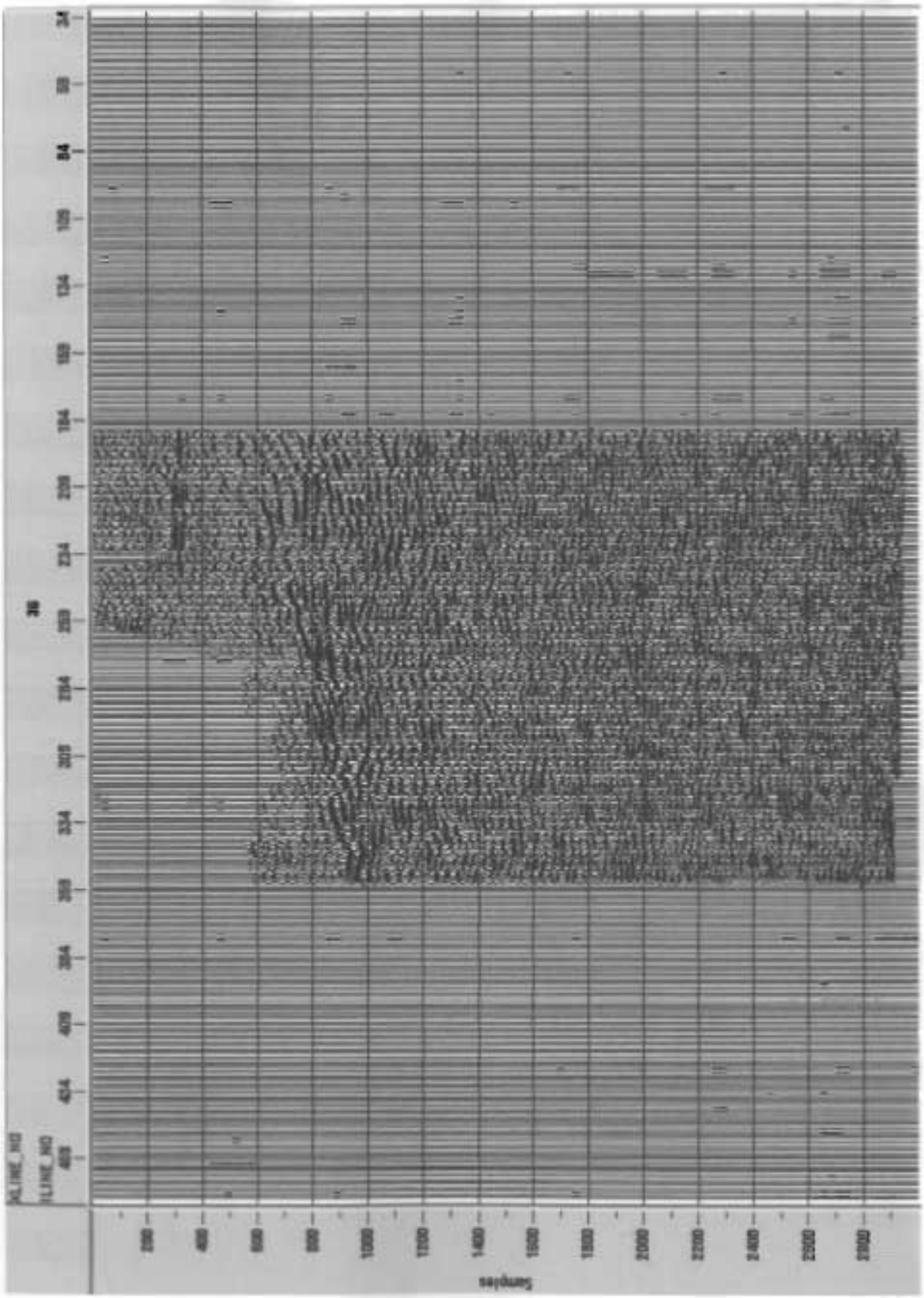
XLINE_NO
YLINE_NO
Samples

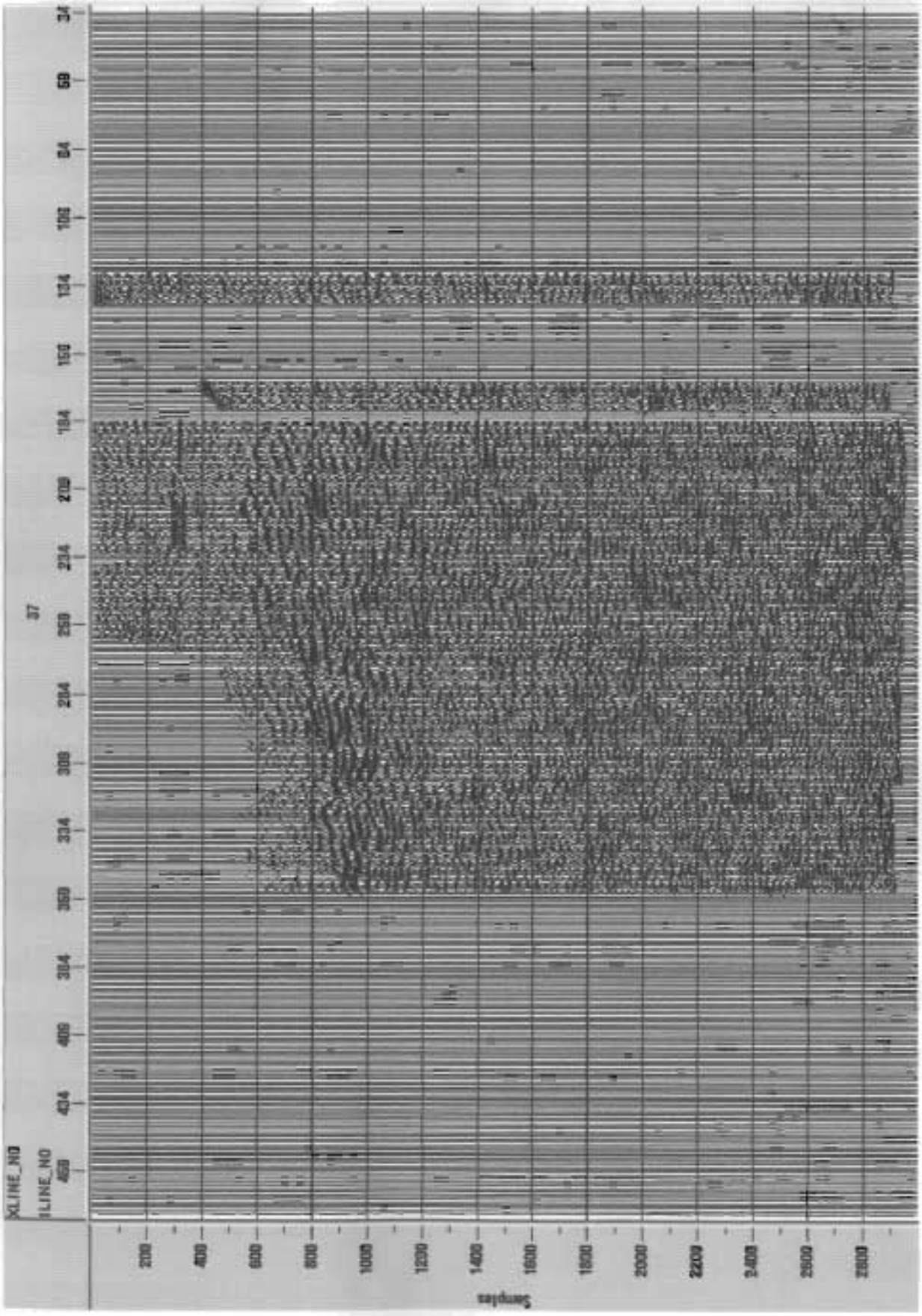
XLINE_NO
ILINE_NO
459
434
409
384
359
334
309
284
259
234
209
184
159
134
109
84
59
34
37
200
400
600
800
1000
1200
1400
1600
1800
2000
2200
2400
2600
2800
Samples

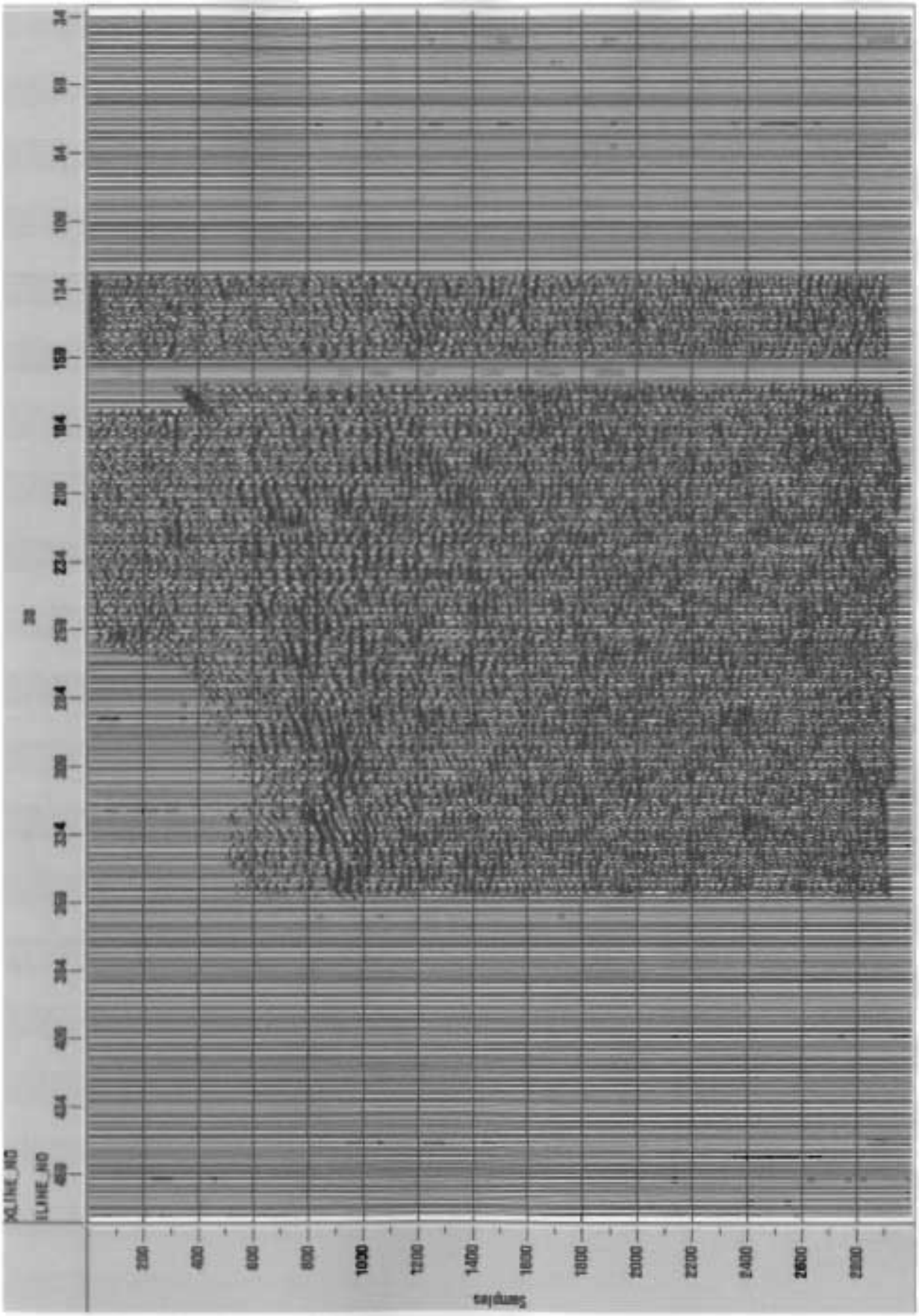
XLINE_NO
ILINE_NO
Samples

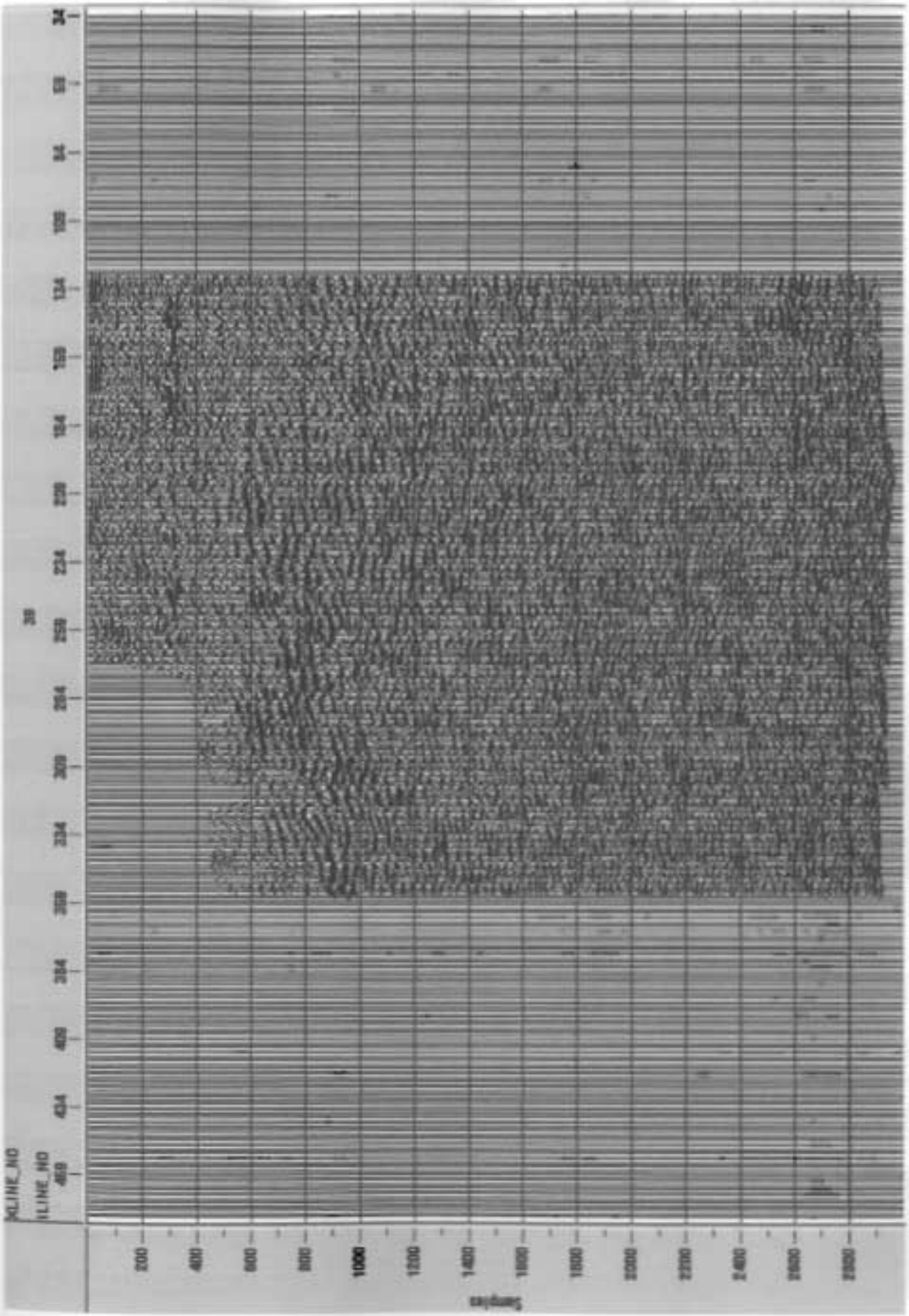
XLINE_NO
ILINE_NO
Samples

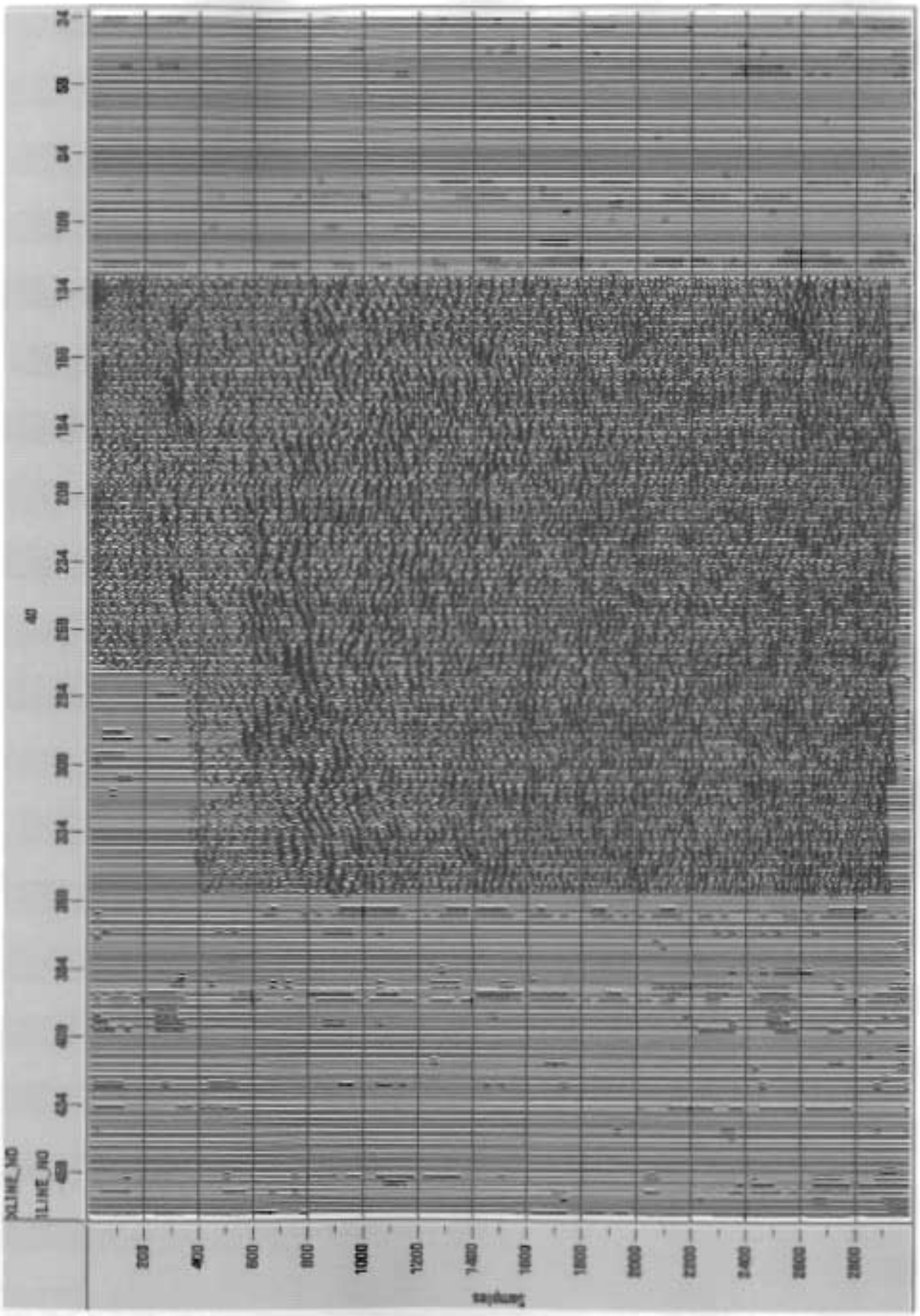
XLINE_NO
ILINE_NO
40
Samples

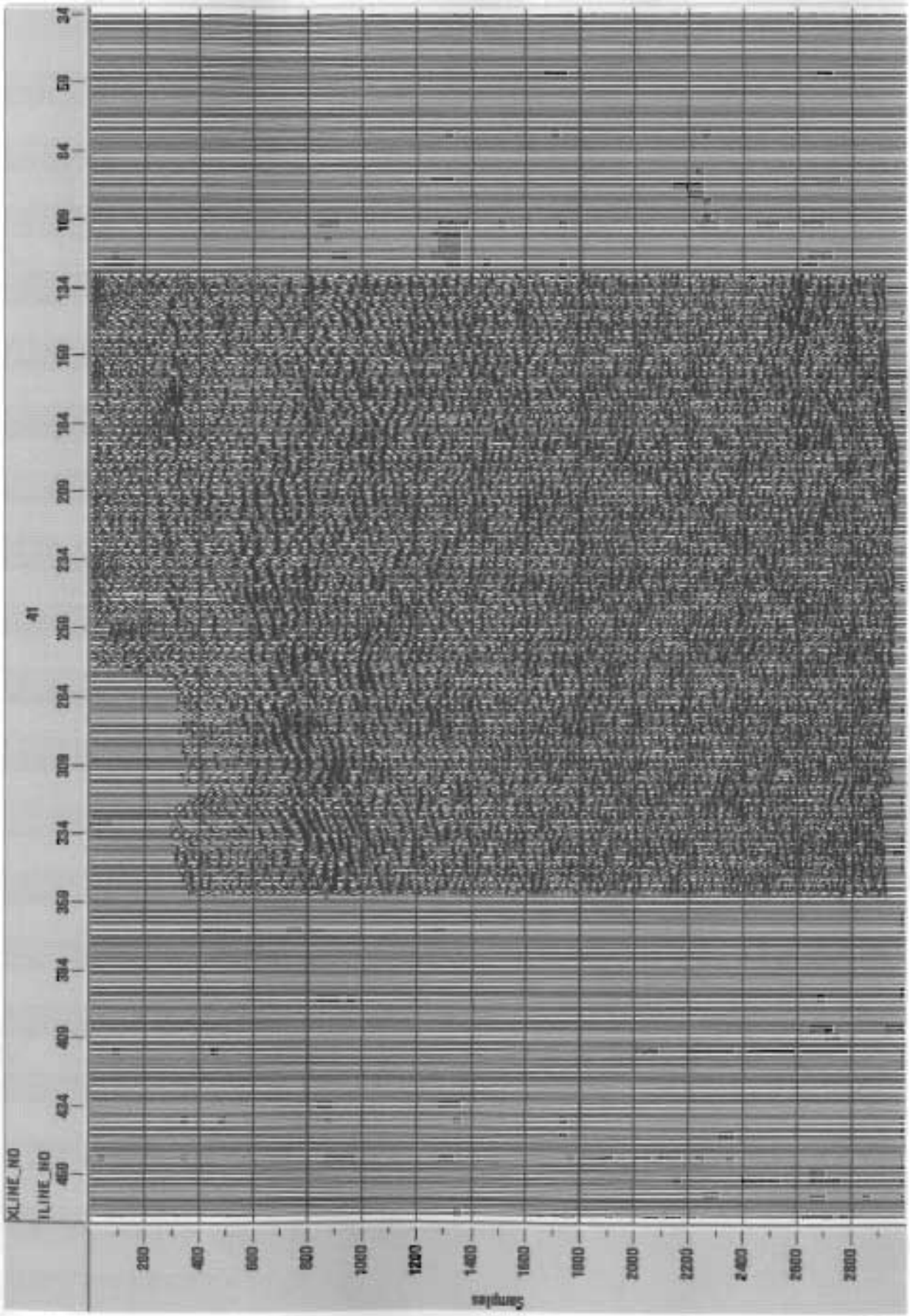
XLINE_NO
ILINE_NO
Samples

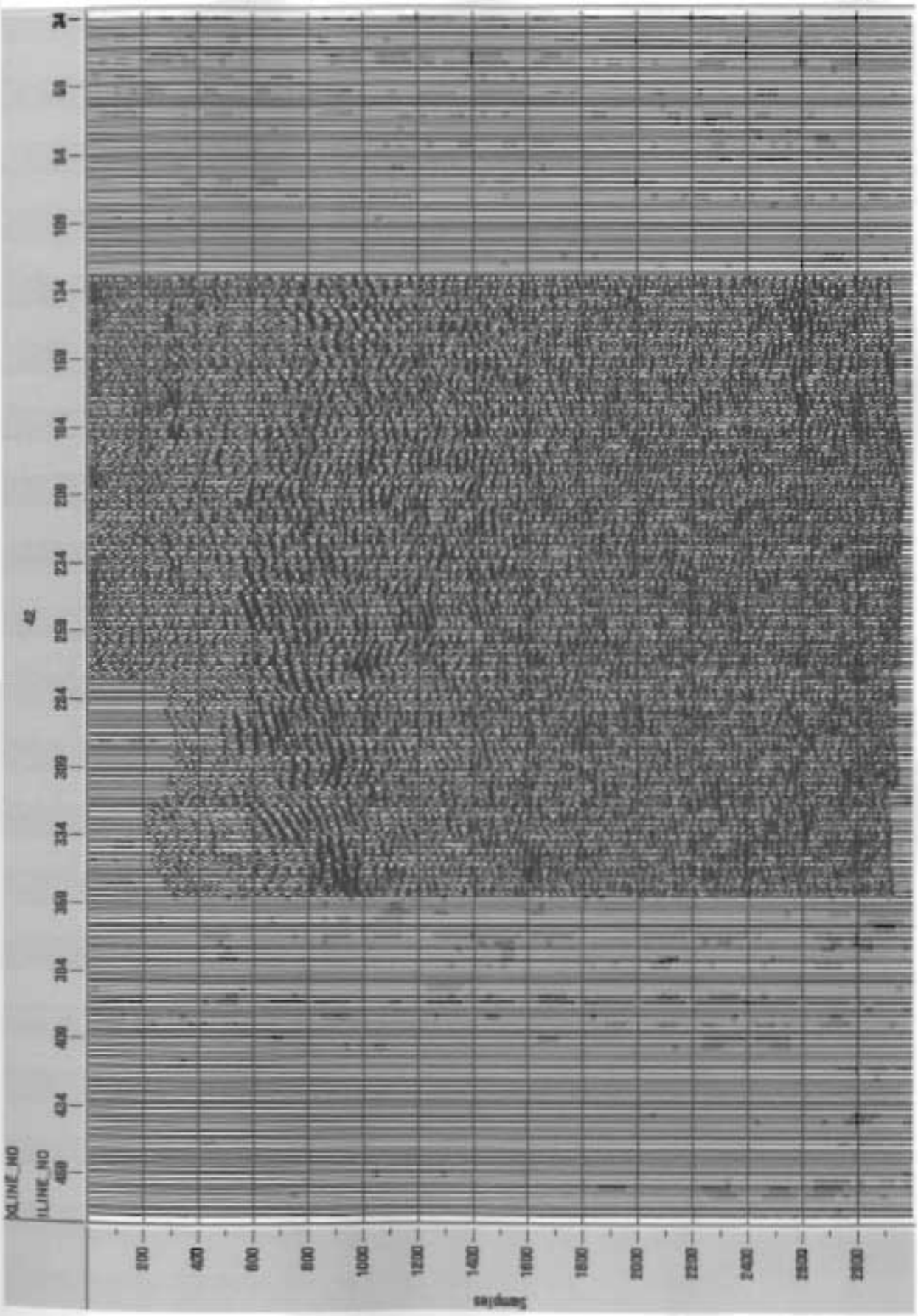
XLINE_NO
ILINE_NO
Samples

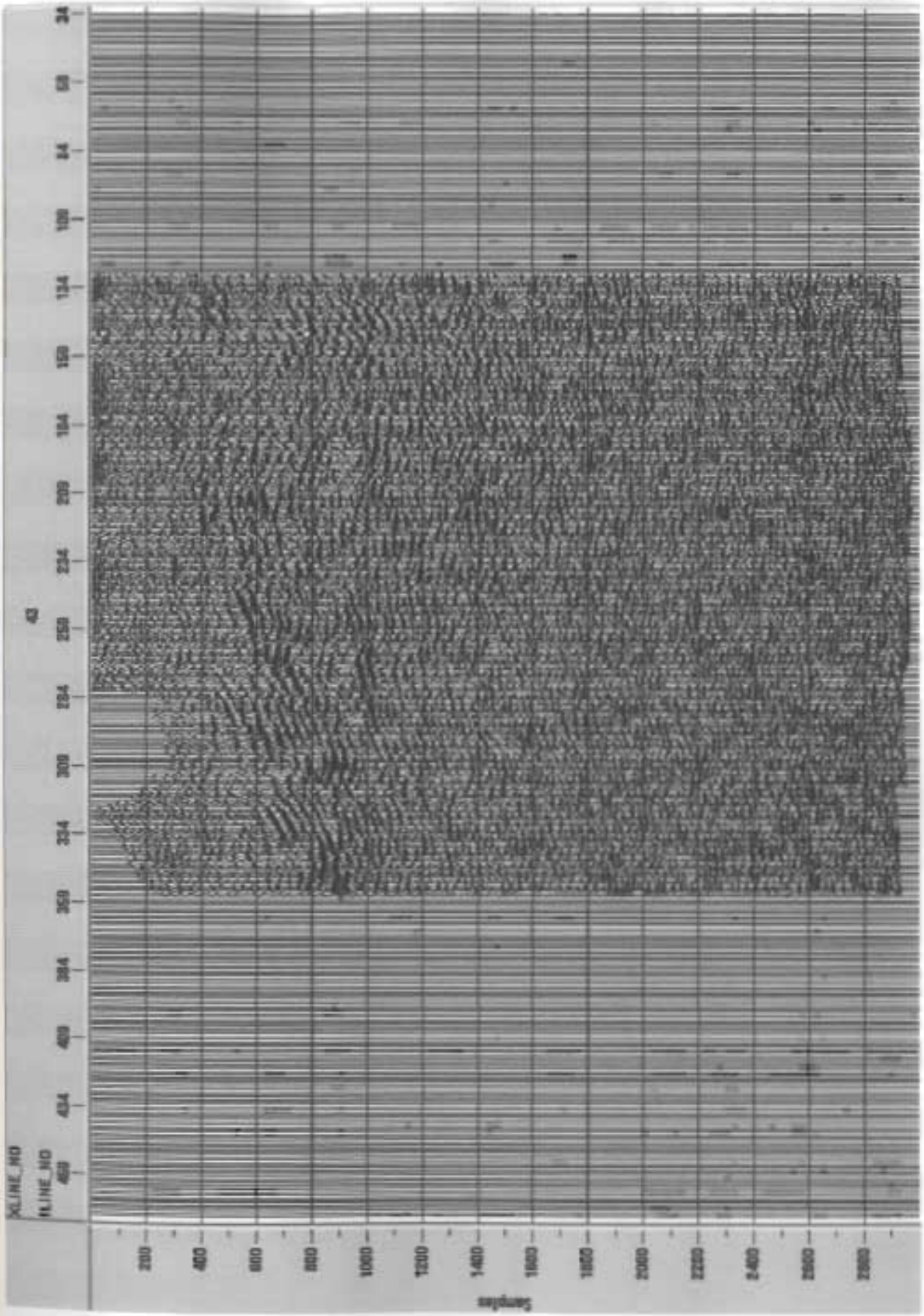
XLINE_NO
ILINE_NO
43
Samples

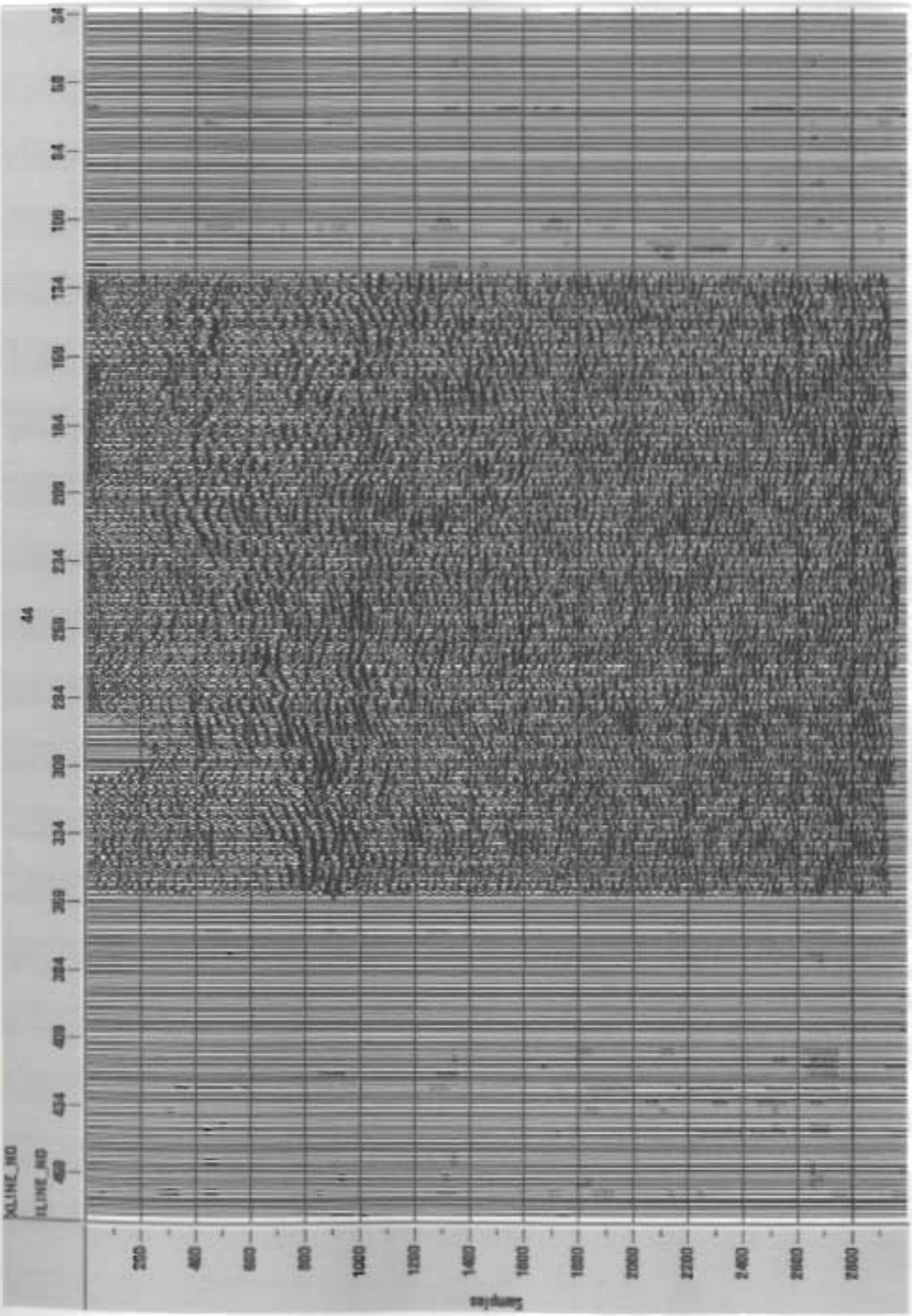
XLINE_NO
ILINE_NO
44
Samples

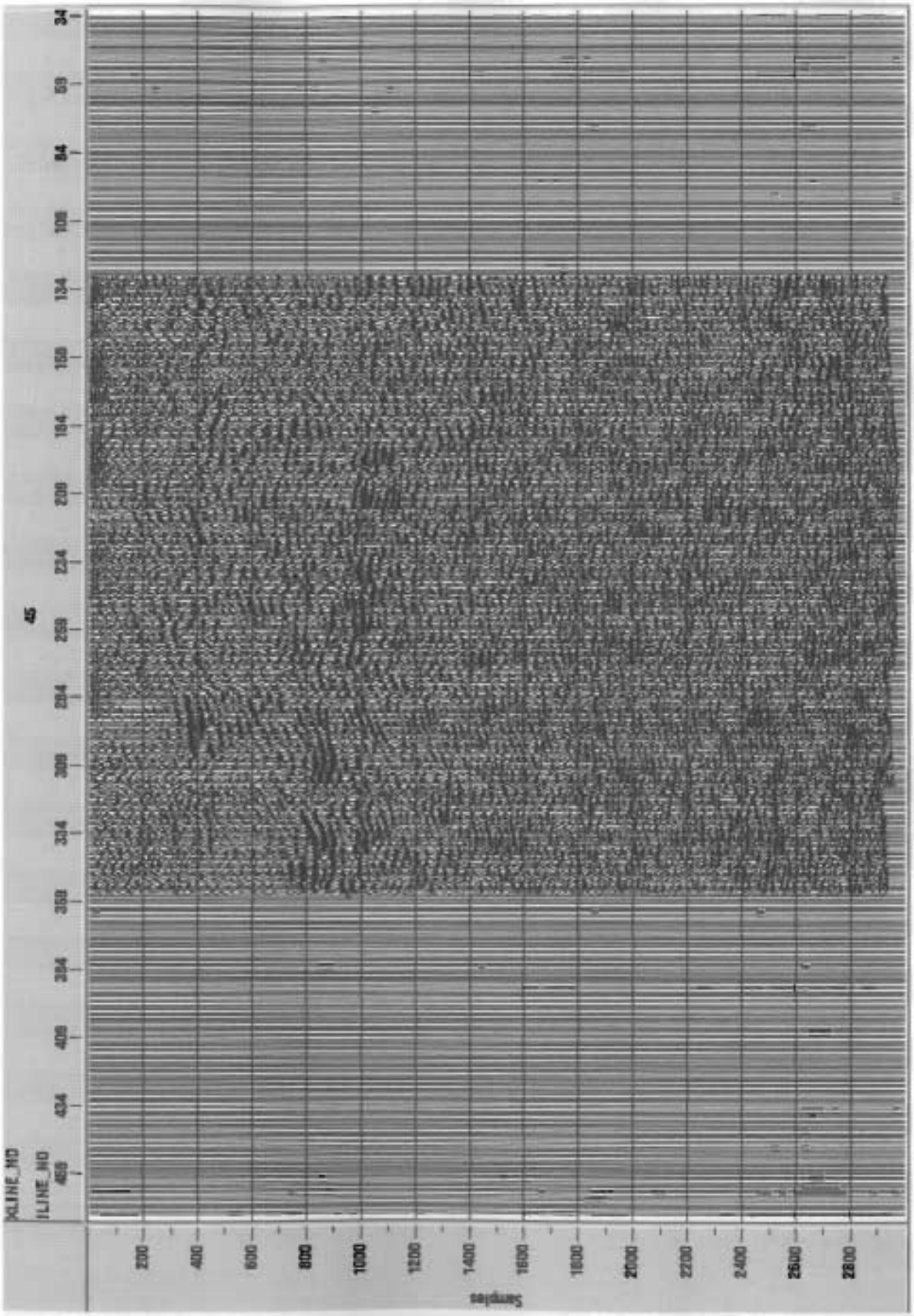
XLINE_NO
ILINE_NO
45
34
59
84
109
134
159
184
209
234
259
284
309
334
359
384
409
434
459
Samples
200
400
600
800
1000
1200
1400
1600
1800
2000
2200
2400
2600
2800

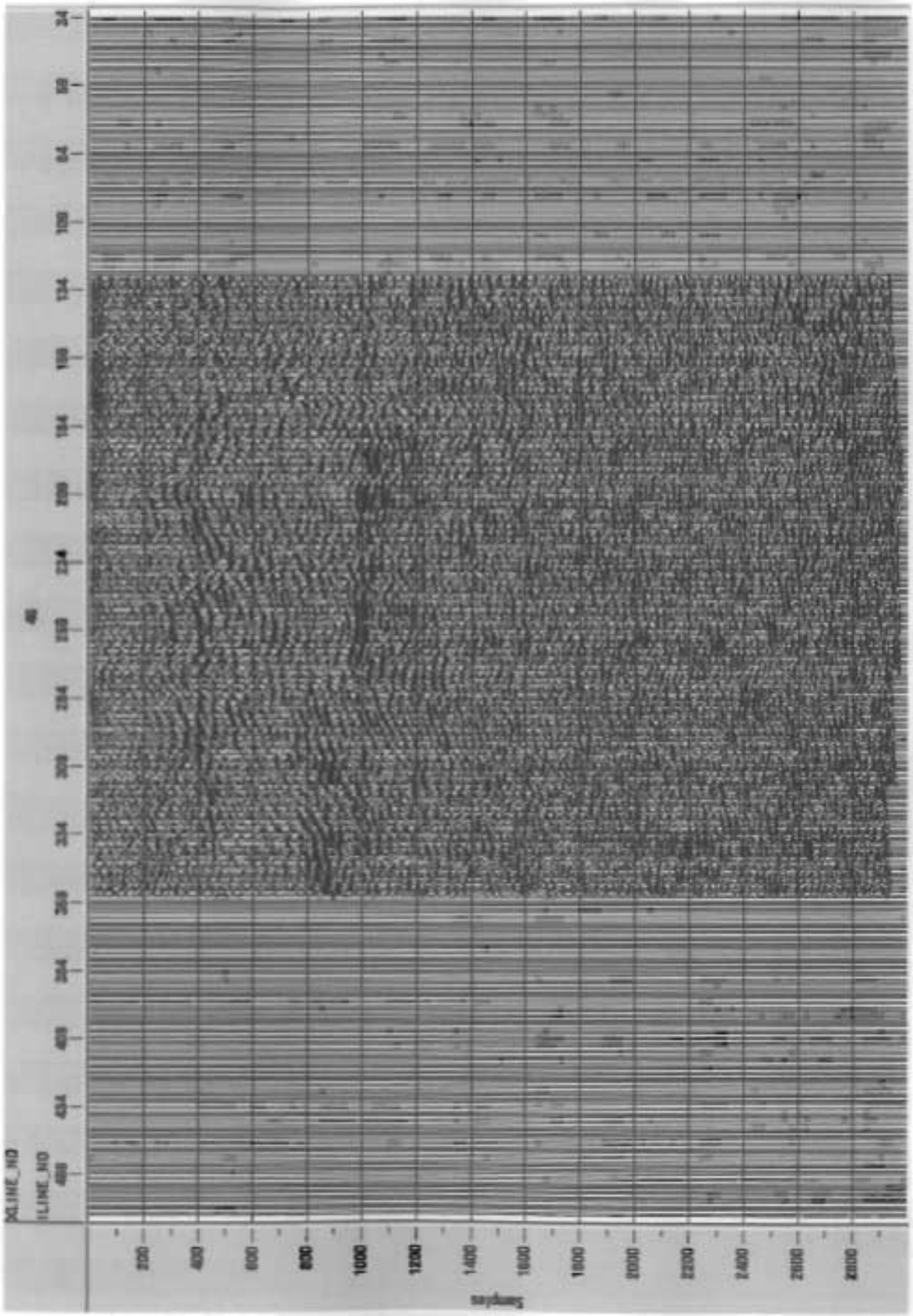
XLINE_NO
YLINE_NO
Samples

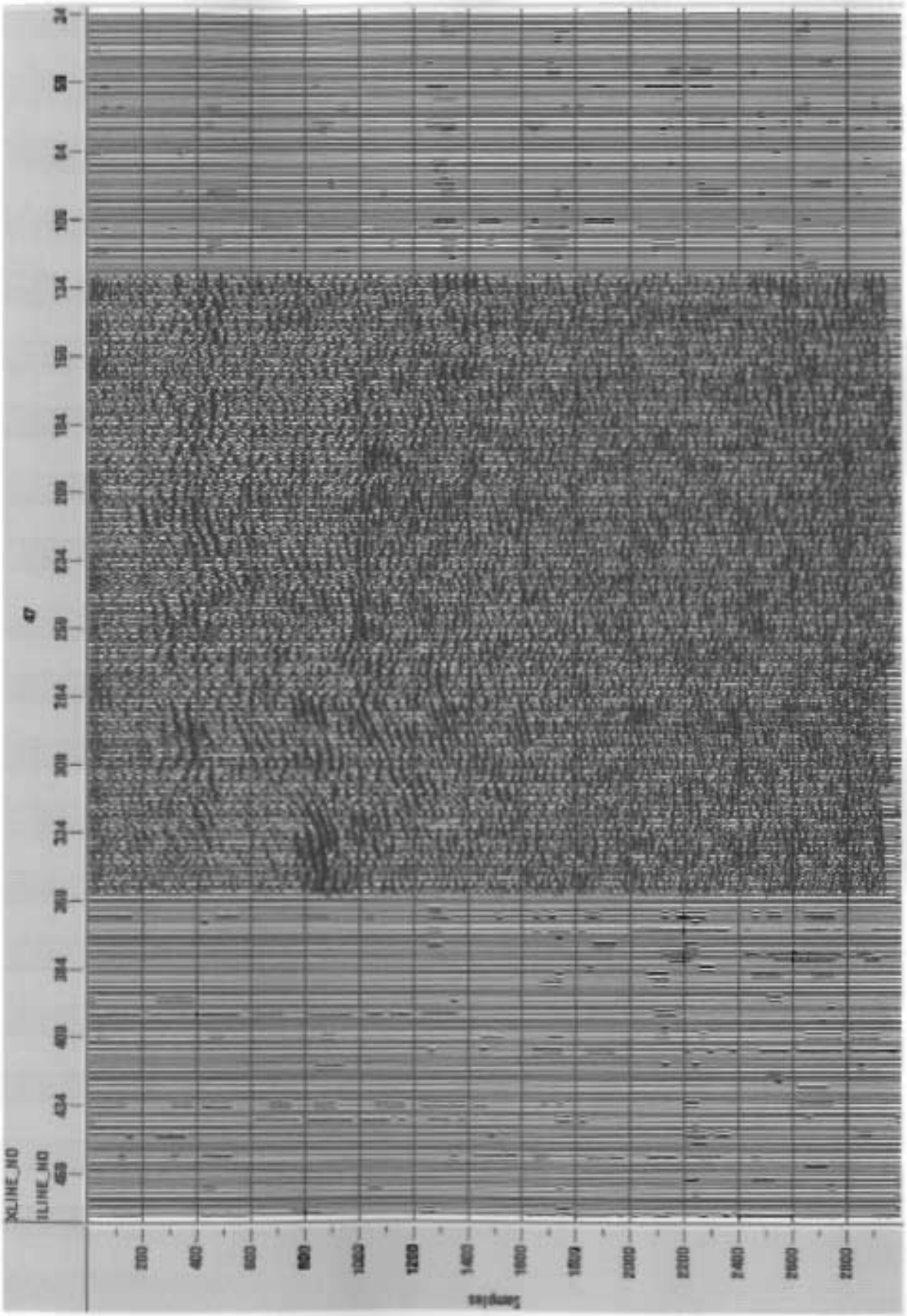
XLINE_NO
ILINE_NO
459
434
409
384
359
334
309
284
259
234
209
184
159
134
109
84
59
34
47
Samples
200
400
600
800
1000
1200
1400
1600
1800
2000
2200
2400
2600
2800

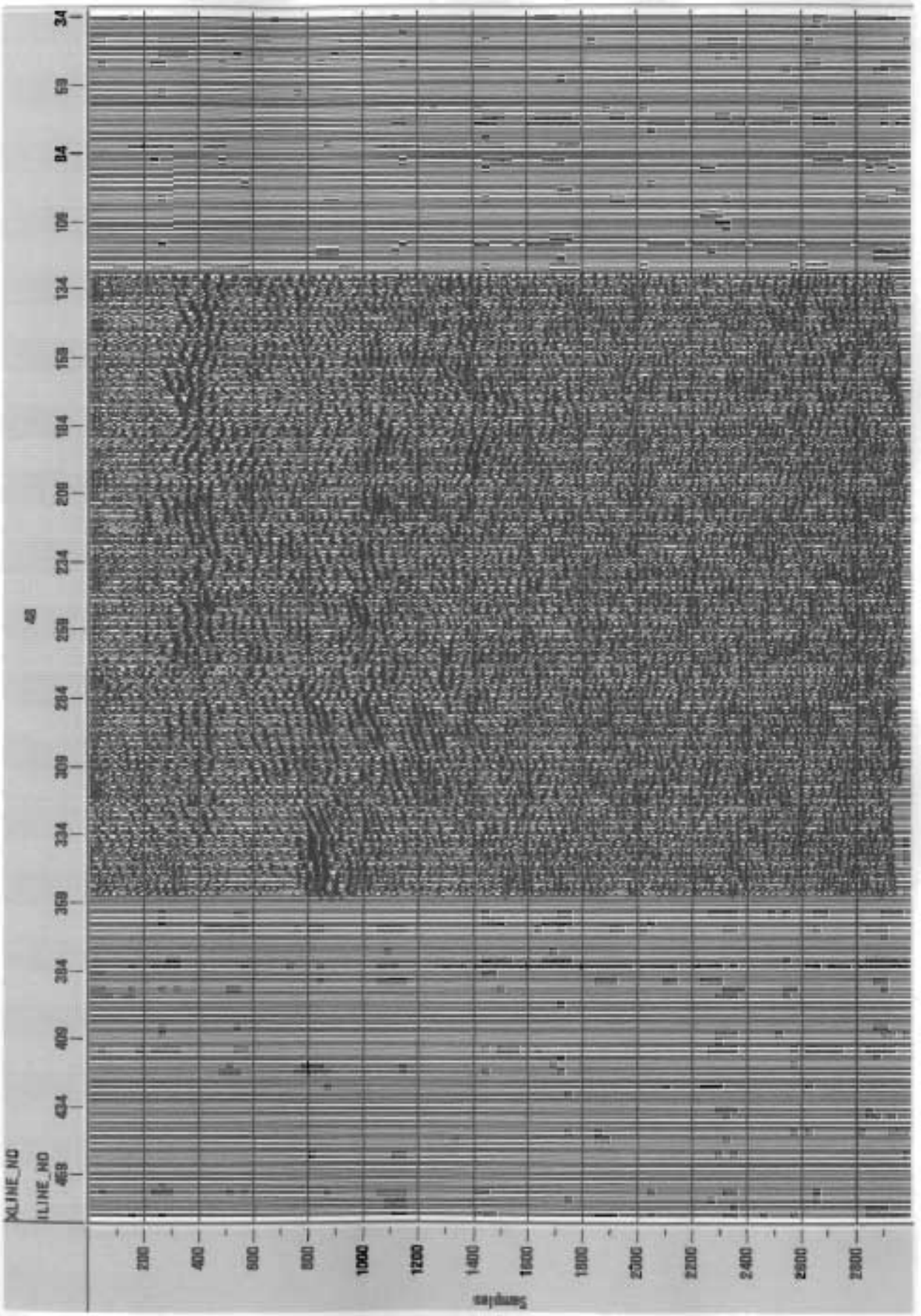
XLINE_NO
ILINE_NO
34
59
84
109
134
159
184
209
234
259
284
309
334
359
384
409
434
459
200
400
600
800
1000
1200
1400
1600
1800
2000
2200
2400
2600
2800
Samples

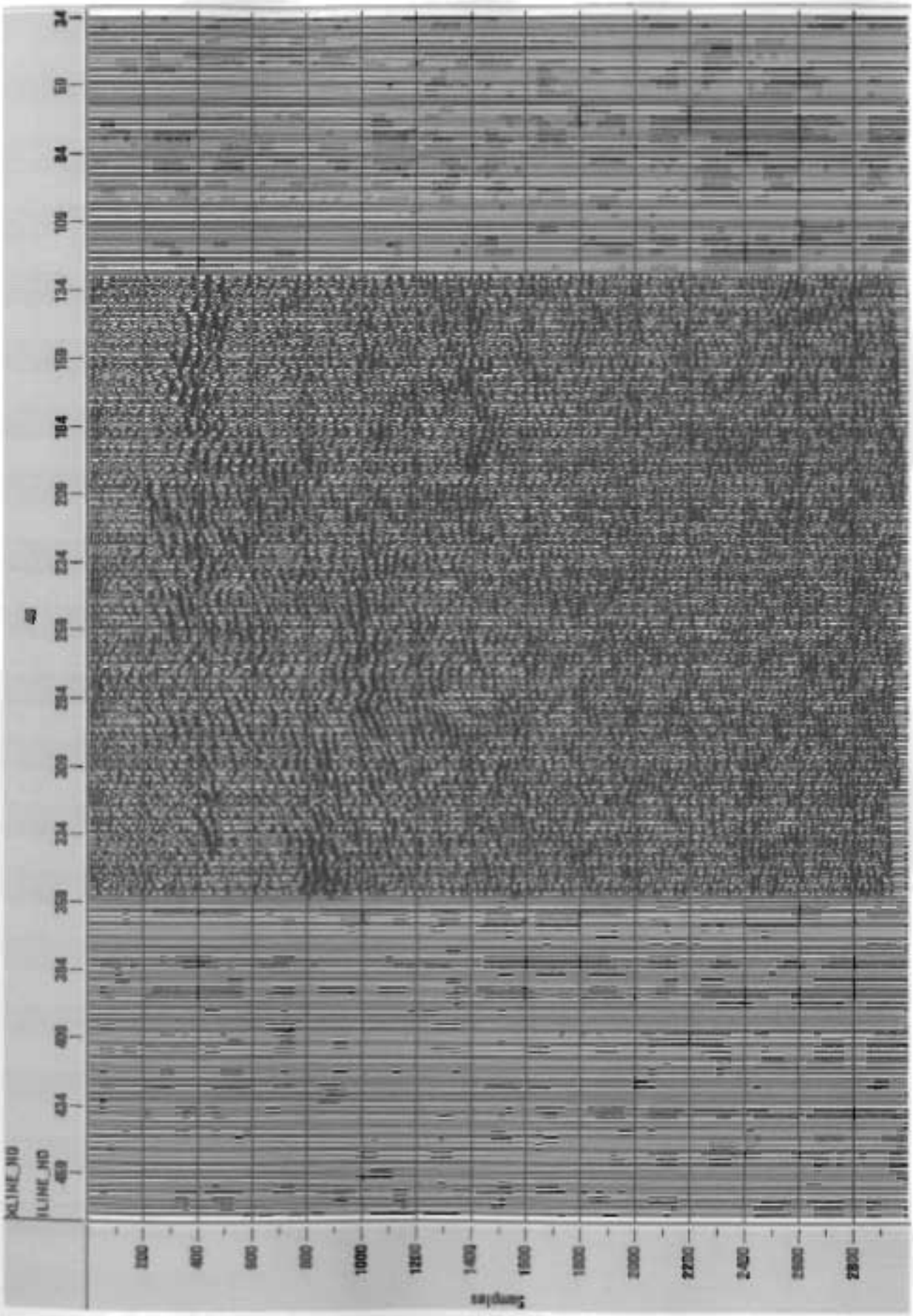
XLINE_NO
ILINE_NO
Samples

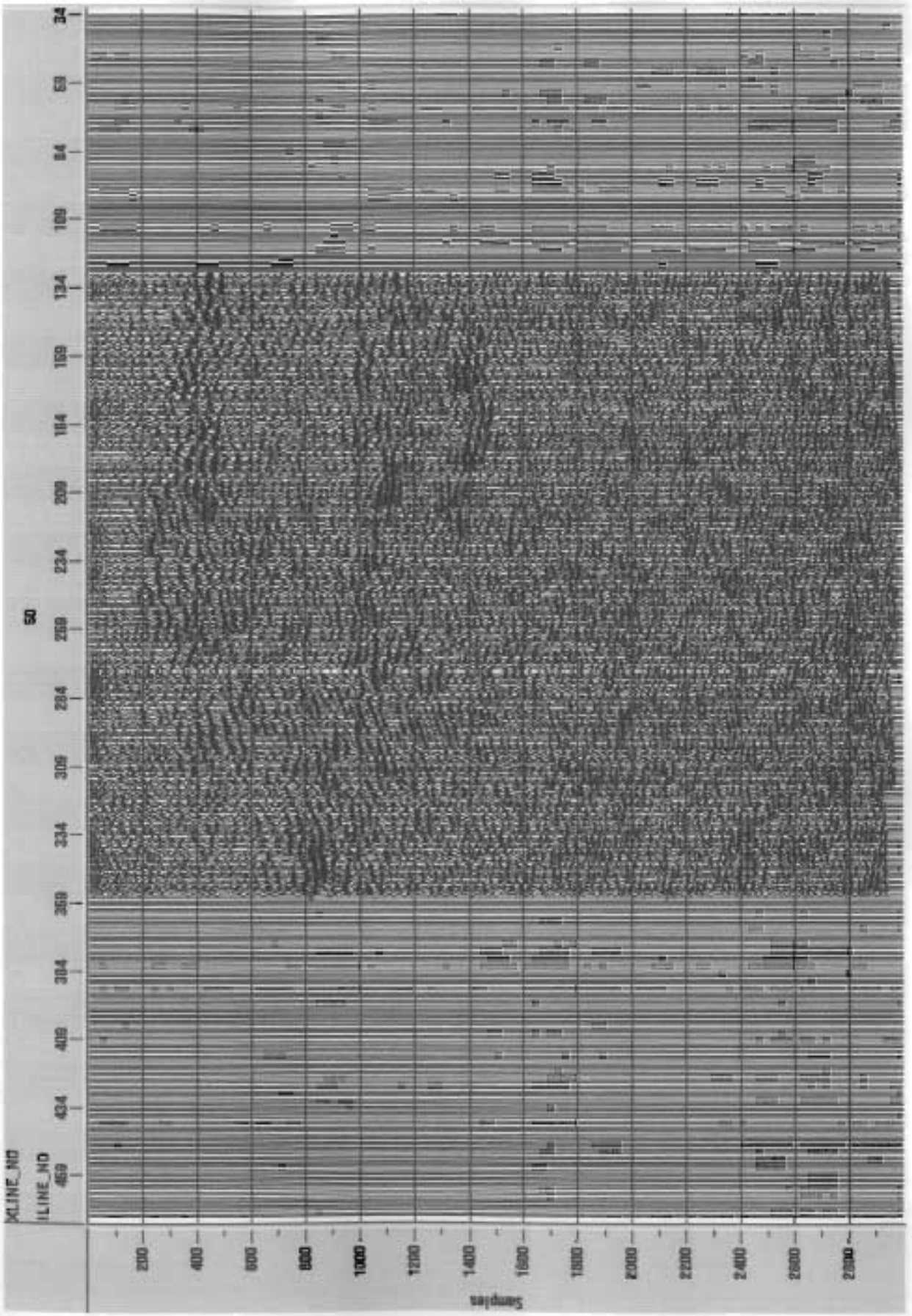
XLINE_NO
ILINE_NO
Samples

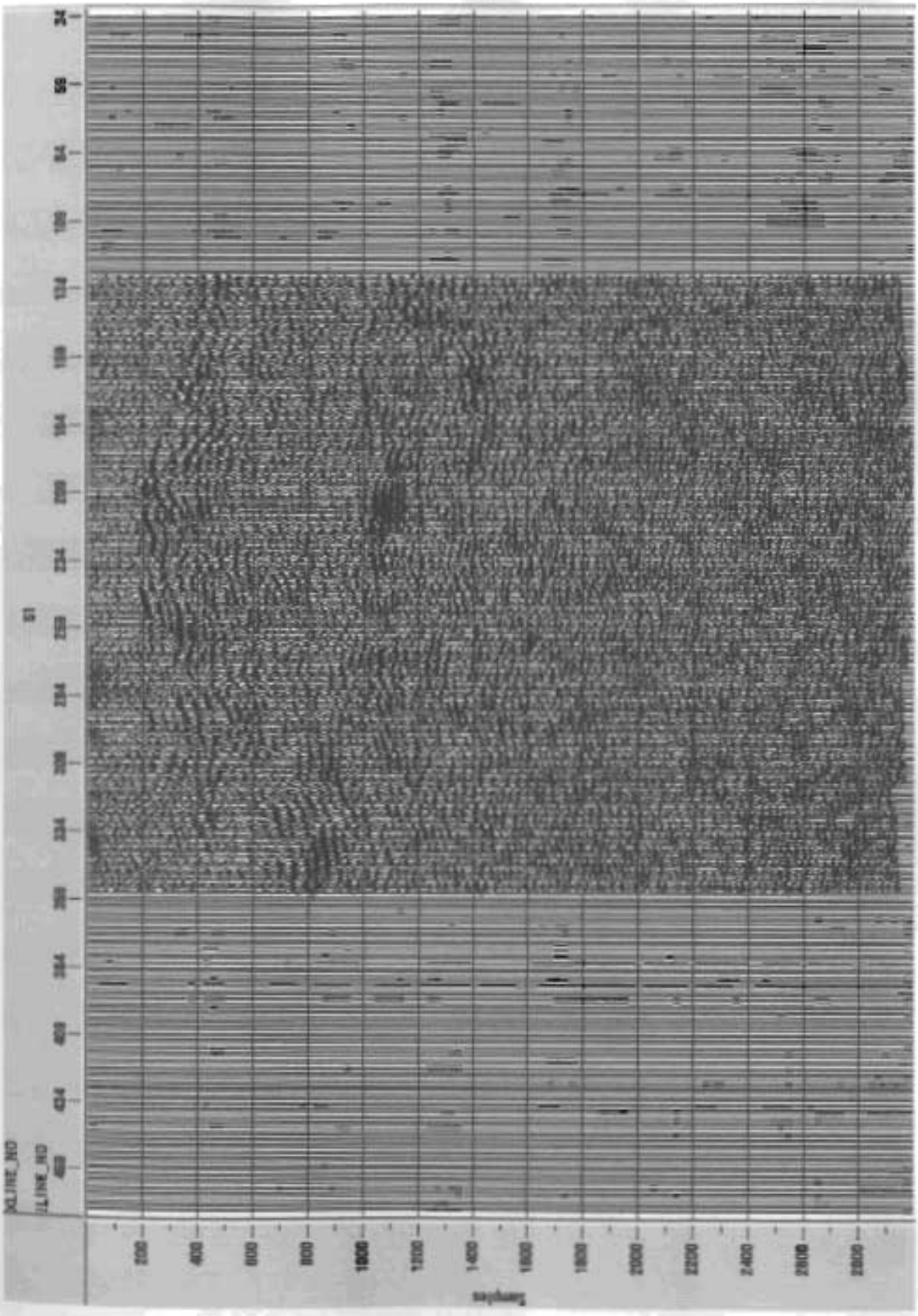
XLINE_NO
ILINE_NO
Samples

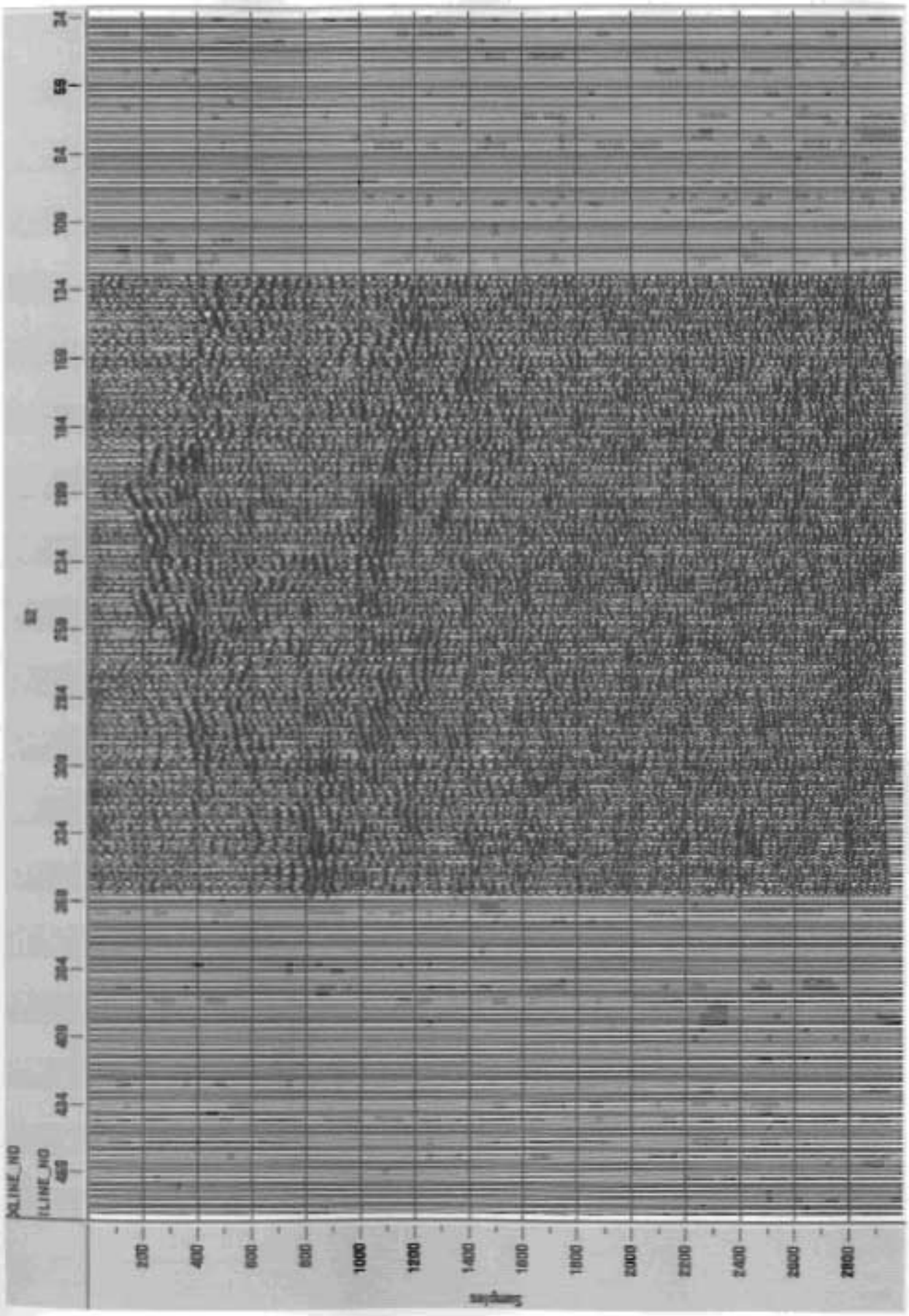
XLINE_NO
YLINE_NO
Sample

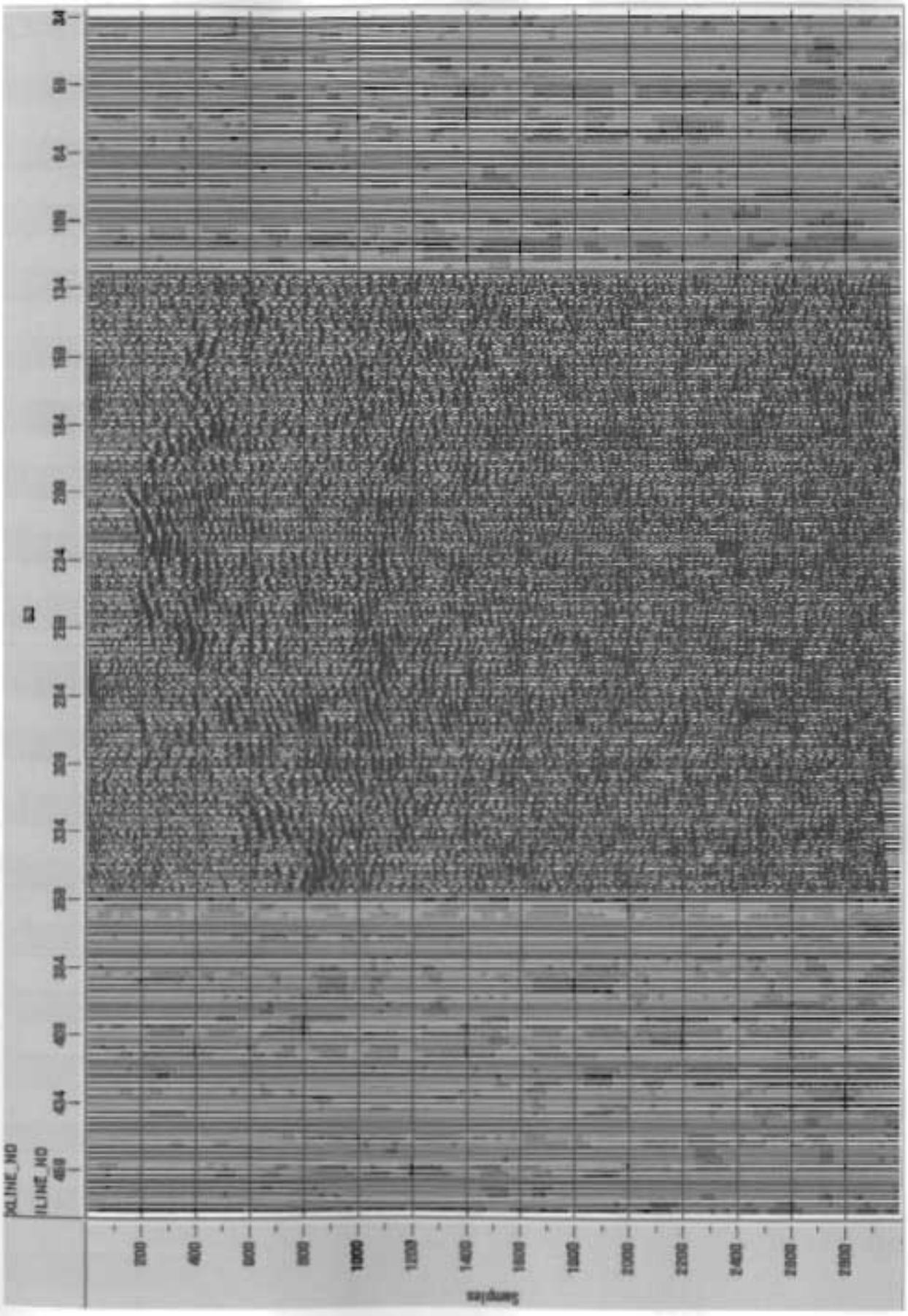
XLINE_NO
ILINE_NO
Samples

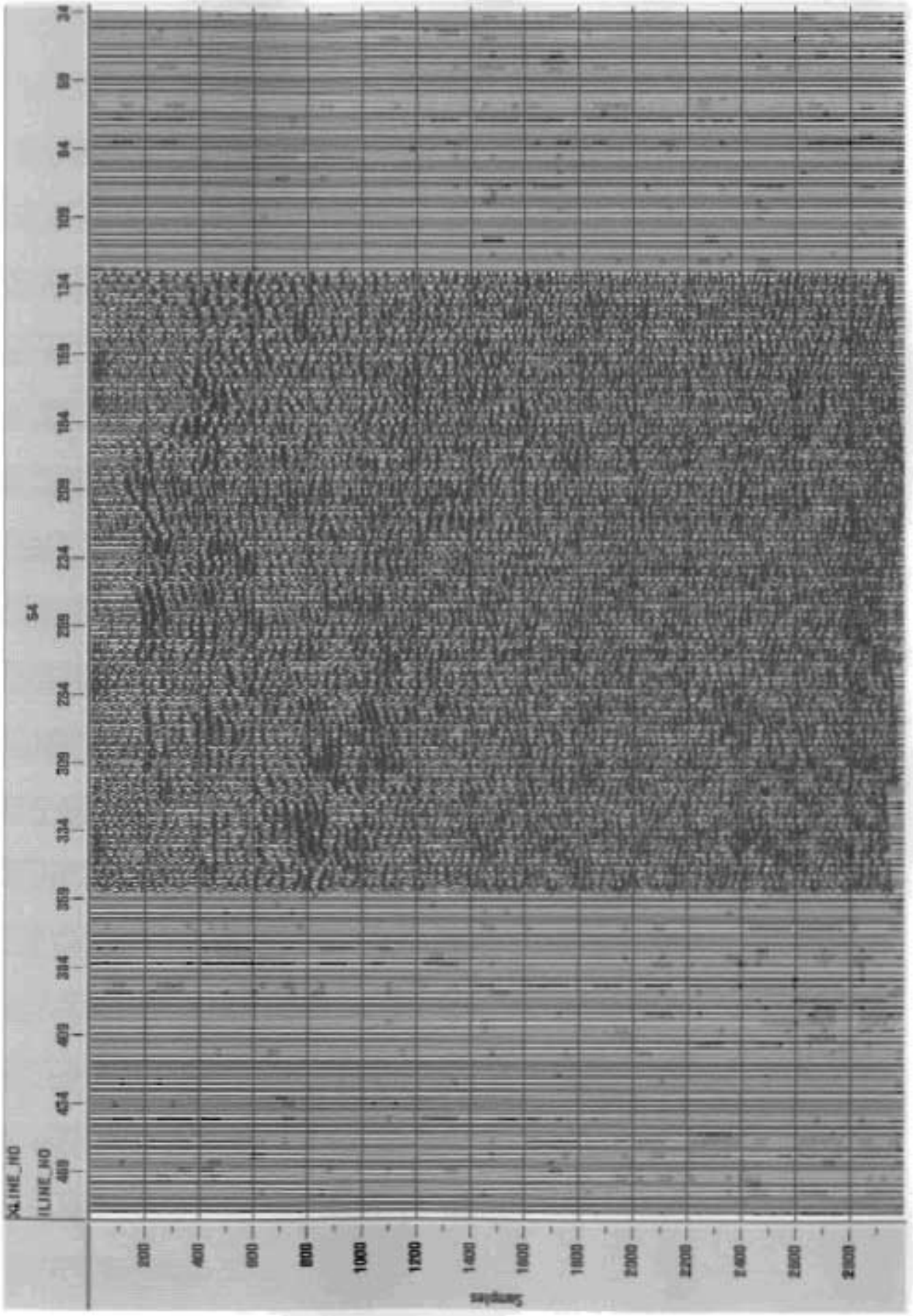
XLINE_NO
ILINE_NO
54
Samples

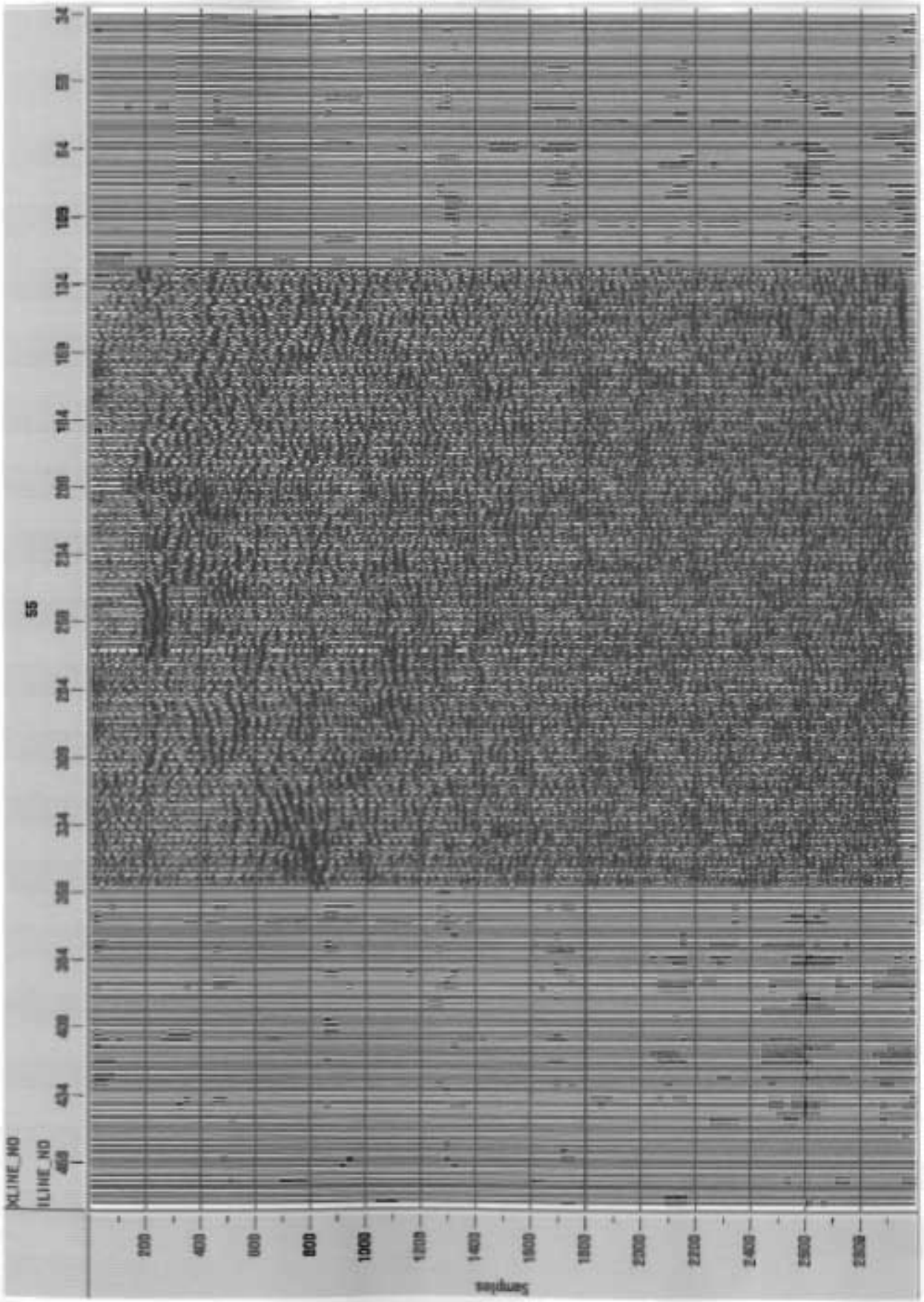
XLINE_NO
ILINE_NO
55
Samples

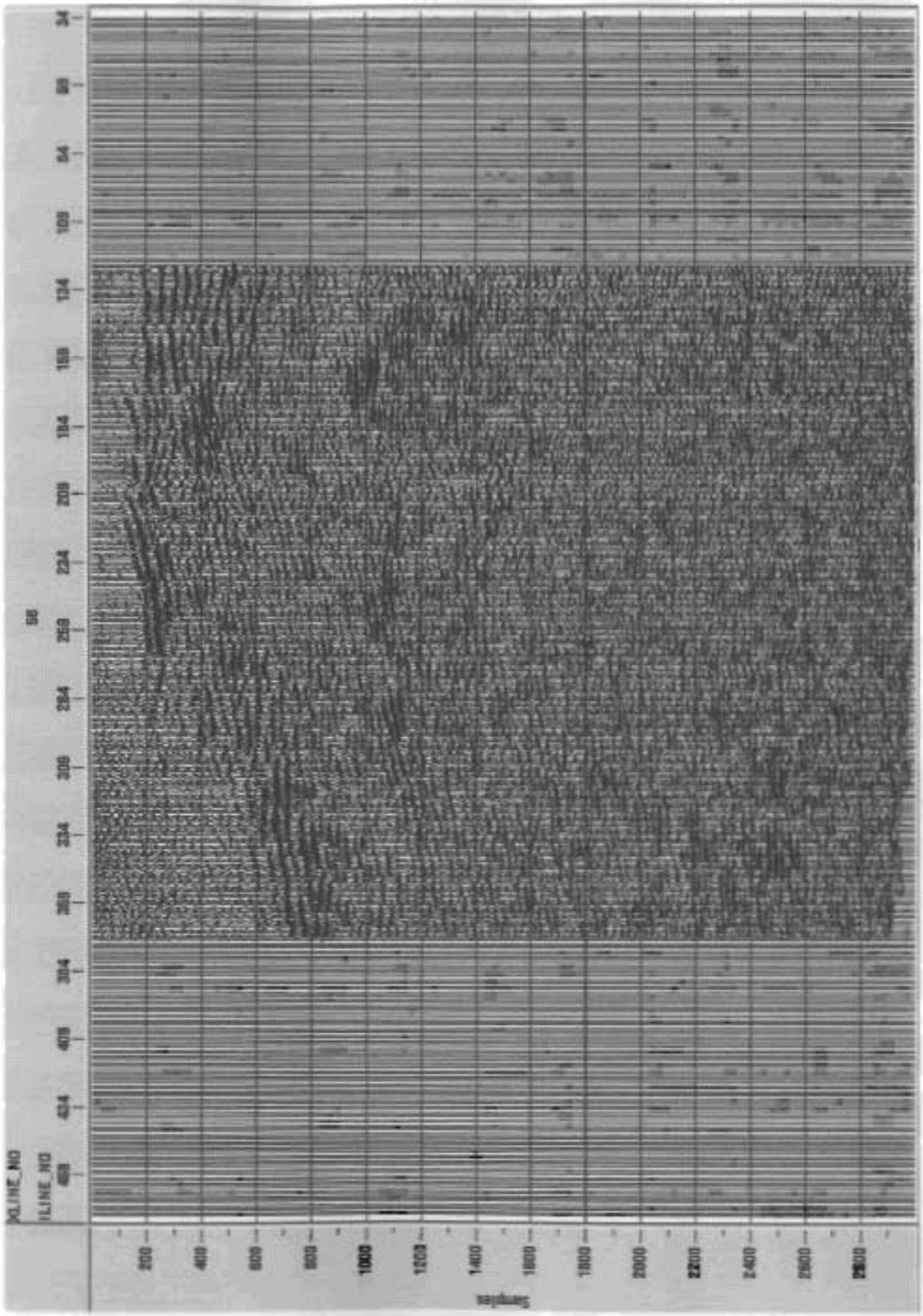
XLINE_NO
ILINE_NO
Sample

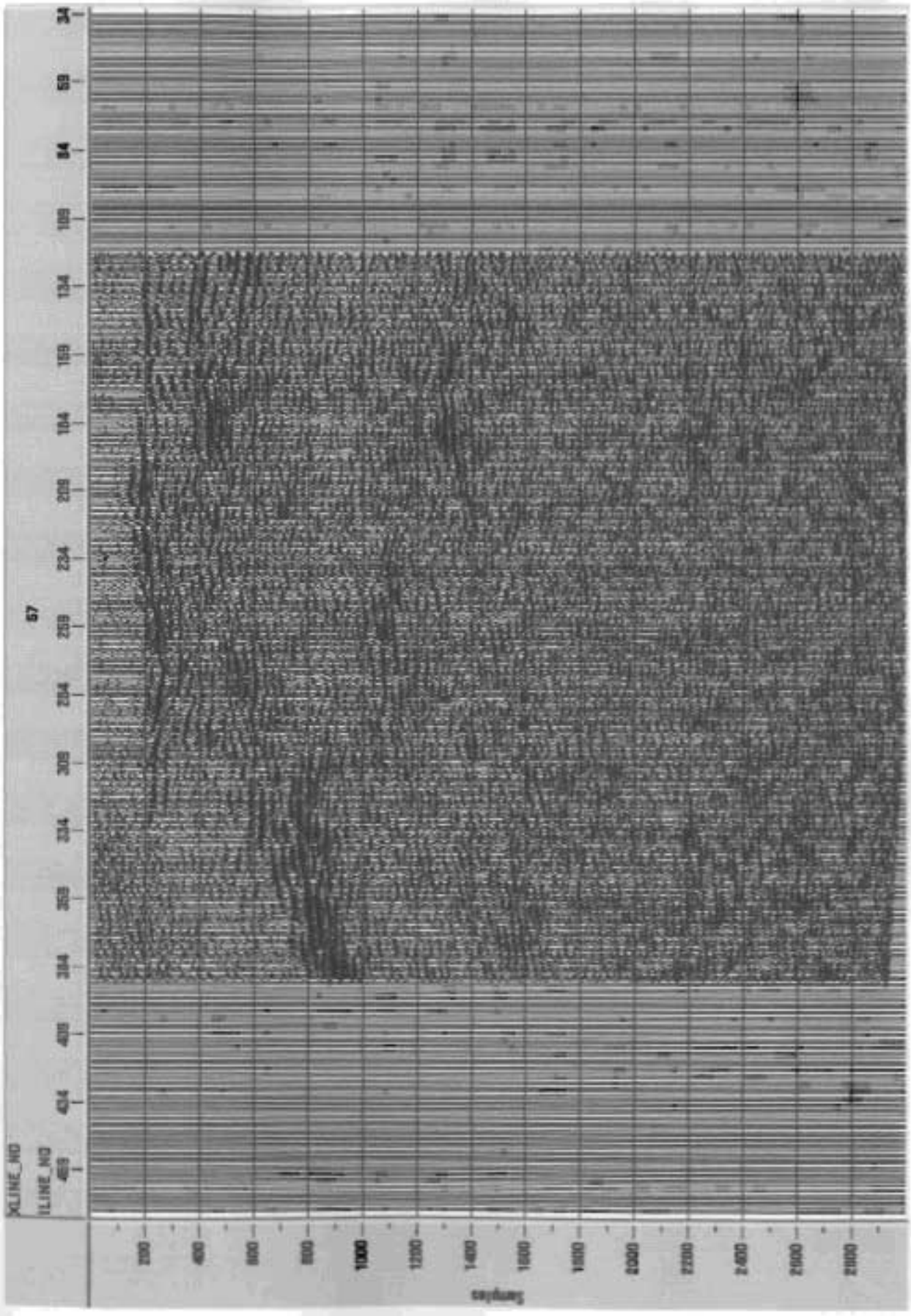
XLINE_NO
ILINE_NO
469
434
400
384
359
334
309
284
259
234
209
184
159
134
109
84
59
34
67
Samples
200
400
600
800
1000
1200
1400
1600
1800
2000
2200
2400
2600
2800

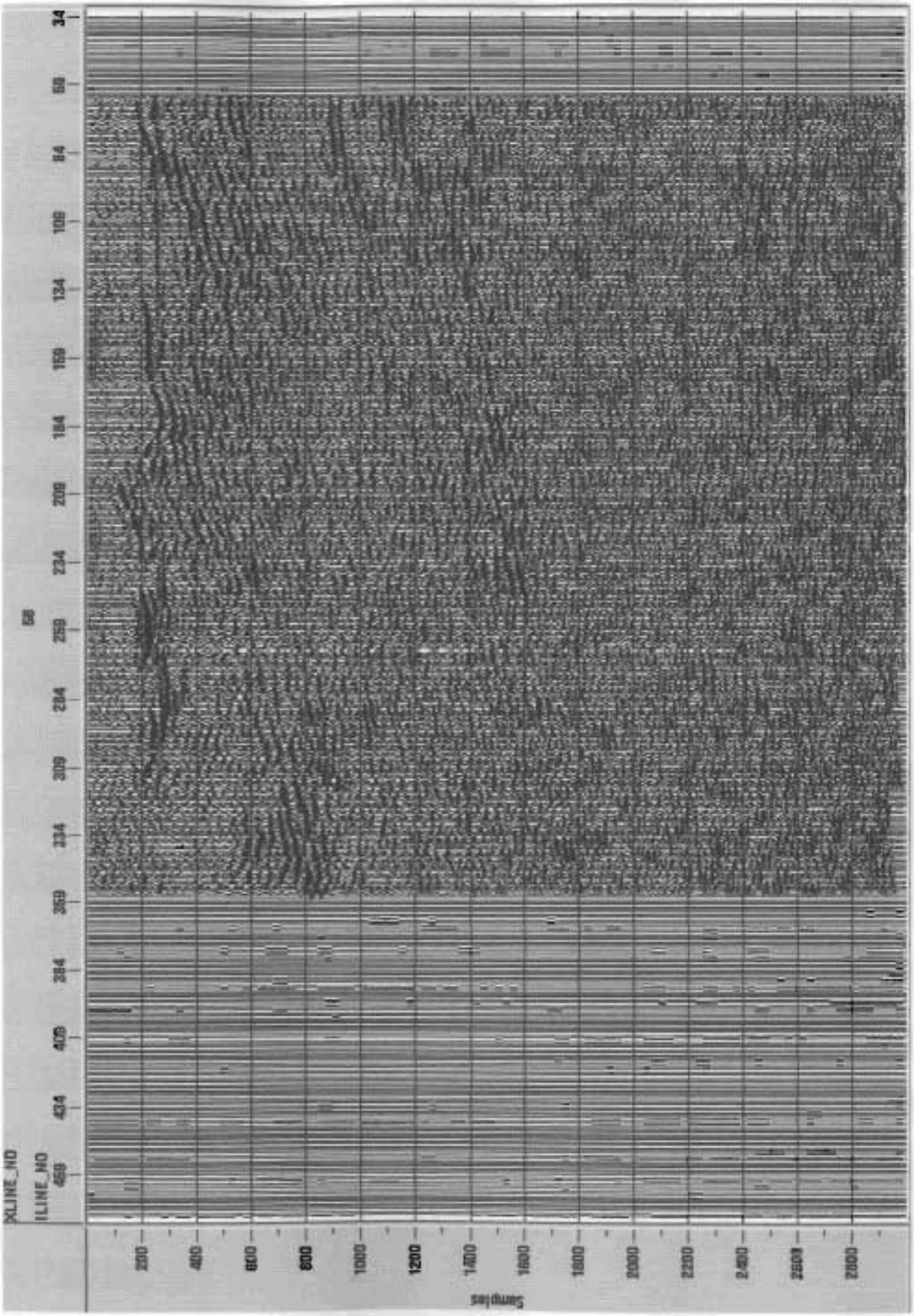
XLINE_NO
ILINE_NO
459
434
409
384
359
334
309
284
259
234
209
184
159
134
109
84
59
34
Samples
200
400
600
800
1000
1200
1400
1600
1800
2000
2200
2400
2600
2800

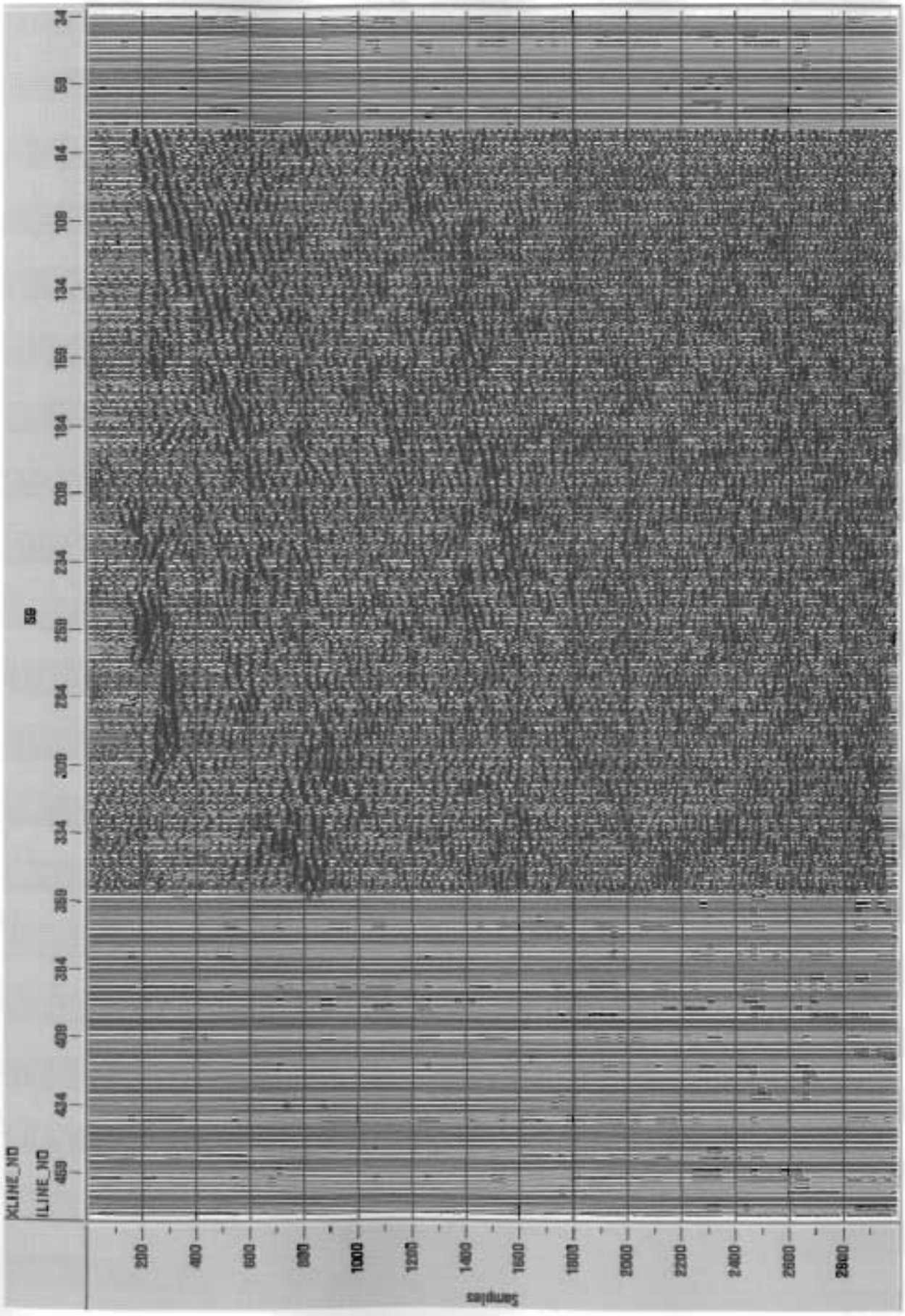
XLINE_NO
ILINE_NO
Samples

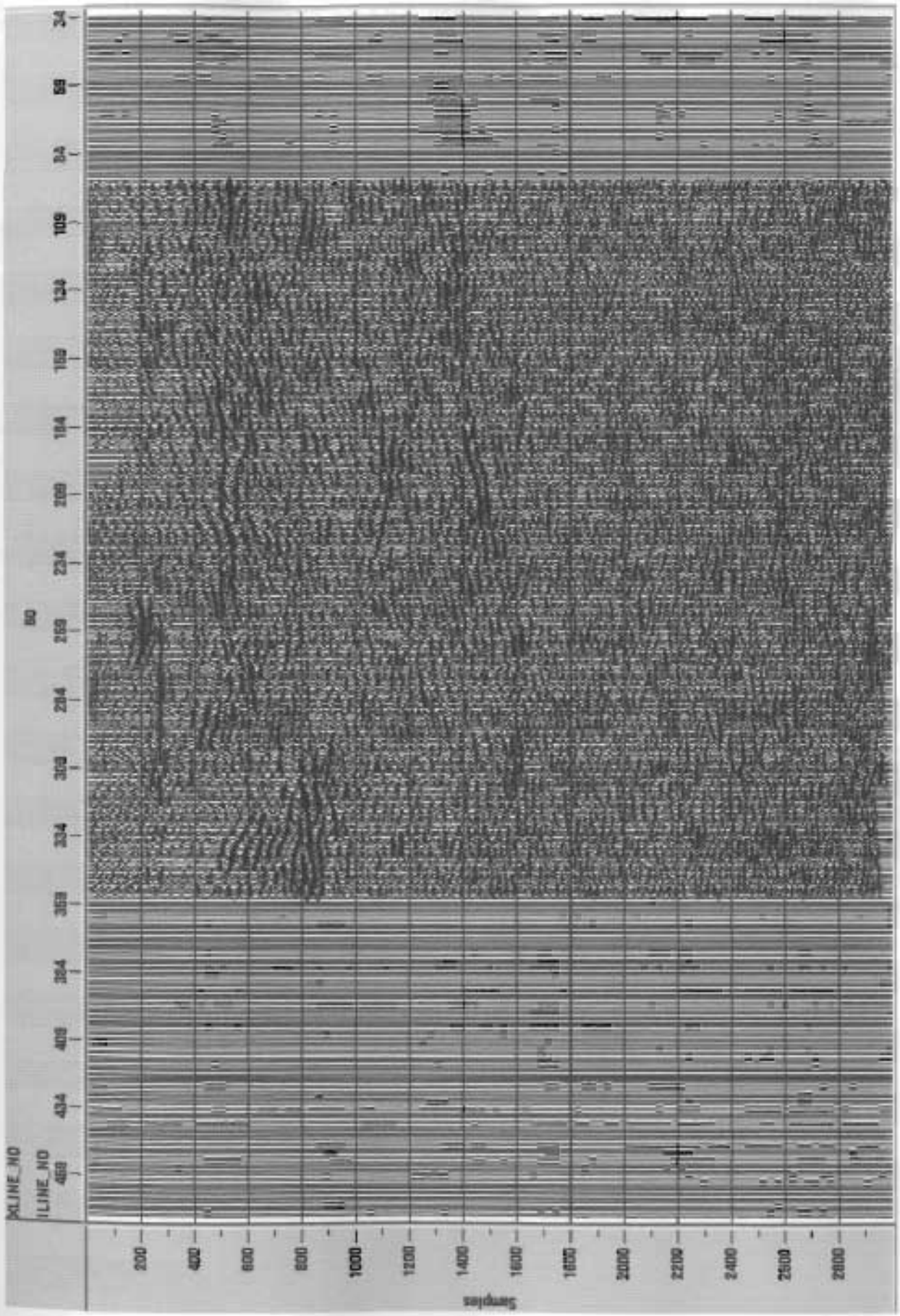
XLINE_NO
ILINE_NO
459
434
409
384
359
334
309
284
259
234
209
184
159
134
109
84
59
34
50
Samples
200
400
600
800
1000
1200
1400
1600
1800
2000
2200
2400
2600

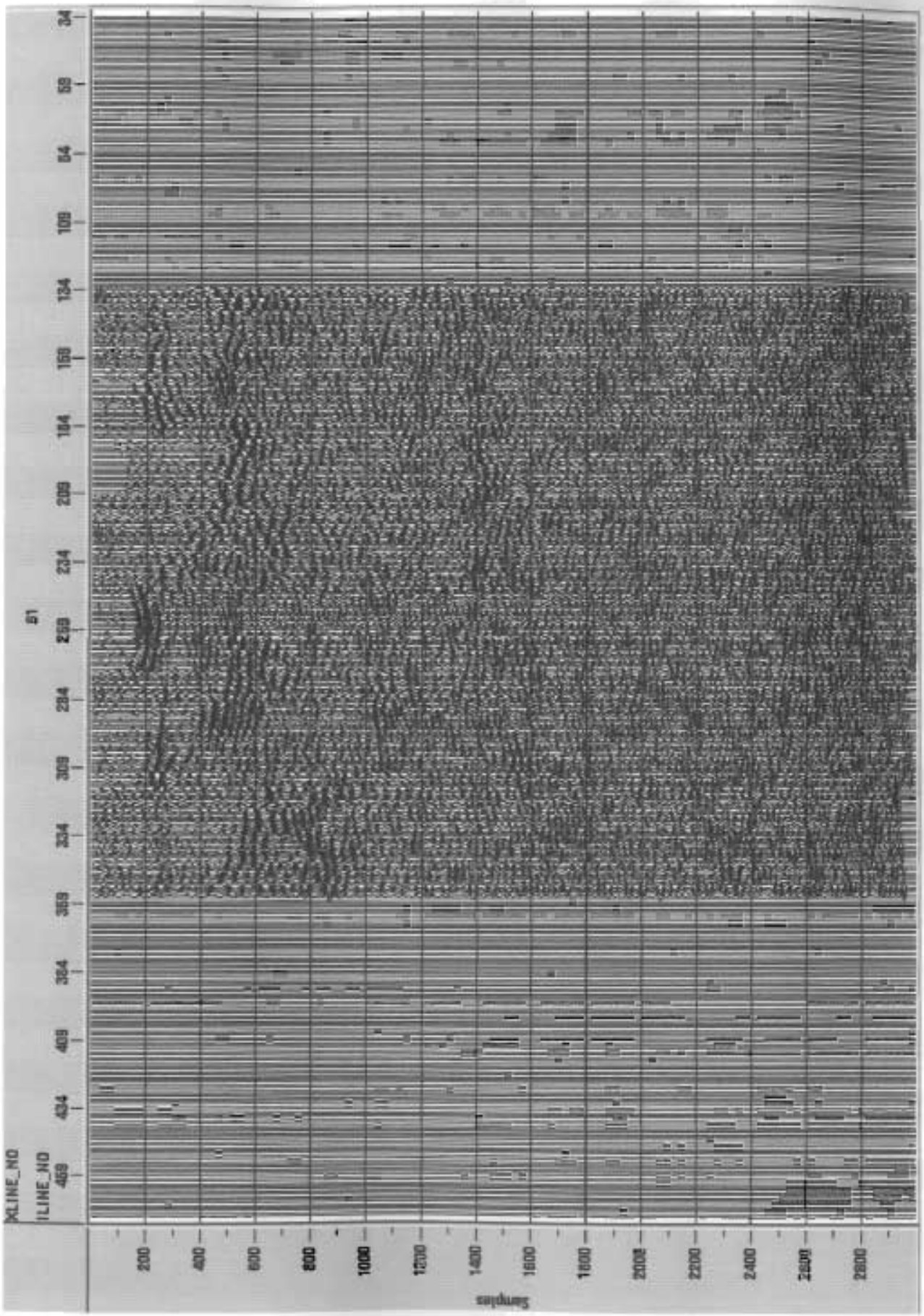
XLINE_NO
ILINE_NO
459
434
409
384
359
334
309
284
259
234
209
184
159
134
109
84
59
34
61
samples
200
400
600
800
1000
1200
1400
1600
1800
2000
2200
2400
2600

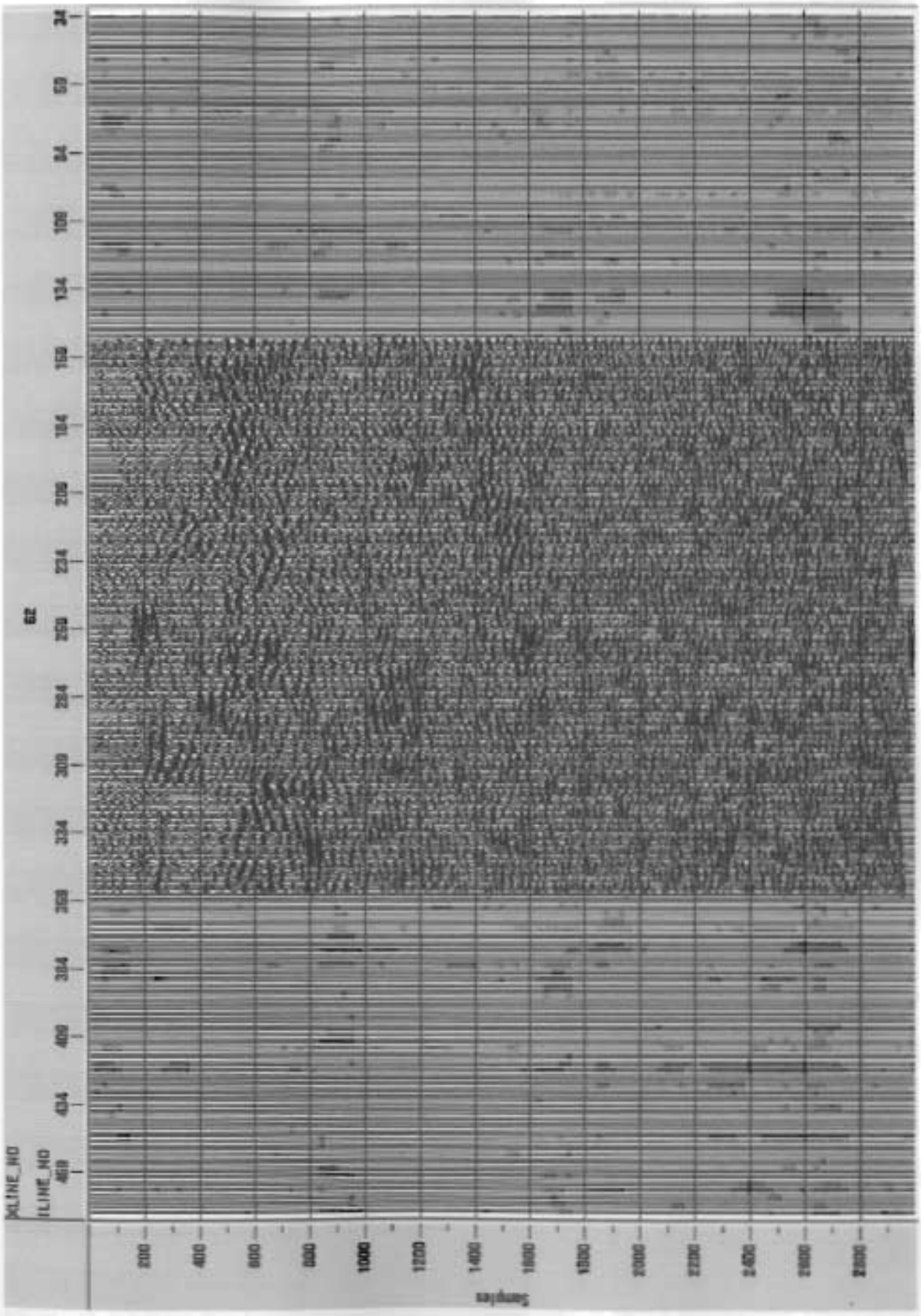
XLINE_NO
ILINE_NO
469
434
409
384
359
334
309
284
259
234
209
184
159
134
109
84
59
34
Samples
200
400
600
800
1000
1200
1400
1600
1800
2000
2200
2400
2600
2800

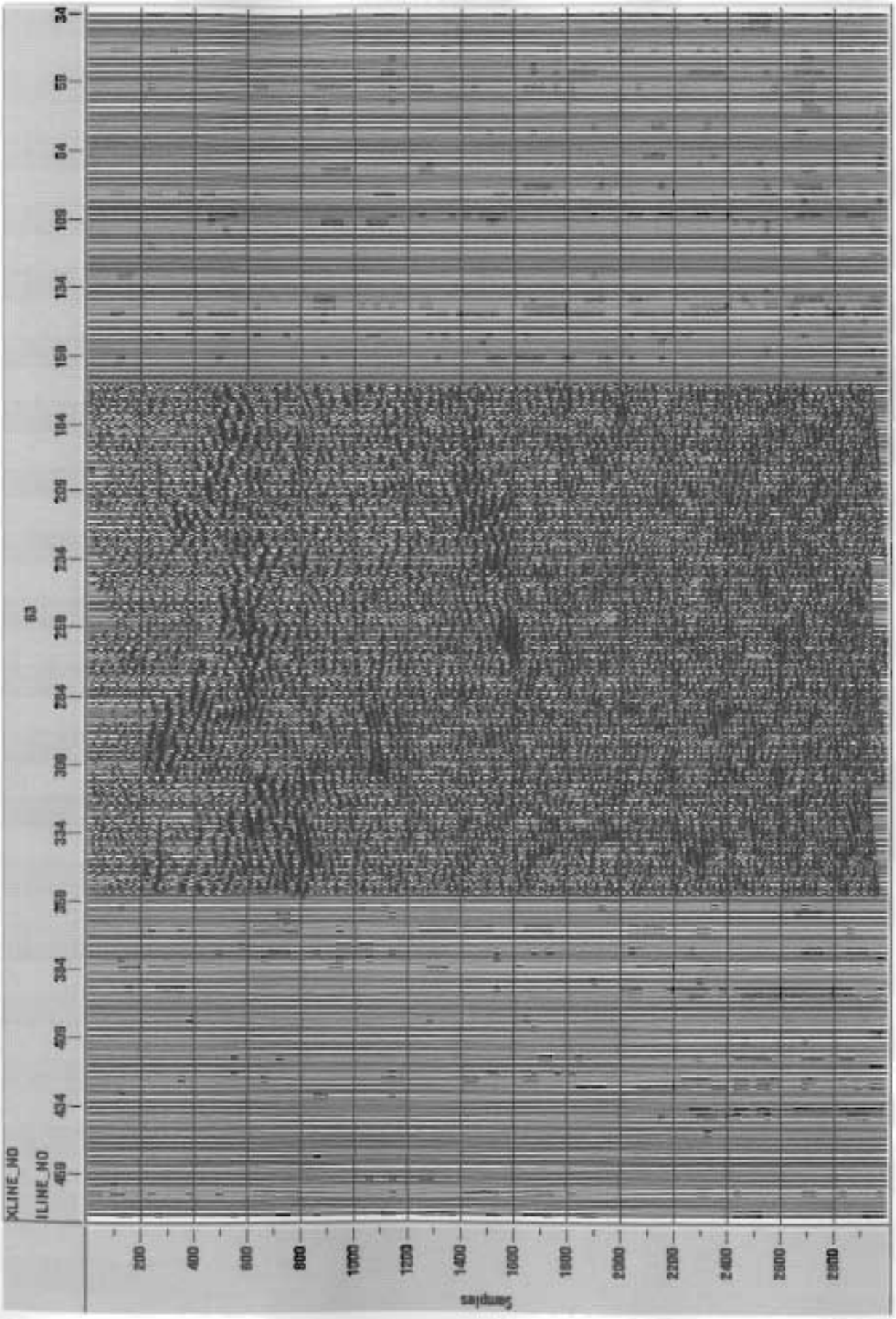
XLINE_NO
ILINE_NO
Samples

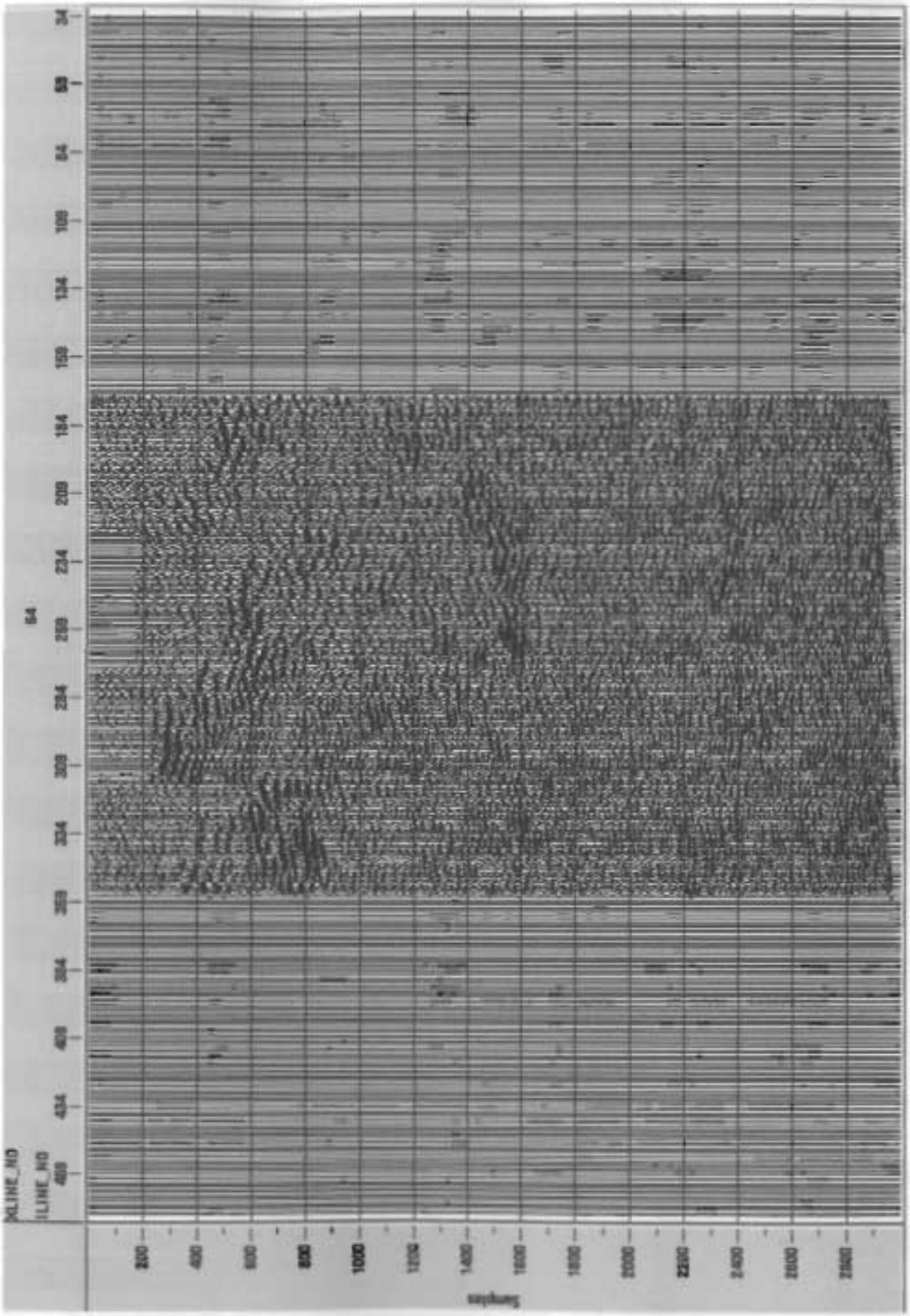
XLINE_NO
ILINE_NO
54
Samples

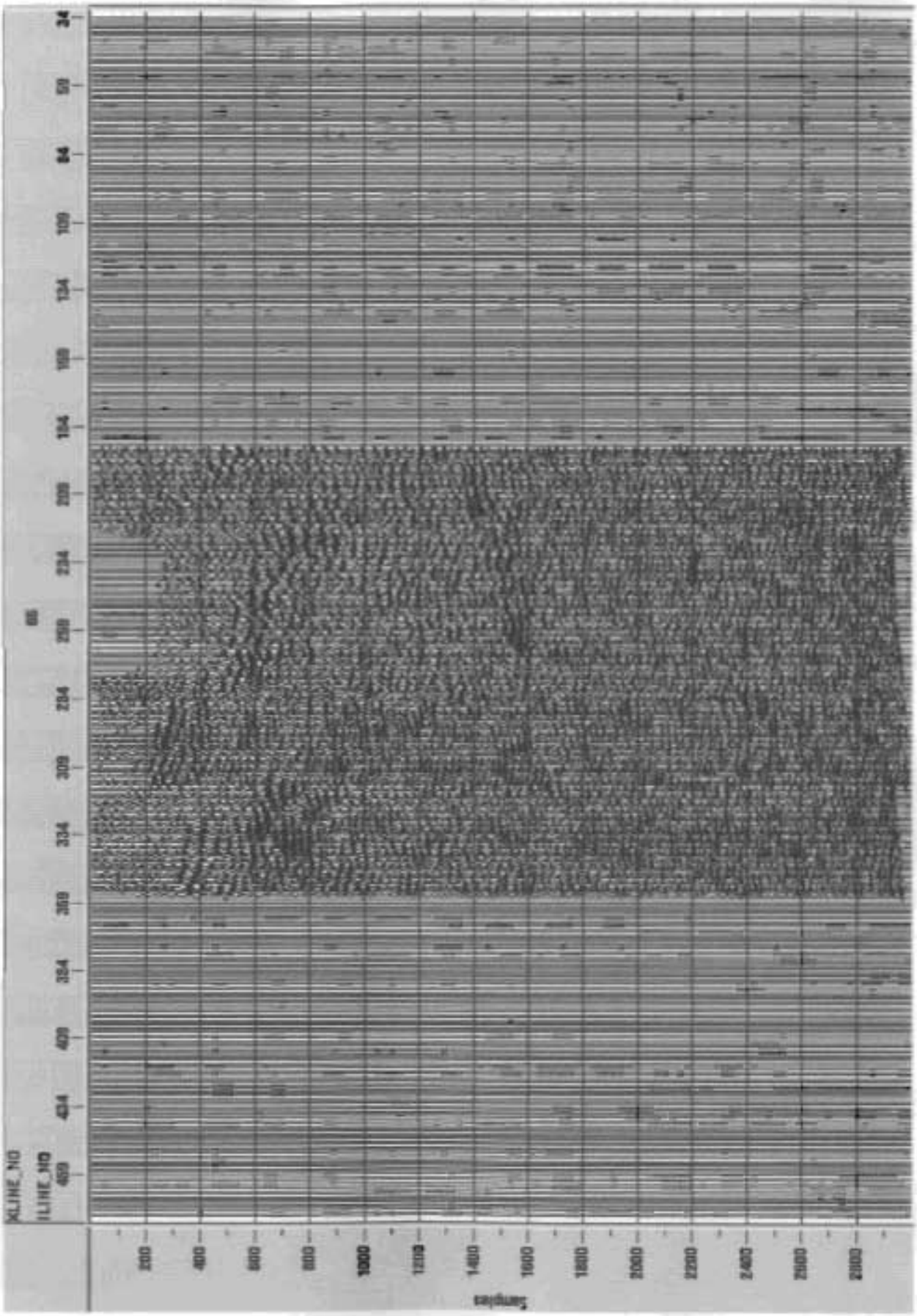
XLINE_NO
ILINE_NO
Samples

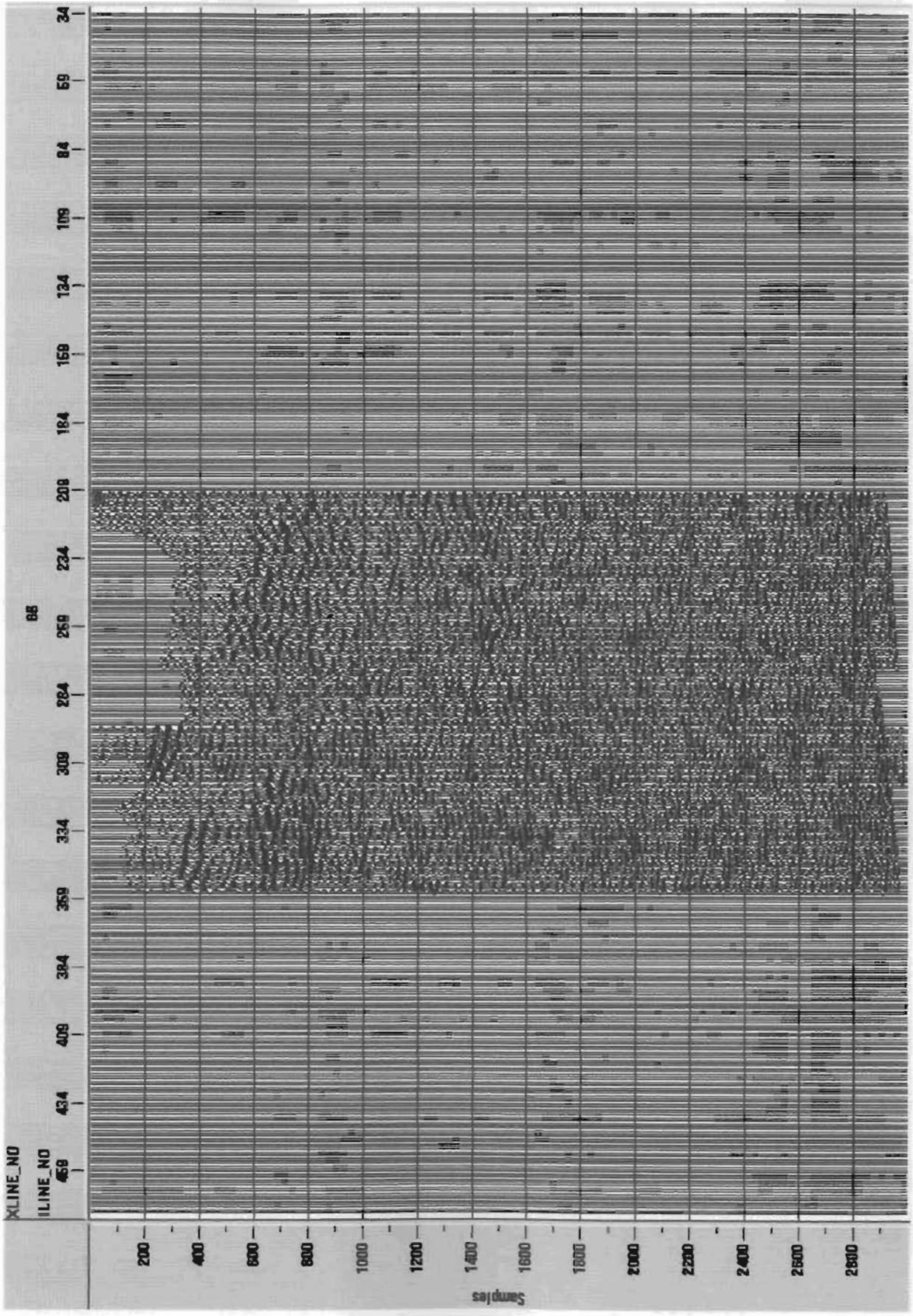
XLINE_NO
ILINE_NO
Samples

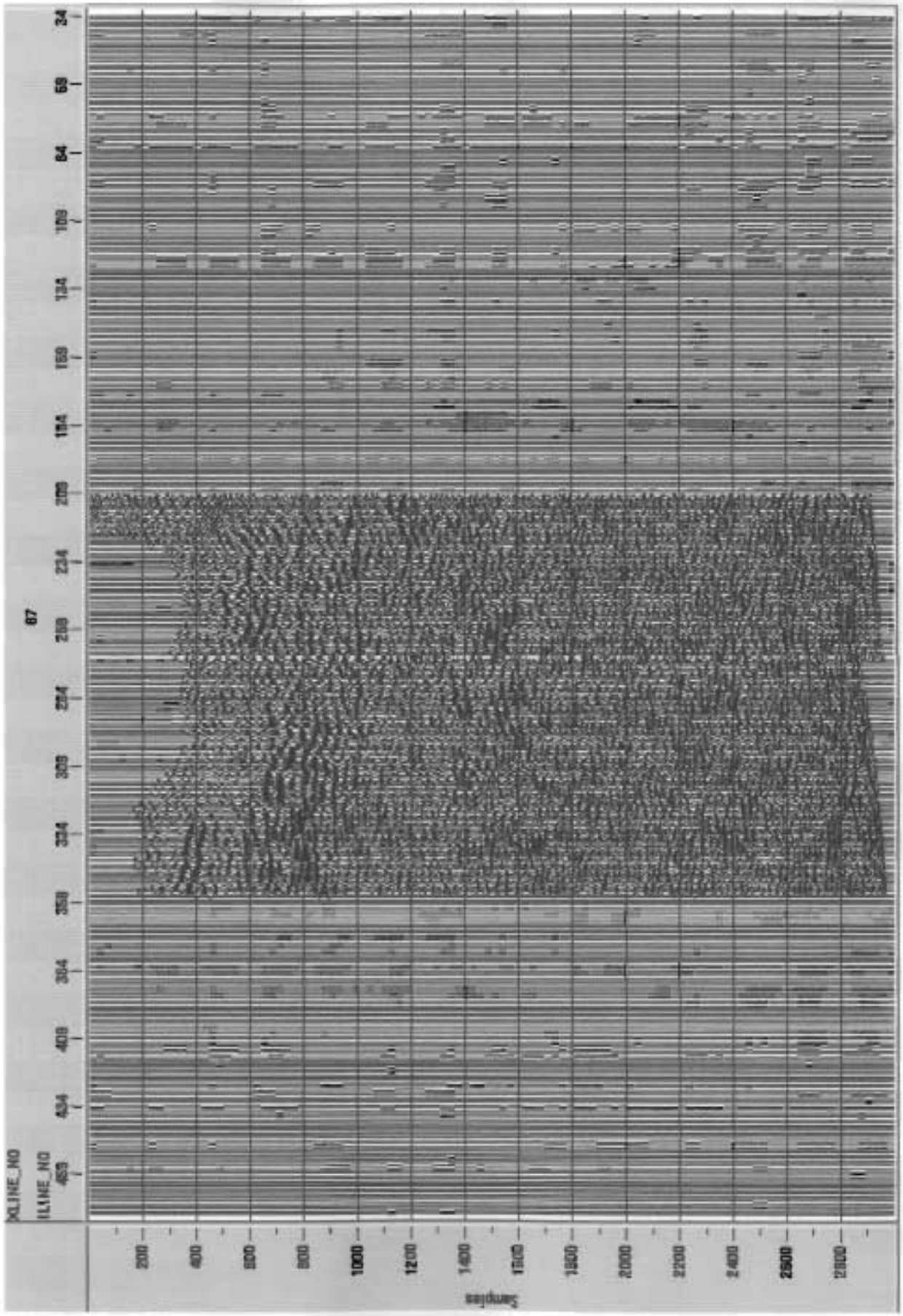
XLINE_NO
ILINE_NO
459
434
409
384
359
334
309
284
259
234
209
184
159
134
109
84
59
34
87
Samples
200
400
600
800
1000
1200
1400
1600
1800
2000
2200
2400
2600
2800

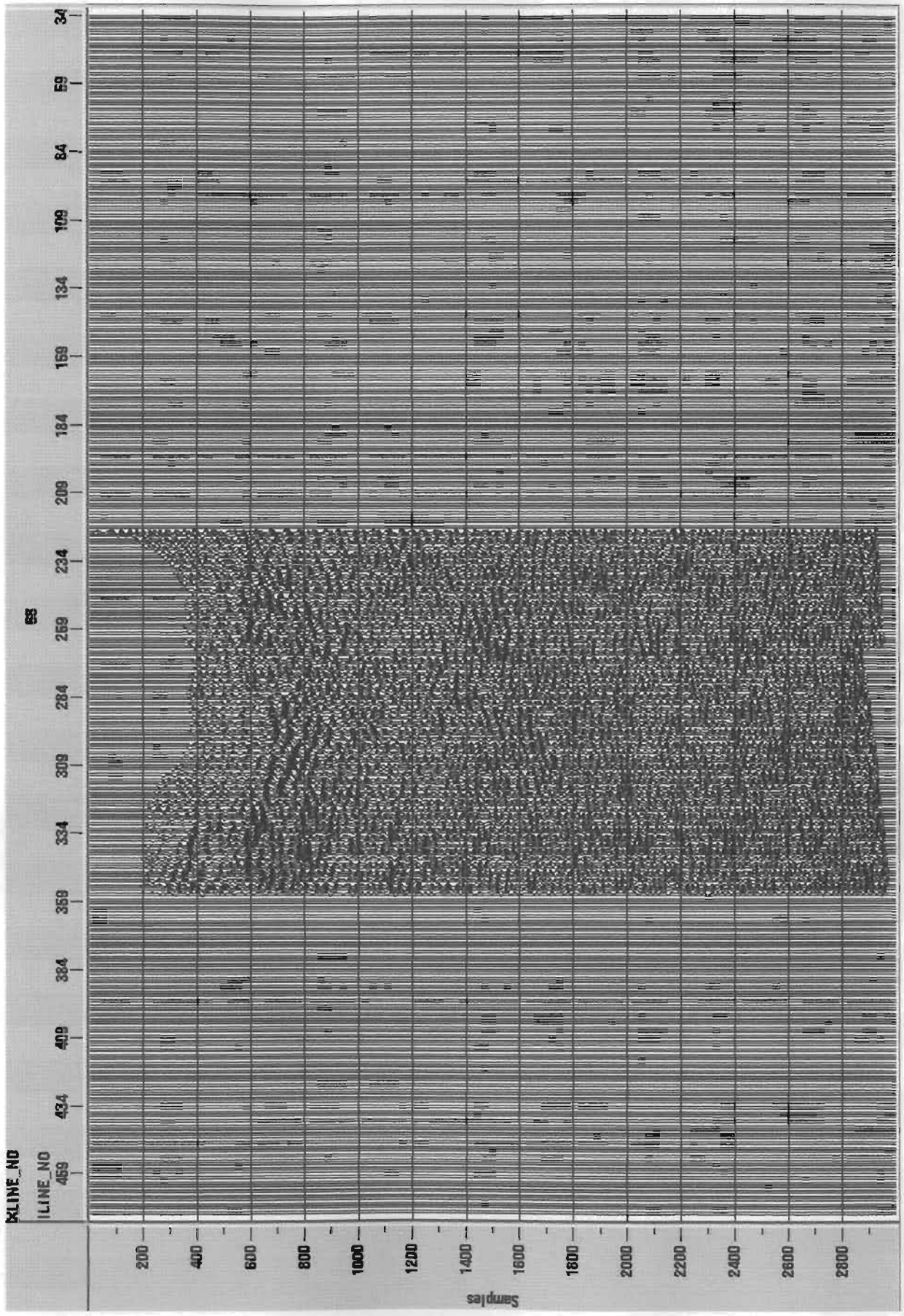
XLINE_NO
ILINE_NO
Samples

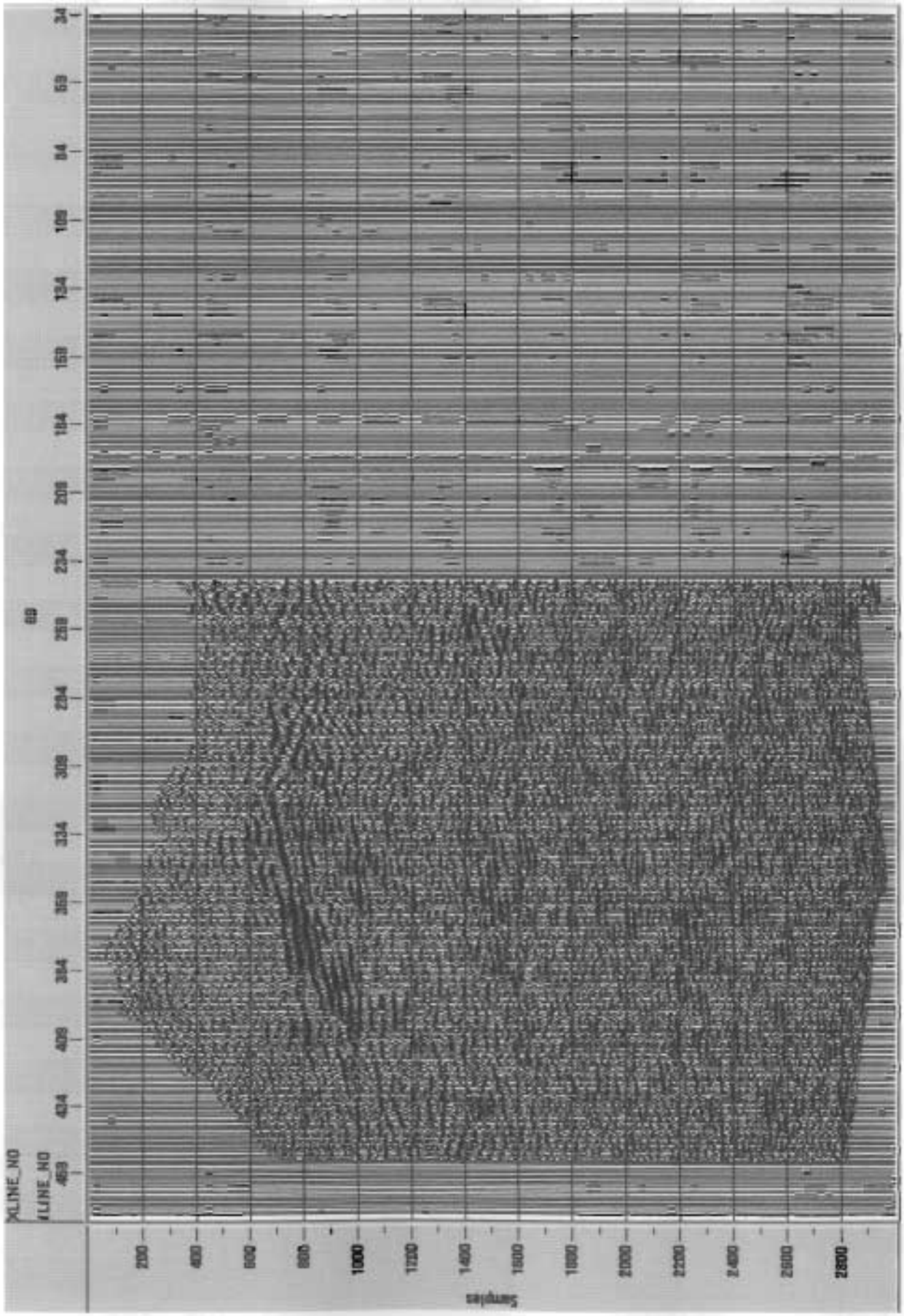
XLINE_NO
ILINE_NO
459
434
409
384
359
334
309
284
259
234
209
184
159
134
109
84
59
34
Samples
200
400
600
800
1000
1200
1400
1600
1800
2000
2200
2400
2600

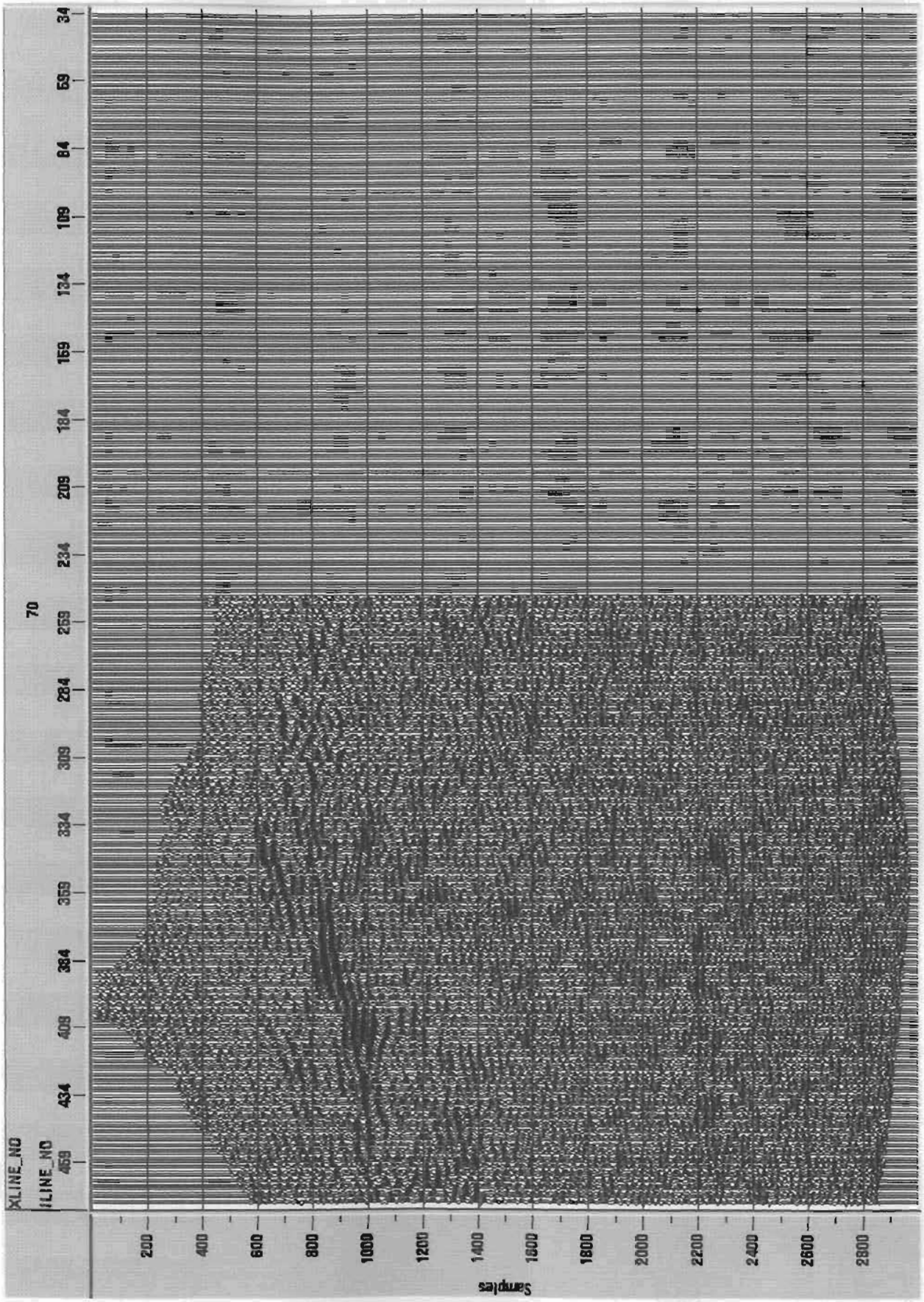
XLINE_NO
ILINE_NO
459
434
409
384
359
334
309
284
259
234
209
184
159
134
109
84
59
34
70
Samples
200
400
600
800
1000
1200
1400
1600
1800
2000
2200
2400
2600
2800

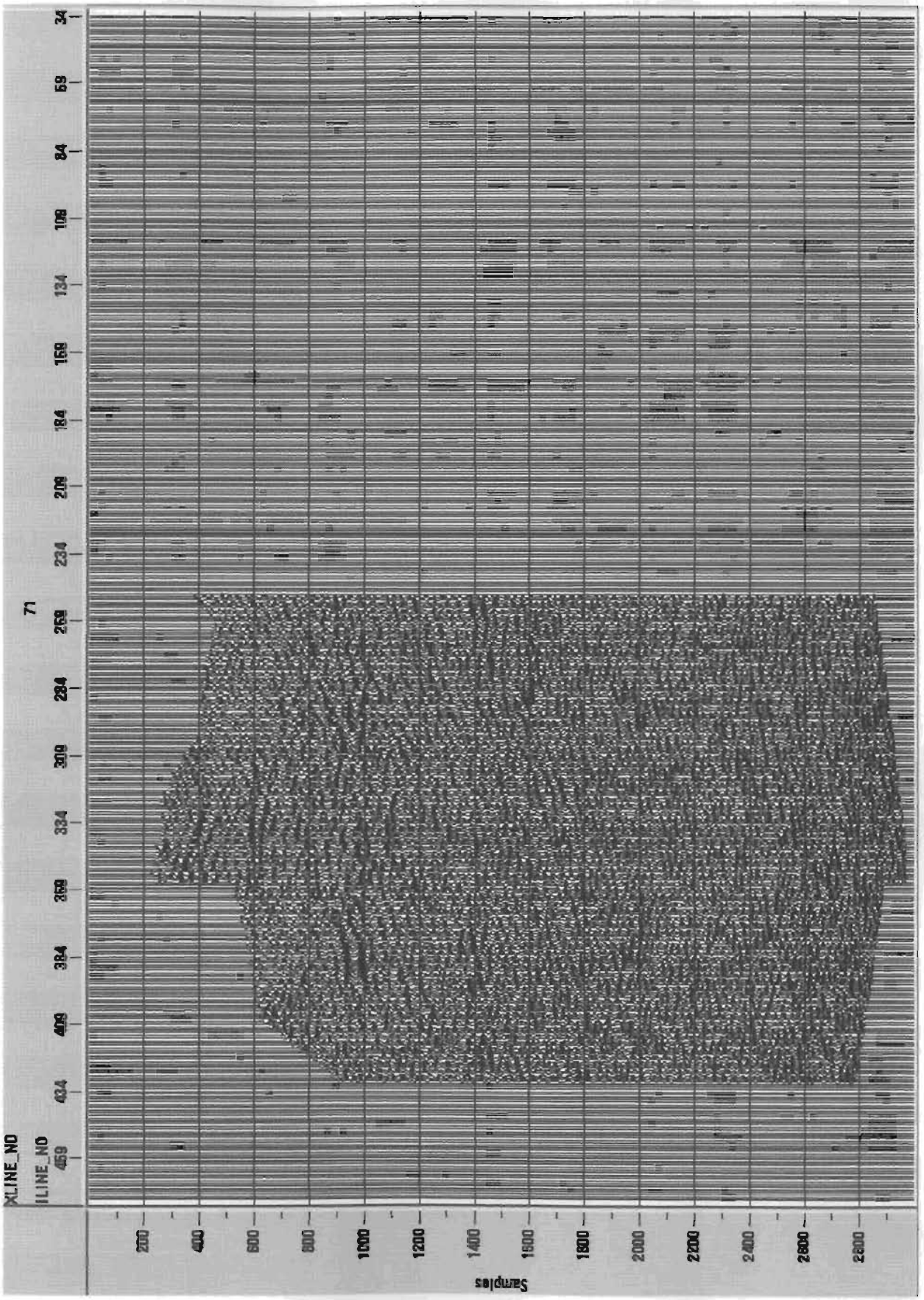
XLINE_NO
ILINE_NO
459
434
409
384
359
334
309
284
259
234
209
184
159
134
109
84
59
34
71
Samples
200
400
600
800
1000
1200
1400
1600
1800
2000
2200
2400
2600
2800

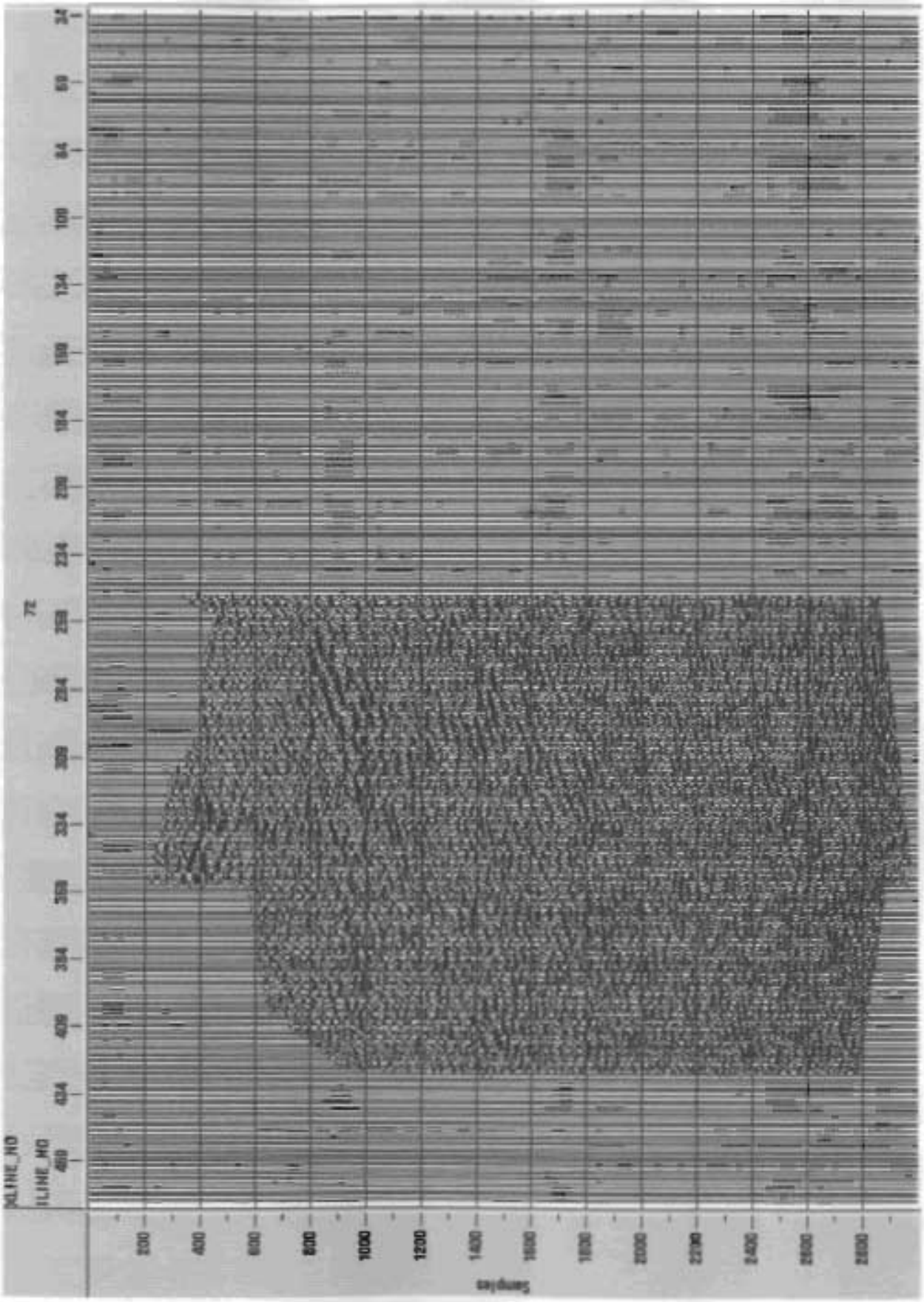
XLINE_NO
ILINE_NO
TIME
Samples

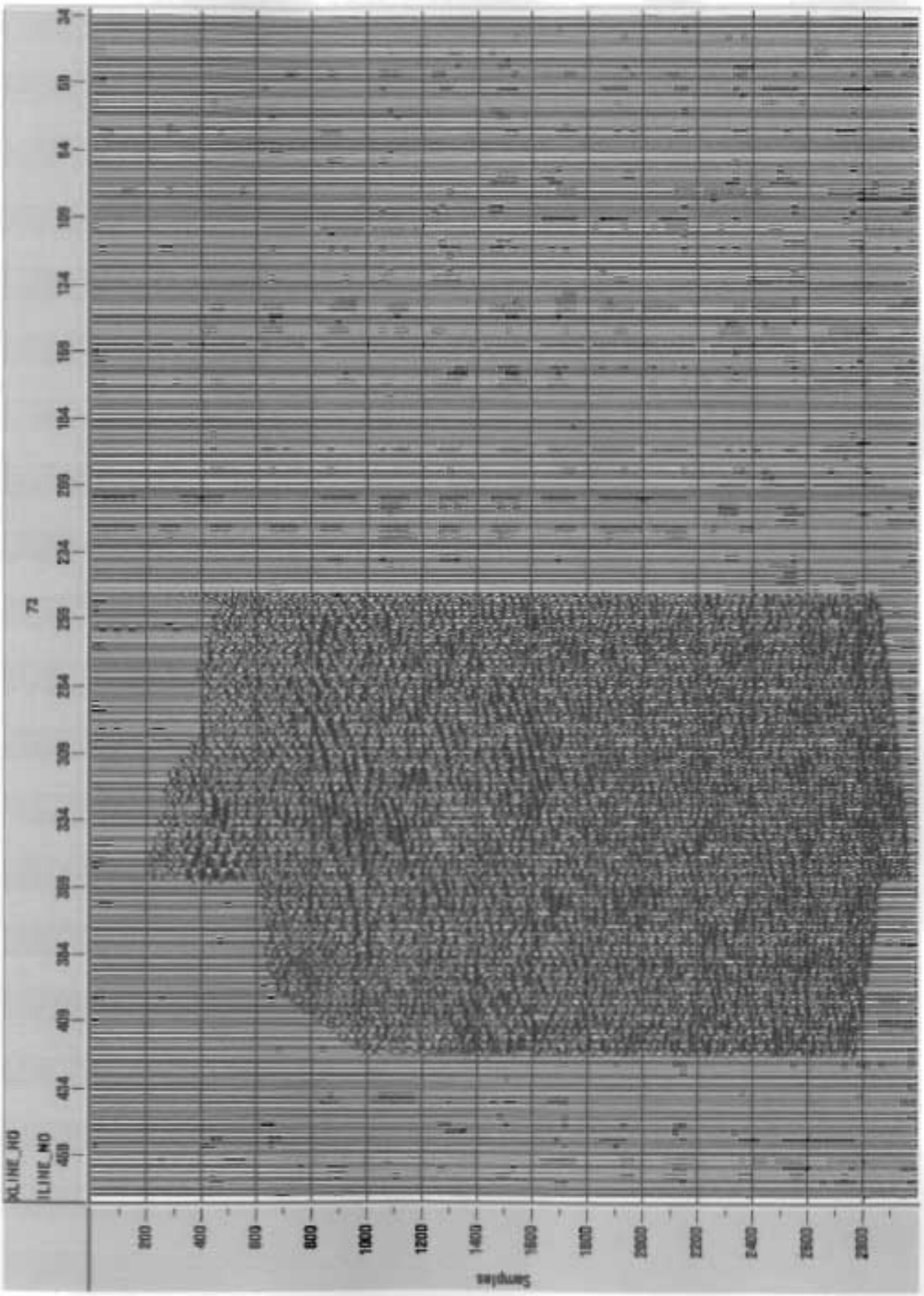
XLINE_NO
ILINE_NO
73
Samples

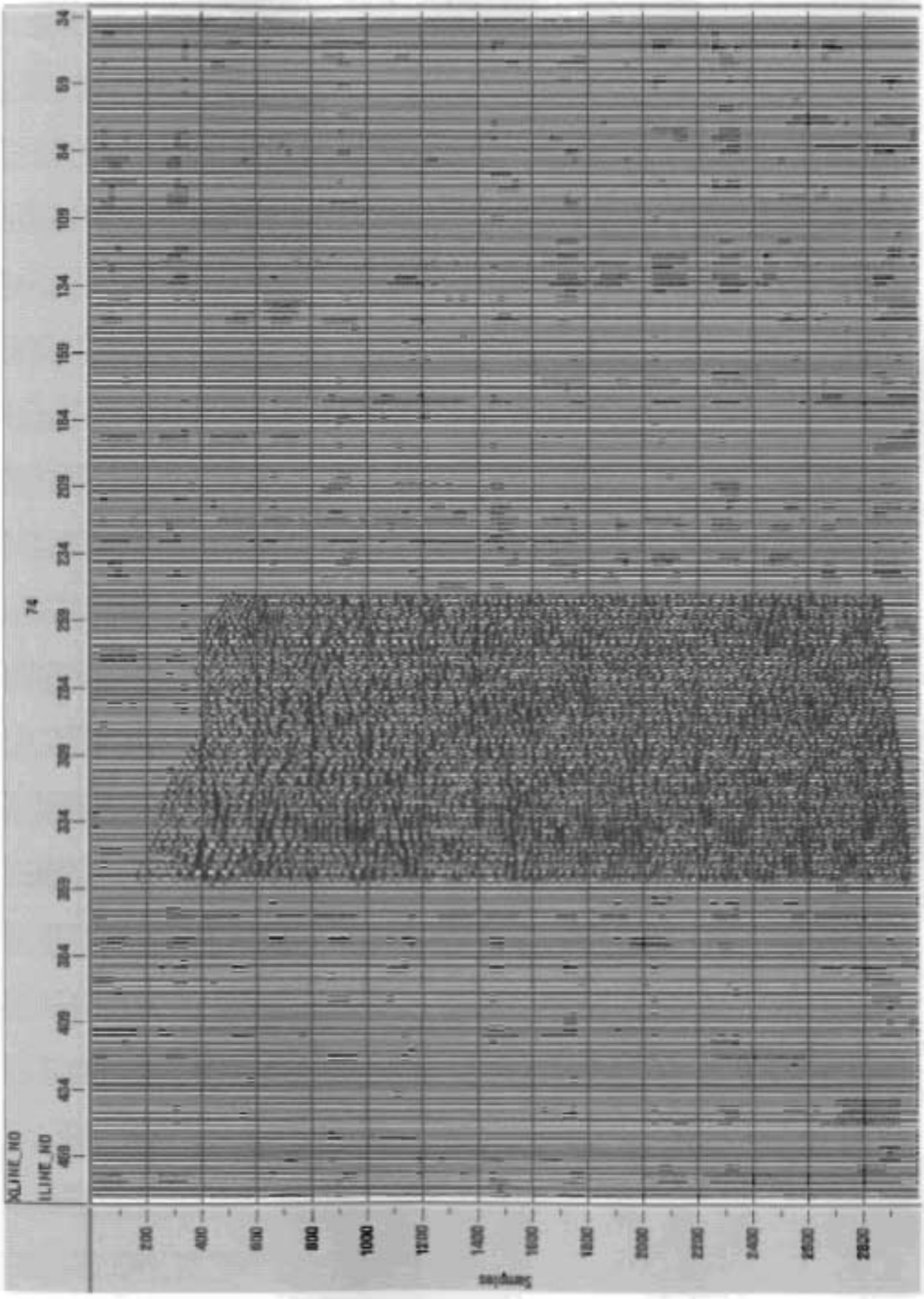
XLINE_NO
ILINE_NO
74
Samples

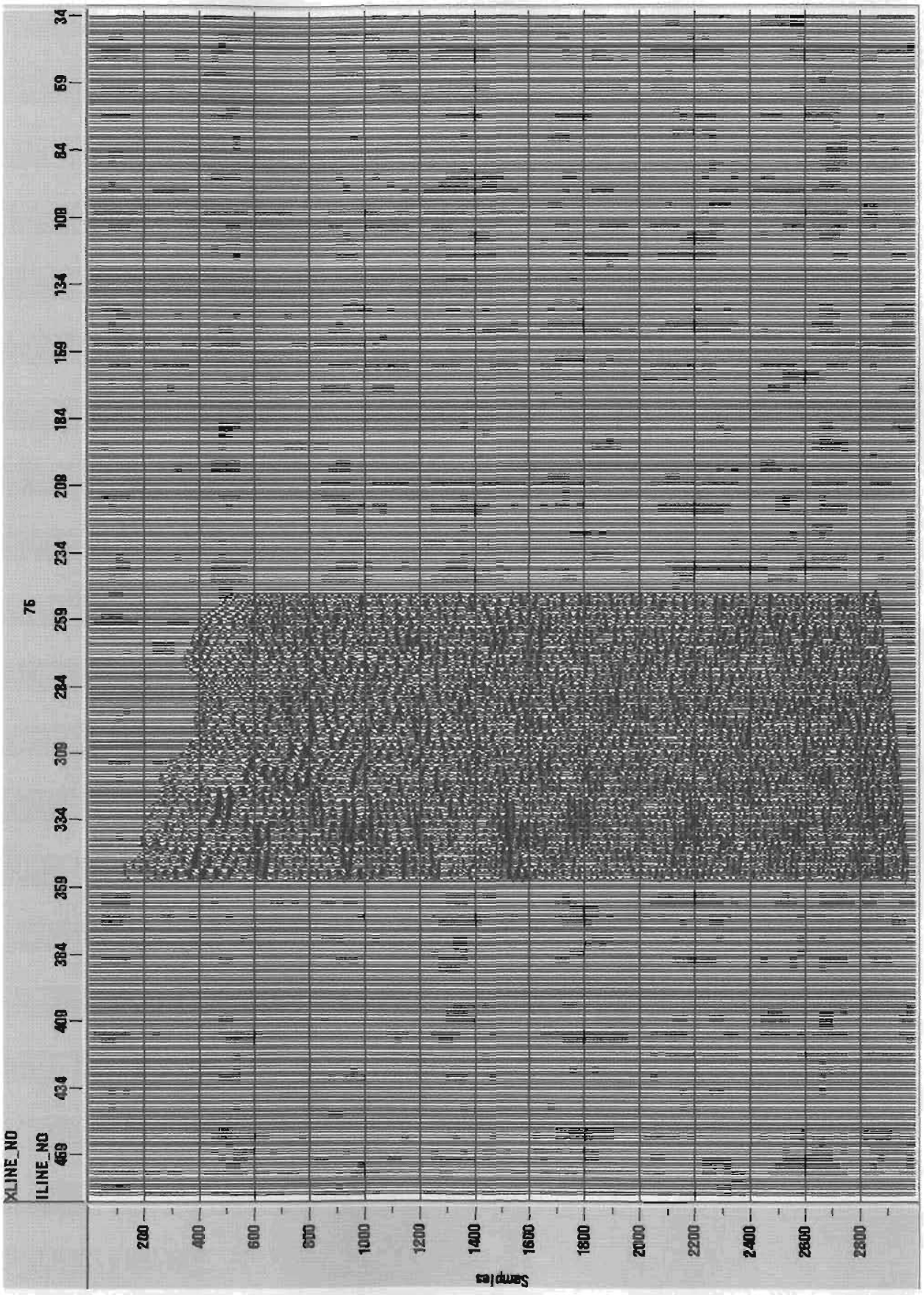
XLINE_NO
ILINE_NO
469
434
409
384
359
334
309
284
259
234
208
184
159
134
108
84
59
34
76
Samples
200
400
600
800
1000
1200
1400
1600
1800
2000
2200
2400
2600
2800

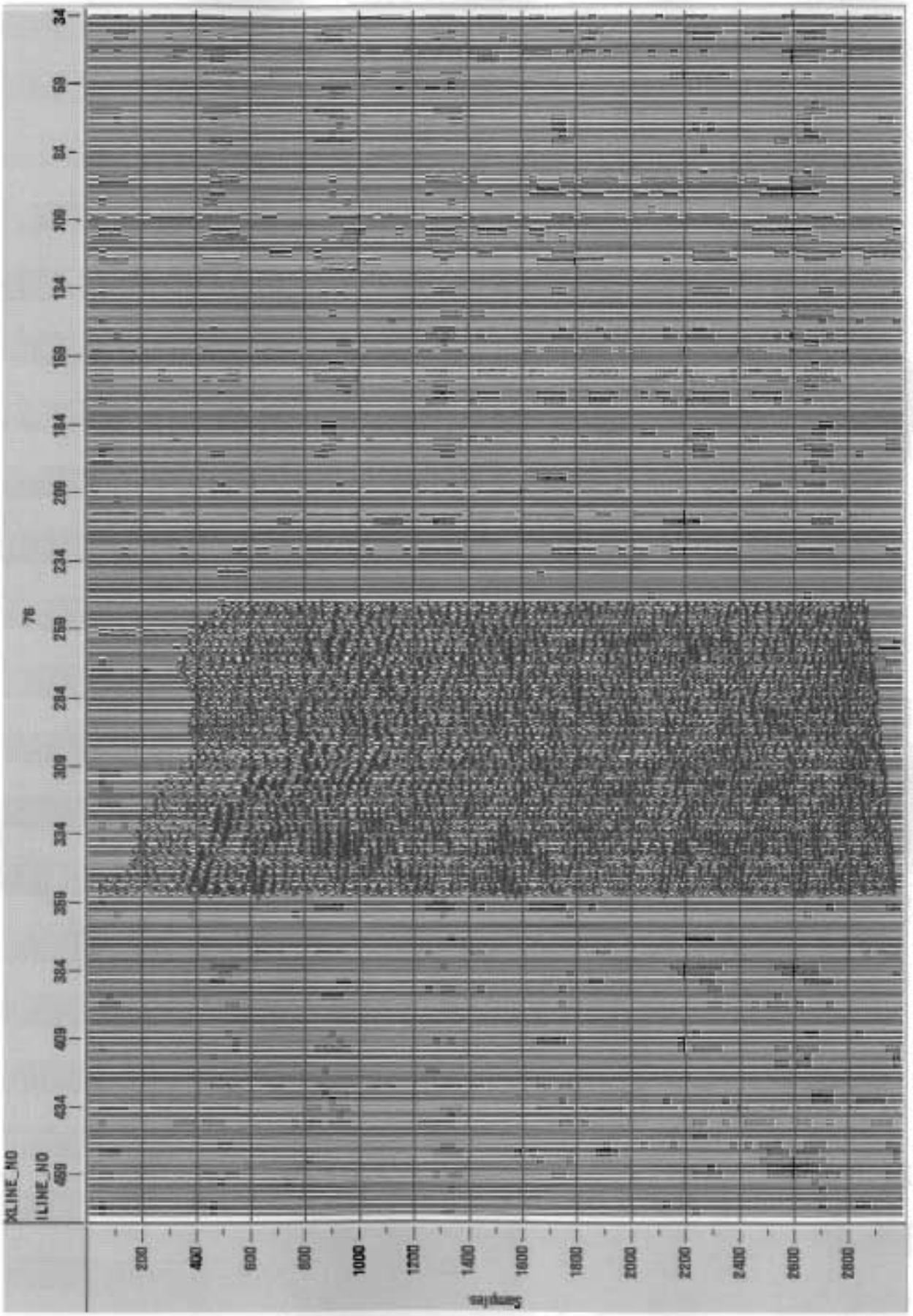
XLINE_NO
ILINE_NO
78
34
59
84
109
134
159
184
209
234
259
284
309
334
359
384
409
434
459
200
400
600
800
1000
1200
1400
1600
1800
2000
2200
2400
2600
2800
Sample

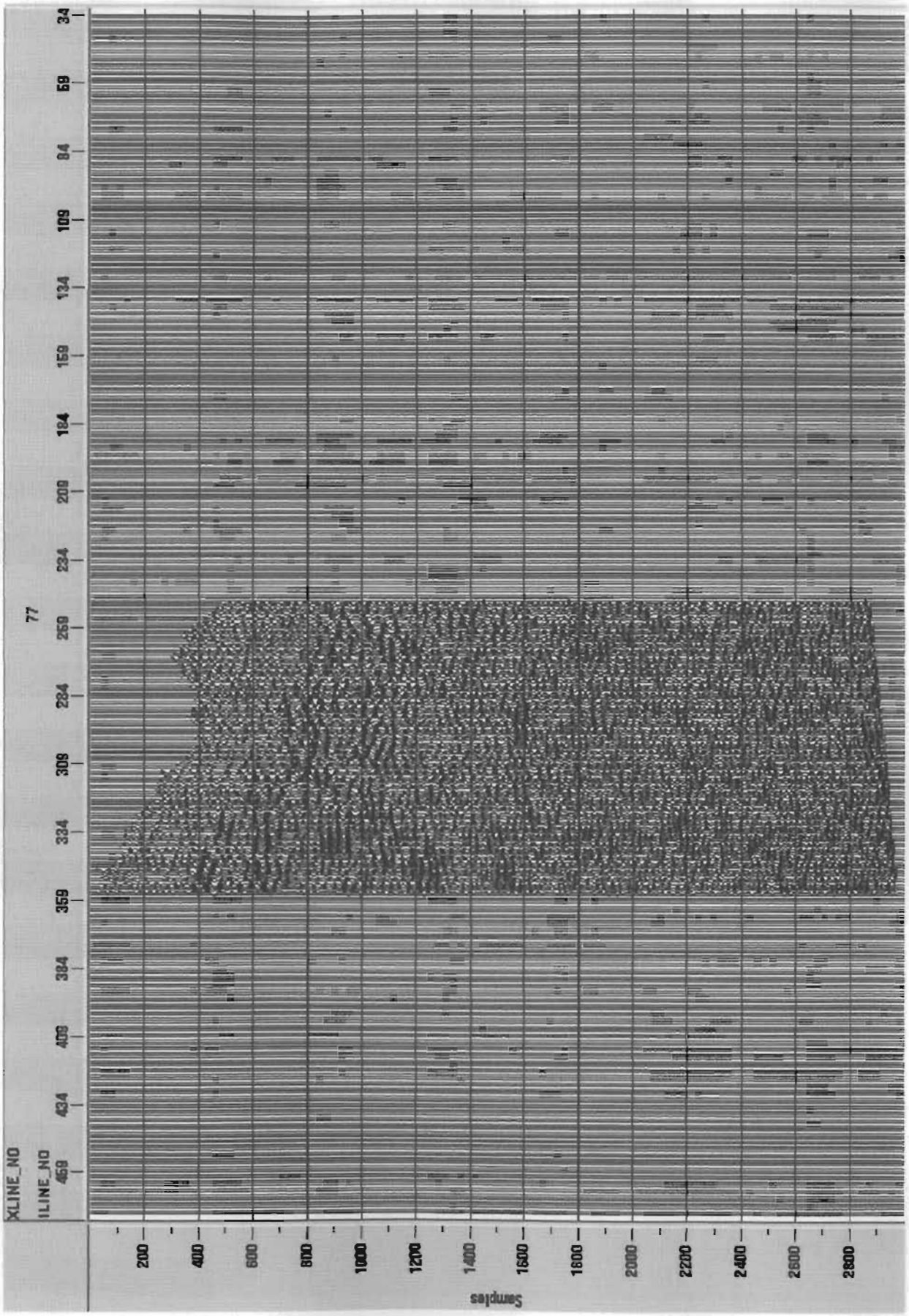
XLINE_NO
ILINE_NO
77
Samples

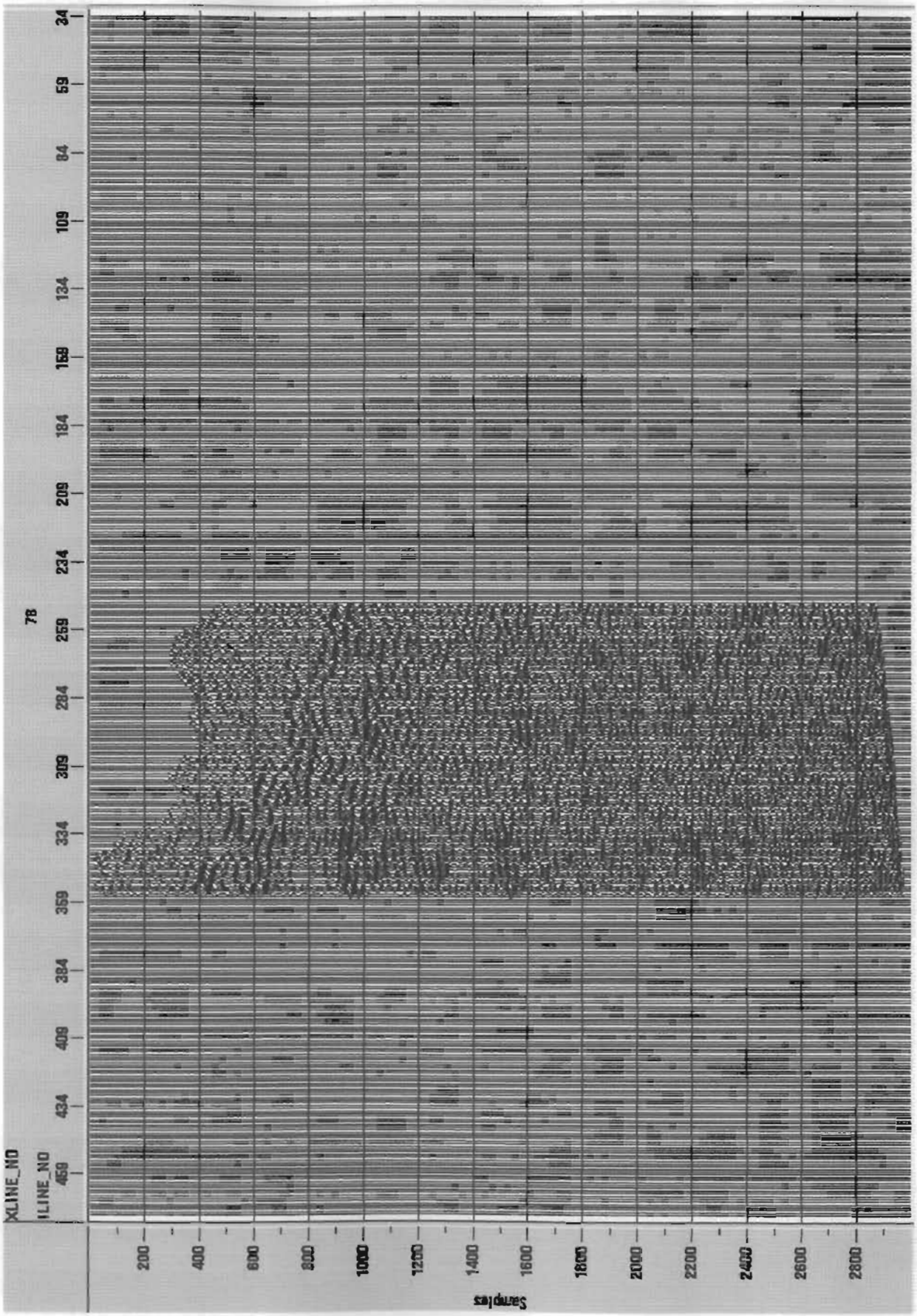
XLINE_NO
ILINE_NO
78
Samples

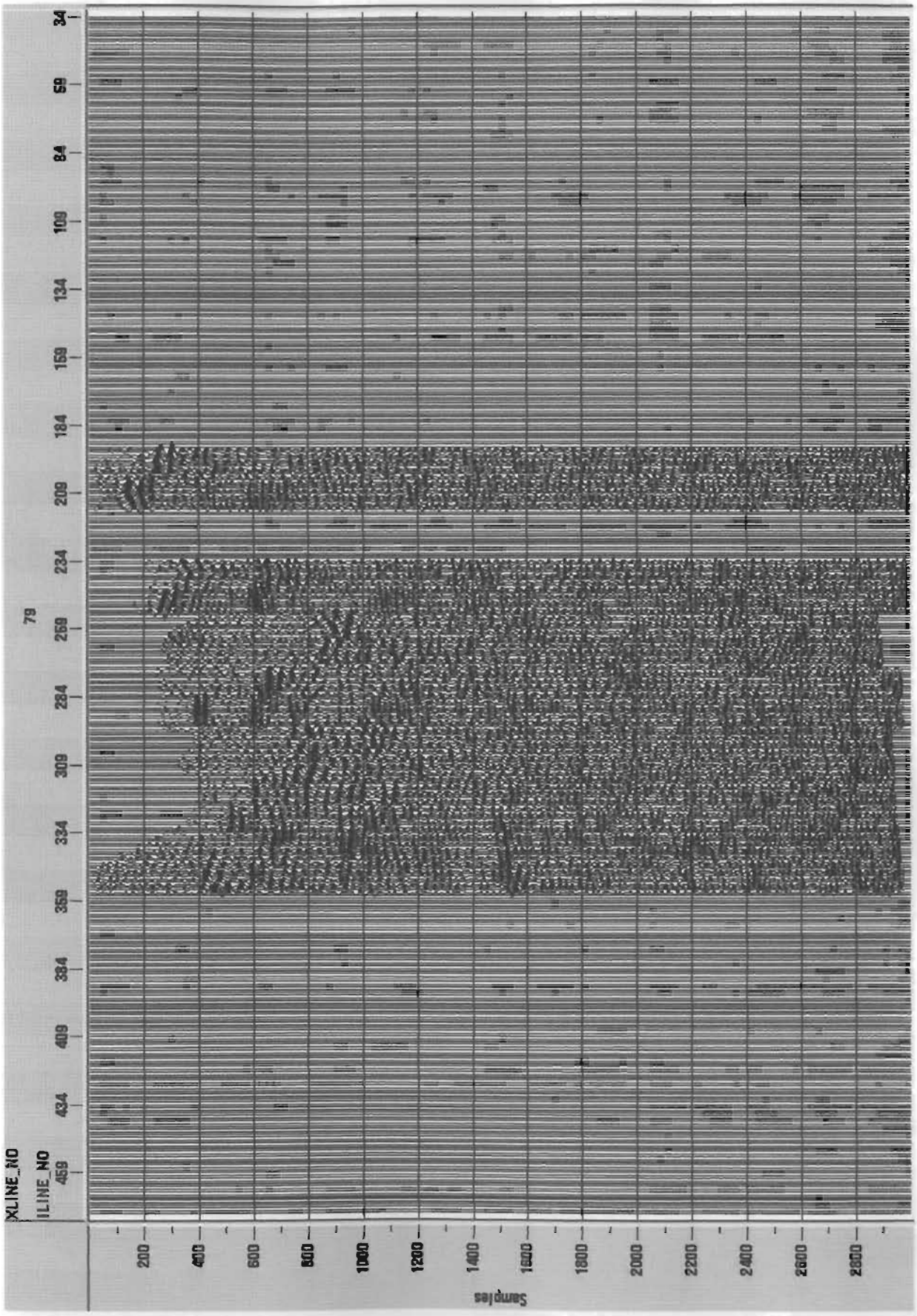
XLINE_NO
ILINE_NO
Samples
79

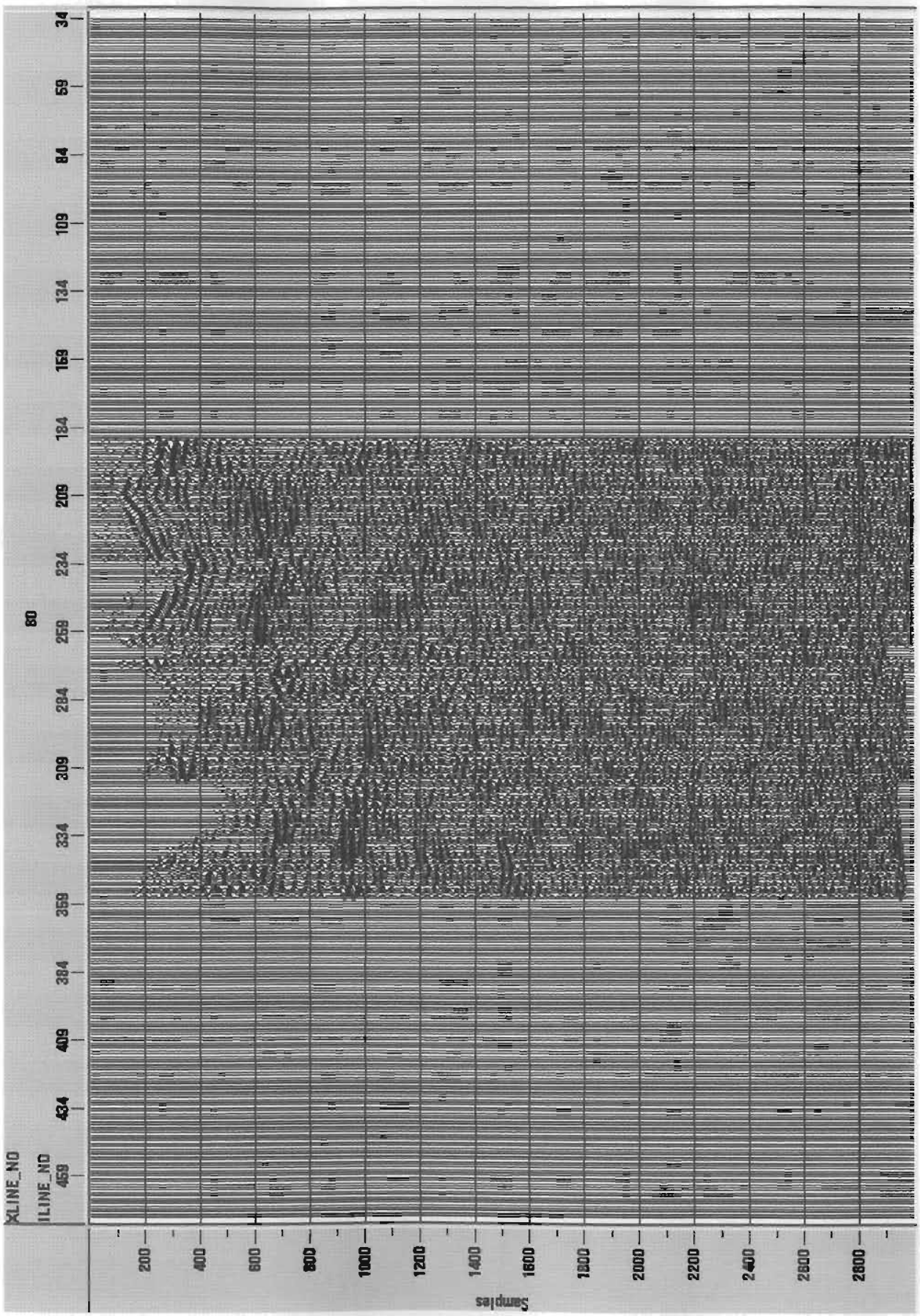
XLINE_NO
ILINE_NO
459
434
409
384
359
334
309
284
259
234
209
184
159
134
109
84
59
34
80
Samples
200
400
600
800
1000
1200
1400
1600
1800
2000
2200
2400
2600
2800

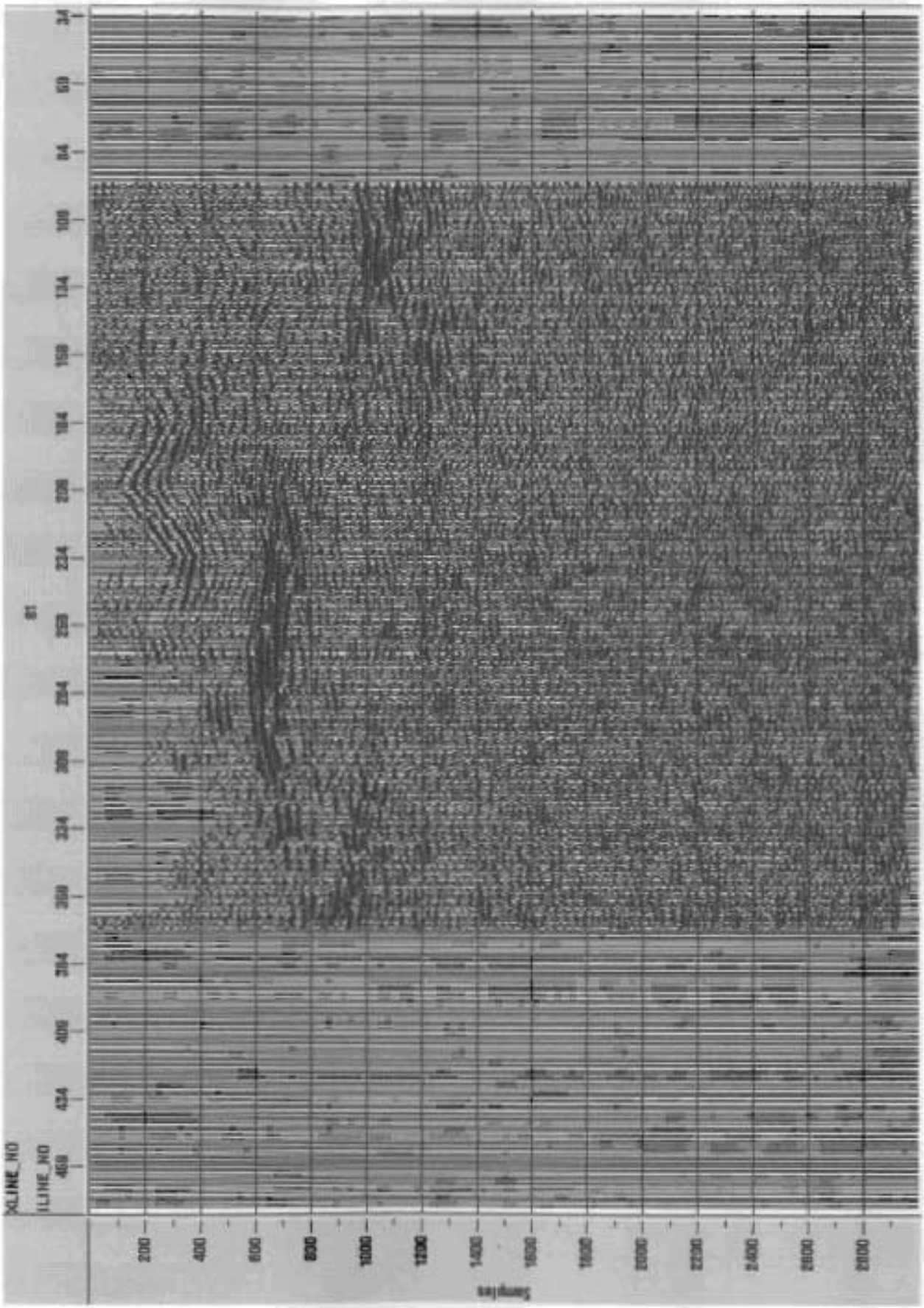
XLINE_NO
ILINE_NO
Samples

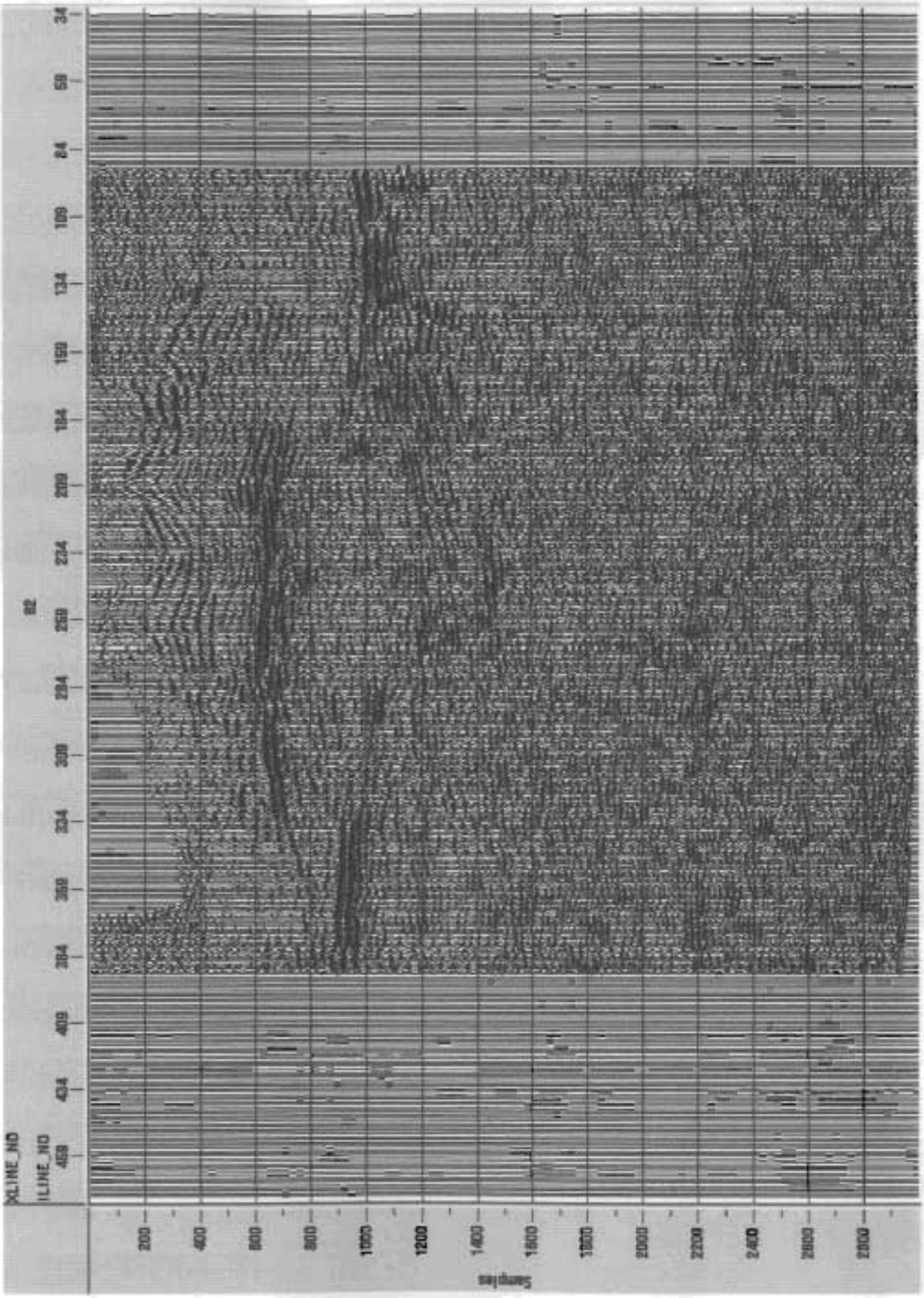
XLINE_NO
ILINE_NO
459
434
409
384
359
334
309
284
259
234
209
184
159
134
109
84
59
34
82
Samples
200
400
600
800
1000
1200
1400
1600
1800
2000
2200
2400
2600
2800

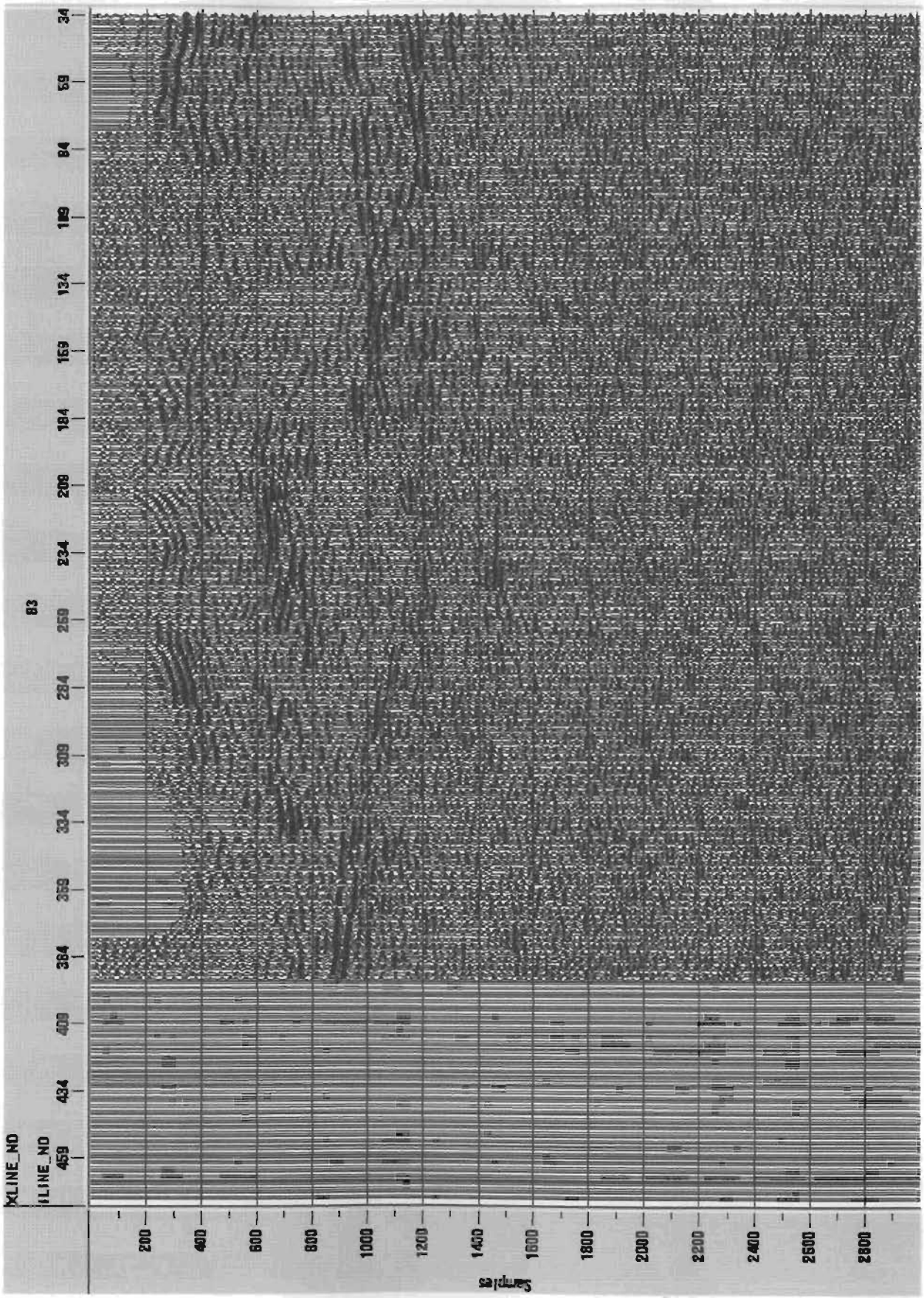
XLINE_NO
ILINE_NO
459
434
409
384
359
334
309
284
259
234
209
184
159
134
109
84
59
34
83
200
400
600
800
1000
1200
1400
1600
1800
2000
2200
2400
2600
2800
Samples

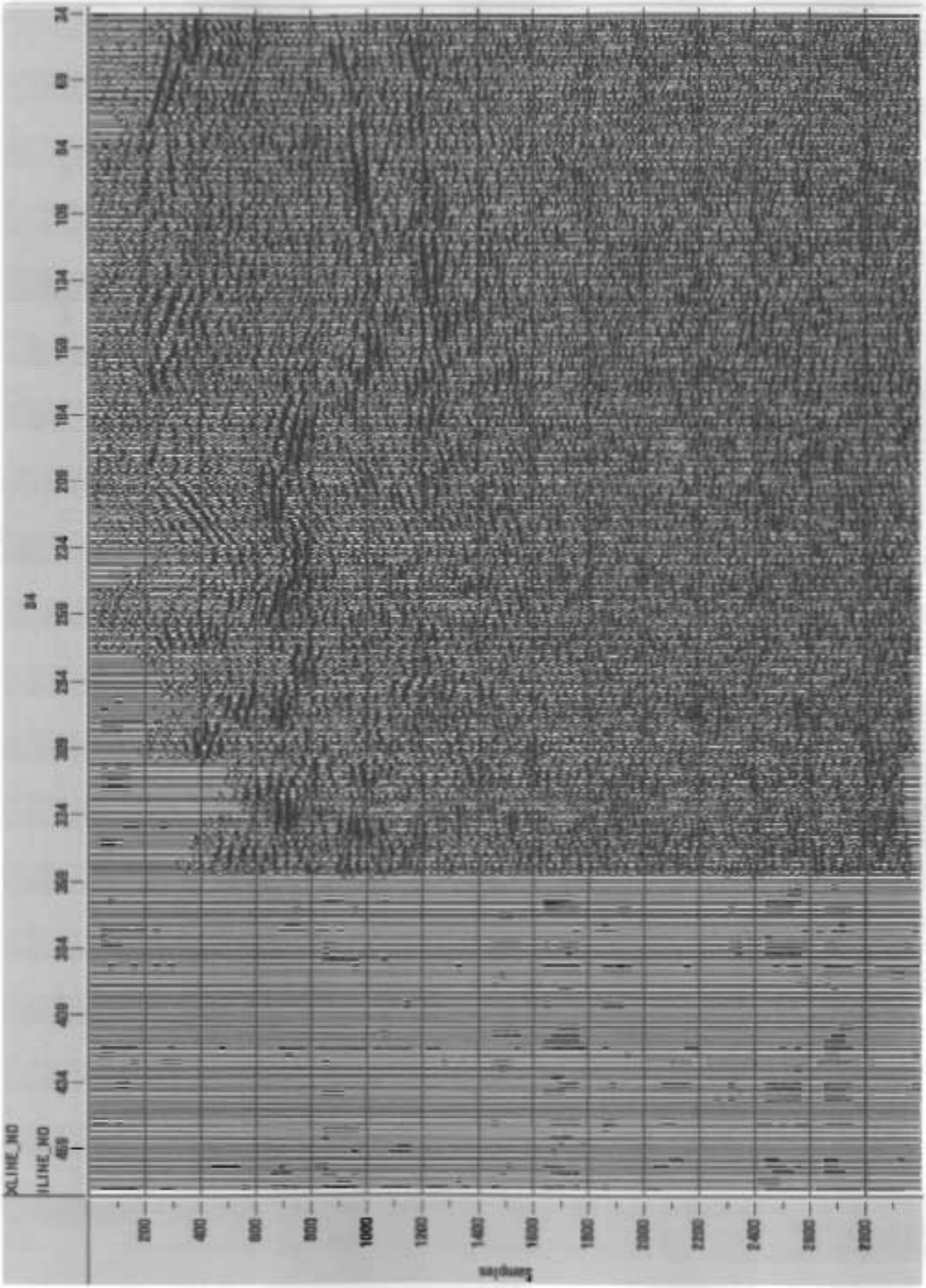
XLINE_NO
ILINE_NO
84
Samples

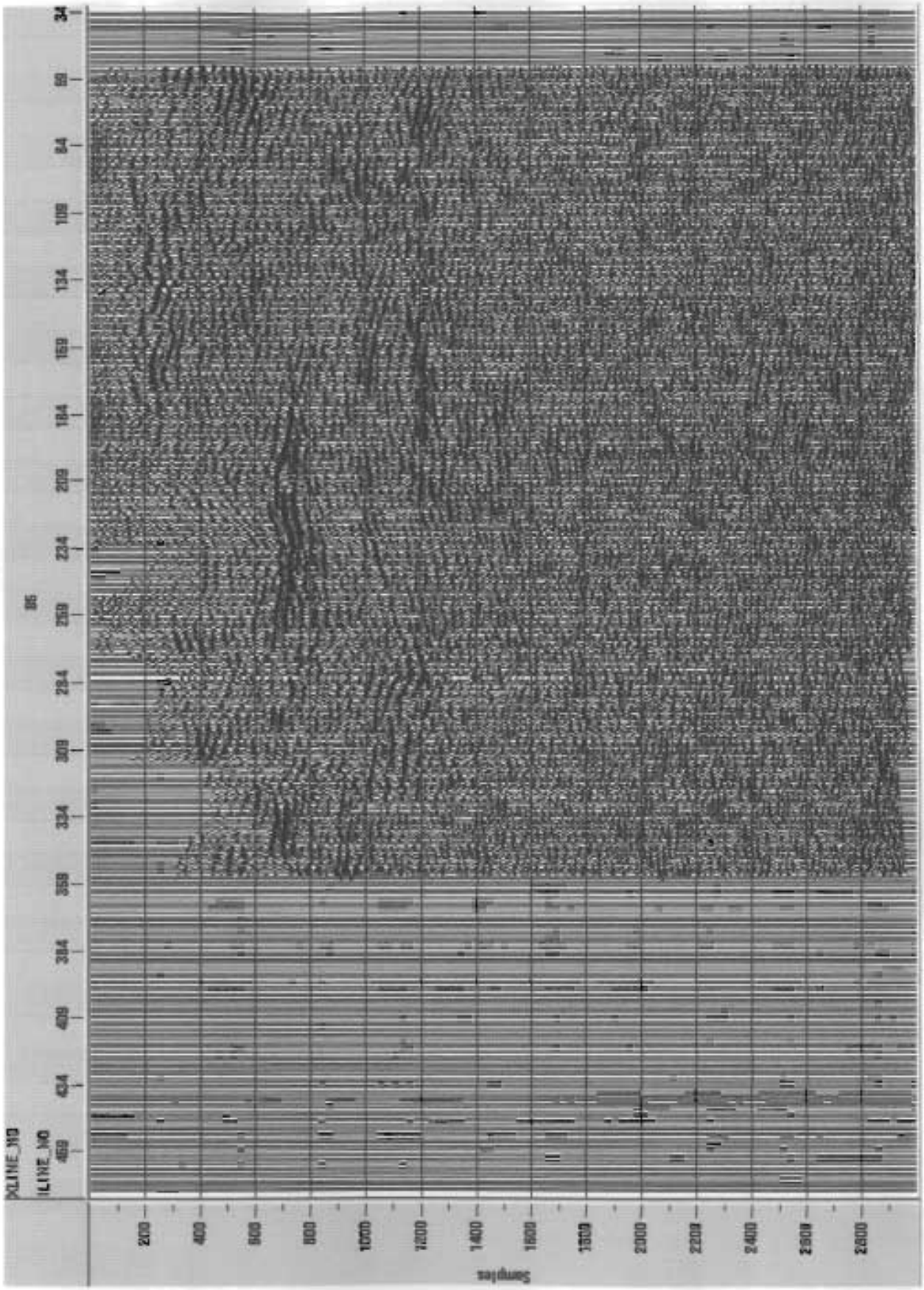
XLINE_NO
ILINE_NO
Samples

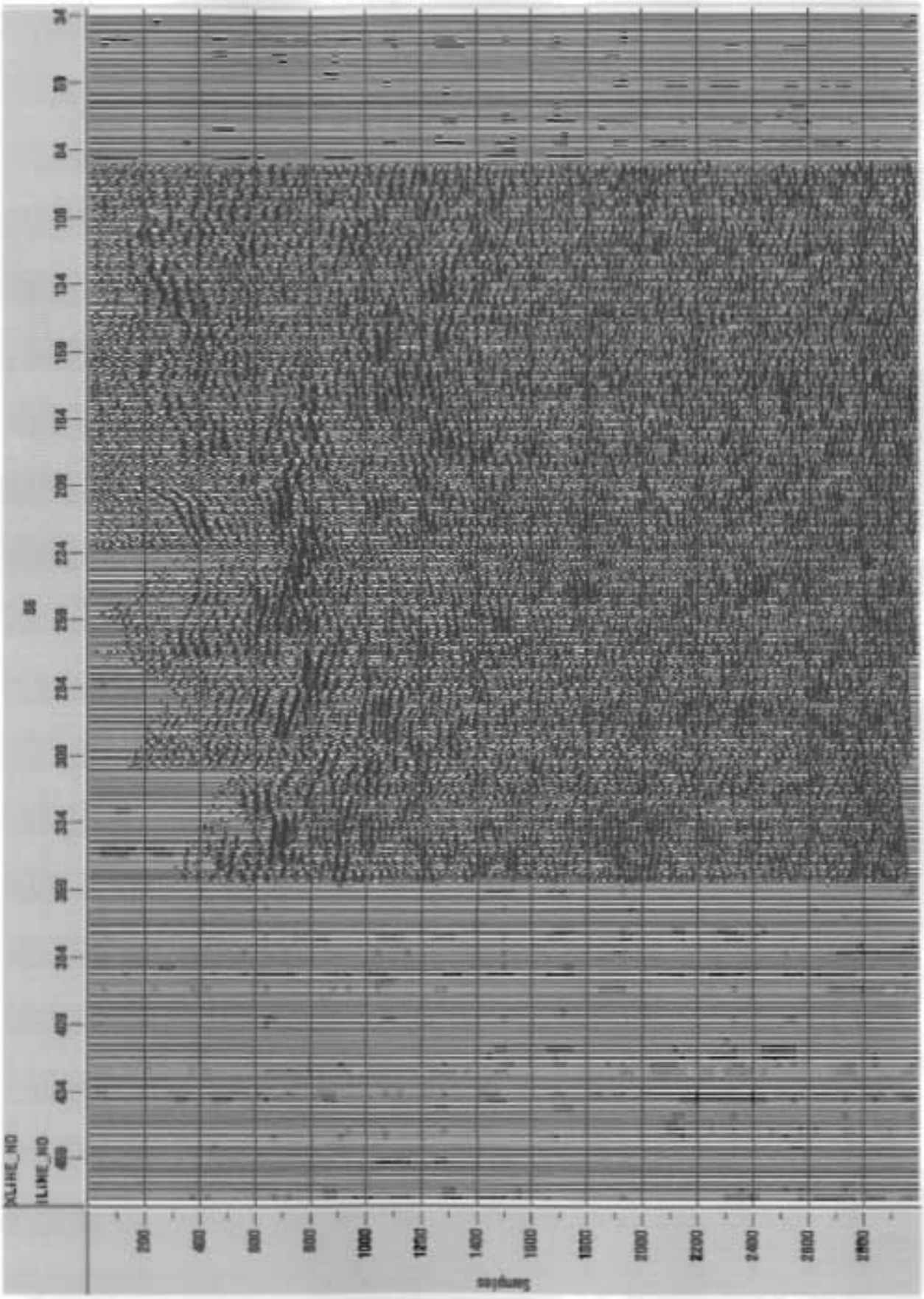
XLINE_NO
ILINE_NO
Samples

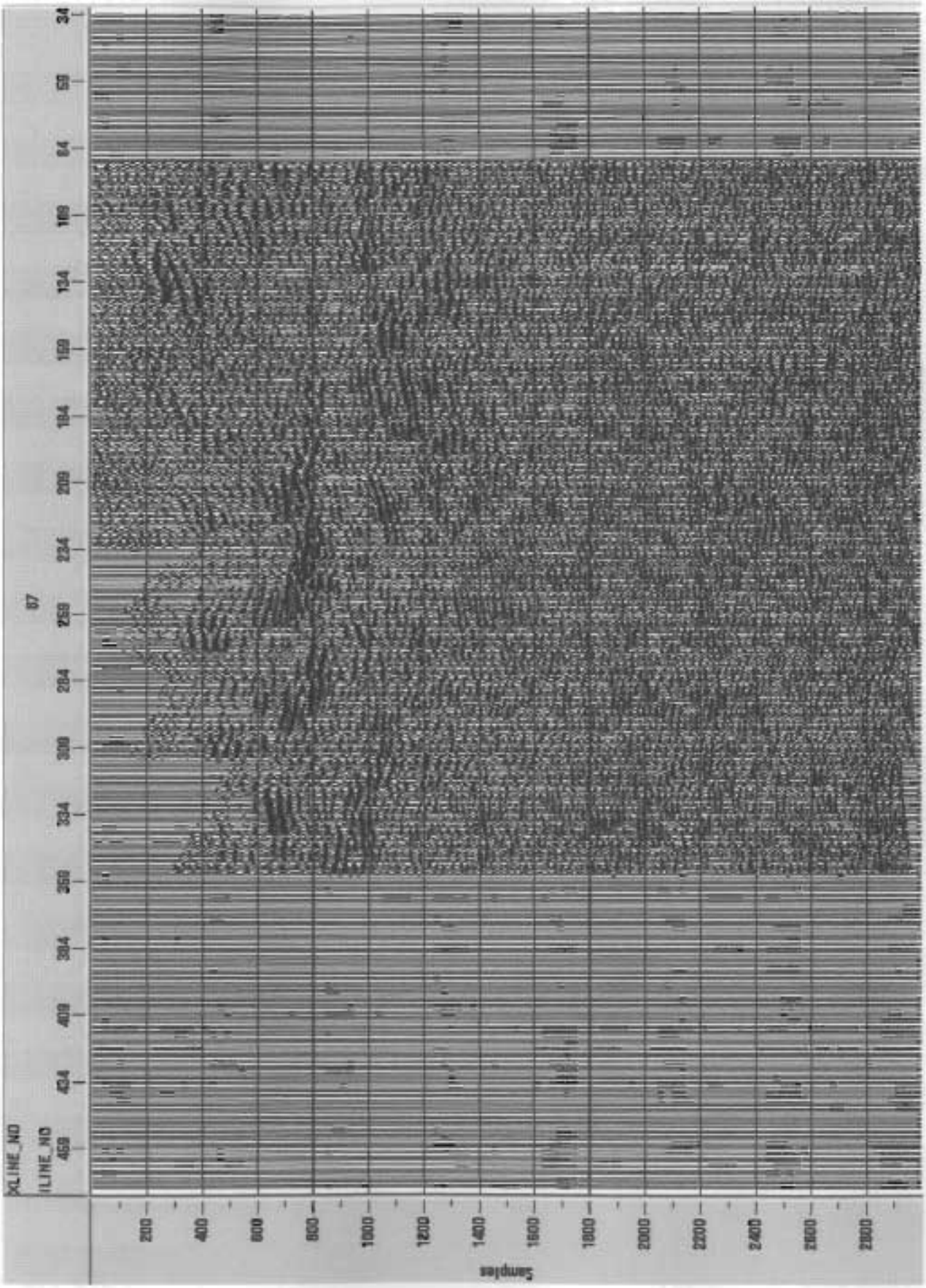
XLINE_NO
ILINE_NO
459
434
409
384
359
334
309
284
259
234
209
184
159
134
109
84
59
34
97
Samples
200
400
600
800
1000
1200
1400
1600
1800
2000
2200
2400
2600
2800

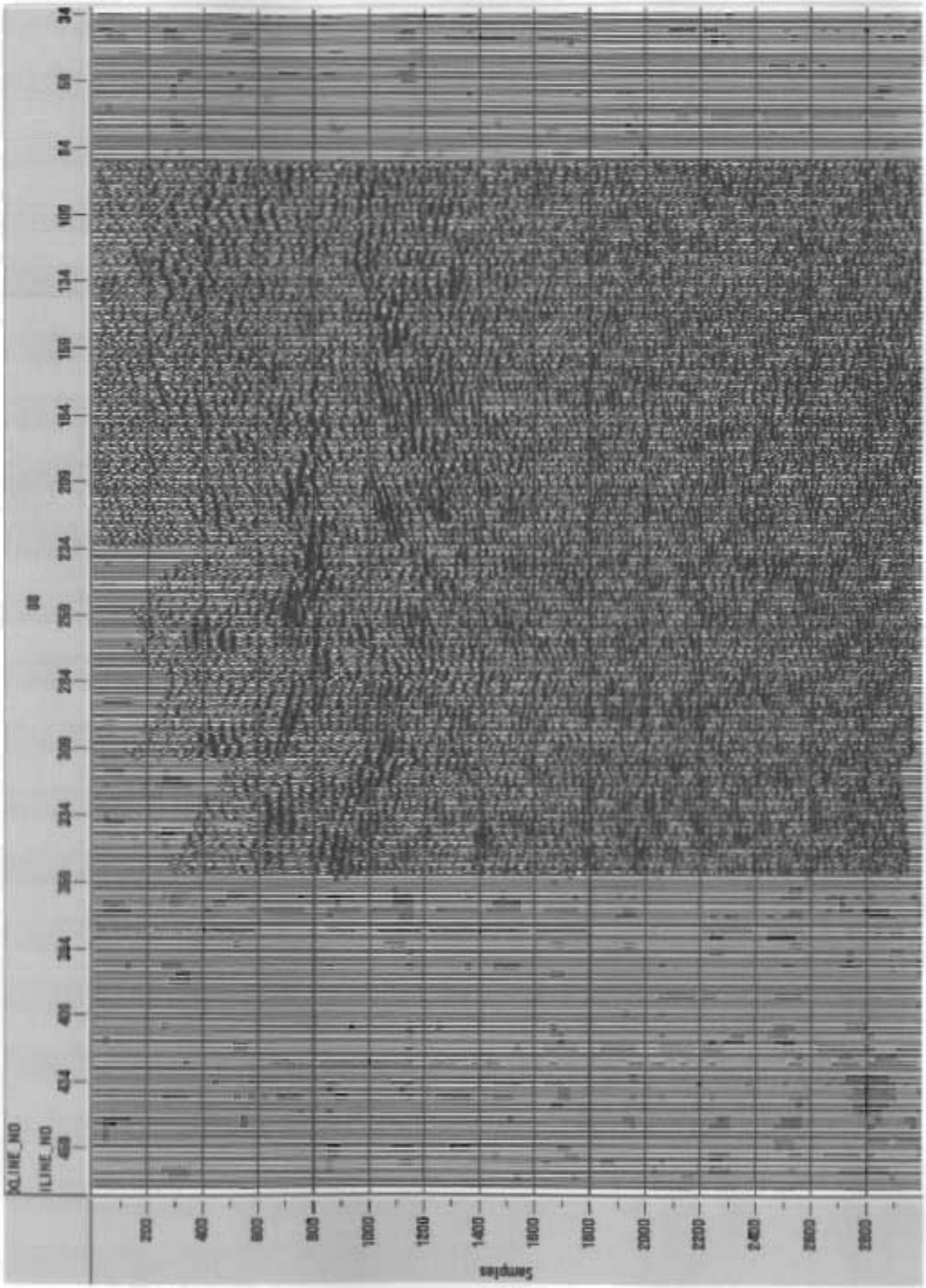
XLINE_NO
ILINE_NO
Samples

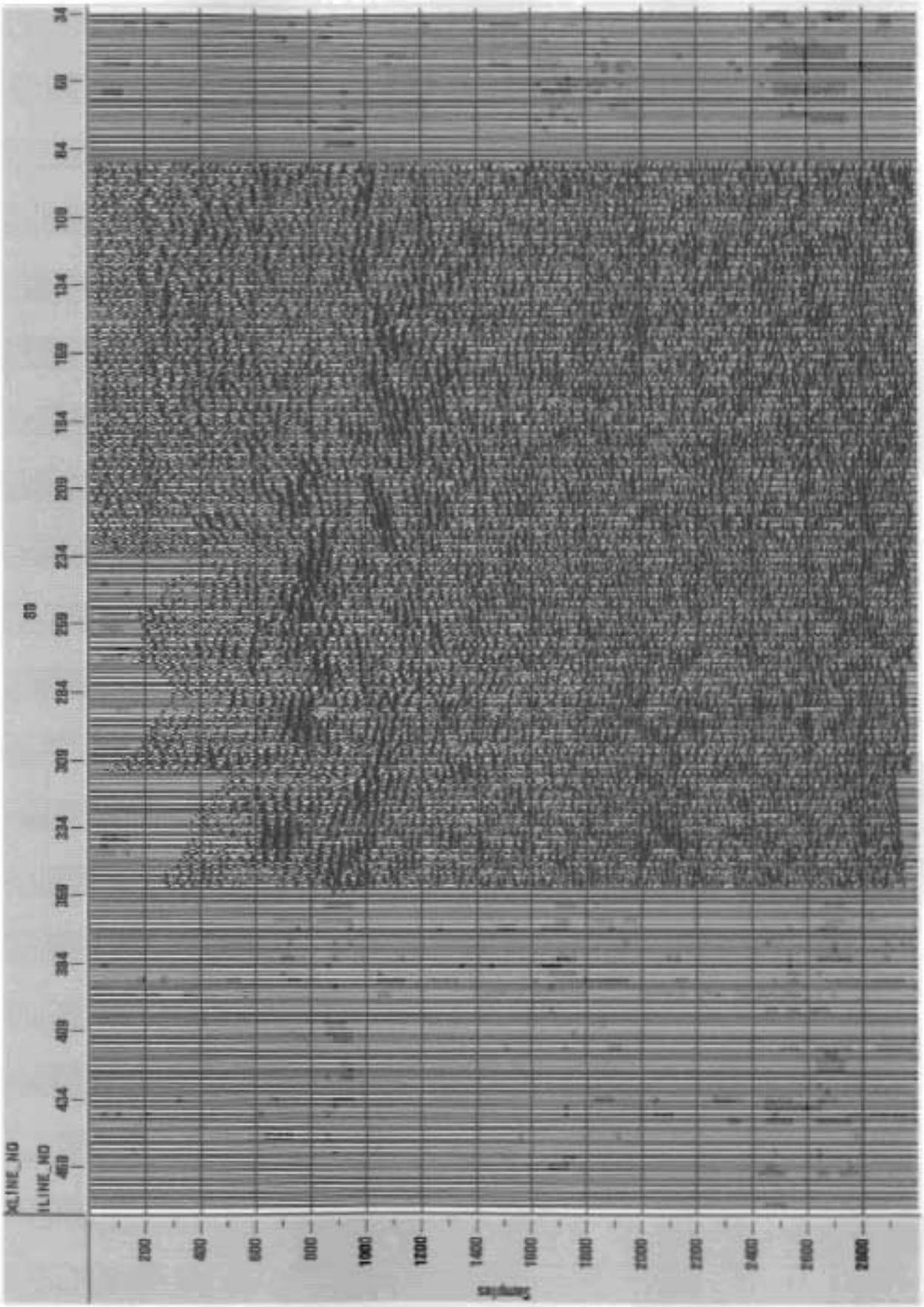
XLINE_NO
ILINE_NO
469
434
399
384
359
334
309
284
259
234
209
184
159
134
109
84
59
34
Samples

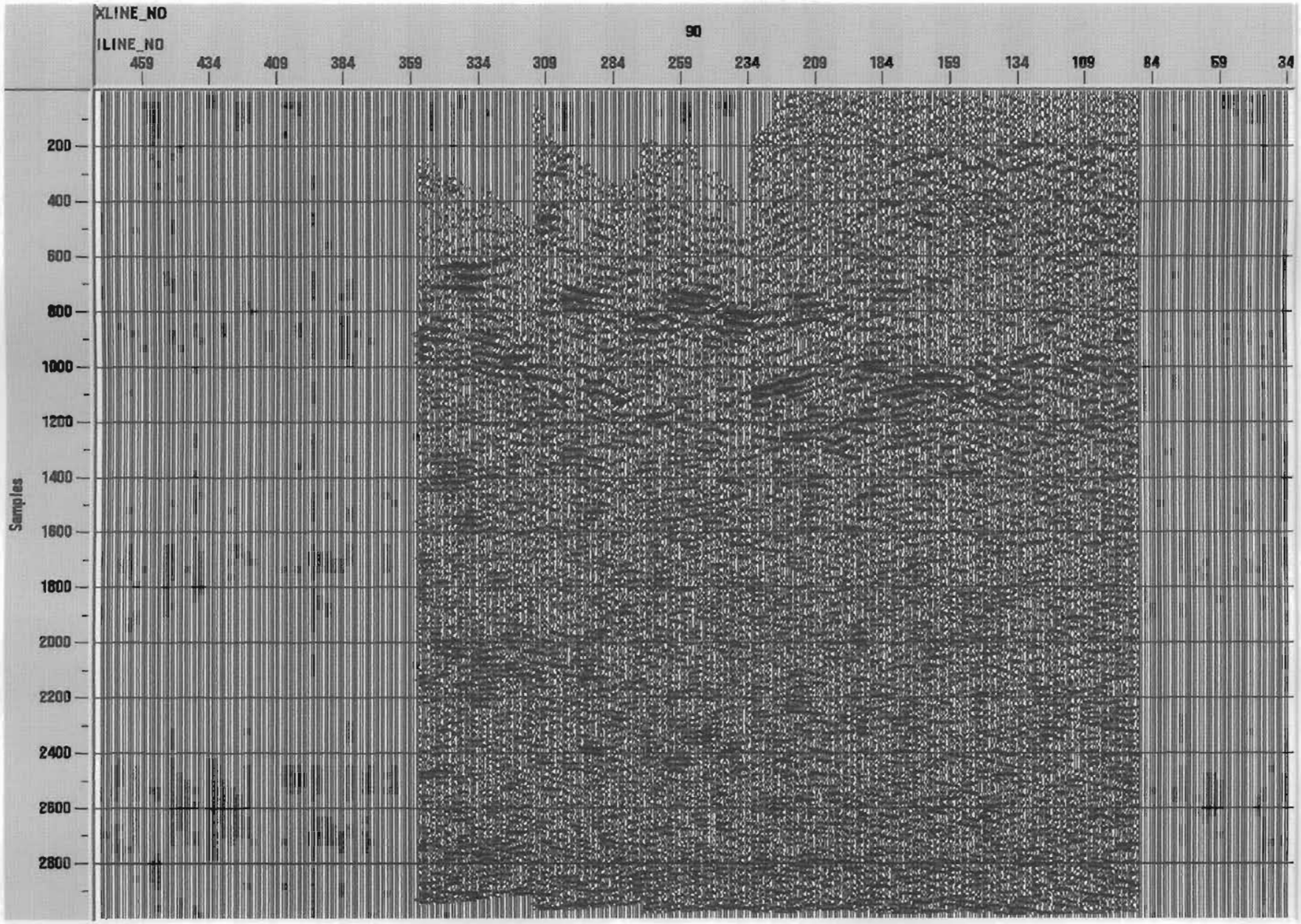
XLINE_NO
ILINE_NO
90
459
434
409
384
359
334
309
284
259
234
209
184
159
134
109
84
59
34
Samples
200
400
600
800
1000
1200
1400
1600
1800
2000
2200
2400
2600
2800

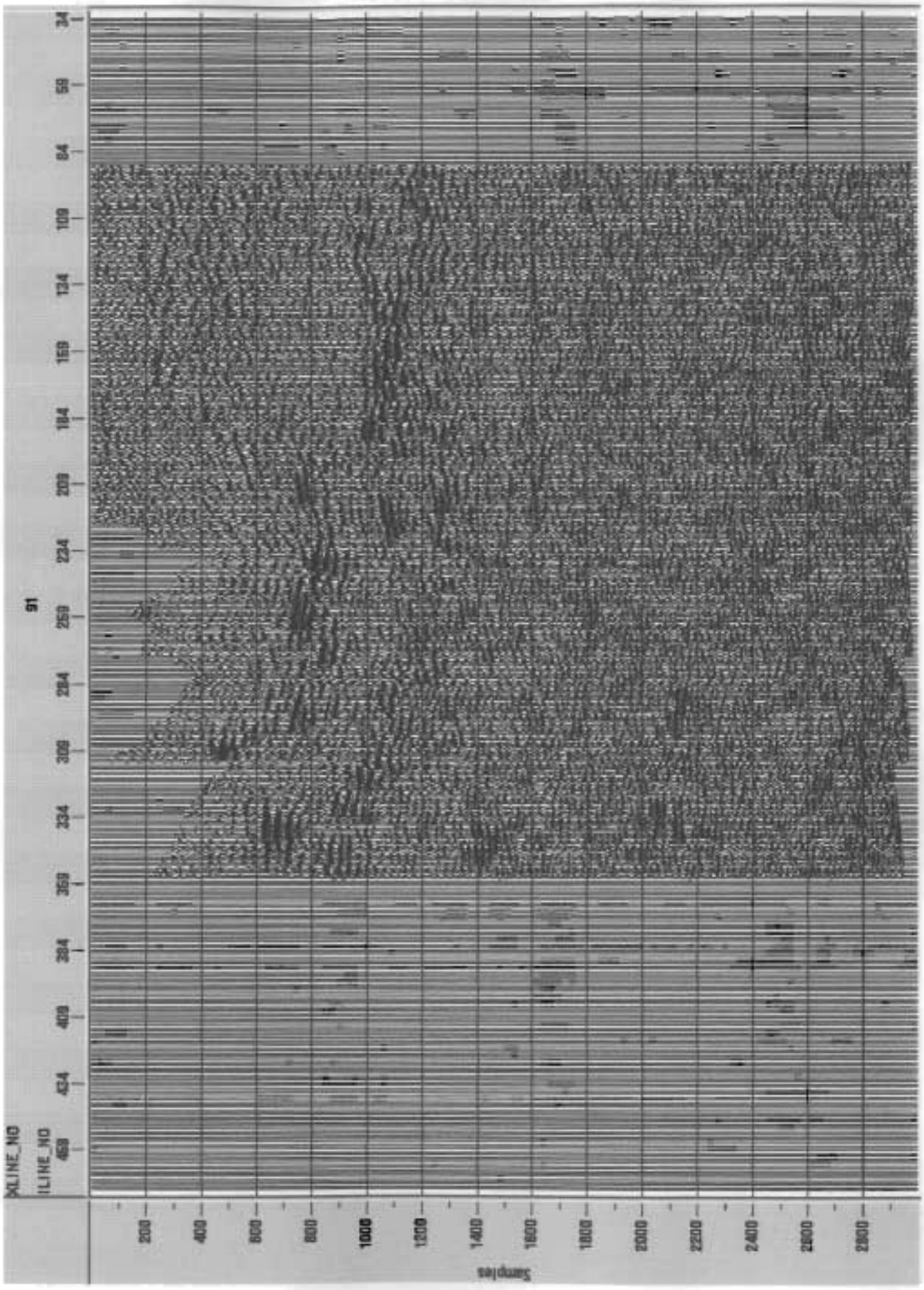
XLINE_NO
ILINE_NO
Samples

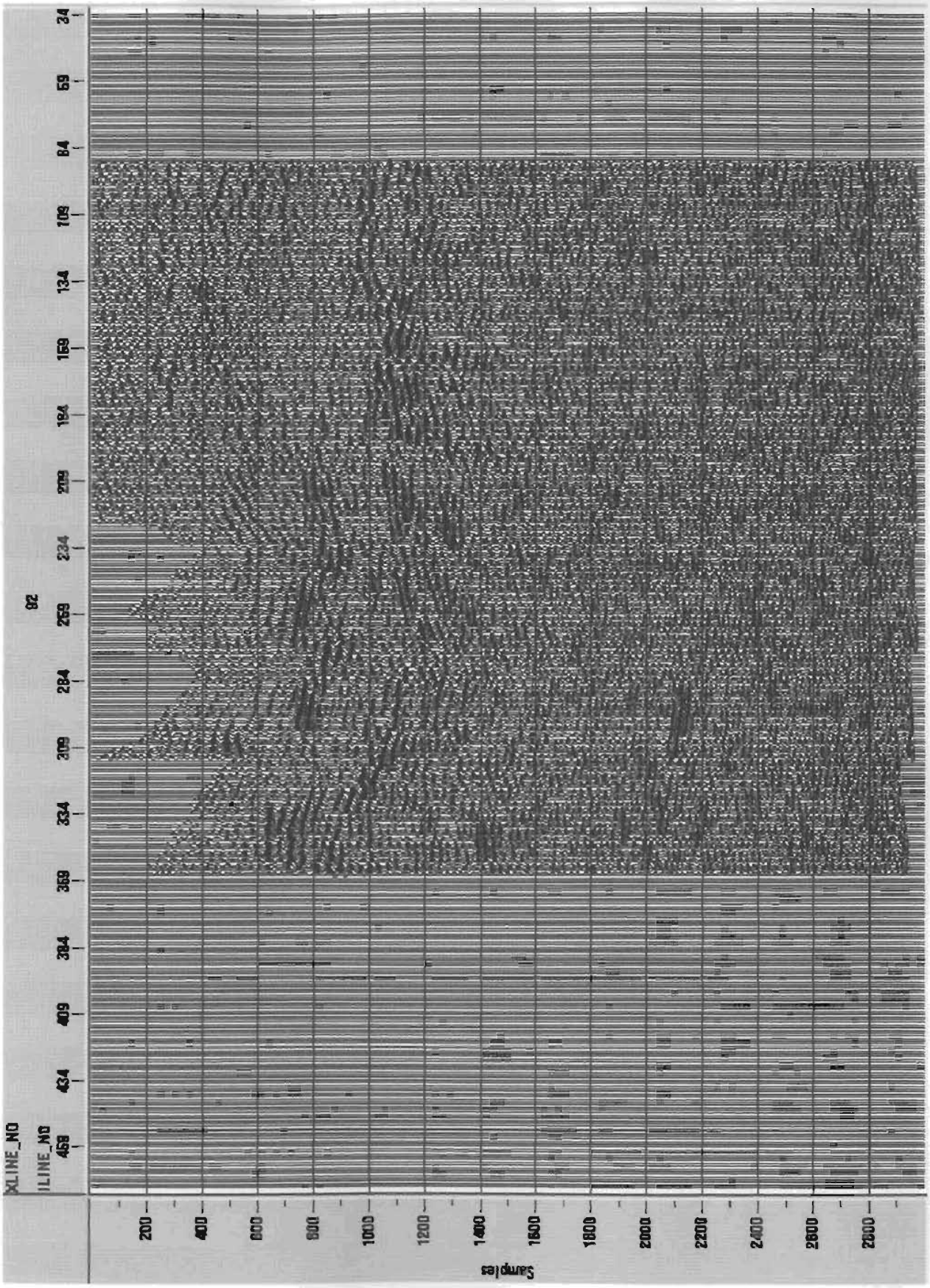
XLINE_NO
ILINE_NO
459
434
409
384
359
334
309
284
259
234
209
184
159
134
109
84
59
34
92
Samples
200
400
600
800
1000
1200
1400
1600
1800
2000
2200
2400
2600
2800

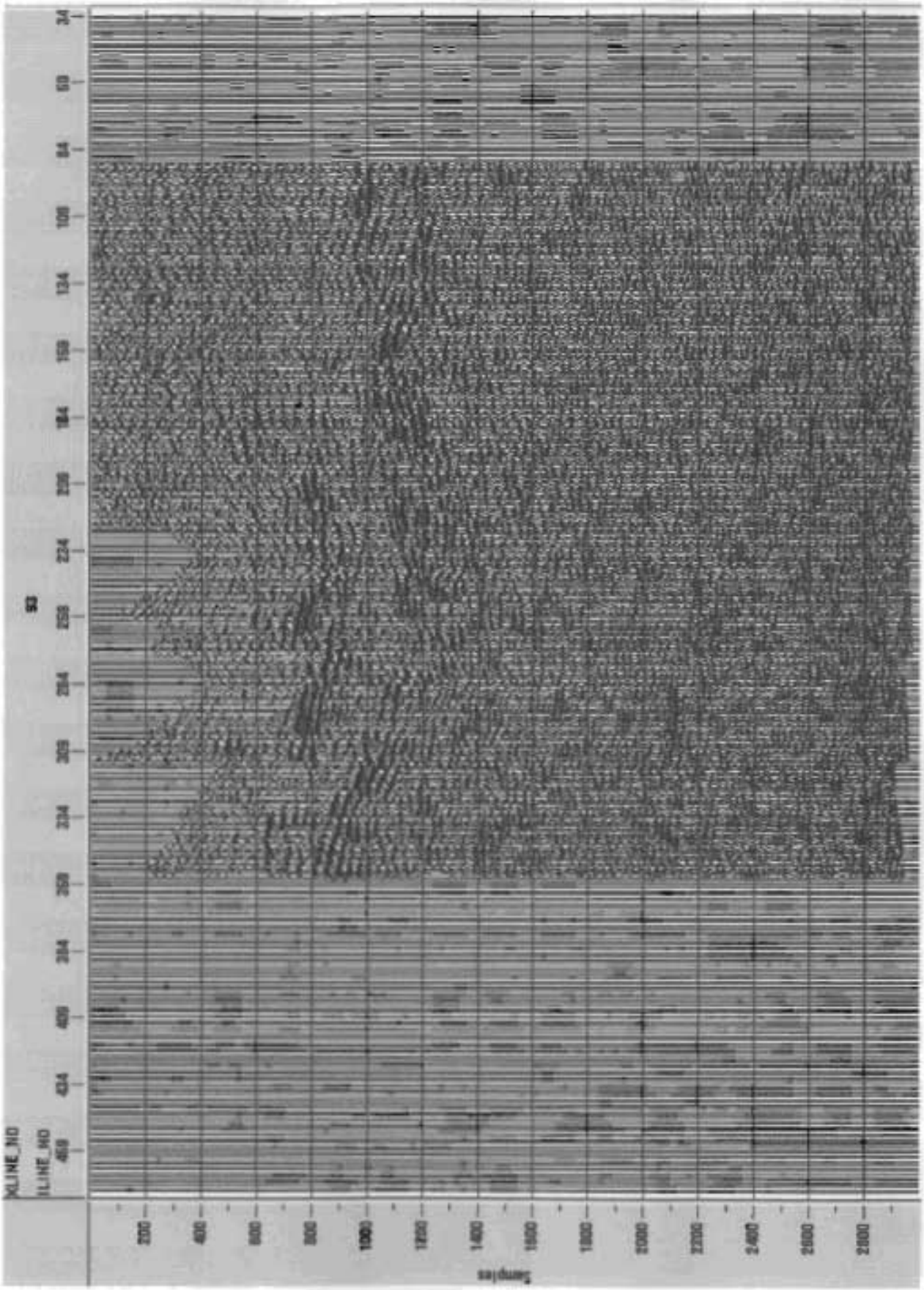
XLINE_NO
ILINE_NO
93
Samples

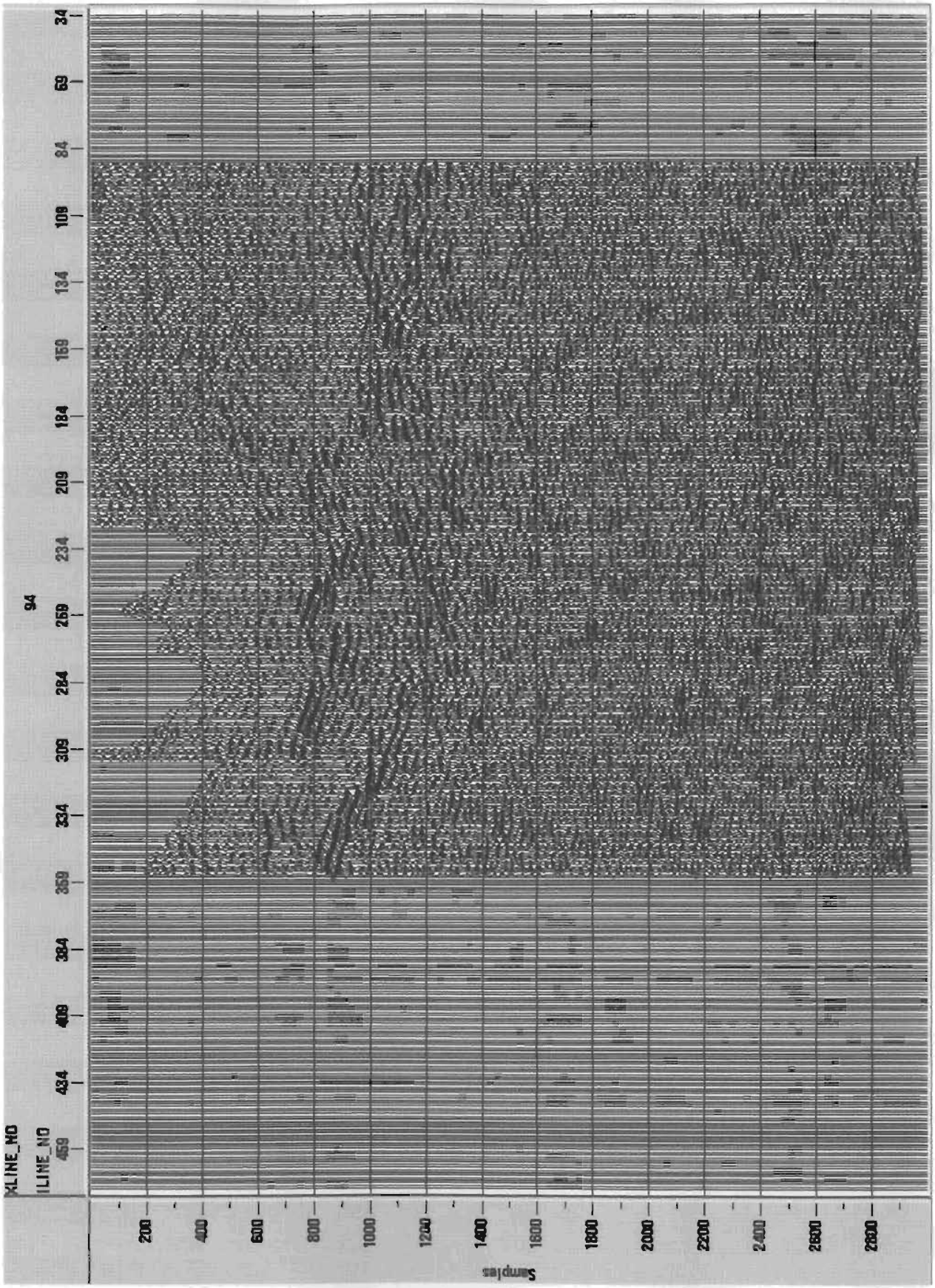
XLINE_NO
ILINE_NO
459
434
409
384
359
334
309
284
259
234
209
184
159
134
109
84
59
34
94
Samples
200
400
600
800
1000
1200
1400
1600
1800
2000
2200
2400
2600
2800

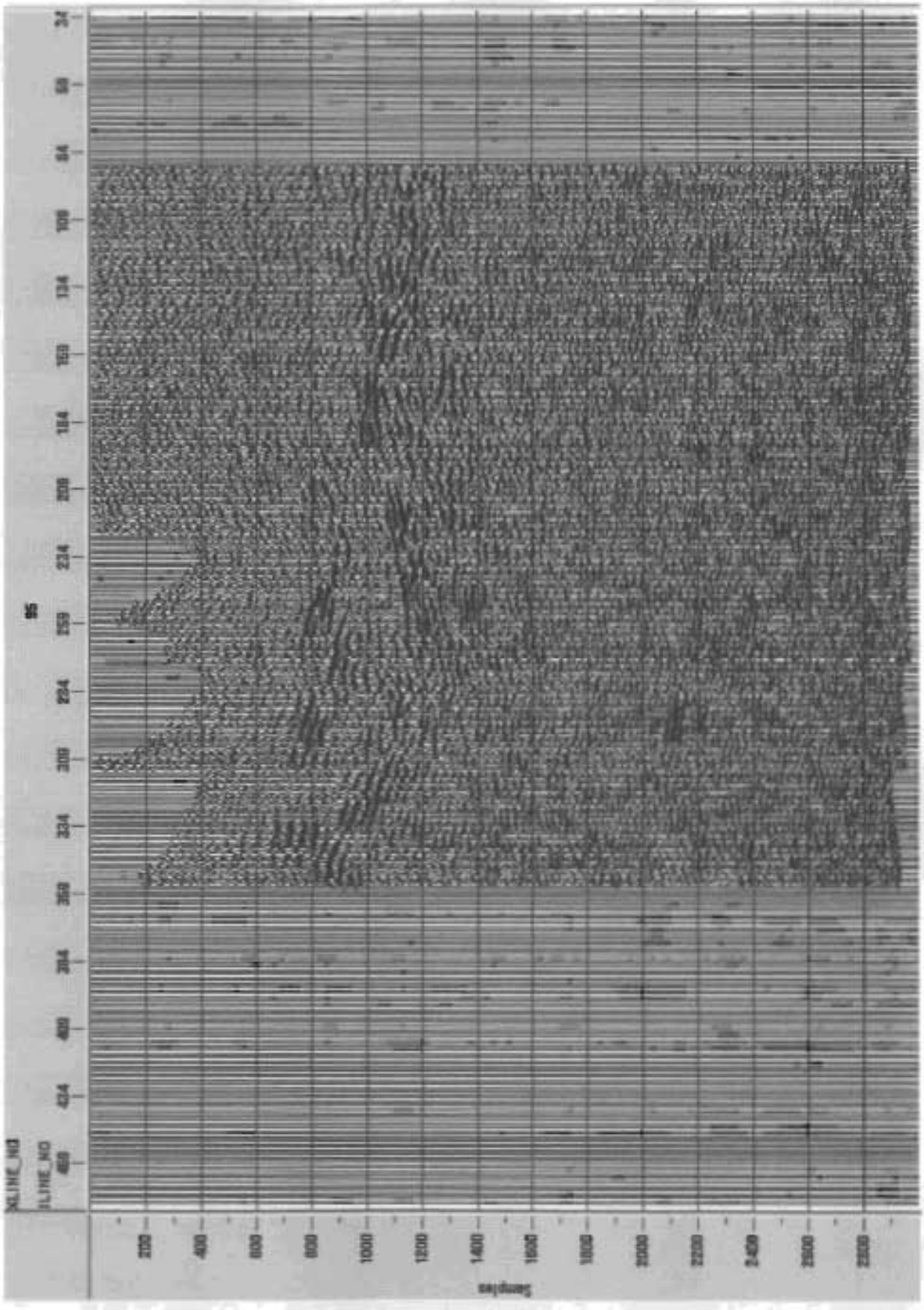
XLINE_NO
ILINE_NO
95
Samples

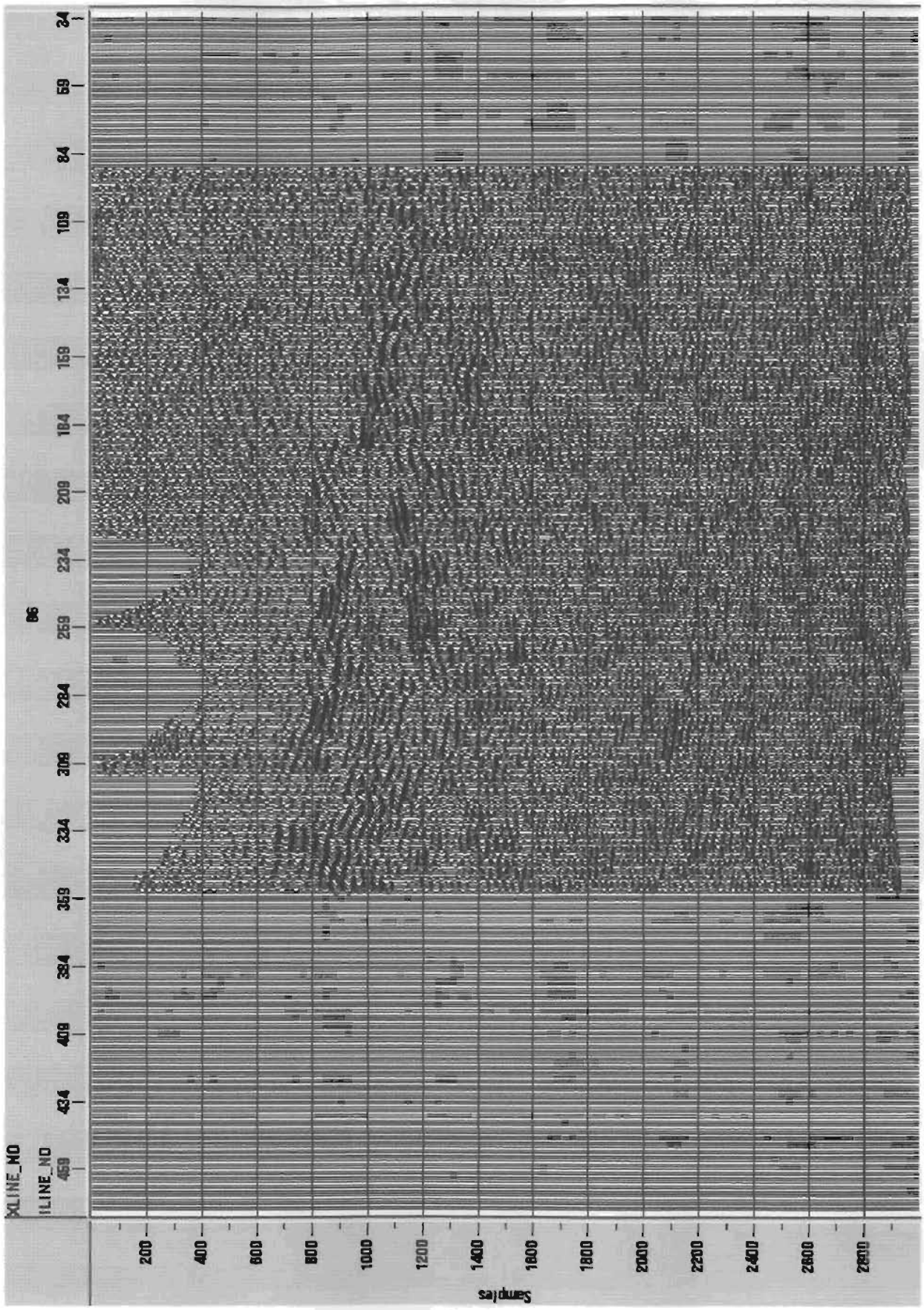
XLINE_NO
ILINE_NO
Samples
200
400
600
800
1000
1200
1400
1600
1800
2000
2200
2400
2600
2800
34
59
84
109
134
159
184
209
234
259
284
309
334
359
384
409
434
459

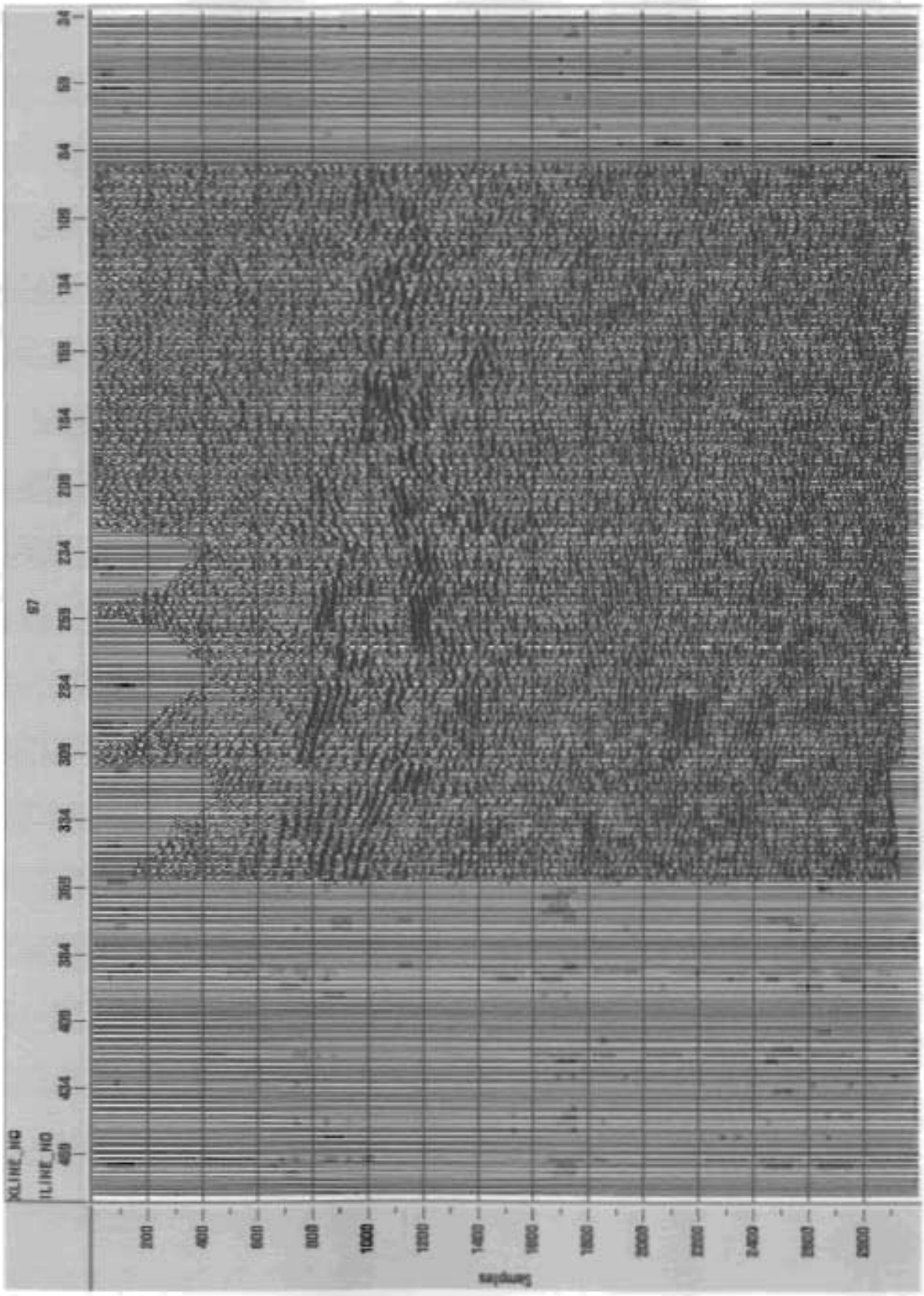
XLINE_NO
ILINE_NO
67
Samples

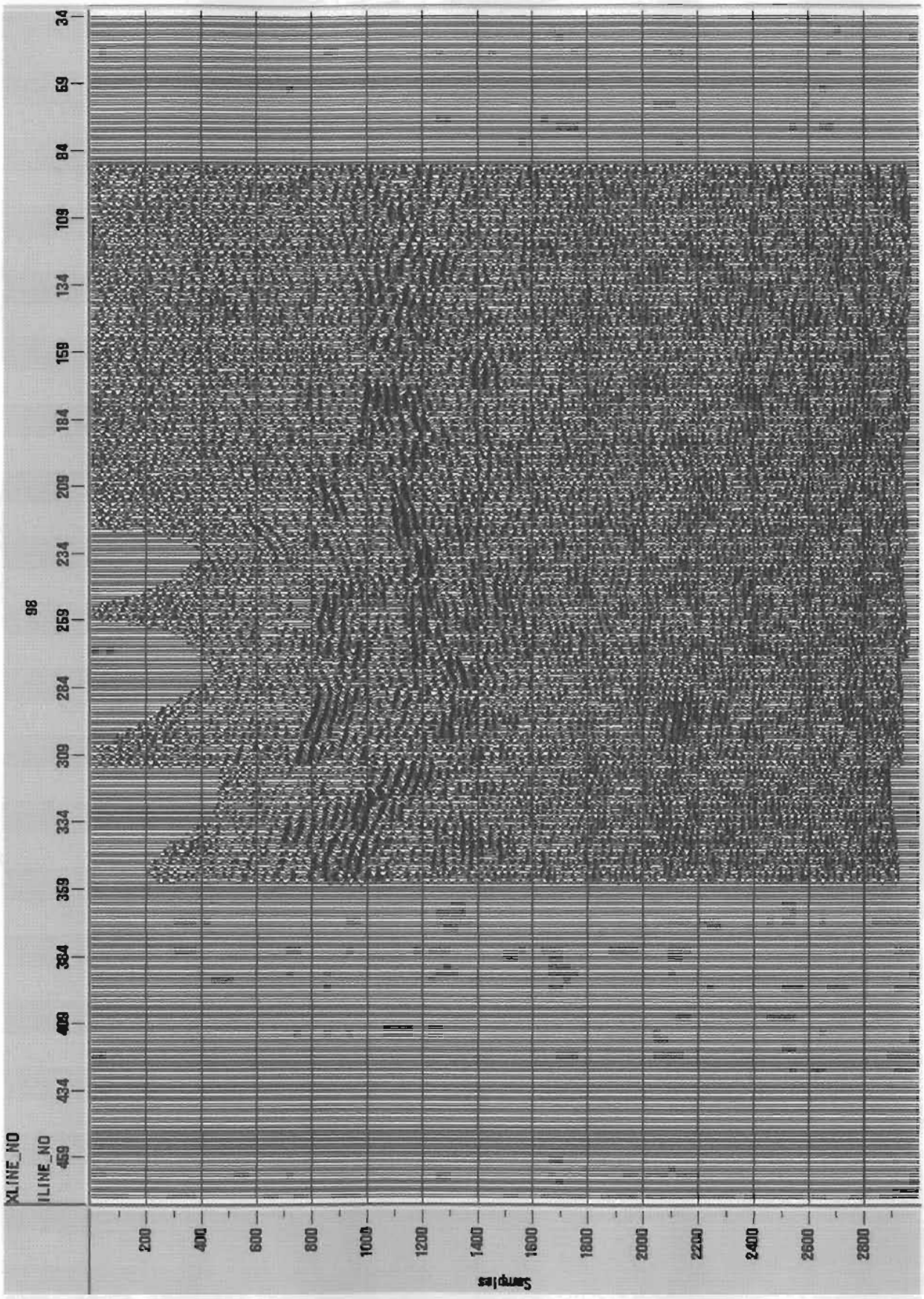
XLINE_NO
ILINE_NO
459
434
409
384
359
334
309
284
259
234
209
184
159
134
109
84
59
34
96
Samples
200
400
600
800
1000
1200
1400
1600
1800
2000
2200
2400
2600
2800

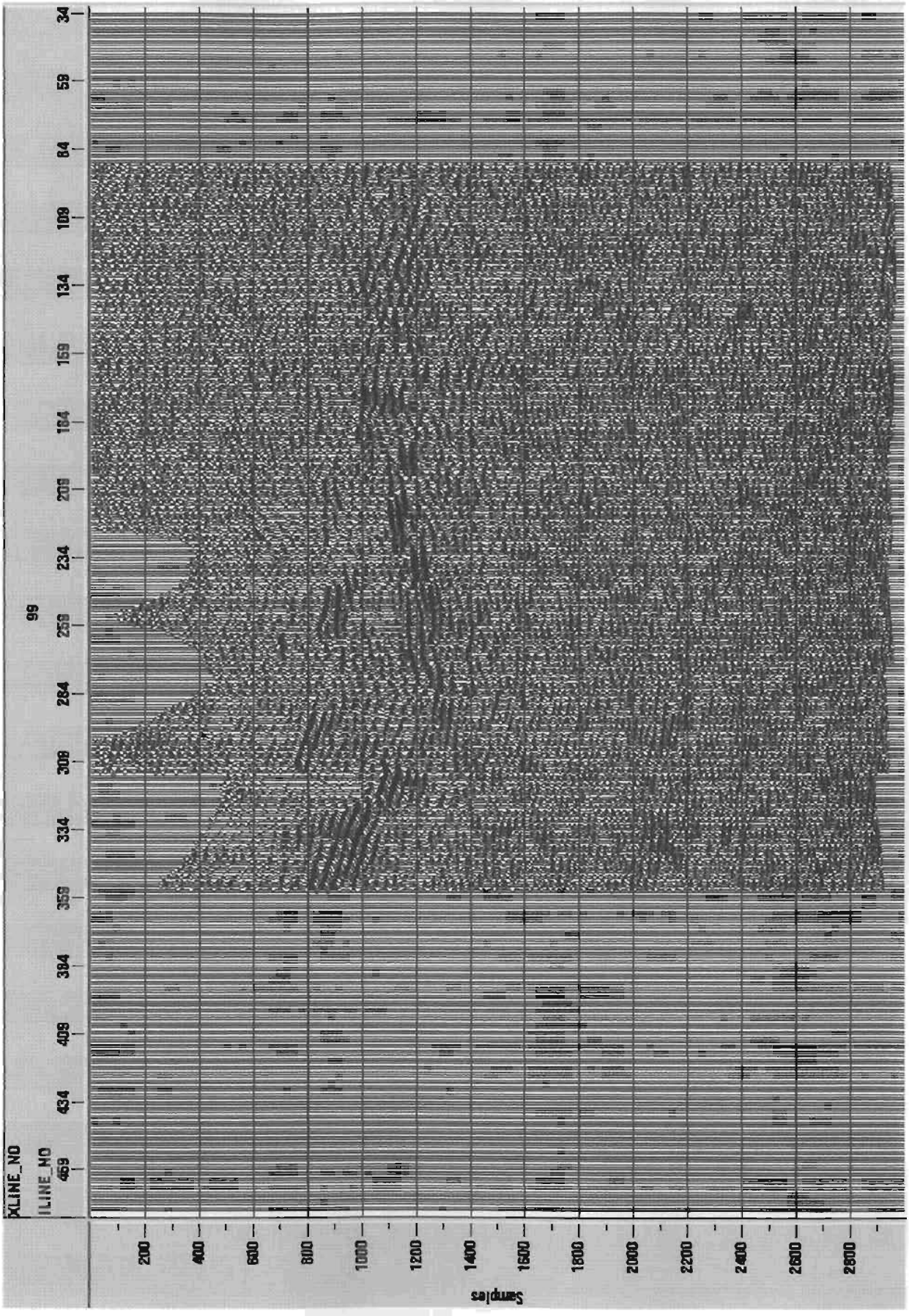
XLINE_NO
ILINE_NO
469
434
408
384
359
334
308
284
259
234
209
184
159
134
109
84
59
34
99
Samples
200
400
600
800
1000
1200
1400
1600
1800
2000
2200
2400
2600

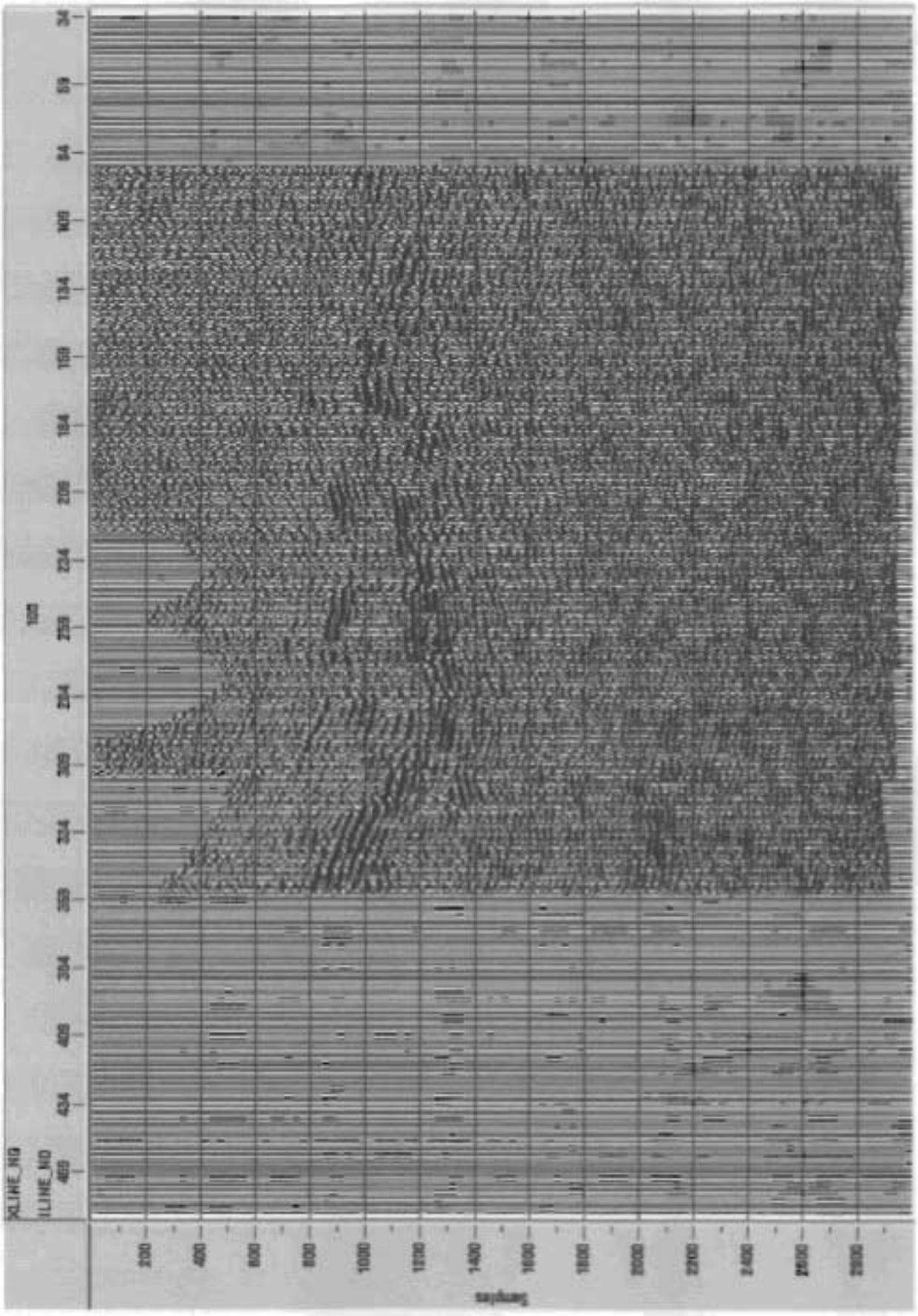
XLINE_NO
ILINE_NO
Samples

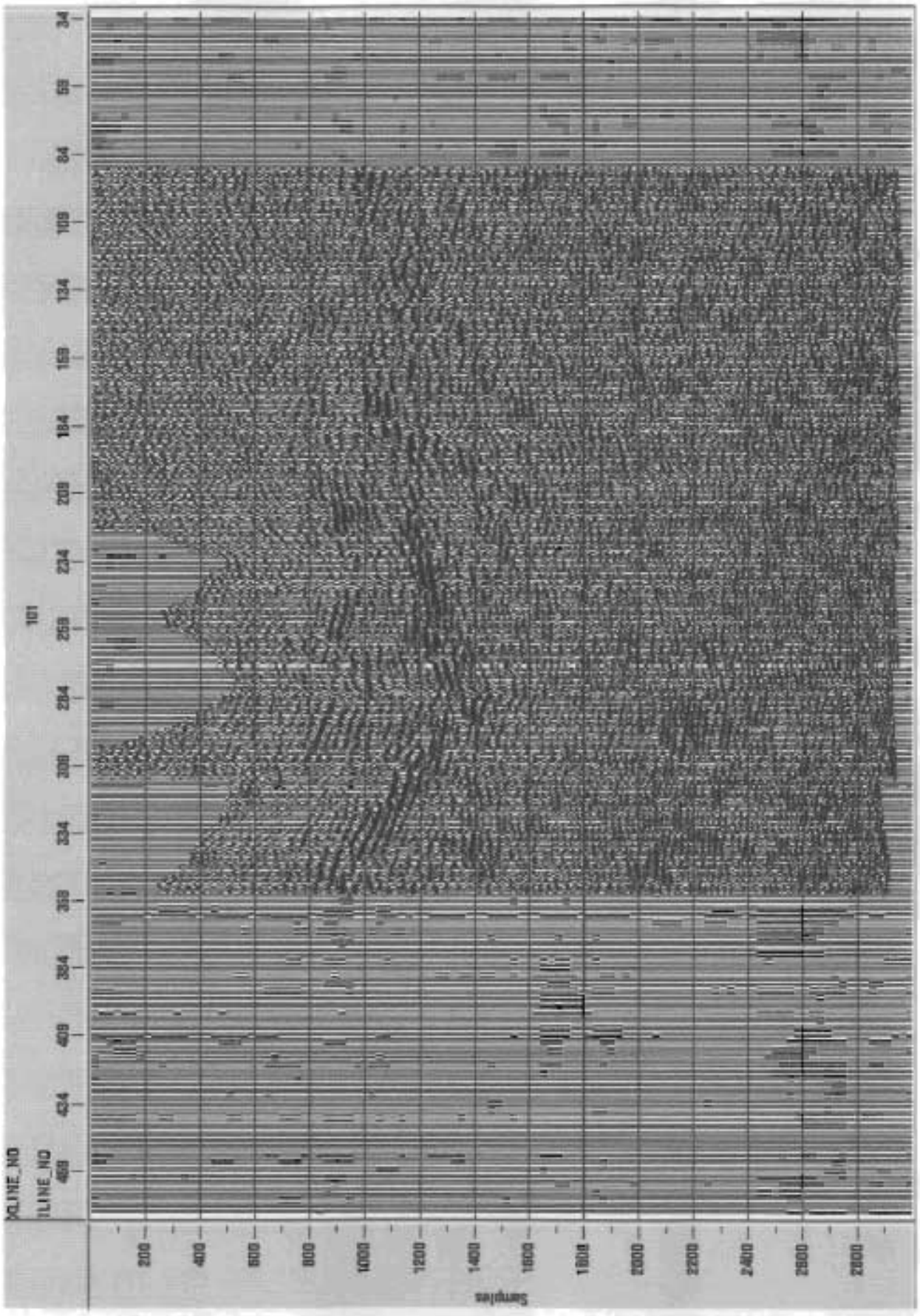
XLINE_NO
ILINE_NO
101
Samples

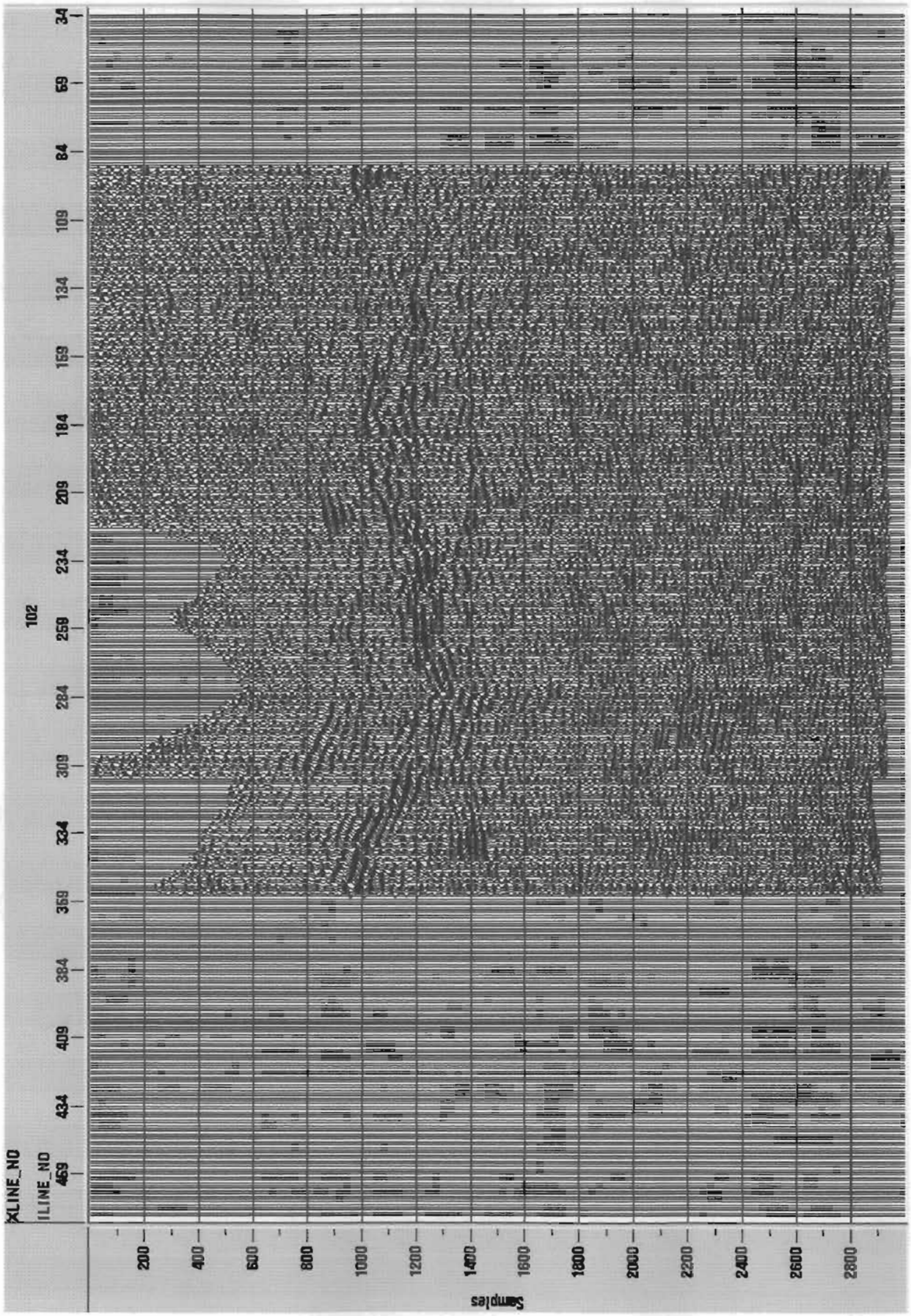
XLINE_NO
ILINE_NO
469
434
409
384
359
334
309
284
259
234
209
184
159
134
109
84
59
34
102
Samples
200
400
600
800
1000
1200
1400
1600
1800
2000
2200
2400
2600
2800

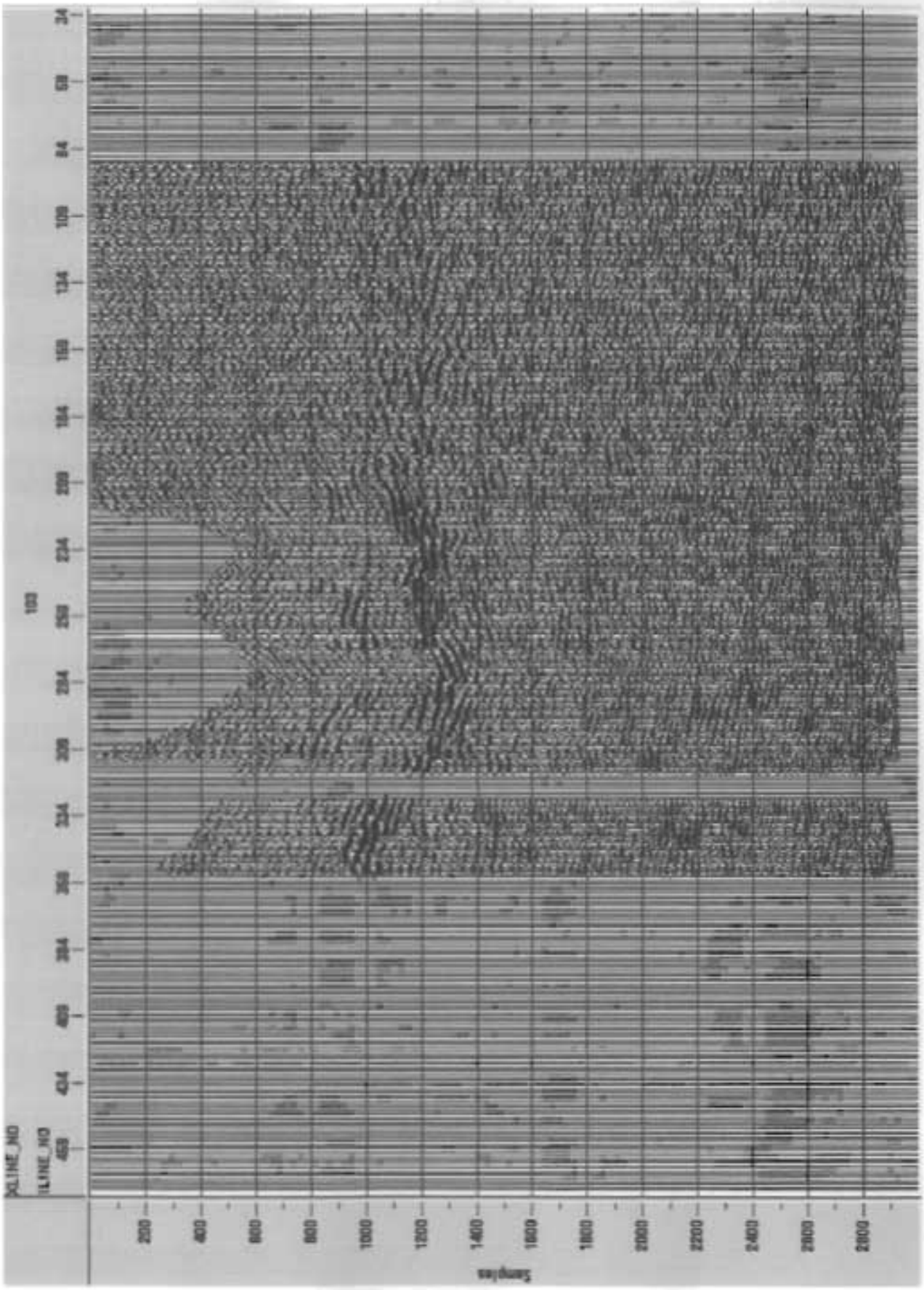
XLINE_NO
ILINE_NO
Samples

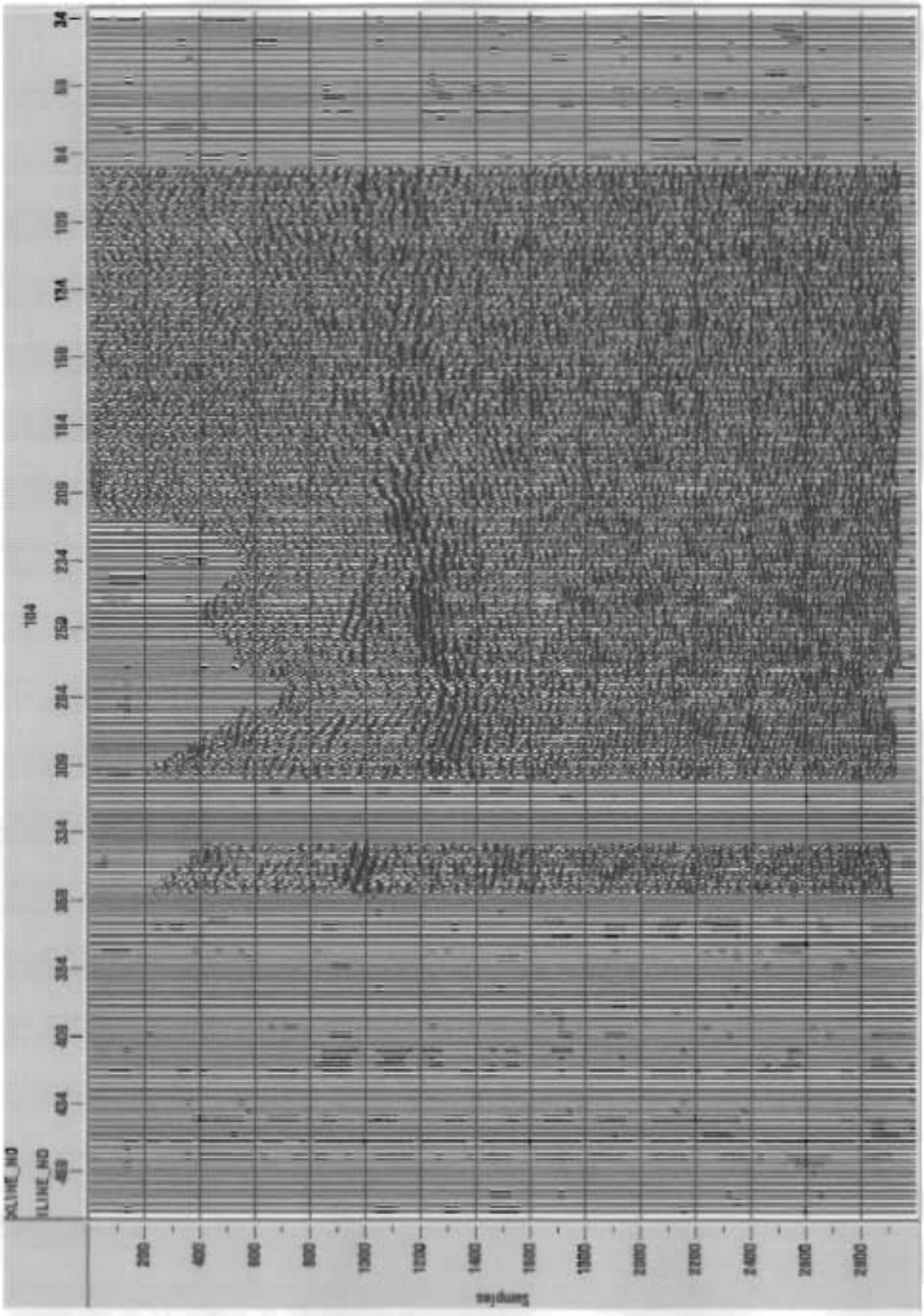
XLINE_NO
ILINE_NO
Samples

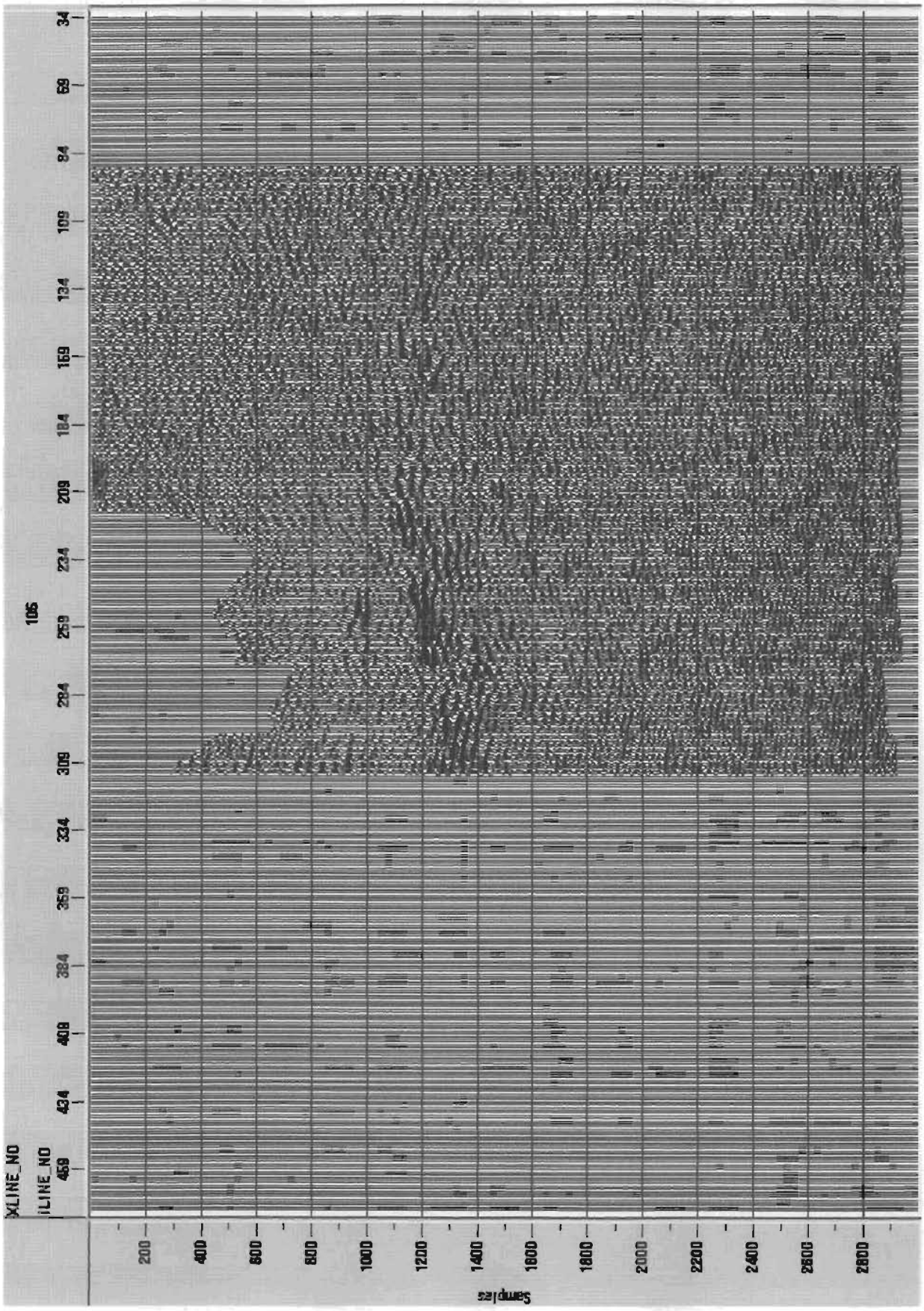
XLINE_NO
ILINE_NO
459
434
409
384
359
334
309
284
259
234
209
184
159
134
109
84
59
34
105
Samples
200
400
600
800
1000
1200
1400
1600
1800
2000
2200
2400
2600
2800

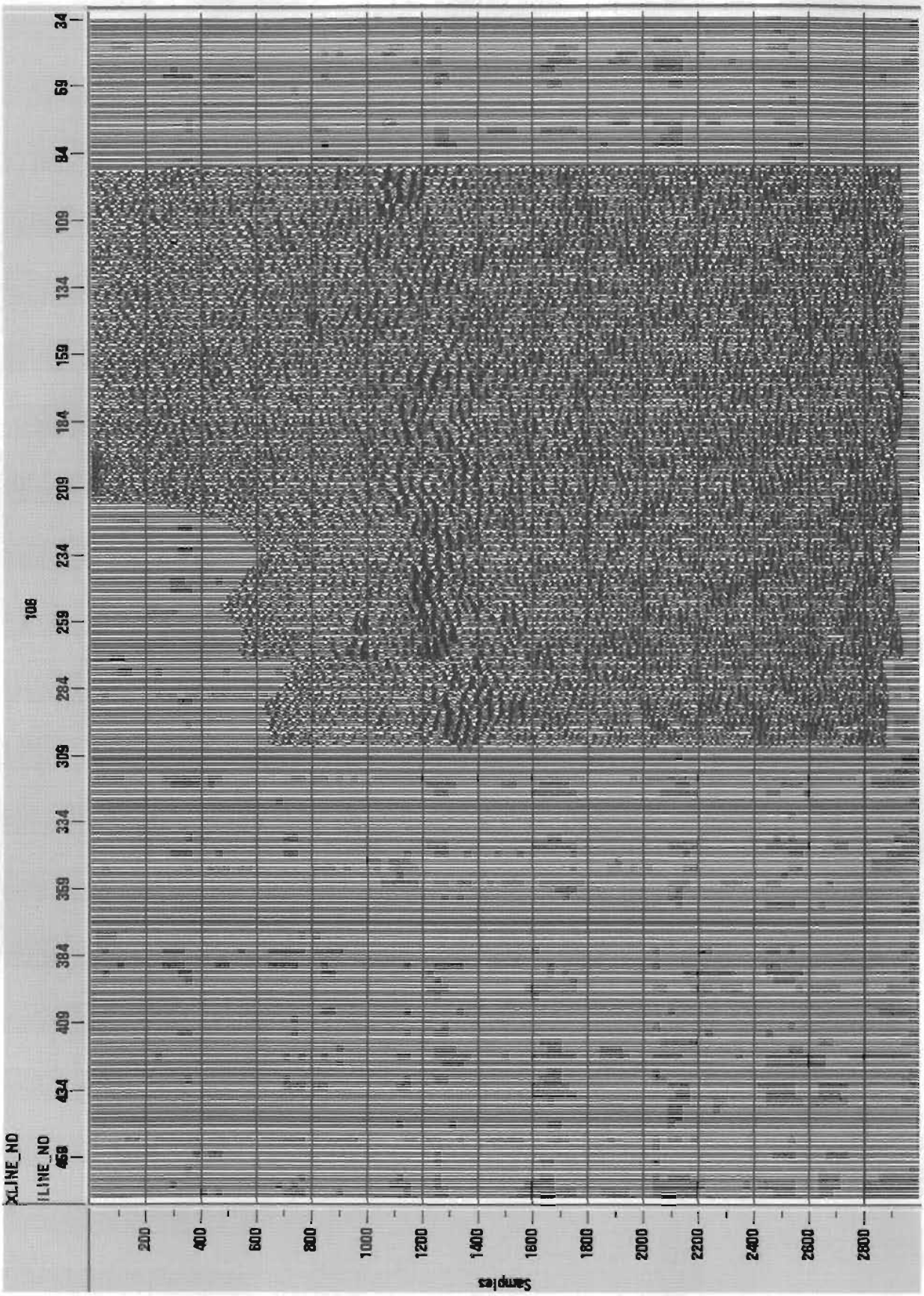
XLINE_NO
ILINE_NO
458
434
409
384
359
334
309
284
259
234
209
184
159
134
109
84
59
34
108
Samples
200
400
600
800
1000
1200
1400
1600
1800
2000
2200
2400
2600
2800